Engineering turbulence modelling for CFD with a focus on explicit algebraic Reynolds stress models

by

Stefan Wallin

February 2000
Technical Reports from
Royal Institute of Technology
Department of Mechanics
S-100 44 Stockholm, Sweden

Typsatt i $\mathcal{AMS}$-LaTeX med KTH's *thesis*-stil.

Akademisk avhandling som med tillstånd av Kungliga Tekniska Högskolan i Stockholm framlägges till offentlig granskning för avläggande av teknologie doktorsexamen fredagen den 25 februari 2000 kl 10.15 i Kollegiesalen, Administrationsbyggnaden, Kungliga Tekniska Högskolan, Valhallavägen 79, Stockholm.

Norstedts Tryckeri AB, Stockholm 2000

Engineering turbulence modelling for CFD with a focus on explicit algebraic Reynolds stress models

Stefan Wallin 2000
Department of Mechanics, Royal Institute of Technology
SE-100 44 Stockholm, Sweden

Abstract

Modelling of complex turbulent flows using explicit algebraic Reynolds stress and scalar flux models (EARSM and EASFM) has been considered. The eddy-viscosity or eddy-diffusivity assumption has been replaced by a more general constitutive relation for the second-order correlation in the Reynolds averaged equations. This relation has been derived using a formal approximation of the corresponding second-order transport model equations in the weak-equilibrium limit. The proposed EARSM is an exact solution of the implicit algebraic Reynolds stress model (ARSM) for two-dimensional mean flows and a reasonable approximation also in three-dimensional mean flows where the fully three-dimensional tensorial form is kept. Asymptotically correct near-wall treatment, extension to compressible mean flows and approximations of the neglected advection and diffusion terms are proposed. The resulting model behaves well in a number of different engineering and generic test cases giving significant improvements compared to standard eddy-viscosity models and the computational effort was comparable to standard two-equation models. The proposed EASFM is an exact solution of the corresponding implicit algebraic model in both two- and three-dimensional mean flows. *Á priori* tests show good model behaviour in homogeneous shear flows, channel and wake flow for the scalar flux vector.

Descriptors: Turbulence model, Reynolds stress, passive scalar flux, explicit algebraic models, computational fluid dynamics, aerodynamics, nonequilibrium turbulence, weak-equilibrium assumption.

Preface

This thesis considers the modelling of turbulent flows using explicit algebraic Reynolds stress and scalar flux models. The thesis is based on and contains the following papers.

Paper 1. Wallin, S. & Johansson, A. V. (2000) An explicit algebraic Reynolds stress model for incompressible and compressible turbulent flows. *J. Fluid Mech.* **403**, 89–132.

Paper 2. Lindblad, I.A.A., Wallin, S., Johansson, A.V., Friedrich, R., Lechner, L., Krogmann, P., Schülein, E., Courty, J.-C., Ravachol, M. & Giordano, D. (1998) A prediction method for high speed turbulent separated flows with experimental verification. AIAA Paper No. 98-2547.

Paper 3. Wallin, S. & Girimaji, S.S. (2000) Evolution of an isolated turbulent trailing vortex. Accepted for publication in *AIAA J.*

Paper 4. Wallin, S., Wang, D., Berggren, M. & Eliasson, P. (2000) A computational study of unsteady turbulent buffet aerodynamics. To be submitted.

Paper 5. Wikstrm, P.M., Wallin, S. & Johansson, A.V. (2000) Derivation and investigation of a new explicit algebraic model for the passive scalar flux. Accepted for publication in *Phys. Fluids.*

Paper 6. Wallin, S. (1999) An efficient explicit algebraic Reynolds stress k–ω model (EARSM) for aeronautical applications. FFA TN 1999-71.

Paper 7. Eliasson, P. & Wallin, S. (1999) A robust and positive scheme for viscous, compressible steady state solutions with two-equation turbulence models. FFA TN 1999-81.

The papers are here re-set in the present thesis format, and some minor differences are present as compared to published versions. The first part of the thesis is both a short introduction to the field and a summary of the most important

results presented in the papers given above. The main reults of the papers are presented in the context of a general introduction to the field of engineering turbulence modelling.

In memory of my father

Contents

CHAPTER 1

Introduction

Two brothers on a windy field on one of the barrier islands of North Carolina are getting ready for the first test flight of the day. It is December 17 (a special date in the history of fluid mechanics) and the conditions are perfect. It is Orville's turn to control the airplane. The engine starts and he takes off for a 36 m flight and Wilbur and Orville Wright became historic with the first controlled flight.

This event in 1903 marks the beginning of the amazing history of aeronautics during the 20th century. It was rather the pioneering work of Wilbur and Orville in flight mechanics and aerodynamic research preceding the historic flight that had the largest scientific value. Carrying out tedious experiments in a primitive wind tunnel they found that the relation for the lift force that they used was basically wrong and, moreover, they discovered wing profiles that produced much more lift than the previously used circular arc shapes. These experiments during the first years of the century became the necessary basis for the successful flight.

Since then wind tunnel techniques have been greatly improved. Most of the airplanes today are designed based on data from wind tunnel experiments and empirical correlations derived from such experiments and from experiences of previous airplane designs. It is not until the last few decades that computational fluid dynamics (CFD) has begun to be an alternative (or rather a complement) to expensive wind tunnel experiments. Earlier computational methods had severe physical restrictions, and were typically based on potential methods and boundary layer methods. These methods were, and still are, mainly used for approximative concept studies rather than for complete validations of final designs.

The major problem in CFD is the strong nonlinearity in the governing equations along with the corresponding nonlinearity in the dynamics of the physical reality. The nonlinearity causes anomalies in the flow, such as discontinuities (shock waves), and that small disturbances in some critical points may cause major effects in the flow. However, progress in numerical methods and computer performance have solved many of these problems and today it is possible to, with at least some confidence, obtain a numerical solution of the flow field around a complete aircraft configuration including all major physical effects, such as *e.g.*, shock waves, turbulent boundary layers and vortices. In some applications, such as the reentry of space vehicles back to earth, representative wind tunnel experiments are not possible and one must rely on CFD methods.

There is, however, one major physical approximation still present in the present CFD methods namely the modelling of the turbulence. The flow in the boundary layer closest to the solid walls of all moving bodies, including airplanes, cars, trains, ships and whales are mostly turbulent. This is also the case in most internal flows, such as pipe flows and flows in engines and pumps. This means that the flow is chaotic and stochastic with eddies in a wide range of sizes. This can quite literally be felt in the wind on a stormy day. The turbulent boundary layer very much controls the performance of the airplane, such as drag and maximum lift forces, which set the fuel consumption and landing and take-off speeds. Thus, it is crucial to be able to accurately predict, and possibly also to control, the turbulent boundary layer.

The equations that govern the turbulent flow are known, so in principal the turbulent field may be computed directly in a, so called, direct numerical simulation (DNS). If the Reynolds number is large (it almost always is), *i.e.* the internal viscosity of the fluid is small, the smallest turbulent eddies are very small compared to the largest eddies and the computational effort to capture all the dynamics is enormous. Years of computational time on the fastest supercomputers is needed to simulate the turbulence in just a small strip (say 10×1 cm^2) on a typical airplane wing. For that reason the turbulence needs to be modelled. Hence the turbulent flow is described by statistical methods, just like the meteorologist talking about the mean wind speed and direction even if the wind in the gusts are varying wildly.

Turbulence research and modelling efforts go back to the late 19th century with landmark events such as the first attempt to model turbulence in terms of a turbulent viscosity proposed by Boussinesq[5] (1877) contemporary with the Reynolds[40] pipe experiments in 1880. First, the turbulent viscosity was assumed to be constant and not until 1925 the more useful mixing-length idea was proposed by Prandtl[38] from which the well known, and in CFD much used, Baldwin & Lomax[3] model originates. Other pioneering work in more advanced models are the first two-equation model by Kolmogorov[27] (1942) and the first Reynolds stress transport model by Rotta[46] (1951). It was not until the 70's the modelling efforts started to make real progress when the computers started to be useful for CFD applications. Worth notice are the Jones & Launder[22] K–ε model and the Launder, Reece & Rodi[29] RST model.

Engineering turbulence flows are often, by nature, complex. This means that different turbulence effects are present simultaneously and are interacting. The most important demand on an engineering turbulence model is thus generality. Complex flows often mean three-dimensional complex geometries and another, equally strong demand is that the computational effort must be limited. The major contribution of this work is the extension of validity for a class of turbulence models that is affordable for engineering CFD methods.

CHAPTER 2

Basic concepts in turbulence modelling

2.1. Governing equations and Reynolds averaging

Compressibility is an important aspect of many engineering flows. However, most of the basic turbulence theories, modelling developments, and experimental as well as numerical simulations are made for incompressible flows. Simple extensions of incompressible turbulence models to account for mean-density variations are successfully used as long as the Morkovin's hypothesis holds, that is when the compressibility effects due to turbulent fluctuations are negligible.

For attached boundary layers, compressibility effects due to turbulent fluctuations begin to be important for a Mach number around five, but in free shear flows these effects become important at much lower Mach numbers. For a detailed description of the intricate aspects of compressibility effects due to turbulent fluctuations, please consult Friedrich[11].

To illustrate the basic approaches for turbulence modelling we will here restrict ourself to incompressible flows. The extension to compressible flows is described in Paper 1 (see also Johansson & Burden[19]). Turbulent flows are supposed to be governed by conservation of mass and momentum through the Navier–Stokes equations, which read

$$\frac{\partial \widetilde{u}_i}{\partial x_i} = 0 \tag{1}$$

$$\frac{\partial \widetilde{u}_i}{\partial t} + \widetilde{u}_j \frac{\partial \widetilde{u}_i}{\partial x_j} = -\frac{1}{\rho}\frac{\partial \widetilde{p}}{\partial x_i} + \frac{\partial}{\partial x_j}\left(2\nu \widetilde{s}_{ij}\right) \tag{2}$$

where $\widetilde{u}_i$ and $\widetilde{p}$ are the instantaneous velocity and pressure fields. ρ and ν are the (constant) density and kinematic viscosity respectively. The instantaneous strain rate tensor is defined as $\widetilde{s}_{ij} \equiv (\widetilde{u}_{i,j} + \widetilde{u}_{j,i})/2$.

These equations completely describe the turbulent field and may, in principal, be solved directly in a so called direct numerical simulation (DNS). The smallest length and time scales in a turbulent field then need to be resolved, and thus the computational effort grows rapidly with increasing Reynolds number, which relates the largest or geometrical scales to the smallest or viscous scales. Therefore, direct numerical simulation is mainly used as a research tool for studying turbulence in detail and for calibration of turbulence models. The simulations are typically run for geometrically simple generic cases like different kinds of homogeneous turbulence, channel and pipe flows, or boundary layers.

In practically all engineering cases, the turbulence needs to be considered using a statistical approach. The flow-field variables are then decomposed into mean and fluctuating parts such as $\widetilde{u}_i = U_i + u_i$ and $\widetilde{p} = P + p$ where U_i and P are defined as the ensemble average over a large number of independent realizations of the flow field, $U_i \equiv \overline{\widetilde{u}_i}$ and $P \equiv \overline{\widetilde{p}}$. u_i and p are the fluctuating parts, for which $\overline{u_i} = 0$ and $\overline{p} = 0$.

The Reynolds averaged Navier–Stokes (RANS) equations are formed by taking the mean of the Navier–Stokes equations using the decomposition defined above

$$\frac{\partial U_i}{\partial x_i} = 0 \tag{3}$$

$$\frac{\mathrm{D}\, U_i}{\mathrm{D}t} = -\frac{1}{\rho}\frac{\partial P}{\partial x_i} + \frac{\partial}{\partial x_j}\left(2\nu S_{ij} - \overline{u_i u_j}\right) \tag{4}$$

where the mean strain rate tensor $S_{ij} \equiv (U_{i,j} + U_{j,i})/2$. The notation $\mathrm{D}/\mathrm{D}t \equiv \partial/\partial t + U_j \partial/\partial x_j$ is used to denote the rate of change following the mean flow.

The momentum equation for the mean flow field contains an additional term that originates from the average of the nonlinear term. That term is called the Reynolds stress $-\overline{\rho u_i u_j}$ and is felt by the mean field as an additional stress due to the turbulent fluctuations. In incompressible flows the density, ρ, is constant and gives no additional information and, thus, it is common to denote only the velocity correlation as the Reynolds stress.

Turbulence modelling in engineering CFD methods is simply a matter of finding an expression for the Reynolds stress tensor in terms of known quantities. Its complexity ranges from purely algebraic relations to relations that consider one or several extra transport equations for different turbulent correlations.

The transport equation for the Reynolds stress tensor may be derived from the Navier–Stokes equations

$$\frac{\mathrm{D}\,\overline{u_i u_j}}{\mathrm{D}t} = \mathcal{P}_{ij} - \varepsilon_{ij} + \Pi_{ij} + \mathcal{D}_{ij}. \tag{5}$$

The terms represent production, dissipation, pressure-strain rate, and diffusion (molecular and turbulent), respectively. The exact expressions for these are given by, *e.g.*, Johansson & Burden[19]. One should particularly note that the production term is explicit in the Reynolds stresses, whereas the other terms need to be modelled.

The transport equation for the turbulent kinetic energy, $K \equiv \overline{u_i u_i}/2$, is derived by taking half of the trace of the transport equation for the Reynolds stress tensor

$$\frac{\mathrm{D}\, K}{\mathrm{D}t} = \mathcal{P} - \varepsilon + \mathcal{D}^{(K)}. \tag{6}$$

The production, dissipation and diffusion (molecular and turbulent) terms on the right-hand side are given by half the trace of the respective terms in the Reynolds stress transport equation.

The trace of the pressure-strain term is zero so that it does not contribute to the energy equation. The Reynolds stresses may also be expressed in terms of the Reynolds stress anisotropy tensor

$$a_{ij} \equiv \frac{\overline{u_i u_j}}{K} - \frac{2}{3}\delta_{ij} \tag{7}$$

which is symmetric and traceless ($a_{ij} = a_{ji}$ and $a_{ii} = 0$).

2.2. Eddy-viscosity models

The analogy between the viscous stress generation caused by fluctuations on the molecular level and the generation of turbulent stresses caused by macroscopic velocity fluctuations lead historically to an eddy (or turbulent) viscosity formulation or the Reynolds stress. The first attempt to model the Reynolds stresses was made by Boussinesq[5] who introduced an eddy viscosity, ν_T, in complete analogy with the molecular viscosity for a Newtonian fluid. The original Boussinesq assumption or the eddy viscosity assumption related the shear component of the Reynolds stress tensor in nearly parallel shear flows to the cross stream mean velocity gradient. This approach was later generalized for modelling turbulent flows in general geometries. The Reynolds stress tensor is then related to the mean flow field through

$$\overline{u_i u_j} = -2\nu_T S_{ij} + \frac{2}{3}K\delta_{ij} \tag{8}$$

The last term is often included in the pressure term. In that way a somewhat modified pressure is obtained, but is a necessary approach in, *e.g.*, simple algebraic eddy-viscosity models where K is not available.

The eddy viscosity may be interpreted as a diffusivity coefficient (of momentum) related to the velocity scale V and length scale L of the large energetic turbulent eddies ($\nu_T \sim VL$). By applying the eddy-viscosity hypothesis, turbulence modelling reduces to a matter of modelling the eddy viscosity ν_T.

2.2.1. Algebraic and one-equation models. Models where the eddy viscosity is completely determined in terms of the local mean flow variables are referred to as zero-equation or algebraic models. In these models the turbulent velocity scale is related to the mean flow velocity or vorticity and the length scale is related to some geometrical length, for example wall distance or wake thickness. Well known and much used is the Baldwin–Lomax[3] model.

In one-equation models, one of the two turbulence scales (or a combination of both) is determined from a transport equation. As for algebraic models additional information from the mean flow field or geometrical measures is needed. Many one-equation models are based on the transport equation for the turbulent kinetic energy originally proposed by Prandtl[39]. The one-equation model of Spalart & Allmaras[58] is based on a transport equation for the eddy viscosity itself. This model has attracted considerable attention recently and has been shown to perform reasonably well in typical aeronautical applications.

2.2.2. Two-equation models. The major deficiency in algebraic and one-equation models is that the turbulence scales need to be related to the global flow or geometrical scales. Many of the ad hoc corrections and relations present in such models are caused by this 'incompleteness' of the model. A complete model is characterized by the feature that the Reynolds stresses are completely determined from the local state of the mean flow and mean turbulence quantities. No global measures are thus needed such as, *e.g.*, the wall distance, boundary layer thickness or free stream velocities.

The lowest modelling level that is complete in that sense is the two-equation modelling approach where the turbulence scales are determined from two transport equations. The natural choice for the turbulent velocity scale is the square root of the turbulent kinetic energy K and the turbulent length scale is determined from K and the auxiliary quantity, *i.e.* ε in the K–ε model where $L{\sim}K^{3/2}/\varepsilon$. Auxiliary quantities other than ε have been used, *e.g.*, $\omega \sim \varepsilon/K$ and $\tau \sim K/\varepsilon$ together with K.

The exact transport equation for K is given by (6) where the different terms need to be modelled in terms of known quantities. The production term needs no further modelling after applying the eddy-viscosity assumption

$$\mathcal{P} = 2\nu_T S_{ij} S_{ji}. \tag{9}$$

The turbulent diffusion is usually modelled using the gradient diffusion assumption which gives the total diffusion

$$\mathcal{D}^{(K)} = \frac{\partial}{\partial x_j}\left(\left(\nu + \frac{\nu_T}{\sigma_K}\right)\frac{\partial K}{\partial x_j}\right) \tag{10}$$

where the diffusivity is related to the turbulent viscosity through the turbulent Schmidt number σ_K.

The dissipation rate ε is modelled in form of an additional transport equation for ε or some other quantity Z related to K and ε, such as $Z = K^m\varepsilon^n$. The standard structure of the transport equation for Z is

$$\frac{\mathrm{D}\,Z}{\mathrm{D}t} = \left(C_{Z1}\mathcal{P} - C_{Z2}\varepsilon\right)\frac{Z}{K} + \mathcal{D}^{(Z)} \tag{11}$$

The diffusion term usually reads

$$\mathcal{D}^{(Z)} = \frac{\partial}{\partial x_j}\left(\left(\nu + \frac{\nu_T}{\sigma_Z}\right)\frac{\partial Z}{\partial x_j}\right) \tag{12}$$

but additional, so called cross diffusion terms, could be added

$$+C_{Z3}\frac{\partial K}{\partial x_j}\frac{\partial Z}{\partial x_j}. \tag{13}$$

Such terms result from straightforward transformations between different bases for Z, *e.g.*, between ε and ω.

Finally the eddy viscosity is related to K and Z, for instance through

$$\nu_T = C_\mu \frac{K^2}{\varepsilon} \qquad \text{or} \qquad \nu_T = \frac{K}{\omega} \tag{14}$$

in case of a K–ε or a K–ω model respectively.

In wall bounded flows the very near-wall region ($y^+ \lesssim 50$) needs special attention. Typically, the coefficients in the Z equation and C_μ need to be multiplied with so called damping functions based on y^+, Re_y or Re_T or a combination of these nondimensional numbers

$$y^+ \equiv \frac{y u_\tau}{\nu} \qquad Re_y \equiv \frac{y\sqrt{K}}{\nu} \qquad Re_T \equiv \frac{K^2}{\varepsilon\nu} \tag{15}$$

where y is the wall distance and $u_\tau \equiv \sqrt{\tau_w/\rho}$ is the wall friction velocity. There are, however, models that are defined completely without any near-wall damping functions, *e.g.* the Wilcox[66] standard K–ω model.

Another alternative is the use of wall function boundary condition which means that the boundary conditions are set outside of the viscous sub-layer. The very near-wall stiffness is then avoided and a considerable amount of computational grid points and computational effort are saved. However, the numerical solutions are sensitive to the distance to the first computational point above the surface and the law of the wall does not always hold, *e.g.*, near boundary layer separation.

The standard two-equation models are insensitive to rotation. The K–Z equations and the stress-strain relation contain no explicit dependence on the rotation rate tensor $\Omega_{ij} \equiv (U_{i,j} - U_{j,i})/2$ and thus the equations expressed in a rotating coordinate system are identical to the ones written in an inertial system. Also the effect of local rotation is lost, that could be related to the absence of rotation near stagnation points and the excessive rate of rotation within vortices. This is a major deficit of standard eddy-viscosity two-equation models and one of the reasons for the fact that such models fail in predicting the correct rate of production in complicated turbulent flows.

Moreover, even in the simplest possible equilibrium shear flows, or in the log-layer of boundary layers, the eddy-viscosity assumption completely fails in predicting all but one of the components in the Reynolds stress anisotropy tensor. However, the well predicted component is the only one that is of primarly importance in thin shear layers.

Another deficit is that two-equation eddy-viscosity models may produce unphysical values of the Reynolds stresses in nonequilibrium flows where the production to dissipation ratio is large, $\mathcal{P}/\varepsilon \gg 1$. Any normal component of the Reynolds stress tensor must be positive $\overline{u_\alpha^2} \geq 0$ regardless of the choice of unit vector $e_i^{(\alpha)}$. This is the so called realizability of turbulence models and gives that the components of the anisotropy tensor are bounded. The Reynolds stress anisotropy for the K–ε model may be expressed as $a_{ij} = -2C_\mu(K/\varepsilon)S_{ij}$. In

rapidly strained turbulence the term $(K/\varepsilon)S_{ij}$ may become large, which obviously may result in unphysical values of the anisotropy. This could lead to unphysical growth of turbulence in regions where low-level free-stream turbulence interacts with flow distortions such as around stagnation points and near shocks in compressible flows.

To avoid unphysical growth of the turbulence in practical computations, the production is often limited by the dissipation rate $\mathcal{P}<C\varepsilon$ where C is some sufficiently high number, typically around 10. The problem with this form is that in rapidly growing turbulence the growth rate should be independent of the dissipation rate. An alternative limiter for the production is described in Paper 6 where $\mathcal{P}<K\sqrt{S_{ij}S_{ji}}$, which is based on realizability constraints. A similar effect is obtained with the Menter SST K–ω model[32], where the Bradshaw assumption is used. Here, the shear anisotropy a_{12} is limited to -0.3 for $\mathcal{P}/\varepsilon$ ratios greater than unity, which has been observed in adverse pressure gradient boundary layers and also in homogeneous shear flows. This model has been found to perform well for typical aeronautical applications.

However, in many engineering flows the boundary layers are attached without strong curvature or rotational effects, and thus the eddy-viscosity assumption has been, and still is, relatively successful. The absolute majority of turbulence models used in industrial CFD methods are based on the eddy-viscosity assumption.

2.3. Reynolds stress models

Eddy-viscosity models perform reasonably well in attached boundary layer flows as long as only one component of the Reynolds stress tensor is of significant importance. In these cases one could consider the eddy viscosity as a representative for the significant Reynolds stress component. However, if the flow becomes more complicated the eddy-viscosity assumption fails and, thus, there is not much hope for a more general validity of the eddy-viscosity approach.

Models that are based on the exact transport equation for the Reynolds stress tensor (5) contain much more of the fluid mechanics needed in complicated turbulent flows. The advection and diffusion terms account for transport effects for the individual Reynolds stress components, whereas eddy-viscosity two-equation models only consider such effects for the trace of the Reynolds stress tensor. These effects are of significant importance for the development of the trace of the Reynolds stress tensor, *i.e.*, the kinetic energy, as well as the individual components in nonequilibrium flows where $\mathcal{P}/\varepsilon\ll 1$.

More important are the different local source terms. No modelling is needed for the production term, $\mathcal{P}_{ij}$, which is a significant improvement compared to the modelling of the trace of the production present in eddy-viscosity models described in the previous section. The intercomponent energy transfer, represented by Π_{ij} needs to be modelled, but already the simplest possible models represent

improvements compared to eddy-viscosity two-equation models in which this effect is not present at all.

2.3.1. Differential Reynolds stress models (DRSM). In differential Reynolds stress models, or Reynolds stress transport (RST) models, all different terms in (5) are kept or modelled which results in a transport equation for every individual Reynolds stress component. In general three-dimensional mean flows this implies six equations due to symmetry in the Reynolds stress tensor.

The dissipation rate tensor ε_{ij} is usually decomposed into an isotropic part and a deviation from that, $\varepsilon_{ij} = \varepsilon(e_{ij} + 2\delta_{ij}/3)$. First, the total dissipation rate ε is modelled through a transport equation, similar to the ε equation in the K–ε models. Also here other alternatives to ε, such as ω or τ exist. The dissipation rate anisotropy e_{ij} is typically explicitly modelled in terms of the Reynolds stress anisotropy or included into the modelling of the pressure strain rate. Turbulent diffusion, $\mathcal{D}_{ij}$, may be modelled using the generalized gradient diffusion model by Daly & Harlow[10].

The focus of the modelling in this context is that of the pressure strain rate. The classical decomposition into two parts, the rapid and slow parts, is based on the formal solution of the Poisson equation for the pressure field. The rapid part responds directly to changes in the mean flow field while the source term for the slow part does not contain any mean flow field information. Originally these terms were modelled linearly in the Reynolds stress tensor, see Rotta[46] and Launder, Reece & Rodi[29]. More recently higher order models that are nonlinear in the Reynolds stresses have been proposed mainly in order to satisfy strong realizability, which is not possible for linear models, see Sjögren & Johansson[56] and Sarkar, Speziale & Gatski[60].

The most general quasi-linear model for the pressure-strain rate and dissipation rate anisotropy e_{ij} lumped together reads

$$\begin{aligned}\frac{\Pi_{ij}}{\varepsilon} - e_{ij} = &-\frac{1}{2}\left(C_1^0 + C_1^1\frac{\mathcal{P}}{\varepsilon}\right)a_{ij} + C_2\tau S_{ij} \\ &+\frac{C_3}{2}\tau\left(a_{ik}S_{kj} + S_{ik}a_{kj} - \frac{2}{3}a_{kl}S_{lk}\delta_{ij}\right) - \frac{C_4}{2}\tau\left(a_{ik}\Omega_{kj} - \Omega_{ik}a_{kj}\right), \quad (16)\end{aligned}$$

for example, see Girimaji[13]. $\tau = K/\varepsilon$ is the turbulent timescale. Classical linear models, such as the Launder, Reece & Rodi[29] (LRR) or the simplified, so called isotropization of production (IP) model (see also Naot[35]) may be written in this form. Also the Sarkar, Speziale & Gatski[60] (SSG) model linearized around equilibrium homogeneous shear flows may be expressed in this form, see for example Gatski & Speziale[12] for linearization of the SSG model. The C coefficients for these models are given in Table 2.1. By quasi-linear pressure-strain models we here mean that the model is linear in the Reynolds stress anisotropy, but may contain the scalar nonlinearity $a_{ij}\mathcal{P}/\varepsilon \equiv -\tau a_{kl}S_{lk}a_{ij}$.

TABLE 2.1 The values of the C coefficients for different quasi-linear pressure-strain models

	C_1^0	C_1^1	C_2	C_3	C_4
Original LRR	3.0	0	0.8	1.75	1.31
Recalibrated LRR (W&J)	3.6	0	0.8	2	1.11
Linearized SSG	3.4	1.8	0.36	1.25	0.40

An alternative to using the Reynolds stress transport equations (5) is to reformulate the equations in terms of the Reynolds stress anisotropy and the turbulent kinetic energy. The transport equation for the Reynolds stress anisotropy reads

$$K\left(\frac{\mathrm{D}\,a_{ij}}{\mathrm{D}t}-\mathcal{D}_{ij}^{(a)}\right)=\left(\mathcal{P}_{ij}-\frac{\overline{u_iu_j}}{K}\mathcal{P}\right)-\left(\varepsilon_{ij}-\frac{\overline{u_iu_j}}{K}\varepsilon\right)+\Pi_{ij}, \tag{17}$$

where diffusion of the anisotropy is defined as

$$\mathcal{D}_{ij}^{(a)}\equiv\frac{\mathcal{D}_{ij}}{K}-\frac{\overline{u_iu_j}}{K^2}\mathcal{D}^{(K)}. \tag{18}$$

Inserting the quasi-linear pressure-strain rate model (16) into (17) gives

$$\begin{aligned}\tau\left(\frac{\mathrm{D}\,a_{ij}}{\mathrm{D}t}-\mathcal{D}_{ij}^{(a)}\right)\;=\;A_0\Bigg[&\left(A_3+A_4\frac{\mathcal{P}}{\varepsilon}\right)a_{ij}+A_1S_{ij}^*-\left(a_{ik}\Omega_{kj}^*-\Omega_{ik}^*a_{kj}\right)\\&+\;A_2\left(a_{ik}S_{kj}^*+S_{ik}^*a_{kj}-\frac{2}{3}a_{kl}S_{lk}^*\delta_{ij}\right)\Bigg]\end{aligned} \tag{19}$$

where the strain and rotation rate tensors are normalized by the turbulent timescale, $S_{ij}^*=\tau S_{ij}$ and $\Omega_{ij}^*=\tau\Omega_{ij}$. The A coefficients are related to the C coefficients through

$$A_0=\frac{C_4}{2}-1,\;\;A_1=\frac{3C_2-4}{3A_0},\;\;A_2=\frac{C_3-2}{2A_0},\;\;A_3=\frac{2-C_1^0}{2A_0},\;\;A_4=\frac{-C_1^1-2}{2A_0}. \tag{20}$$

The transport equation for the Reynolds stress anisotropy may be written in the following symbolic form

$$\mathrm{tr}(a_{ij})=\mathrm{f}_{ij}\left(a_{kl},S_{kl}^*,\Omega_{kl}^*\right) \tag{21}$$

where $\mathrm{tr}(a_{ij})$ represents the advection and diffusion of the Reynolds stress anisotropy and f_{ij} the production, dissipation and redistribution terms.

2.3.2. Algebraic Reynolds stress models (ARSM). In flows where the anisotropy varies slowly in time and space, the transport equation for the Reynolds stress anisotropy tensor is reduced to an implicit algebraic relation. Also in many inhomogeneous flows of engineering interest the flow is steady and the advection and diffusion of the Reynolds stress anisotropy may be neglected. This is equivalent to the assumption by Rodi[42, 43] that the advection and

diffusion of the individual Reynolds stresses scale with those of the turbulent kinetic energy. The set of transport equations for the Reynolds stress anisotropy is then reduced to an algebraic equation system, which in the case of quasi-linear pressure-strain models may be written as

$$0 = \left(A_3 + A_4\frac{\mathcal{P}}{\varepsilon}\right)a_{ij} + A_1 S^*_{ij} - \left(a_{ik}\Omega^*_{kj} - \Omega^*_{ik}a_{kj}\right) + A_2\left(a_{ik}S^*_{kj} + S^*_{ik}a_{kj} - \frac{2}{3}a_{kl}S^*_{lk}\delta_{ij}\right). \tag{22}$$

This system is implicit in the Reynold stress anisotropy. It is also nonlinear in the Reynolds stresses, even with linear modelling of the pressure-strain rate term, because of the term $(\mathcal{P}/\varepsilon)a_{ij} \equiv -a_{kl}S^*_{lk}a_{ij}$. The set of equations may be written in the following symbolic form

$$0 = \mathrm{f}_{ij}\left(a_{kl}, S^*_{kl}, \Omega^*_{kl}\right). \tag{23}$$

and may, in principle, be solved for any kind of model for the pressure-strain rate and dissipation rate tensors.

2.3.3. Explicit algebraic Reynolds stress models (EARSM). The system of equations (22) has been found to be numerically and computationally cumbersome since there is no diffusion or damping present in the equations. In many applications the computational effort has been found to be excessively large and the benefit of using ARSM instead of the full transport form is then lost. In a pioneering work of Pope[36] (1975) an explicit form was proposed for two-dimensional flows, but the approach did not attract significant attention until the beginning of the 90's. The work in this area of algebraic Reynolds stress modelling has been focused on finding explicit expressions. EARSMs are much more numerically and computationally robust and have been found to be comparable to standard two-equation models in computational effort.

So far explicit solutions of algebraic Reynolds stress models have been restricted to linear or quasi-linear pressure-strain models where the ARSM equations can be written as (22). The procedure proposed by Pope[36] to obtain an explicit form was to avoid the nonlinearity by considering $\mathcal{P}/\varepsilon$ as an extra unknown. The resulting linear equation system can then be written as

$$0 = \mathrm{L}_{ij}\left(a_{kl}, S^*_{kl}, \Omega^*_{kl}, \mathcal{P}/\varepsilon\right). \tag{24}$$

and may, in principal, be solved directly. However, by the inspection of (22) one realizes that the anisotropy tensor is dependent on only two other tensors, S^*_{ij} and Ω^*_{ij}, which can be used to form a complete base for the anisotropy. Following Spencer & Rivlin[59] and Pope[36] the complete expression consists of

ten tensorially independent groups

$$\begin{aligned}\mathbf{a} = & \beta_1\mathbf{S} \\ & + \beta_2\left(\mathbf{S}^2 - \frac{1}{3}II_S\ \mathbf{I}\right) + \beta_3\left(\mathbf{\Omega}^2 - \frac{1}{3}II_\Omega\ \mathbf{I}\right) + \beta_4\left(\mathbf{S\Omega} - \mathbf{\Omega S}\right) \\ & + \beta_5\left(\mathbf{S}^2\mathbf{\Omega} - \mathbf{\Omega S}^2\right) + \beta_6\left(\mathbf{S\Omega}^2 + \mathbf{\Omega}^2\mathbf{S} - \frac{2}{3}IV\ \mathbf{I}\right) \\ & + \beta_7\left(\mathbf{S}^2\mathbf{\Omega}^2 + \mathbf{\Omega}^2\mathbf{S}^2 - \frac{2}{3}V\ \mathbf{I}\right) + \beta_8\left(\mathbf{S\Omega S}^2 - \mathbf{S}^2\mathbf{\Omega S}\right) + \beta_9\left(\mathbf{\Omega S\Omega}^2 - \mathbf{\Omega}^2\mathbf{S\Omega}\right) \\ & + \beta_{10}\left(\mathbf{\Omega S}^2\mathbf{\Omega}^2 - \mathbf{\Omega}^2\mathbf{S}^2\mathbf{\Omega}\right). \end{aligned} \tag{25}$$

The β coefficients may be functions of the five independent invariants of $\mathbf{S}$ and $\mathbf{\Omega}$, which can be written as

$$II_S = \mathrm{tr}\{\mathbf{S}^2\},\ \ II_\Omega = \mathrm{tr}\{\mathbf{\Omega}^2\},\ \ III_S = \mathrm{tr}\{\mathbf{S}^3\},\ \ IV = \mathrm{tr}\{\mathbf{S\Omega}^2\},\ \ V = \mathrm{tr}\{\mathbf{S}^2\mathbf{\Omega}^2\}. \tag{26}$$

Other scalar parameters may also be involved. For simplicity, we have used boldface for denoting second-rank tensors and tr{} is the trace. We have also omitted the *, so that $\mathbf{S}{\equiv}S^*_{ij}$ and $\mathbf{\Omega} \equiv \Omega^*_{ij}$.

The ARSM equation system (22) may now be solved by mapping every term onto this base and solve the linear equation system for the β coefficients. The β coefficients are thus completely determined in terms of the coefficients in the basic RST model. Pope[36] derived a solution for two-dimensional mean flows, where only the three terms associated to β_1, β_2 and β_4 are needed. In three-dimensional mean flows Taulbee[62] obtained a solution for a specific choice of ARSM where $A_2 = 0$ and Gatski & Speziale[12] determined the solution for the general quasi-linear ARSM. Also more general nonlinear models may be mapped onto the base (25) but the corresponding equation system for the β coefficients is then no longer linear.

Now, we return to the assumption by Pope of leaving the production to dissipation ratio as an unknown quantity. The solution may be written in the following form

$$a_{ij} = \mathrm{A}_{ij}\left(S^*_{kl}, \Omega^*_{kl}, \mathcal{P}/\varepsilon\right). \tag{27}$$

Remembering that $\mathcal{P}/\varepsilon{\equiv} - a_{ij}S^*_{ji}$ the following equation must hold for consistency

$$\mathcal{P}/\varepsilon = -\mathrm{A}_{ij}\left(S^*_{kl}, \Omega^*_{kl}, \mathcal{P}/\varepsilon\right) S^*_{ji}. \tag{28}$$

Models that fulfill this so called consistency condition may be considered as 'self consistent'. The condition (28) may be fulfilled implicitly by some iteration procedure or as a part of the solution process, as Pope[36] and Taulbee[62] suggest. Self consistency may also be obtained explicitly by expanding and solving (28), which results in a third-order polynomial equation with an exact solution in two-dimensional mean flows. That approach was taken by Girimaji[13] and

Johansson & Wallin[20]. The latter also extended the solution with an approximation valid also in three-dimensional mean flows, see Paper 1.

A different approach was taken by Gatski & Speziale[12] where the equilibrium value for $\mathcal{P}/\varepsilon$ in homogeneous shear flows was taken as a universal constant. This model is thus only exactly self consistent in equilibrium homogeneous shear flows. The major motivation behind that assumption was that the basic equilibrium assumption of neglecting $\mathrm{D}a_{ij}/\mathrm{D}t$ and $\mathcal{D}_{ij}^{(a)}$ is strictly valid only in equilibrium flows, and thus it might be considered as inconsistent to extend $\mathcal{P}/\varepsilon$ to beyond equilibrium flows. The assumption of a constant $\mathcal{P}/\varepsilon$ resulted in a model with the wrong asymptotic behaviour in rapidly distorted flows and that also may become singular under some conditions. Additional corrections were therefore needed, see Gatski & Speziale[12] and Speziale & Xu[61].

More recently it has become quite well accepted that the consistency condition improves the predictive performance and that it is important for avoiding numerical problems, see *e.g.* Rumsey, Gatski & Morrison[47], Jongen, Machiels & Gatski[24] and the analysis of the consequences of the consistency condition by Jongen & Gatski[25]. Approximate self consistency was obtained in the model proposed by Rung *et al.*[48], which performs similarly to fully self-consistent models.

Extensions of EARSMs to account for anisotropic dissipation rate have been proposed by Xu & Speziale[68] and extended to inhomogeneous flows by Jongen, Mompean & Gatski[26]. Some improvements compared to the basic EARSM was reported for S-duct flow using this composite model.

2.3.4. Nonlinear eddy-viscosity models (NL-EVM). A different family of models, that has the same principal form (25) as EARSMs, are the nonlinear eddy-viscosity models (NL-EVM). A standard eddy-viscosity model is recalled by setting $\beta_1 = -2C_\mu$ and $\beta_{2-10} = 0$ in (25). By adding additional terms from the general constitutive relation (25) and by letting the β coefficients be functions of the invariants (26) more of the turbulence physics may be captured. The method is typically to relate each term, or group of terms, to a specific generic flow case, to find a suitable functional form for the β coefficients and calibrate the coefficients. Also more analytical considerations, such as realizability, may be considered when formulating the β-functions in terms of the invariants.

When formulating a NL-EVM one should consider that the components of the Reynolds stress anisotropy tensor are restricted to order of unity due to realizability constraints. Eddy-viscosity models with constant C_μ (or constant β_1) become unrealizable for large strain rates since the anisotropy is proportional to the normalized strain rate, $\|a_{ij}\| \sim \sigma$, where σ is some representative measure of the normalized deformation rate, *e.g.* $\sigma \sim \tau\|\partial U_i/\partial x_j\|$. Adding higher-order terms makes this problem worse if the corresponding β coefficients are constant. For example, second-order terms give $\|a_{ij}\| \sim \sigma^2$ and third-order terms $\|a_{ij}\| \sim \sigma^3$.

The β coefficients should, therefore, be functions of the strain rate so that for large strain rates they become inversely proportional to the strain rate to a power at least equal to the degree of the corresponding term. An example of such a form is

$$\beta_1 = \frac{\beta_1^0}{1+\beta_1^1\sigma}, \quad \beta_{2-4} = \frac{\beta_{2-4}^0}{1+\beta_{2-4}^1\sigma^2}, \quad \beta_{5-6} = \frac{\beta_{5-6}^0}{1+\beta_{5-6}^1\sigma^3}, \cdots \tag{29}$$

where the constants β_α^β need to be calibrated. Examples of this kind of model are Shih, Zhu & Lumley[53] and Craft, Launder & Suga[9]. Self-consistent EARSMs naturally fulfill this condition and are, thus, realizable in this respect.

2.4. Scalar flux models

In turbulent flows where transport of some additional scalar $\widetilde{\theta}$ is present a velocity–scalar correlation $\overline{u_i\theta}$ appears in the governing Reynolds averaged equations. The additional scalar may be the temperature in compressible flows, species concentrations in combustion flows or pollutant concentration in atmospheric or ocean flows. The Reynolds decomposition of the scalar $\widetilde{\theta}$ into the average Θ and the turbulent fluctuation θ reads $\widetilde{\theta} = \Theta + \theta$, and the Reynolds averaged equation (in constant density flows) becomes

$$\frac{\partial\Theta}{\partial t} + U_j\frac{\partial\Theta}{\partial x_j} = \frac{\partial}{\partial x_j}\left(\alpha\frac{\partial\Theta}{\partial x_j} - \overline{u_j\theta}\right) \tag{30}$$

where α is the molecular diffusivity.

The modelling of the scalar flux has many similarities with the modelling of the Reynolds stresses. The, by far, most used model is the eddy-diffusivity model or gradient flux model that relates the scalar flux vector to the mean scalar gradient by an eddy diffusivity α_T

$$\overline{u_i\theta} = -\alpha_T\frac{\partial\Theta}{\partial x_i}. \tag{31}$$

The eddy diffusivity is related to the eddy viscosity by $\alpha_T = \nu_T/Sc_T$ where the Schmidt number (or Prandtl number if Θ is the temperature) is a model constant or sometimes a function of the ratio between the scalar (thermal) and dynamic timescales.

In reality the scalar flux vector is not aligned with the mean scalar gradient vector and, thus, the eddy-diffusivity approach fails in predicting the flux components in the other directions. These components are often of the same order as the component in the gradient direction. However, in thin shear layers, such as attached boundary layers, these effects are of minor importance for the mean scalar field and the eddy-diffusivity approach may be used.

In more complicated flow situations higher level modelling is needed. Analogous to Reynolds stress transport modelling, a transport model for the flux

vector may symbolically be written as

$$\frac{\mathrm{D}\,\overline{u_i\theta}}{\mathrm{D}t} - \mathcal{D}_i = \mathcal{P}_{\theta i} + \Pi_{\theta i} - \varepsilon_{\theta i}. \tag{32}$$

The right-hand side may in general be assumed to be a function of the Reynolds stress tensor $\overline{u_iu_j}$, the scalar flux vector $\overline{u_i\theta}$, the gradients of the mean velocity $\partial U_i/\partial x_j$ and scalar $\partial\Theta/\partial x_j$, the turbulent kinetic energy K and its dissipation rate ε, and the scalar flux variance K_θ and its dissipation rate ε_θ. Additional equations for K_θ and ε_θ are thus needed together with transport equations for $\overline{u_iu_j}$ and ε.

The production term $\mathcal{P}_{\theta i}$ is explicit in the primary quantities and needs no further modelling. The pressure-scalar gradient correlation $\Pi_{\theta i}$ and the destruction term $\varepsilon_{\theta i}$ need modelling and are often lumped together[28, 50, 54]. The diffusion term $\mathcal{D}_i$ is usually modelled using the Daly & Harlow[10] gradient-diffusion model.

There is a renewed interest in algebraic models which are obtained from the transport equations using some equilibrium assumption. The most common approach is the weak equilibrium assumption, where the advection and diffusion of the normalized scalar flux $\overline{u_i\theta}/\sqrt{KK_\theta}$ is neglected, rather than the scalar flux itself[1, 2, 16, 45, 52, 54]. A different approach is taken by Shabany & Durbin [50] where the advection and diffusion of the normalized dispersion tensor $\mathcal{D}_{ij}$, defined as $\overline{u_i\theta} = -\mathcal{D}_{ij}(K^2/\varepsilon)\partial\Theta/\partial x_j$, is neglected.

CHAPTER 3

The proposed modelling approach

Engineering problems are typically characterized by complexity in that different physical effects are present simultaneously and are interacting. Generality of the turbulence models used for such problems is thus of major importance.

Two-equation eddy-viscosity turbulence models are today widely used in industrial CFD codes and have been found to be reasonably numerically robust and computationally efficient. The objective with the present study is to extend the generality of two-equation models while retaining the computational efficiency of standard models.

The model, or class of models, derived and evaluated in Paper 1 is the basis of the present study. Models published by others in this field have similarities and also differences compared to the present model. In this chapter motivations of the different choices are given and the different approaches are explained in some detail.

3.1. The weak equilibrium assumption

The classical definition of equilibrium turbulence is the condition when the production rate of turbulent energy at the larger scales is balanced by the dissipation rate at the smallest scales. This means that neither the mean flow scales nor the turbulence scales vary significantly in time or space. This condition can never exactly be fulfilled since the turbulence in a constant mean-flow field is always evolving in time. However, the condition may be satisfied in the sense that the energy produced by the larger scales is approximately balanced by the dissipation rate at the smaller scales. The energy is said to cascade down from the large to the small scales. For sufficiently large Reynolds numbers there is an intermediate range of scales, the inertial subrange for which the net rate of change is negligible. This is the basis for the Kolmogorov's universal equilibrium theory, see ,*e.g.*, Tennekes and Lumley[63]. Let us call this *perfect equilibrium*.

Another definition of equilibrium is that the evolution of the turbulent scales should be similar to that of the mean-flow scales. A measure of the ratio between the mean-flow and turbulence scales is the production to dissipation ratio $\mathcal{P}/\varepsilon$ or the normalized deformation rate $\sigma \equiv SK/\varepsilon$ where S is some measure of the mean flow deformation rate. In such *strong equilibrium* flows $\mathcal{P}/\varepsilon$ or σ is constant in time and space. This is the case in free shear flows after some initial transients

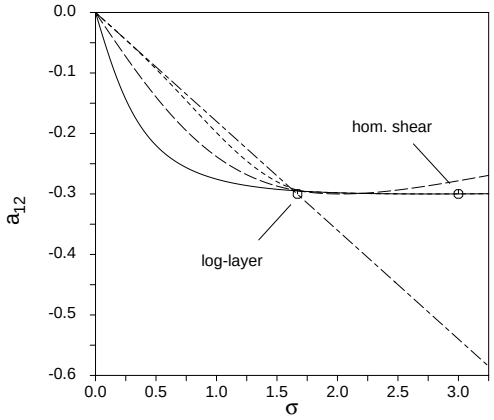

FIGURE 3.1 The a_{12} anisotropy versus strain rate σ for parallel shear flow. The Johansson & Wallin[20] self-consistent model (——) compared with fixed $\mathcal{P}/\varepsilon = 1$ (– – –), with the diffusion model (·····), and with a standard eddy-viscosity model (– · –).

and also in the log-region of wall bounded flows, in the latter only $\mathcal{P}/\varepsilon$, not σ, is constant. In these flows $\mathcal{P}/\varepsilon$ is of the order of unity.

The assumption introduced by Rodi[42, 43] for obtaining an algebraic relation for the Reynolds stresses is referred to as the *weak equilibrium* assumption, characterized by a Reynolds stress anisotropy tensor that is constant in time and space, or

$$\frac{\mathrm{D}\, a_{ij}}{\mathrm{D}t} - \mathcal{D}_{ij}^{(a)} = 0. \tag{33}$$

The relaxation of some nonequilibrium initial state where $\mathcal{P}/\varepsilon > 1$ is characterized by a rapid and slow time scale[15]. The anisotropy relaxes rapidly to some quasi-equilibrium state for prescribed mean flow and turbulence scales. The weak equilibrium assumption (33) could not be expected to capture this initial process. After the initial transient the turbulence scales adjust slowly with the mean flow where the anisotropy is nearly in local equilibrium. This slow process could be reasonably well captured using the algebraic Reynolds stress approach since the transport effects on the turbulence scales are captured through the transport equations for, *e.g.*, K and ε.

3.1.1. The consistency condition. Since the weak equilibrium assumption (33) may be valid also in flows that depart from the strong equilibrium condition (for $\mathcal{P}/\varepsilon \gg 1$), it is natural to invoke the consistency condition (28). The effect of the consistency condition is illustrated in Figure 3.1 where the shear component a_{12} of the Reynolds stress anisotropy tensor is plotted versus the normalized strain rate $\sigma \equiv \sqrt{II_S/2}$ in parallel flow ($II_S = -II_\Omega$). It is

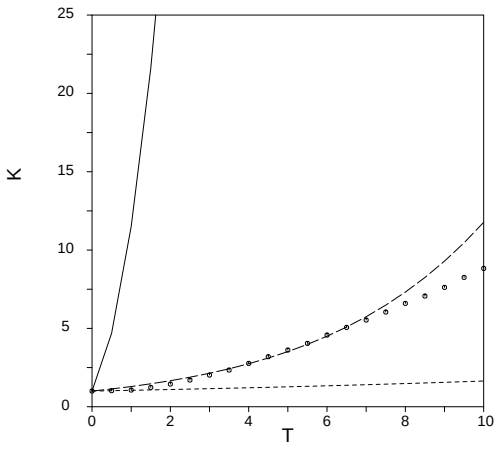

FIGURE 3.2 Time evolution of the turbulent kinetic energy in rapidly sheared homogeneous flow, $SK/\varepsilon = 50$. Eddy-viscosity model (——), the Johansson & Wallin[20] self-consistent EARSM (– – –) and the Gatski & Speziale[12] EARSM (------) compared with RDT (◦).

clearly seen that the consistency condition makes a significant difference away from the equilibrium choice for $\mathcal{P}/\varepsilon$. The differences in this σ-range between the two EARSM approaches are, however, small compared to the difference between EARSM and the eddy-viscosity model that gives unrealizable anisotropies for large strain rates.

The asymptotic behaviour for large strain rates in parallel flow can be investigated by letting $\sigma \to \infty$. The production to dissipation ratio then becomes $\mathcal{P}/\varepsilon \sim \sigma$ and $\beta_1 \sim C_\mu^{\text{eff}} \sim 1/\sigma$. The asymptotic behaviour is consistent with the asymptotic characteristics of homogeneous shear flow. With a model assumption of a constant production to dissipation ratio the wrong asymptote, $\beta_1 \sim 1/\sigma^2$, is obtained, as also noticed by Speziale & Xu[61].

To illustrate the behaviour for large shear rates the model is tested in homogeneous shear flow at high initial shear rate ($SK/\varepsilon = 50$), see figure 3.2. As expected, the eddy-viscosity model fails, giving a far too high growth rate. Interesting to note is that also the Gatski & Speziale[12] model with fixed $\mathcal{P}/\varepsilon$ fails because of the wrong asymptotic behaviour. This flow is a case where one should expect differences between the algebraic approach and the full differential model due to the fact that the anisotropies undergo a temporal evolution ($\partial a_{ij}/\partial t \neq 0$) in the development towards an asymptotic state. Moreover, the LRR model gives quite poor predictions of this case when used in a differential form. The very good predictions of the present EARSM can thus be regarded as a bit fortuitous. Nevertheless, the self-consistent approach gives a model with the correct asymptotic behaviour, which is a prerequisite for reasonable predictions in the limit of high shear. It is important to make clear that the proposed model is not

intended for these extreme high shear rates and the normal stress components are not as well predicted as the turbulent kinetic energy. It is, however, an important step towards a more general engineering model that the model is able to give reasonable results also in extreme flow cases.

3.1.2. Slowly distorted turbulence. In slowly distorted turbulence where $\mathcal{P}/\varepsilon \ll 1$, such as in the outer parts of boundary layers and free shears or at the centre of channel, wake, or jet flows, the source terms are weak compared to the advection or diffusion terms. In such cases the weak equilibrium assumption does not hold and (E)ARSMs that do not consider this behave worse than eddy-viscosity models with constant C_μ. In many flows, such as wall bounded flows, this deficit does not influence the mean flow much, whereas it is more important in some other flows like free shear flows, jets, and wakes.

The slow distortion problem was noticed by Taulbee[62], who suggested an alternative method of obtaining the algebraic relation based on an approximation of the usually neglected advection. Improvements were reported in cases where the advection was important. Another alternative is proposed in Paper 1 where an approximation of the turbulent diffusion was included, which improved the behaviour in cases with nonnegligible diffusion. These approaches are somewhat unsatisfying because they do both give effects in both advection dominated and diffusion dominated flows although they both are motivated from only one of these effects. These *ad hoc* corrections do, however, give some of the wanted effects, but more work is needed on this specific topic. The effect of the diffusion approximation in Paper 1 is shown in Figure 3.1 where we can see that the corrected model behaves much like the eddy-viscosity model for small strain rates.

3.1.3. Streamline curvature effects. Turbulent flows over curved surfaces, near stagnation and separation points, in vortices and in rotating frames of reference are all affected by streamline curvature effects. Strong curvature effects form a major cornerstone problem also at the Reynolds stress transport modelling level, and pressure-strain rate models that are able to accurately capture strongly rotating turbulence are rare. In more moderate situations the SSG[60] model, and derivations thereof, show rather good behaviour in rotating flows such as rotating homogeneous shear flows, see Gatski & Speziale[12]. Standard eddy-viscosity models fail in describing effects of local as well as global rotation and thus completely fail.

In Paper 3, a schematic wingtip vortex was studied where the SSG model behaves qualitatively correct while the standard eddy-viscosity K–ε model highly overestimates the turbulence diffusion. More surprisingly, it was found that also the EARSM based on the SSG model completely failed. The reason for this is that the advection term in the anisotropy transport equation (17) is significant

and cannot be neglected in strongly curved flows, also noticed by Rumsey, Gatski & Morrison[47].

A schematic vortex, where the axial $\hat{\mathbf{z}}$ and azimuthal $\hat{\boldsymbol{\theta}}$ directions are homogeneous, may be used for illustrating this mechanism. In the homogeneous directions all scalar quantities are constant and from continuity the mean velocity has no radial $\hat{\mathbf{r}}$ component and thus the advection $\mathrm{D}/\mathrm{D}t$ is zero for any scalar (neglecting the small $\partial/\partial t$ term). This means that the advection of the anisotropy invariants, $II_a \equiv a_{ij}a_{ji}$ and $III_a \equiv a_{ij}a_{jk}a_{ki}$, are zero. However, the principal axes of the anisotropy tensor varies in the azimuthal direction and thus also the individual components a_{ij} varies and $\mathrm{D}a_{ij}/\mathrm{D}t \neq 0$.

Advection of the anisotropy tensor (or any symmetric tensor) may be written in the following form

$$\frac{\mathrm{D}\, a_{ij}}{\mathrm{D}t} = \frac{\partial a_{ij}}{\partial t} + \mathrm{G}\left(a_{ij}\right) - \frac{\varepsilon}{K}\left(a_{ik}\Omega^{(r)}_{kj} - \Omega^{(r)}_{ik}a_{kj}\right) \tag{34}$$

where G contains spatial derivatives evaluated in a curvilinear coordinate system, see Sjögren[55]. $\Omega^{(r)}_{ij}$ is an antisymmetric tensor that represents the rotation rate of the coordinate system metrics following the mean flow. In a Cartesian coordinate system $\Omega^{(r)}_{ij} = 0$ and $\mathrm{G} = U_k\partial/\partial x_k$. If the generic vortex is expressed in a streamline based coordinate system (cylindrical) the rotation tensor reads

$$\boldsymbol{\Omega}^{(r)} = \frac{V(r)}{r}\left(\hat{\boldsymbol{\theta}}\hat{\mathbf{r}} - \hat{\mathbf{r}}\hat{\boldsymbol{\theta}}\right) \tag{35}$$

and the spatial derivative of the anisotropy components becomes zero $G = 0$. The advection term may thus be exactly included in the EARSM formulation for this case. Here it becomes clear that $\Omega^{(r)}_{ij}$ represents the local rotation rate of the anisotropy tensor following the streamline.

The last term in (34) may be fully accounted for and included into the EARSM solution without increasing the complexity of the solution. This was done in Paper 3 for the generic vortex and it was found that the predictions using the extended EARSM were much improved. The results were in line with the corresponding full RST models. In general three-dimensional mean flows the problem is to determine a streamline-based coordinate system for obtaining $\Omega^{(r)}_{ij}$. Girimaji[14] proposed to use the local acceleration vector, $\mathbf{a}$, and the rate of change of that, $\dot{\mathbf{a}}$, following the mean flow in obtaining the base of the curvilinear coordinate system. The algebra becomes very tedious in general three-dimensional mean flows involving also gradients of the coordinate system metrics (*i.e.* gradients of $\mathbf{a}$ and $\dot{\mathbf{a}}$) and such a method is thus of limited practical use.

A more simple and straightforward alternative could be to directly formulate the $\Omega^{(r)}_{ij}$ tensor in terms of the $\mathbf{a}$ and $\dot{\mathbf{a}}$ vectors by recalling that $\Omega^{(r)}_{ij}$ represents the rotation rate of the coordinate system metrics following the mean flow. The

local rotation vector may be obtained as

$$\boldsymbol{\omega} = \frac{\mathbf{a} \times \dot{\mathbf{a}}}{\mathbf{a}^2} \tag{36}$$

and the rotation tensor reads

$$\Omega_{ij}^{(r)} = -e_{ijk}\omega_k = \frac{\dot{a}_i a_j - a_i \dot{a}_j}{a_k a_k}. \tag{37}$$

This new approach is identical to the more complete relation above in circular flows, such as the generic vortex. It also behaves well in linearly accelerated or decelerated flows, such as on the symmetry line of a stagnation flow since $\mathbf{a}$ and $\dot{\mathbf{a}}$ have the same direction and thus $\mathbf{a} \times \dot{\mathbf{a}} = 0$. This approach has not yet been tested in general three-dimensional mean flows.

The acceleration vector and its rate of change fulfill Galilean invariance, that is independency of solid-body motion of the frame of reference. However, any incompressible flow field should also be independent of a superimposed solid-body constant acceleration, according to Spalart & Speziale[57], except for a modified pressure field. The proposed modification must thus be used with caution in accelerated frames of reference. Extensions of EARSMs for including approximations of the usually neglected transport terms could never be expected to be completely general, but could anyway be motivated by improved model performance in a reasonably wide class of flows.

If the curvature effects are smaller the advection term is of lesser importance and the standard EARSM approach may be used successfully. The stabilizing and destabilizing effects in curved wall bounded flows or in a rotating channel are naturally incorporated in also the standard EARSM. Launder[31] stated that cubic terms are needed in nonlinear eddy-viscosity models for capturing these effects, but, in the proposed EARSM these effects are actually captured already with the linear term because of the rotation rate dependency in the β_1 (or C_μ^{eff}) coefficient.

3.1.4. Pressure-strain rate model. The method to derive an EARSM described in Paper 1 requires that the pressure-strain rate model is quasi-linear, which means that it can be written on the form given in (16). The linearized SSG and the LRR models may be written on this form and are thus basically very similar. However, the two models behave rather differently when used in a full RST model and the SSG model has been found to perform better than the LRR in a number of situations.

The EARSM proposed in Paper 1 was based on a somewhat recalibrated LRR model for the pressure-strain rate which was motivated by the simplification in three-dimensional mean flows, as compared to the general expression. With this recalibrated LRR model five of the ten tensor groups in (25) vanish. Moreover, the resulting EARSM is guaranteed not to become singular for any parameter choice which cannot be proven for the general case. The proposed EARSM in Paper 1 was demonstrated to give reasonable predictions in different

TABLE 3.1 The values of the A-coefficients for different quasi-linear pressure-strain models

	A_0	A_1	A_2	A_3	A_4
Original LRR	-0.34	1.54	0.37	1.45	2.89
Recalibrated LRR (W&J)	-0.44	1.20	0	1.80	2.25
Linearized SSG	-0.80	1.22	0.47	0.88	2.37

flows and the choice of the recalibrated LRR model does not significally degenerates the results. However, in Paper 3 the wing tip vortex was significally better predicted using the SSG based EARSM rather than the LRR based EARSM.

The reason for the LRR based EARSM to behave similarly to SSG in many cases is mainly because of the recalibration of the original LRR model. The value of c_2 in the rapid pressure–strain model was originally suggested to be 0.4 by Launder *et al.*[29], but more recent studies have suggested a higher value close to 5/9[30, 51]. By setting $c_2 = 5/9$ one obtains the simplification in three-dimensional mean flows. The Rotta coefficient, c_1, was originally set to 1.5, but also that has more recently been recalibrated and is here set to 1.8. This recalibration gives a model that behaves well in the log-layer in wall bounded flows as well as in homogeneous shear flows. The normal components in the streamwise and spanwise directions, a_{11} and a_{33}, are, however, predicted better using the SSG model. That has been found to be of minor importance since these components, in contrast to a_{12} and a_{22}, do not influence the mean flow or the turbulent scale equations in parallel flows.

The full quasi-linear RST model may be written in terms of five model coefficients, A_{0-4} in (19). In the corresponding ARSM (22) one of these coefficients, A_0, may be eliminated which means that the ARSM approximations of different RST models may be identical. The A-coefficients are listed in Table 3.1. Comparing the A_{1-4}-coefficients that defines the EARSM, one can see that the A_1 and A_4 coefficients are very similar between the recalibrated LRR and the linearized SSG. These coefficients have the strongest impact on the a_{12} component in parallel flows and thus the two models behave similarly. More important is that the A_0-coefficient differs by almost a factor of two and since that factor multiplies the complete right-hand side in the transport equation (19) the RST models behave very differently in nonequilibrium flows. This is also the case when some part of the advection or diffusion terms in (19) is included into the EARSM, which is the case in the vortex computations in Paper 3. The A_0-coefficient then enters into the EARSM and may cause important differences that explain the differences between the EARSM results based on LRR and SSG. Actually, in Paper 3, the vortex was recomputed using the LRR-based EARSM but with the A_0-coefficient changed to that of the SSG model resulting in much closer agreement with the SSG based EARSM.

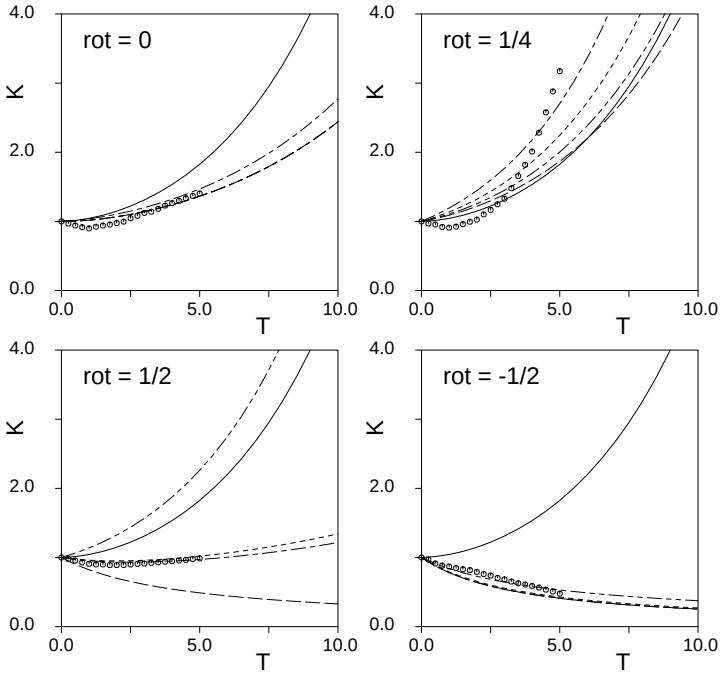

FIGURE 3.3 Computed evolution of the turbulent kinetic energy K in rotating homogeneous shear flow compared to large eddy simulation (◦), Bardina *et al.*[4]. Eddy-viscosity model (——), Wallin & Johansson basic EARSM (– – –), modified EARSM with $A_0 = -0.8$, (------) and $A_0 \to \infty$ (– – –), and EARSM based on SSG (– · –). $SK/\varepsilon = 3.4$ initially.

Rotating homogeneous shear flow is another example in which the A_0-coefficient may cause differences, see Figure 3.3. The proposed EARSM was computed using different values for the A_0-coefficient, the basic model with $A_0 = -0.44$, the modified model with $A_0 = -0.8$ (same as for SSG) and the model without advection correction ($A_0 \to \infty$). If was only the modified EARSM with $A_0 = -0.8$ that gives reasonable predictions comparable to EARSM based on SSG.

To conclude, if it is based on the recalibrated LRR the EARSM is simplified in three-dimensional mean flows without major deficits in model predictions compared to EARSM based on SSG. However, the A_0-coefficient needs to be recalibrated if some part of the advection or diffusion terms is included into the EARSM. The full three-dimensional form of the EARSM has been found to be important in fully developed pipe flow rotating around the symmetry axis in order to capture the secondary swirl flow, see Paper 1.

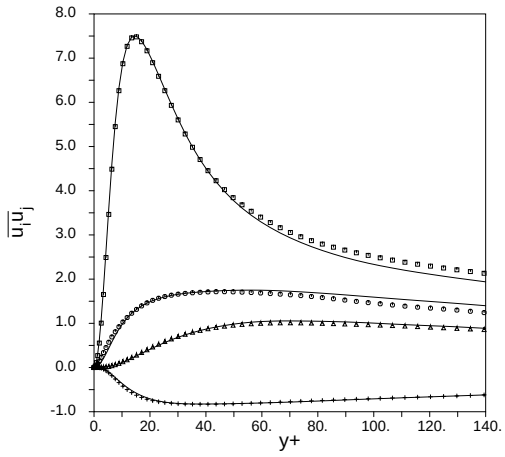

FIGURE 3.4 The Reynolds stresses in channel flow. Comparison of the Wallin & Johansson near-wall correct EARSM (——) with DNS data (symbols) of Moser *et al.*[33]. From top to bottom: $\overline{uu}$, $\overline{ww}$, $\overline{vv}$ and $\overline{uv}$ components. The predicted Reynolds stresses were evaluated by use of the DNS data for the mean flow, K and ε fields.

3.2. Near-wall treatment

The near-wall region usually needs special treatment in turbulence models through the use of wall-damping functions. This is the case also for EARSMs, but the situation is somewhat better compared to standard eddy-viscosity models.

The very near-wall behaviour is studied by using channel DNS data of Moser, Kim & Mansour[33] at $Re_\delta \approx 7800$. The mean velocity, K and ε profiles obtained from the DNS data have been used to compute the modelled anisotropy, which is compared to the anisotropy determined directly from the DNS data.

The modelled a_{12} anisotropy without any near-wall corrections has been computed from the channel DNS data. It was found in Paper 1 that a_{12} is nearly constant as the wall is approached while DNS data exhibit a behaviour similar to an exponential decay. The obvious choice of 'wall damping function' is of van Driest type $f_1 = 1 - \exp(-y^*/A^+)$, which gives almost perfect agreement with the DNS data. A standard eddy-viscosity K–ε model, without any near-wall damping function, gives strongly negative values for a_{12} in the buffer layer, almost down to -2. Note that this is well outside the range of physically realizable values, that are limited to be between ± 1. The K–ε model cannot be correctly damped towards the wall as easily as the EARSM, which is much better suited to be integrated down to the wall. This is due to the correct asymptotic model behaviour for large strain rates, giving a balanced a_{12} anisotropy (cf. figure 3.1).

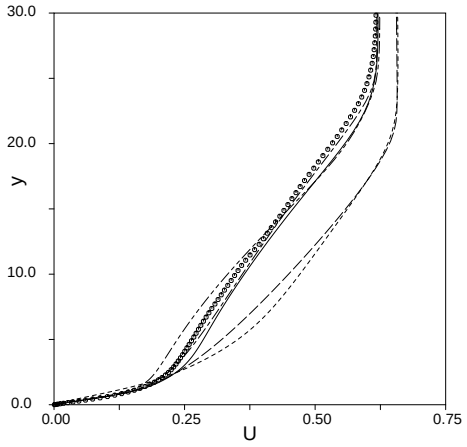

FIGURE 3.5 The velocity profile for an adverse pressure gradient boundary layer ($U_\infty \sim x^{-0.25}$). Computations with standard Wilcox[66] K–ω (– – –), Chien[7] K–ε (– – –), EARSM based on K–ω and y^+ (------) or y^* (——) and the Hanjalić[17] RST model (– · –). Comparisons with DNS data (∘), (M. Skote, personal communication)

Also the normal components of the Reynolds stress tensor are fitted to the DNS data by applying the same damping function f_1 to the β_2 and β_4 coefficients and also considering the correct anisotropies at the wall, for example $a_{22} = -2/3$ at the wall. All Reynolds stress components are, thus, well fitted to the DNS data, see Figure 3.4.

The damping function, f_1, is formulated in terms of y^* defined as $y^+ \equiv yu_\tau/\nu$ in the original van Driest function. The scaling with the local wall skin friction is, however, not valid in flows near separation and reattachment and the y^* is defined in terms of the Reynolds number $Re_y \equiv \sqrt{K}y/\nu$ so that $y^* \approx y^+$ for $y^+ \lesssim 100$ in zero-pressure gradient boundary layers. The importance of the y^* choice is illustrated in Figure 3.5 where the models based on y^+ fail (the Chien K–ε model uses damping functions based on y^+). For this case it is obvious that the y^+ scaling degenerates the model performance and should be avoided.

An alternative to the asymptotically correct near-wall treatment is presented in Paper 6 in an approach without any damping functions or wall distance dependence. That is possible if the EARSM is based on the Wilcox[66] K–ω model or derivates of that, such as the Menter BSL model[32]. These models reproduce the log-layer without near-wall corrections and, thus, the EARSM approach may be invoked without the wall damping function f_1. Obviously this model does not reproduce the correct near-wall behaviour for the Reynolds stresses, but that may be of lesser importance in high Reynolds number flows and this approach is an alternative that somewhat simplifies the formulation.

3.3. Numerical behaviour and some applications

The major argument for EARSMs is to increase the validity and generality of two-equation models without significantly increased computational cost, so the numerical treatment is one of the cornerstones in this study in spite of the relative small attention to this in the attached papers.

3.3.1. Effective eddy viscosity. The Reynolds stresses expressed by the EARSM may be written in terms of an effective eddy viscosity ν_T and an extra anisotropy $a_{ij}^{(\mathrm{ex})}$

$$\overline{u_i u_j} = \frac{2}{3} K \delta_{ij} - 2\nu_T S_{ij}^* + K a_{ij}^{(\mathrm{ex})} \tag{38}$$

where the effective turbulent viscosity reads

$$\nu_T = -\frac{1}{2} \left(\beta_1 + I\!I_\Omega \beta_6\right) K\tau \tag{39}$$

and the extra anisotropy

$$\begin{aligned} \mathbf{a}^{(\mathrm{ex})} \;=\; & \beta_3 \left(\mathbf{\Omega}^2 - \frac{1}{3} I\!I_\Omega \, \mathbf{I} \right) + \beta_4 \left(\mathbf{S\Omega} - \mathbf{\Omega S} \right) \\ & + \beta_6 \left(\mathbf{S\Omega}^2 + \mathbf{\Omega}^2 \mathbf{S} - I\!I_\Omega \mathbf{S} - \frac{2}{3} I\!V \, \mathbf{I} \right) + \beta_9 \left(\mathbf{\Omega S \Omega}^2 - \mathbf{\Omega}^2 \mathbf{S \Omega} \right). \end{aligned} \tag{40}$$

The β-coefficients are given in Paper 1.

This formulation is identical to that in (25) and the reason for invoking the eddy viscosity is that many CFD solvers already have different eddy-viscosity two-equation models implemented so the model implementation becomes easier with a formulation in terms of an eddy viscosity. It has also been found that the extra anisotropy may be treated in a fully explicit way without degenerating the overall performance of the solution process.

3.3.2. Positivity. It is well known that positivity of the turbulence variables (K, ε) at any time during iteration to a steady-state solution is crucial. Ad hoc methods, like a lower limit of the turbulent variables, often prevent the convergence or cause divergence of the iterative process which means that positivity must be maintained by the numerical scheme. First, the spatial scheme must suppress spurious oscillations that may give negative values, which is obtained by imposing TVD-like conditions[23]. Then the time integration method, or iterative process, must guarantee positivity. The CFD solver EURANUS[41] used in this study uses explicit pseudotime marching to steady state, so the positive time integration described here will be focused on explicit methods.

In Paper 7 a novel approach is suggested for updating the turbulence variables guaranteeing positivity. The approach is based on an estimate of the spectral radius of the complete turbulent equations and produces an underrelaxed

update of the turbulence variables q. This may be written in the following form

$$q^{n+1} = q^n + \frac{\Delta t R^{(q)}}{1 - \min\left(\Delta t R^{(q)}/q^n, 0\right)}. \tag{41}$$

The underrelaxation depends on the local residual $R^{(q)} = \partial q/\partial t$ and is significant only in those regions where the residual is large compared to the variable itself and is only active if the variable is decreasing. The method does not affect the asymptotic convergence rate and is most important initially.

Multigrid methods are important for convergence acceleration, especially for explicit methods, and are considered in Paper 7. The update of the turbulence variables from the prolongated correction may result in spurious oscillations that may cause negative values locally. Also here the method for positive updating (41) is used.

3.3.3. Compressible flow applications. A straightforward extension of the proposed EARSM for compressible mean flow effects is described in Paper 1. Compressible effects due to turbulent fluctuations have not been considered. The extended EARSM was tested on a supersonic boundary layer at Mach 5 interacting with an impinging shock of different strengths (Schülein, Krogmann, & Stanewsky[49]). The proposed EARSM was used with both the Chien[7] K–ε and the Wilcox[66] K–ω models as platforms and substantial differences between the baseline two-equation models were found. The EARSM approach significantly improved the prediction of the size of the separation zone over the corresponding eddy-viscosity models, which severely underpredicted the separation length. Also the influence of different shock strengths was accurately captured, ranging from almost separated for the weakest shock to a large separation region for the strongest shock. The Chien K–ε models, both the eddy-viscosity and the EARSM version, severely overpredicted the skin friction coefficient in the reattachment region. The K–ω models behaved much better in that respect. Detailed results are reported in Paper 2.

Figure 3.6 shows the computational results for the two-dimensional RAE2822 aerofoil profile using the Wallin & Johansson EARSM compared to the Wilcox[67] K–ω model. The EARSM approach clearly improves the prediction of the position of the shock and the results are very much in line with differential Reynolds stress computations by Hellström, Davidsson & Rizzi[18] for the same conditions and geometry.

Computations are made where the damping function f_1 in the EARSM is formulated in terms of y^+ as well as y^* and the figure shows no major differences between these approaches except in the separated region where the y^+ formulation gives a somewhat larger negative skin friction. The figure also shows a computation using the proposed EARSM, together with the Wilcox[66] K–ω model, without any damping functions whatsoever. Even if this model is unable to reproduce the correct near-wall behaviour for the turbulence quantities, the

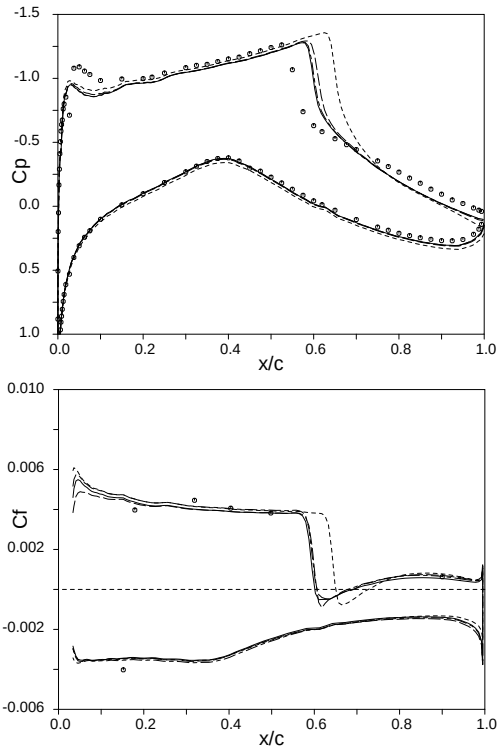

FIGURE 3.6 Wall pressure and skin friction coefficients for the RAE2822 wing profile ($M = 0.754$, $\alpha = 2.57^\circ$ and $Re = 6.2 \times 10^6$). Predictions using Wilcox[67] K–ω (------) and the Wallin & Johansson EARSM based on K–ω with damping function based on y^+ (– – –), y^* (——) or without any damping functions (–·–·–), compared to experimental data (∘) by Cook *et al.*[8]. The geometry is the measured one including a camber correction.

mean velocity profiles are well reproduced and there are no major differences between the EARSM with or without damping functions.

The convergence history is shown in figure 3.7 where we can see that there are no major differences in convergence rate between the different approaches. Actually, the proposed EARSM converges to a somewhat lower residual than the corresponding eddy-viscosity model for this case. The numerical parameters are the same for these two cases and the computational time for the 5000 iteration steps is 6% higher for the EARSM computation. This case was found not to be completely numerically stationary which results in the residual 'hanging' as for the K–ω model. The fluctuations are, however, very small and could not be seen in the solution. In other cases without separation the convergence curves are even closer to each other, and the convergence rates are in general faster than for the case shown in figure 3.7.

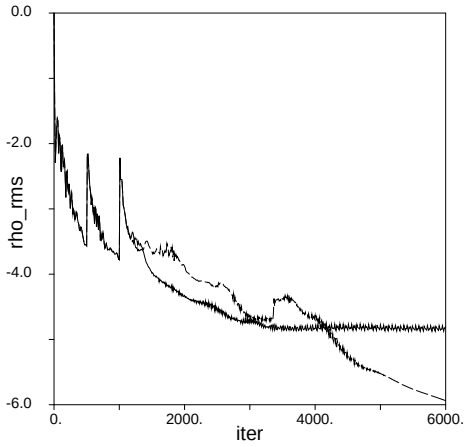

FIGURE 3.7 Convergence history for the RAE2822 wing profile. Wilcox[67] K–ω (——) compared with the Wallin & Johansson EARSM based on K–ω (– – –). The computational time is increased by 6% by using EARSM. Three levels of full multigrid is used.

A further example with a three-dimensional transonic supercritical wing was computed using the standard Wilcox[66] K–ω model and the EARSM based on that, see Paper 6. Again, the predicted shock position was found to be improved compared to the eddy-viscosity model. This case illustrates the benefit of the proposed model which is also viable in expensive three-dimensional cases, here with almost one million grid points. Most importantly, there is no substantial increase in the computational cost compared to the, in many cases, robust standard K–ω model.

3.4. Time-dependent turbulence

The mean flow is considered as unsteady when the time scale of the unsteadiness is much larger than the characteristic integral time scale of the turbulence. In that case the turbulence energy spectrum is well separated from the unsteadiness. Thus, the turbulence may be modelled while the mean flow unsteadiness is left to be resolved in the unsteady RANS solution. This is known as the quasi-steady approach where a standard RANS turbulence model, with the time derivatives included, may be used. No additional modification of the turbulence model is in principal needed due to the unsteadiness.

If there is no clear separation between the turbulence scales and the unsteadiness, then standard RANS turbulence models should not be used. Therefore this class of problems needs to be tackled using large eddy simulations (LES) where subgrid-scale models are used to represent the unresolved stresses. The Reynolds averaged and the filtered Navier-Stokes equations are in principal similar, but the unknown correlation $\overline{u_i u_j}$ is modelled in completely different ways in RANS

TABLE 3.2 Computed reduced frequency for unsteady transonic airfoil flow compared to experiment by McDevitt[34].

model	EARSM	K–ω	B–L	Exp.
reduced frequency	0.493	0.441	0.461	~ 0.49

and LES. A RANS model could not be used as a subgrid-scale model, mainly because a RANS model is unable to capture the decreased subgrid-scale energy with decreased filter width. Actually, it gives the opposite trend of increased eddy viscosity.

Unsteady turbulent flows are often by nature, or forced to be, periodic and the mean is thus conveniently defined as a phase average. The flow variables are decomposed into three parts, $\widetilde{\phi} = \overline{\phi} + \phi" + \phi$, where $\overline{\phi}$ is the time-averaged value, $\phi"$ is the periodic component and ϕ the turbulent fluctuations. The phase-averaged variable is then defined as $\langle\phi\rangle \equiv \overline{\phi} + \phi"$.

In the quasi-steady approach, RANS turbulence models will be used without any explicit modifications due to the unsteadiness. However, the unsteadiness of the mean flow poses some additional requirements on the turbulence model, or will emphasize existing requirements on models for steady flows even more. The following general requirements can thus be identified: (i) No y^+ or log-law dependency, (ii) correct near-wall asymptotic behavior, (iii) good prediction of nonequilibrium turbulence and (iv) good prediction of boundary layer separation. The Wallin & Johansson EARSM is thus a good candidate also for modelling unsteady turbulent flows.

The periodic self-excited turbulent flow around an 18-percent thick circular-arc airfoil at transonic speeds has been computed in Paper 4 using three different turbulence models: the Baldwin & Lomax (B–L) algebraic model[3], the Wilcox $K-\omega$ model[67], and the Wallin & Johansson EARSM. The EARSM predicts the unsteadiness due to shock and boundary layer separation better than the eddy-viscosity models. The EARSM predicts the frequency of self-exited unsteady transonic flow to high accuracy, see Table 3.2, and the motion of the shock agrees well with the experimental data.

3.5. Passive scalar modelling

In Paper 5 an explicit algebraic relation for the scalar flux is proposed. This is intended to be used in an explicit algebraic approximation approach for the transport equations for the Reynolds stress tensor and scalar flux vector. The relation for the scalar flux vector is derived by neglecting the advection and diffusion of the normalized scalar flux $\overline{u_i\theta}/\sqrt{KK_\theta}$. This gives in general an implicit, nonlinear set of algebraic equations. The nonlinearity in the algebraic equations for the normalized scalar fluxes may be eliminated directly by using a nonlinear term in the model of the pressure scalar-gradient correlation and the

TABLE 3.3 Predicted scalar fluxes in homogeneous shear flow using the WWJ model proposed in Paper 5 compared to the DNS data of Rogers *et al.*[44]. Case 1, 2 and 3 corresponds to a scalar gradient in the streamwise, cross-stream and spanwise directions respectively.

	Case 1		Case 2		Case 3
	$\overline{u\theta}$	$\overline{v\theta}$	$\overline{u\theta}$	$\overline{v\theta}$	$\overline{w\theta}$
DNS data	-2.41	0.45	0.94	-0.36	-0.67
WWJ model	-2.05	0.42	1.13	-0.46	-0.70

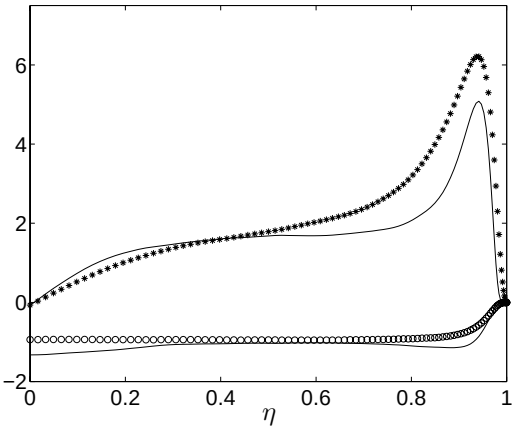

FIGURE 3.8 Predicted scalar fluxes in the channel flow using the WWJ model (——) compared to DNS data for $-\overline{u\theta}$ ($*$) and $\overline{v\theta}$ ($\circ$) of Wikström *et al.*[64]. The predicted fluxes were evaluated from (42) by use of the DNS data.

destruction and thus results in an algebraically simple model for both two- and three-dimensional mean flows. The resulting model may be written as

$$\overline{u_i\theta} = -A_{ij}^{-1}\overline{u_j u_k}\frac{K}{\varepsilon}\frac{\partial\Theta}{\partial x_k} \tag{42}$$

where the tensor A_{ij}^{-1} is an explicit function of the normalized mean velocity gradients $\tau\partial U_i/\partial x_j$, the production to dissipation ratio $\mathcal{P}/\varepsilon$ and the ratio of the scalar to dynamical timescales r.

The proposed model is, however, not complete since transport equations for the scalar variance $\overline{\theta^2} \equiv 2K_\theta$ and its dissipation rate ε_θ are needed for obtaining the timescale ratio r. The modelling of these equations is not considered in Paper 5. These issues are investigated to some extent in Johansson & Wikström [21].

The performance of the present model is investigated in three different flow situations in Paper 5. These are homogeneous shear flow with an imposed mean

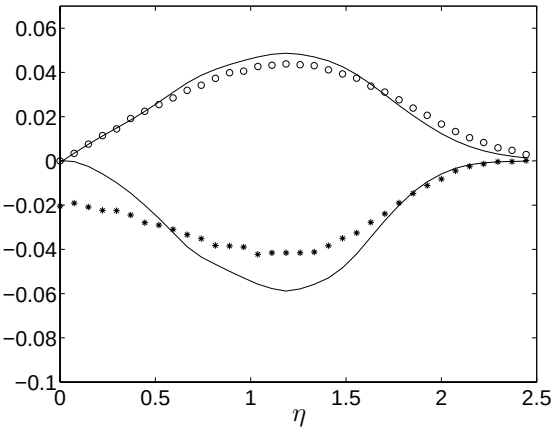

FIGURE 3.9 Predicted scalar fluxes in the cylinder wake using the WWJ model (——) compared to experimental data for $-\overline{u\theta}$ ($*$) and $\overline{v\theta}$ ($\circ$) of Wikström *et al.*[65]. The predicted fluxes were evaluated from (42) by use of the experimental data.

scalar gradient (Table 3.3), turbulent channel flow (Figure 3.8), and the flow field downstream a heated cylinder (Figure 3.9). DNS data are used to analyse the passive scalar flux in the homogeneous shear and channel flow cases, and experimental data are used in the case of the heated cylinder wake. Good predictions in all three cases are demonstrated. It is interesting to note that, both for the channel flow and the heated cylinder wake, $\overline{u\theta}$ and $\overline{v\theta}$ are of the same order of magnitude. This is well captured by the EASFM, whereas eddy-diffusivity models would predict a zero $\overline{u\theta}$.

CHAPTER 4

Conclusions and outlook

The ultimate goal in turbulence modelling is to obtain a universally valid model. Since that is, by far, out of reach, a more realistic goal must be set and could be what Pope[37] referes to as an *optimal* turbulence model. This he defines as the best particular model within each class of models. For a given such class of models, the validity and generality should be increased to the limit of the applicability of that class. In this effort one really needs to be aware of the physical limitations for different types of models.

This work fits into the efforts to increase the validity and generality of two-equation models during the last decade by abandoning the eddy-viscosity hypothesis. Bradshaw[6] writes "Using eddy viscosity is like keeping one foot on the bottom when learning to swim – a restriction, but helpful if one does not venture into deep water", an argument that can be used both for keeping and leaving the eddy-viscosity hypothesis. The improvements result in more general constitutive relations between the second moments ($\overline{u_i u_j}$ and $\overline{u_i \theta}$) and the mean flow.

The proposed models are the results of careful and well-motivated approximations of the corresponding second-order transport model equations. The major advantage of this approach compared to more empirical nonlinear extensions to eddy-viscosity models is that the model coefficients and behaviour of the full second-order model is inherited in the algebraic form. This means that it is possible to estimate the validity of the model prediction based on the expected behaviour of the full second-order model and the validity of the approximations. Empirical extensions of eddy-viscosity models have many degrees of freedom and may be adjusted to a large number of different test cases. These kind of models could, however, not with confidence be extended outside of the range of the set of validation and calibration cases used for finding appropriate functional forms and calibration of the different terms.

The EARSM proposed in Paper 1 is derived from the recalibrated LRR model. The method, at least for two-dimensional mean flows, are general and the EARSM could in principal be derived also from the linearized SSG model. There is actually a strong argument for deriving the EARSM from the SSG model and that is that the SSG model has previously been found to perform better than LRR in a number of cases, especially in nonequilibrium and rotating flows. The LRR used in this study was, however, found to give results comparable

to the SSG when used in the algebraic forms and after recalibration of the LRR model coefficients. An explanation of why the algebraic forms perform more similarly than the corresponding full differential forms has been proposed. The slight degeneration in model performance using EARSM derived from LRR is well balanced by the fact that the full three-dimensional form of the proposed EARSM is simple enough to be useful only for the EARSM derived from LRR. The full three-dimensional form is necessary for capturing, for instance, the secondary swirl in axially rotating pipes.

In the case of strong streamline curvature, the weak-equilibrium assumption must be derived in a streamline based coordinate system. In some specific cases, such as symmetric vortices and rotating homogeneous shear flows, the streamline based coordinate system may explicitly be defined and the advection term may be exactly included into the EARSM form. For these specific cases the proper treatment of the advection term has been found to be of crucial importance. When approximations of the advection term is included into the EARSM formulation, the proposed EARSM fails because of the basic LRR model. However, by an ad hoc modification of the coefficient preceding the complete right-hand side of the anisotropy transport equation (19), it is possible to get a model behaviour similar to EARSM derived from SSG in these kind of flows and also keeping the simplified three-dimensional form.

One should here start to consider if it is worth the effort to include approximations of the transport terms from the full RST model within the EARSM form instead of leaving this class of models for full RST models where such effects enters naturally. The only, and so far completely relevant, argument for EARSM is the troublesome numerical treatment and computational cost of full RST models. One should, thus, put more efforts on improvements of the numerical methods for full RST models and entice specialists in numerical methods to leave the island of constant coefficients for the world of these strongly nonlinear problems. Hopefully, one would expect that improvements in numerical methods and computer performance would decrease the importance of the argument for EARSM in the near future and, thus, the importance of RST models in engineering CFD methods could be expected to increase. Also in such a situation it is worthwhile to continue the struggle for the search of the ‘optimal’ model within both the class of two-equation models and that of full differential Reynolds stress models.

Acknowledgments

I wish to thank my supervisor Professor Arne Johansson for introducing me into the field of turbulence modelling. During our numerous discussions, which he always had time for, Arne guided me with his great knowledge in this field. The atmosphere at the department has been inspiring and friendly. I would especially like to thank Doctor Petra Wikström for a fruiful collaboration on passive scalars and Martin Skote for providing me with DNS data.

I also wish to thank Doctor Ingemar Lindblad, head of my department at FFA, for believing in my ideas and supporting me even when I seemed to have disappeared into the boundary layer. The professionalism and wide range of experience of my colleagues at FFA were the prerequisite and basis of my work. I particularly want to thank Doctor Peter Eliasson for helping me with numerical treatment and implementation issues.

I would like to thank Doctor Torbjörn Sjögren for our discussions concerning representation theory and automatic code generation. Professor Sharath Girimaji is kindly acknowledged for fruitful discussions and for making the visit of me and my family at ICASE very pleasant.

Finally, I want to thank Ingela for always supporting me. Tack Tommy och Cecilia för att ni är så mysiga.

Financial support from FFA, ESA, EU, NUTEK and FMV is gratefully acknowledged.

Bibliography

[1] Abe, K., Kondoh, T. & Nagano, Y. 1996 A two-equation heat transfer model reflecting second-moment closures for wall and free turbulent flows. *Int. J. Heat and Fluid Flow* **17**, 228-237.

[2] Adumitroaie, V., Taulbee, D.B. & Givi, P. 1997 Explicit Algebraic Scalar-Flux Models for Turbulent Reacting Flows. *A. i. ch. e. J.* **8**, 1935-2147.

[3] Baldwin, B. & Lomax, H. 1978 Thin Layer Approximation and Algebraic Model for Separated Turbulent Flow. AIAA Paper 78-257.

[4] Bardina, J., Ferziger, J.H. & Reynolds, W.C. 1983 Improved turbulence models based on large-eddy simulation of homogeneous, incompressible turbulent flows. *Stanford University Tech. Rep.* TF-19.

[5] Boussinesq, J. 1877 Essai sur la théorie des eaux courantes. *Mém. prés. Acad. Sci.*, 3rd edn, Paris XXIII, 46.

[6] Bradshaw, P. 1997 The best turbulence models for engineers. In Modeling complex turbulent flows, Eds. M.D. Salas, J.N. Hefner, L. Sakell, Kluwer (1999).

[7] Chien, K.Y. 1982 Predictions of Channel and Boundary-Layer Flows with a Low-Reynolds-Number Turbulence Model. *AIAA J.* **20**, 33–38.

[8] Cook, P.H., MacDonald, M.A. & Firmin, M.C.P. 1979 Aerofoil 2822 - Pressure distributions, boundary layer and wake measurements. *AGARD AR 138*.

[9] Craft, T.J., Launder, B.E. & Suga, K. 1993 Extending the applicability of eddy viscosity models through the use of deformation invariants and non-linear elements. In *Proc. 5th Int. Symp. on Refined Flow Modelling and Turbulence Measurements*, 125–132, Presses Ponts et Chaussées, Paris.

[10] Daly, B.J. & Harlow, F.H. 1970 Transport equations in turbulence. *Phys. Fluids* **13**, 2634–2649.

[11] Friedrich, R. 1998 Modelling of turbulence in compressible flows. Chapter 5 of **Transition, Turbulence and Combustion Modelling**, Eds. A. Hanifi, P.H. Alfredsson, A.V. Johansson and D.S. Henningson. Kluwer.

[12] Gatski, T.B & Speziale C.G. 1993 On explicit algebraic stress models for complex turbulent flows. *J. Fluid Mech.* **254**, 59–78.

[13] Girimaji, S.S. 1996 Fully-explicit and self-consistent algebraic Reynolds stress model *Theor. and Comp. Fluid Dyn.* **8** 387–402 (also *ICASE Report No. 95-82*).

[14] Girimaji, S.S. 1997 A Galilean invariant explicit algebraic Reynolds stress model for turbulent curved flows *Phys. Fluids.* **9** 1067–1077 (also *ICASE Report No. 96-38*).

[15] Girimaji, S.S. 1997 Development of algebraic Reynolds stress model for non-equilibrium turbulence. In Modeling complex turbulent flows, Eds. M.D. Salas, J.N. Hefner, L. Sakell, Kluwer (1999).

[16] Girimaji, S.S. & Balachandar, S. 1998 Analysis and modeling of boyancy-generated turbulence using numerical data. *Int. J. Heat Mass Transfer* **41**, 915-929.

[17] Hanjalić, K., Jakirlić, S. & Hadžić, I. 1995 Computation of oscillating turbulent flows at transitional *Re*-numners *Turbulent Shear Flows* **9** pp 323–342. Eds F. Durst, N. Kasagi & B.E. Launder. Springer-Verlag, Berlin.

[18] Hellström, T., Davidson, L. & Rizzi, A. 1994 Reynolds stress transport modelling of transonic flow around the RAE2822 airfoil. *AIAA 94-0309* 32nd Aerospace Sciences Meeting, Reno, Jan 1994

[19] Johansson, A.V. & Burden, A.D. 1998 An introduction to turbulence modelling. Chapter 4 of **Transition, Turbulence and Combustion Modelling**, Eds. A. Hanifi, P.H. Alfredsson, A.V. Johansson and D.S. Henningson. Kluwer.

[20] Johansson, A.V. & Wallin, S. 1996 A new explicit algebraic Reynolds stress model. Proc. Sixth European Turbulence Conference, Lausanne, July 1996, Ed. P. Monkewitz, 31–34.

[21] Johansson, A.V. & Wikström, P.M. 2000 DNS and modelling of passive scalar transport in turbulent channel flow with a focus on scalar dissipation rate modelling. To appear in *ERCOFTAC J.*

[22] Jones, W.P. & Launder, B.E. 1972 The prediction of laminarization with a two-equation model of turbulence. *Int. J. Heat Mass Trans.* **15**, 310–314.

[23] Jongen, T. & Marx, Y.P. 1997 Design of an unconditionally stable positive scheme for the K–ε and two-layer turbulence models. *Computers & Fluids* **26**, 469–487.

[24] Jongen, T., Machiels, L. & Gatski, T.B. 1998 Predicting noninertial effects with linear and nonlinear eddy-viscosity, and algebraic stress models. *Flow Turbul. Combust.* **60** (2), 215–234.

[25] Jongen, T. & Gatski, T.B. 1998 A new approach to characterizing the equilibrium states of the Reynolds stress anisotropy in homogeneous turbulence. *Theoret. Comput. Fluid Dynamics* **11**, 31–47.

[26] Jongen, T., Mompean, G. & Gatski, T.B. 1998 Predicting S-duct flow using a composite algebraic stress model. *AIAA J.* **36**, 327–335.

[27] Kolmogorov, A.N. 1942 Equations of turbulent motions of an incompressible fluid. Izvestia Academy of Sciences, USSR; Physics, **6**, 56–58.

[28] Launder, B.E. 1978 Heat and mass transport. In Turbulence, P. Bradshaw (ed.), Springer, Berlin, 231-287.

[29] Launder, B.E., Reece, G.J. & Rodi, W. 1975 Progress in the development of a Reynolds-stress turbulence closure. *J. Fluid Mech.* **41**, 537–566.

[30] Lumley, J.L. 1978 Computational modeling of turbulent flows. *Adv. Appl. Mech.* **18**, 123–176.

[31] Launder, B.E. 1996 Advanced turbulence models for industrial applications Chapter 5 of **Turbulence and Transition Modelling**, Eds. M. Hallbäck, D.S. Henningson, A.V. Johansson and P.H. Alfredsson. Kluwer.

[32] Menter, F.R. 1994 Two-equation eddy-viscosity turbulence models for engineering applications. *AIAA J.* **32**, 1598–1604.

[33] Moser, R.D, Kim J. & Mansour N.N. 1998 DNS of Turbulent Channel Flow up to $Re_\tau = 590$. *Phys. Fluids* **11**, 943–945.

[34] McDevitt, J. 1979 Supercritical Flow about a Thick Circular-Arc Airfoil. NASA TM-78549.

[35] Naot, D., Shavit, A. & Wolfstein, M. 1973 Two-point correlation model and the redistribution of Reynolds stresses. *Phys. Fluids* **16**, 738–743.

[36] Pope, S.B. 1975 A more general effective-viscosity hypothesis *J. Fluid Mech.* **72**, 331–340.

[37] Pope, S.B. 1997 A perspective on turbulence modeling. In Modeling complex turbulent flows, Eds. M.D. Salas, J.N. Hefner, L. Sakell, Kluwer (1999).

[38] Prandtl, L. 1925 Über die ausgebildete Turbulenz. *ZAMM* **5**, 136–139.

[39] Prandtl, L. 1945 Über ein neues Formelsystem für die ausgebildete Turbulenz. Nachr. Akad. Wiss. Göttingen. Math.-Phys. Kl. 1945, 6–19.

[40] Reynolds, O. 1883 An experimental investigation of the circumstances which determine whether the motion of water shall be direct or sinuous, and of the law of resistance in parallel channels. *Philos. Trans. R. Soc. London* **174**, 935–982.

[41] Rizzi, A., Eliasson, P., Lindblad, I., Hirsch C., Lacor, C., Haeuser, J. 1993 The engineering of multiblock/multigrid software for Navier-Stokes flows on structured meshes *Computers Fluids* **22**, 341–367.

[42] Rodi, W. 1972 The prediction of free turbulent boundary layers by use of a two equation model of turbulence. *Ph.D. thesis, University of London.*

[43] Rodi, W. 1976 A new algebraic relation for calculating the Reynolds stresses. *Z. angew. Math. Mech.* **56**, T219–221.

[44] Rogers, M.M., Moin, P. & Reynolds, W.C. 1986 The structure and modeling of the hydrodynamic and passive scalar fields in homogeneous turbulent shear flow. Dept. Mech. Engng. Rep. TF-25, Stanford University, Stanford, California.

[45] Rogers, M.M., Mansour, P. & Reynolds, W.C. 1989 An algebraic model for the turbulent flux of a passive scalar. *J. Fluid Mech.* **203**, 77-101.

[46] Rotta, J.C. 1951 Statistische Theorie nichthomogener Turbulenz. *Z. Phys.* **129**, 547–572.

[47] Rumsey, C.L., Gatski, T.L. & Morrison, J.H. 1999 Turbulence model predictions of extra-strain rate effects in strongly-curved flows. AIAA Paper 99-157

[48] Rung, T., Lübcke, H., Franke, M., Xue, L., Thiede, F. & Fu, S. 1999 Assessment of explicit algebraic stress models in transonic flows. In Proc. Eng. turb. modelling and experiments 4, Ajaccio, France, May 1999, Elsevier.

[49] Schülein, E., Krogmann, P. & Stanewsky, E. 1996 Documentation of Two-Dimensional Impinging Shock/ Turbulent Boundary Layer Interaction Flow. DLR Report: DLR IB 223 - 96 A 49.

[50] Shabany, Y. & Durbin, P.A. 1997 Explicit algebraic scalar flux approximation. *AIAA J.* **35**, 985-989.

[51] Shabbir, A. & Shih, T.H. 1992 Critical Assessment of Reynolds Stress Turbulence Models Using Homogeneous Flows NASA TM 105954, ICOMP-92-24, CMOTT-92-12.

[52] Shih, T.H. & Lumley, J.L. 1993 Remarks on Turbulent Constitutive Relations. *Mathl. Comput. Modelling* **18**(2), 9-16.

[53] Shih, T.H., Zhu, J. & Lumley, J.L. 1992 A Realizable Reynolds Stress Algebraic Equation Model NASA TM 105993, ICOMP-92-27, CMOTT-92-14.

[54] Shih, T.-H. 1996 Constitutive relations and realizability of single-point turbulence closures Chapter 4 of **Turbulence and Transition Modelling**, Eds. M. Hallbäck, D.S. Henningson, A.V. Johansson and P.H. Alfredsson. Kluwer.

[55] Sjögren, T. 1997 Development and Validation of Turbulence Models Through Experiment and Computation Doctoral thesis, Dept. of Mechanics, KTH, Stockholm, Sweden.

[56] Sjögren, T. & Johansson, A.V. 1999 Development and calibration of algebraic nonlinear models for terms in the Reynolds stress transport equations To appear in *Phys. Fluids*

[57] Spalart P.R. & Speziale, C.G. 1999 A note on constraints in turbulence modelling. *J. Fluid Mech.* **391**, 373–376.

[58] Spalart P. & Allmaras, S.R. 1992 A one-equation model for aerodynamic flows. AIAA paper 92-439.

[59] Spencer, A.J.M. & Rivlin, R.S. 1959 The theory of matrix polynomials and its application to the mechanics of isotropic continua *Arch. Rat. Mech. Anal.* **2**, 309–336.

[60] Speziale, C.G., Sarkar, S. & Gatski, T.B. 1991 Modelling the pressure-strain correlation of turbulence: an invariant dynamical systems approach. *J. Fluid Mech.* **227**, 245–272.

[61] Speziale, C.G. & Xu, X.-H. 1996 Towards the development of second-order closure models for nonequilibrium turbulent flows *Int. J. Heat and Fluid Flow* **17**, 238–244.

[62] Taulbee, D.B. 1992 An improved algebraic Reynolds stress model and corresponding nonlinear stress model. *Phys. Fluids A* **4**, 2555–2561.

[63] Tennekes, H. & Lumley, J.L. 1972 A first course in turbulence. The MIT Press, Cambridge, MA, and London, England.

[64] Wikström, P.M. & Johansson, A.V. 1998 DNS and scalar-flux transport modelling in a turbulent channel flow. In proc. Turbulent Heat Transfer II, May 31-June 5, Manchester.

[65] Wikström, P.M., Hallbäck, M., & Johansson, A.V. 1998 Measurements and heat-flux transport modelling in a heated cylinder wake. *Intl. J. Heat Fluid Flow* **19**, 556–562. August 1998.

[66] Wilcox, D.C. 1988 Reassessment of the scale-determining equation for advanced turbulence models. *AIAA J.* **26**, 1299–1310.

[67] Wilcox, D.C. 1994 Simulation of Transition with a Two-Equation Turbulence Model. *AIAA J.* **32**, 247–255.

[68] Xu, X.-H. & Speziale, C.G. 1996 Explicit algebraic stress model of turbulence with anisotropic dissipation. *AIAA J.* **34**, 2186–2189.

1

Paper 1

AN EXPLICIT ALGEBRAIC REYNOLDS STRESS MODEL FOR INCOMPRESSIBLE AND COMPRESSIBLE TURBULENT FLOWS

Stefan Wallin
The Aeronautical Research Institute of Sweden (FFA)
Box 11021, SE-16111 Bromma, Sweden

Arne V. Johansson
Department of Mechanics, KTH, SE-100 44 Stockholm, Sweden

Abstract. Some new developments of explicit algebraic Reynolds stress turbulence models (EARSM) are presented. The new developments include a new near-wall treatment ensuring realizability for the individual stress components, a formulation for compressible flows, and a suggestion for a possible approximation of diffusion terms in the anisotropy transport equation. Recent developments in this area are assessed and collected into a model for both incompressible and compressible three-dimensional wall-bounded turbulent flows. This model represents a solution of the implicit ARSM equations, where the production to dissipation ratio is obtained as a solution to a nonlinear algebraic relation. Three-dimensionality is fully accounted for in the mean flow description of the stress anisotropy. The resulting EARSM has been found to be well suited to integration to the wall and all individual Reynolds stresses can be well predicted by introducing wall damping functions derived from the van Driest damping function. The platform for the model consists of the transport equations for the kinetic energy and an auxiliary quantity. The proposed model can be used with any such platform, and examples are shown for two different choices of the auxiliary quantity.

1. Introduction

Standard two-equation models are still dominant in the context of industrial flow computations. In flows with strong effects of streamline curvature, adverse pressure gradients, flow separation or system rotation, such models fail to give accurate predictions. Turbulence models based on the transport equations for the individual Reynolds stresses have the natural potential for dealing with, for example, the associated complex dynamics of inter-component transfer. The Boussinesq hypothesis may in this context be said to be replaced by transport equations for the individual Reynolds stress anisotropies. As yet, there are non-trivial numerical aspects of flow computations with such models in complex flow situations. This represents an active area of research. In parallel with such efforts there has been a considerable renewed interest in various forms of algebraic approximations of the anisotropy transport equations. In the present work some new developments are presented for explicit formulations of algebraic Reynolds

stress models. The motivation for this work is the general need for improvements in the prediction of complicated turbulent flows using the platform of existing CFD prediction tools based on the two-equation modelling level.

1.1. Algebraic Reynolds stress models. The classical algebraic Reynolds stress model (ARSM), Rodi[26, 27], was developed from the modelled Reynolds stress transport (RST) equation by assuming that the advection minus the diffusion of the individual Reynolds stresses can be expressed as the product of the corresponding quantity for the kinetic energy, K, and the individual Reynolds stresses normalized by K. This results in an implicit relation between the stress components and the mean velocity gradient field that replaces the Boussinesq hypothesis. Since the algebraic Reynolds stress model is determined from the modelled Reynolds stress transport equation no additional model constants are needed and the basic behaviour and experiences of the particular RST model will be inherited. The linearity of the Boussinesq hypothesis excludes any dependence on the rotational (antisymmetric) part of the mean velocity gradient tensor. An ARSM approach here represents a systematic method of constructing a nonlinear stress relationship that includes effects of the rotational part of the mean velocity gradient tensor. Despite this definite improvement one should, however, keep in mind that the ARSM can never represent the transport effects as well as a full RST model, which always should be expected to give a more correct description of the turbulence. Also, the RST models have limitations in predicting turbulence for general and complicated flows, especially in describing the effects of rotation.

The traditional ARSM idea is equivalent to neglecting advection and diffusion terms in the exact transport equation for the Reynolds stress anisotropy, a_{ij}, defined as $a_{ij} \equiv \overline{u_i u_j}/K - 2\delta_{ij}/3$. The advection term is indeed exactly zero for all stationary parallel mean flows, such as fully developed channel and pipe flows. For inhomogeneous flows the assumption of negligible effects of diffusion in the a_{ij} equation can cause problems, particularly in regions where the production term is small or where the inhomogeneity is strong. However, the Rodi ARSM assumption incorporates in a natural way not only effects of rotation but also effects of streamline curvature and three-dimensionality of the flow and has been found to be a reasonable approximation of the full differential RST equations in a number of flow situations, in many respects superior to the eddy-viscosity hypothesis.

To illustrate the natural way in which system rotation, and rotational effects in general, enter in this type of formalism we may take as the starting point the transport equation for the Reynolds stress anisotropy tensor in a rotating Cartesian coordinate system (the formulation of algebraic Reynolds stress models for rotating and curvilinear coordinate systems has recently been studied in some

detail by Sjögren[35])

$$K\frac{\mathrm{D}\,a_{ij}}{\mathrm{D}t} - \left(\frac{\partial T_{ijl}}{\partial x_l} - \frac{\overline{u_iu_j}}{K}\frac{\partial T_l^{(K)}}{\partial x_l}\right) = -\frac{\overline{u_iu_j}}{K}\left(\mathcal{P}-\varepsilon\right) + \mathcal{P}_{ij} - \varepsilon_{ij} + \Pi_{ij} + \varepsilon C_{ij}^{(a)} \tag{1}$$

where $-T_{ijl}$ and $-T_l^{(K)}$ are the fluxes (turbulent and molecular) of the Reynolds stress and turbulent kinetic energy, respectively. The dissipation rate tensor, ε_{ij}, and the pressure strain, Π_{ij}, need to be modelled whereas the production terms, $\mathcal{P}_{ij}$ and $\mathcal{P} = \mathcal{P}_{ii}/2$, and the Coriolis term, $C_{ij}^{(a)}$, do not need any modelling since they are explicit in the Reynolds stress tensor. In a non-rotating coordinate system the Reynolds stress production term is normally written as

$$\mathcal{P}_{ij} = -\overline{u_iu_k}U_{j,k} - \overline{u_ju_k}U_{i,k}, \tag{2}$$

where $U_{i,j}$ denotes the mean velocity gradient tensor. In a rotating system it is convenient to split the mean velocity gradient tensor into a mean strain and a mean rotation tensor. We will here let S_{ij} and Ω_{ij} denote these tensors normalized with the turbulent timescale, $\tau \equiv K/\varepsilon$,

$$S_{ij} = \frac{\tau}{2}\left(U_{i,j} + U_{j,i}\right), \qquad \Omega_{ij} = \frac{\tau}{2}\left(U_{i,j} - U_{j,i}\right). \tag{3}$$

A consistent formulation of (1), valid also in the rotating system, can then be obtained by replacing the mean rotation tensor by the absolute rotation tensor

$$\Omega_{ij}^{*} = \Omega_{ij} + \Omega_{ij}^{\mathrm{s}}, \tag{4}$$

where

$$\Omega_{ij}^{\mathrm{s}} = \tau\epsilon_{jik}\omega_k^{\mathrm{s}} \tag{5}$$

and ω_k^{s} is the constant angular rotation rate vector of the system. This procedure illustrates the origin of the two parts of what normally is referred to as the Coriolis term in the a_{ij} equation. In this way the first part is included in the production term, that now (normalized with ε) can be expressed as

$$\frac{\mathcal{P}_{ij}}{\varepsilon} = -\frac{4}{3}S_{ij} - \left(a_{ik}S_{kj} + S_{ik}a_{kj}\right) + a_{ik}\Omega_{kj}^{*} - \Omega_{ik}^{*}a_{kj}. \tag{6}$$

The second part of the Coriolis term arises from the transformation of the advection term. This part (normalized by ε) is denoted by $C_{ij}^{(a)}$ in (1), and can be expressed as

$$C_{ij}^{(a)} = a_{ik}\Omega_{kj}^{\mathrm{s}} - \Omega_{ik}^{\mathrm{s}}a_{kj}. \tag{7}$$

The ARSM assumption results in the following implicit algebraic equation for a_{ij}:

$$\frac{\overline{u_iu_j}}{K}\left(\mathcal{P}-\varepsilon\right) = \mathcal{P}_{ij} - \varepsilon_{ij} + \Pi_{ij} + \varepsilon C_{ij}^{(a)}, \tag{8}$$

the structure of which, of course, depends on the choice of the models for ε_{ij} and Π_{ij}. For the present modelling purpose we choose an isotropic assumption for the dissipation rate tensor,

$$\varepsilon_{ij} = \frac{2}{3}\varepsilon\delta_{ij}, \tag{9}$$

and the Rotta model[28] for the slow pressure strain

$$\Pi_{ij}^{(s)} = -c_1\varepsilon a_{ij}. \tag{10}$$

For the rapid pressure–strain rate we choose the general linear model of Launder, Reece & Rodi[17], which for a non-rotating system normally is written as

$$\begin{aligned}\Pi_{ij}^{(r)} &= -\frac{c_2+8}{11}\left(\mathcal{P}_{ij}-\frac{2}{3}\mathcal{P}\delta_{ij}\right) - \frac{30c_2-2}{55}K\left(U_{i,j}+U_{j,i}\right)\\ &- \frac{8c_2-2}{11}\left(D_{ij}-\frac{2}{3}\mathcal{P}\delta_{ij}\right)\end{aligned} \tag{11}$$

where $D_{ij} = -\overline{u_iu_k}U_{k,j} - \overline{u_ju_k}U_{k,i}$.

A simple way of obtaining a consistent, frame-independent formulation of the rapid pressure–strain rate model is to apply the same methodology as for the production term. This gives

$$\begin{aligned}\frac{\Pi_{ij}^{(r)}}{\varepsilon} &= \frac{4}{5}S_{ij} + \frac{9c_2+6}{11}\left(a_{ik}S_{kj}+S_{ik}a_{kj}-\frac{2}{3}a_{km}S_{mk}\delta_{ij}\right)\\ &+ \frac{7c_2-10}{11}\left(a_{ik}\Omega^*_{kj}-\Omega^*_{ik}a_{kj}\right).\end{aligned} \tag{12}$$

From (8) we then obtain the implicit algebraic equation for the Reynolds stress anisotropy tensor in the form

$$\begin{aligned}\left(c_1-1+\frac{\mathcal{P}}{\varepsilon}\right)\mathbf{a} &= -\frac{8}{15}\mathbf{S} + \frac{7c_2+1}{11}\left(\mathbf{a\Omega}^{\mathrm{R}}-\mathbf{\Omega}^{\mathrm{R}}\mathbf{a}\right)\\ &- \frac{5-9c_2}{11}\left(\mathbf{aS}+\mathbf{Sa}-\frac{2}{3}\mathrm{tr}\{\mathbf{aS}\}\mathbf{I}\right)\end{aligned} \tag{13}$$

In equation (13) $\mathbf{a}$, $\mathbf{S}$ and $\mathbf{\Omega}$ denote second-rank tensors, and $\mathbf{I}$ is the identity matrix. The inner product of two matrices is defined as $(\mathbf{SS})_{ij} \equiv \left(\mathbf{S}^2\right)_{ij} \equiv S_{ik}S_{kj}$ and tr{} denotes the trace. This notation will be kept through this paper. One should note that (13) represents a nonlinear relation since $\mathcal{P}/\varepsilon \equiv -\mathrm{tr}\{\mathbf{aS}\}$.

It is interesting to note that the 'effective' mean rotation rate tensor, Ω^{R}_{ij}, depends on the choice of model:

$$\Omega^{\mathrm{R}}_{ij} = \Omega^*_{ij} + \frac{11}{7c_2+1}\Omega^{\mathrm{s}}_{ij} = \Omega_{ij} + \frac{7c_2+12}{7c_2+1}\Omega^{\mathrm{s}}_{ij}. \tag{14}$$

The ARSM approximation of the a_{ij} transport equation with this approach is then equivalent to neglecting the advective term (and diffusion) in the chosen rotating coordinate system. Hence, the adequacy of the ARSM approach is coupled to the choice of a coordinate system where the omission of advection

terms in the a_{ij} equation can be justified. The choice of coordinate system is not at all trivial in strongly curved flows and the coordinate direction is not in general aligned with the flow direction. There are, however, methods to construct ARSMs that generally neglect only the advection term in the streamline direction (see e.g. Girimaji[10] and Sjögren[35]).

As is seen from equation (13) the treatment of system rotation is quite straightforward. The superscript R on the mean rotation rate tensor will be dropped in the following.

The turbulent kinetic energy, $K \equiv \overline{u_i u_i}/2$, and its dissipation, ε, are determined from transport equations

$$\frac{\mathrm{D}\,K}{\mathrm{D}t} + \frac{\partial T_l^{(K)}}{\partial x_l} = \mathcal{P} - \varepsilon, \tag{15}$$

$$\frac{\mathrm{D}\,\varepsilon}{\mathrm{D}t} + \frac{\partial T_l^{(\varepsilon)}}{\partial x_l} = (C_{\varepsilon 1}\mathcal{P} - C_{\varepsilon 2} f_\varepsilon \varepsilon)\,\frac{\varepsilon}{K}. \tag{16}$$

There is no direct influence of system rotation on these equations. A substantial improvement over the eddy-viscosity model equations is that the production term, $\mathcal{P}$, does not need to be modelled. The transport terms, $T_l^{(K)}$ and $T_l^{(\varepsilon)}$, are usually modelled using gradient diffusion with the diffusivity coefficient expressed with the aid of the eddy viscosity, but here an improvement can also be achieved by using the knowledge of the complete Reynolds stress tensor. The gradient-diffusion model proposed by Daly & Harlow[3] applied to the turbulent kinetic energy and its dissipation gives

$$T_l^{(K)} = -c_s' \frac{K}{\varepsilon}\overline{u_l u_m}\frac{\partial K}{\partial x_m}, \qquad T_l^{(\varepsilon)} = -c_\varepsilon \frac{K}{\varepsilon}\overline{u_l u_m}\frac{\partial \varepsilon}{\partial x_m}. \tag{17}$$

Launder, Reece & Rodi[17] recommend $c_s' = 0.25$ and $c_\varepsilon = 0.15$.

1.2. Explicit algebraic Reynolds stress models. The implicit relation for $\mathbf{a}$ in the ARSM equations has been found to be numerically and computationally cumbersome since there is no diffusion or damping present in the equation system. In many applications the computational effort has been found to be excessively large and the benefits of using ARSM instead of the full Reynolds stress model are then lost. An explicit algebraic Reynolds stress model, EARSM, where the Reynolds stresses are explicitly related to the mean flow field is much more numerically robust and has been found to have almost a negligible effect on the computational effort as compared to a K–ε model.

The most general form for $\mathbf{a}$ in terms of $\mathbf{S}$ and $\mathbf{\Omega}$ consists of ten tensorially independent groups to which all higher-order tensor combinations can be reduced

with the aid of the Caley–Hamilton theorem:

$$\begin{aligned}\mathbf{a} = {} & \beta_1\mathbf{S} + \beta_2\left(\mathbf{S}^2 - \frac{1}{3}I\!I_S\ \mathbf{I}\right) + \beta_3\left(\mathbf{\Omega}^2 - \frac{1}{3}I\!I_\Omega\ \mathbf{I}\right) + \beta_4\left(\mathbf{S\Omega} - \mathbf{\Omega S}\right) \\ & + \beta_5\left(\mathbf{S}^2\mathbf{\Omega} - \mathbf{\Omega S}^2\right) + \beta_6\left(\mathbf{S\Omega}^2 + \mathbf{\Omega}^2\mathbf{S} - \frac{2}{3}I\!V\ \mathbf{I}\right) \\ & + \beta_7\left(\mathbf{S}^2\mathbf{\Omega}^2 + \mathbf{\Omega}^2\mathbf{S}^2 - \frac{2}{3}V\ \mathbf{I}\right) + \beta_8\left(\mathbf{S\Omega S}^2 - \mathbf{S}^2\mathbf{\Omega S}\right) \\ & + \beta_9\left(\mathbf{\Omega S\Omega}^2 - \mathbf{\Omega}^2\mathbf{S\Omega}\right) + \beta_{10}\left(\mathbf{\Omega S}^2\mathbf{\Omega}^2 - \mathbf{\Omega}^2\mathbf{S}^2\mathbf{\Omega}\right). \end{aligned} \tag{18}$$

The β-coefficients may be functions of the five independent invariants of $\mathbf{S}$ and $\mathbf{\Omega}$, which can be written as

$$I\!I_S = \mathrm{tr}\{\mathbf{S}^2\},\ \ I\!I_\Omega = \mathrm{tr}\{\mathbf{\Omega}^2\},\ \ I\!I\!I_S = \mathrm{tr}\{\mathbf{S}^3\},\ \ I\!V = \mathrm{tr}\{\mathbf{S\Omega}^2\},\ \ V = \mathrm{tr}\{\mathbf{S}^2\mathbf{\Omega}^2\}. \tag{19}$$

Other scalar parameters may also be involved.

The independence of the ten groups and the completeness of expression (18) is further discussed in Appendix B. Shih & Lumley[34] include also an eleventh, sixth-order group. The exact expression for such a group in terms of the lower-order groups is also given in Appendix B. In two-dimensional mean flows, there are only three independent tensor groups, i.e. the $\beta_{1,2,4}$ groups, and two independent invariants, $I\!I_S$ and $I\!I_\Omega$.

Formulation of expression (18) in terms of $\mathbf{S}$ and $\mathbf{\Omega}$ follows Pope[24] and gives a much more compact form than by using the mean velocity gradients directly. It is also more cumbersome to compute matrix products involving $U_{i,j}$ due to the full matrix (eight independent elements) while S_{ij} and Ω_{ij} contain only five and three independent elements respectively. Also, the introduction of a rotating coordinate system is simplified here.

The main problem in obtaining an explicit relation for the anisotropy is that of determining the β-coefficients. A possibility would be to calibrate these from some chosen set of 'basic flows'. Shih, Zhu & Lumley[32] partially adopted this approach combined with conditions related to realizability and restraints on correct behaviour in rapid distortion limits. A more traditional approach is to derive an explicit form from an implicit $\mathbf{a}$-relation based on established models for the terms in the Reynolds stress (or its anisotropy) tensor transport equation, equivalent to equation (13). Pope[24] was the first to propose using the ten tensor groups to form a consistent explicit relation. He also derived a relation for two-dimensional mean flows leaving the production to dissipation ratio ($\mathcal{P}/\varepsilon$) implicit. This approach was later extended and solved for three-dimensional mean flows by Taulbee[41] for the special case of $c_2 = 5/9$ and by Gatski & Speziale[7] for a general linear pressure–strain model.

The nonlinearity of equation (13) ($\mathcal{P}/\varepsilon \equiv -\mathrm{tr}\{\mathbf{aS}\}$) forms a major obstacle for this approach and the studies published so far have circumvented the problem by letting $\mathcal{P}/\varepsilon = -\mathrm{tr}\{\mathbf{aS}\}$ be implicit during the solution of (13), adopted by

Pope[24] and Taulbee[41] or the approach used by Gatski & Speziale[7] where they used the asymptotic equilibrium value for $\mathcal{P}/\varepsilon$ as a universal constant.

The nonlinear system of equations is, however, conveniently solved in the form of a linear system of (five) equations complemented by a nonlinear scalar equation for $\mathcal{P}/\varepsilon$. For two-dimensional mean flows, Johansson & Wallin[15] and Girimaji[8, 9] have independently shown that this equation has a closed and fully explicit solution that can be expressed in a compact form. In the present work it is shown that good approximations are easily found for general three-dimensional mean flows. The complexity of the solution is substantially reduced by setting the coefficient $c_2 = 5/9$ (see e.g. Taulbee[41]).

The removal of the need for *ad hoc* relations for $\mathcal{P}/\varepsilon$ represents a substantial improvement for this type of modelling. A constant $\mathcal{P}/\varepsilon$ gives wrong asymptotic behaviour for large strain rates, also noticed by Speziale & Xu[40], while the fully consistent solution of the nonlinear equation system automatically fulfils the correct asymptotic behaviour. Also, in the very near-wall region, the correct asymptotic behaviour implies that all individual Reynolds stresses can be satisfactorily represented simply by introducing a van Driest damping function.

A straightforward extension to compressible flow is derived in which the mean density variations are taken into account. This model is applied to a complex flow situation with a shock–boundary layer interaction. An extension of the model to account in a simple way for the neglected turbulent transport of the anisotropies is also considered.

2. Formulation of an explicit algebraic model (EARSM)

The value of c_2 in the rapid pressure–strain model was originally suggested to be 0.4 by Launder *et al.*[17], but more recent studies have suggested a higher value close to 5/9[18, 31]. This means that the last term in equation (13) is of quite small influence, also noticed by Taulbee[41]. Setting $c_2 = 5/9$ one obtains the simplified but still implicit equation

$$\left(c_1 - 1 + \frac{\mathcal{P}}{\varepsilon}\right)\mathbf{a} = -\frac{8}{15}\mathbf{S} + \frac{4}{9}\left(\mathbf{a\Omega} - \mathbf{\Omega a}\right). \tag{20}$$

System rotation can easily be accounted for by substituting $\mathbf{\Omega}$ with $\mathbf{\Omega}^{\mathrm{R}} = \mathbf{\Omega} + (13/4)\,\mathbf{\Omega}^{\mathrm{s}}$ according to (14) where $\mathbf{\Omega}^{\mathrm{s}}$ is given by (5) (see section 1). It will be shown later that the removal of the last term in equation (13) gives a substantial simplification of the solution, especially in three-dimensional mean flow. The Rotta coefficient, c_1, is here set to 1.8.

The simplified but implicit algebraic Reynolds stress equation (20) is rewritten in the following form:

$$N\mathbf{a} = -\frac{6}{5}\mathbf{S} + \left(\mathbf{a\Omega} - \mathbf{\Omega a}\right) \tag{21}$$

where N is closely related to the production to dissipation ratio ($\mathcal{P}/\varepsilon = -\mathrm{tr}\{\mathbf{aS}\}$),

$$N = c_1' + \frac{9}{4}\frac{\mathcal{P}}{\varepsilon} \tag{22}$$

and

$$c_1' = \frac{9}{4}\left(c_1 - 1\right). \tag{23}$$

The procedure to solve this equation is the following: First, the general form for the anisotropy, equation (18), is inserted into the simplified ARSM equation (21) where N is not yet determined. The resulting linear equation system for the β-coefficients is then solved by using the fact that higher-order tensor groups can be reduced with the aid of the Cayley–Hamilton theorem where the ten groups in the general form (18) form a complete basis. The β-coefficients are now functions of the production to dissipation ratio, $\mathcal{P}/\varepsilon$, or N. The final step is to formulate and solve the nonlinear scalar equation for N or $\mathcal{P}/\varepsilon$.

2.1. Solution of the simplified ARSM for two-dimensional mean flows. For two-dimensional mean flows the solution is reduced to only two non-zero coefficients, which can be expressed as

$$\beta_1 = -\frac{6}{5}\frac{N}{N^2 - 2II_\Omega}, \quad \beta_4 = -\frac{6}{5}\frac{1}{N^2 - 2II_\Omega} \ . \tag{24}$$

It is clearly seen that the denominator, $N^2 - 2II_\Omega$, cannot become singular since II_Ω is always negative. It will be shown later that an explicit formulation of any quasi-linear ARSM is non-singular if the corresponding nonlinear equation for the production to dissipation ratio is solved, as also noticed by Girimaji[8, 9].

The nonlinear equation for N in two-dimensional mean flow can be derived by introducing the solution of $\mathbf{a}$ for two-dimensional mean flow in the definition of N. The resulting equation is cubic

$$N^3 - c_1' N^2 - \left(\frac{27}{10}II_S + 2II_\Omega\right)N + 2c_1' II_\Omega = 0, \tag{25}$$

and can be solved in a closed form with the solution for the positive root being

$$N = \begin{cases} \dfrac{c_1'}{3} + \left(P_1 + \sqrt{P_2}\right)^{1/3} + \mathrm{sign}\left(P_1 - \sqrt{P_2}\right) \mid P_1 - \sqrt{P_2} \mid^{1/3}, & P_2 \geq 0 \\ \dfrac{c_1'}{3} + 2\left(P_1^2 - P_2\right)^{1/6} \cos\left(\dfrac{1}{3}\arccos\left(\dfrac{P_1}{\sqrt{P_1^2 - P_2}}\right)\right), & P_2 < 0 \end{cases} \tag{26}$$

where the arccos function should return an angle between 0 and π and

$$P_1 = \left(\frac{{c_1'}^2}{27} + \frac{9}{20}II_S - \frac{2}{3}II_\Omega\right)c_1', \quad P_2 = P_1^2 - \left(\frac{{c_1'}^2}{9} + \frac{9}{10}II_S + \frac{2}{3}II_\Omega\right)^3. \tag{27}$$

It can easily be shown that N remains real and positive for all possible values of II_S and II_Ω. The production to dissipation ratio may then be found from (22).

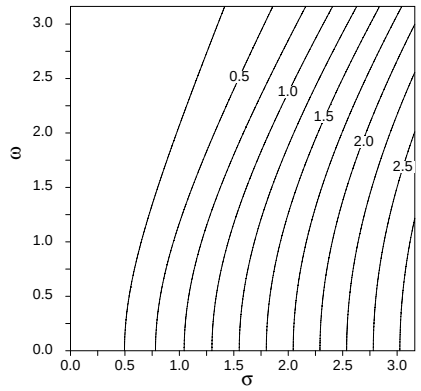

FIGURE 1. Isolines of the production to dissipation ratio for the current model.

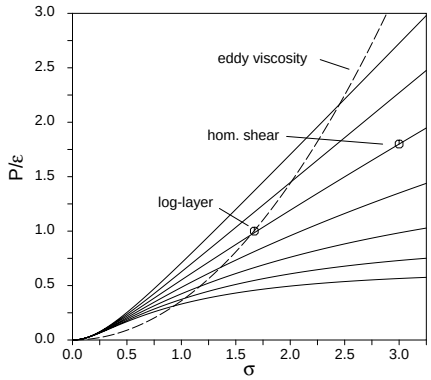

FIGURE 2. Production to dissipation ratio versus strain rate σ for different rotation ratios ω/σ. The current model (——) compared to an eddy-viscosity model (– – –).

The above solution for two-dimensional flows was also given in [15] and is very similar in structure to that of Girimaji[8, 9] who also derives an explicit solution for $\mathcal{P}/\varepsilon$ although for a somewhat more general set of models that yields $\beta_2 \neq 0$ (cf the solutions in Appendix C).

2.1.1. *Illustration of the behaviour of the proposed model.* Figures 1 and 2 illustrate the behaviour of the solution for $\mathcal{P}/\varepsilon$. We note that it is zero for all cases with $\sigma = 0$, i.e. irrespective of the value of ω, where σ and ω are defined as $\sigma \equiv \sqrt{II_S/2}$ and $\omega \equiv \sqrt{-II_\Omega/2}$ and that the $\mathcal{P}/\varepsilon$ ratio decreases monotonically with increasing influence of rotation. For all parallel shear flows $\sigma = \omega$.

Homogeneous shear flow is a classical corner stone case for calibration of turbulence models. Tavoularis & Corrsin[43] have experimentally shown that the asymptotic value of $SK/\varepsilon \approx 6$ corresponding to $\sigma = \omega = 3$. In the experiments

TABLE 1. The computed anisotropy in the log-layer using the current model assuming balance between turbulence production and dissipation compared to channel DNS data by Kim[16].

	a_{12}	a_{11}	a_{22}	a_{33}	σ
DNS	-0.29	0.34	-0.26	-0.08	1.65
Current model	-0.30	0.25	-0.25	0.00	1.69

TABLE 2. The anisotropy in asymptotic homogeneous shear flow using the current model with $\sigma = 3.0$ compared to measurements by Tavoularis & Corrsin[43].

	a_{12}	a_{11}	a_{22}	a_{33}	$\mathcal{P}/\varepsilon$
Experiment	-0.30	0.40	-0.28	-0.12	1.8
Current model	-0.30	0.31	-0.31	0.00	1.8

the production to dissipation ratio was found to be approximately 1.8, marked as a circle in figure 2. The present model exactly replicates that result. Furthermore, in the log-layer of a boundary layer we know that the production balances the dissipation rate, $\mathcal{P} = \varepsilon$, which is obtained with the proposed model when the strain rate $\sigma = 1.69$. This is within the range of σ values found in the log-layer of the DNS data for channel flow [16]. This is also consistent with an effective $C_\mu = 0.09$ which gives $\sigma = 1.67$, also marked as a circle in the figure.

The anisotropies for the two cases are compared in tables 1 and 2. Most important is to correctly predict the a_{12} anisotropy since this is the only component of the anisotropy tensor that contributes to the turbulent production in parallel flows. The a_{22} component is also important since this is the only term that contributes to the turbulent diffusion term. The tables show that a_{12} and a_{22} are well predicted for the two different cases. The a_{11} and a_{33} components are, however, not as well predicted due to the simplification of setting $c_2 = 5/9$ since this implies that $a_{33} = 0$. The inclusion of $c_2 \neq 5/9$ will, however, not be sufficient if one wishes to improve the prediction of the anisotropies, since the particular choice of c_1 and c_2 used here is the only combination that predicts both a_{12} and a_{22} correctly in these two different cases. The good behaviour of the model for these two very different cases justifies the particular choice of model constants, c_1 and c_2, in the pressure–strain model.

A better tuning of the different anisotropies could possibly be achieved by using the most general quasi-linear pressure–strain model, where the coefficients may be functions of the production to dissipation ratio. This will be further discussed in section 2.3.

The asymptotic behaviour for large strain rates in parallel flow can be investigated by letting $\sigma = \omega \to \infty$. The production to dissipation ratio then becomes

$\mathcal{P}/\varepsilon \sim \sigma$ and $\beta_1 \sim 1/\sigma$. This asymptotic behaviour for the β_1-coefficient (equivalent to $-2C_\mu$) is of particular interest since it ensures good model behaviour in the very near-wall buffer- and viscous sub-layers as will be shown later. The asymptotic behaviour is also consistent with the asymptotic characteristics of homogeneous shear flow. With an erroneous model assumption of a constant production to dissipation ratio, $\mathcal{P}/\varepsilon$, the wrong asymptote, $\beta_1 \sim 1/\sigma^2$, is obtained, as also noticed by Speziale & Xu[40], while the solution of the nonlinear equation for $\mathcal{P}/\varepsilon$ automatically gives the correct asymptotic behaviour.

To illustrate the behaviour for large shear rates the model is tested in homogeneous shear flow at high initial shear rate ($SK/\varepsilon = 50$), see figure 3. This flow is a case where one should expect differences between the algebraic approach and the full differential model due to the fact that the anisotropies undergo a temporal evolution ($\partial a_{ij}/\partial t \neq 0$) in the development towards an asymptotic state. Moreover, the Launder *et al.*[17] model gives quite poor predictions of this case when used in a differential form. The very good predictions of the present EARSM can thus be regarded as a bit fortuitous. Nevertheless, the self-consistent approach gives a model with the correct asymptotic behaviour, which is a pre-requisite for reasonable predictions in the limit of high shear. It is important to make clear that the proposed model is not intended for these extreme high shear rates and the normal stress components are not as well predicted as the turbulent kinetic energy. It is, however, an important step towards a more general engineering model that the model is able to give reasonable results in extreme flow cases also.

In flows with an adverse pressure gradient, the production to dissipation ratio is greater than 1 and eddy-viscosity models with constant C_μ overestimate the turbulent viscosity or the a_{12} anisotropy. Bradshaw's assumption, which is adopted by Menter[20] in the shear stress transport (SST) model, forces the a_{12} anisotropy to be constant for $\mathcal{P}/\varepsilon$ ratios greater than unity, which gives $\beta_1 \sim 1/\sigma$. This is fulfilled in the limit of large strain rates by the proposed model, which also gives a nearly constant a_{12} anisotropy in boundary layers with small pressure gradients. This can be seen in figure 4 where the a_{12} anisotropy versus the strain rate is shown for parallel flows. The a_{12} anisotropy computed from the proposed model is nearly constant here for a wide range of strain rates including both the log-layer and asymptotic homogeneous shear. The eddy-viscosity assumption gives $a_{12} = -2C_\mu\sigma$ and has a totally different behaviour, shown in the figure, and becomes physically unrealizable for large strain rates, $\sigma > 5.56$. This is, however, avoided by the SST limitation on the anisotropy which nearly coincides with the proposed model for strain rates larger than those in the log-layer. This feature of the proposed model ensures an improved behaviour in boundary layers with pressure gradients as compared to standard eddy-viscosity models.

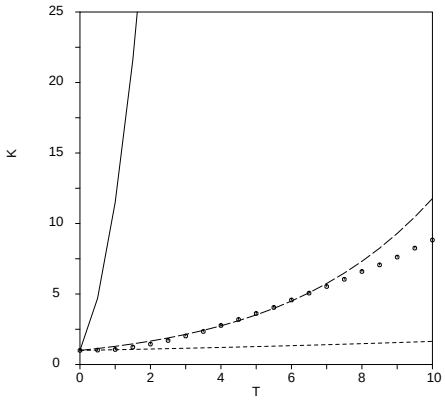

FIGURE 3. Time evolution of the turbulent kinetic energy in rapidly sheared homogeneous flow, $SK/\varepsilon = 50$. Eddy-viscosity model (——), the proposed EARSM (– – –) and the Gatski & Speziale[7] EARSM (·····) compared with RDT (∘).

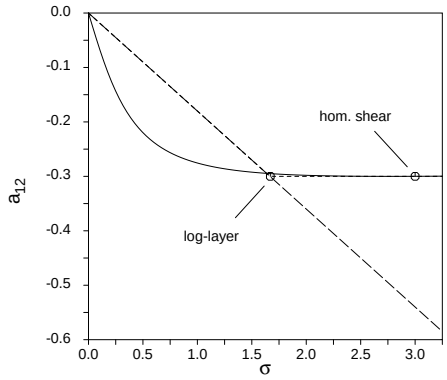

FIGURE 4. Predicted a_{12} anisotropy versus strain rate σ for parallel flow. The current model (——) compared to the eddy-viscosity model (– – –) and the Menter[20] SST model (·····).

Since equation (18) represents the general form of the anisotropy, different explicit algebraic Reynolds stress models can be compared by studying the behaviour of the β-coefficients. In two-dimensional mean flows the β-coefficients can be illustrated as iso-curves in the σ–ω plane. In figure 5 the β_1-coefficient (equivalent to $-2C_\mu$) is shown for the Taulbee[41], Gatski & Speziale[7] and Shih, Zhu & Lumley[32] models. There are substantial differences between the different models for the β_1 coefficient and a similar behaviour can also be seen for the other coefficients. Figure 5(a) is very similar to the results of Pope[24] although the coefficients in the pressure–strain model were somewhat different.

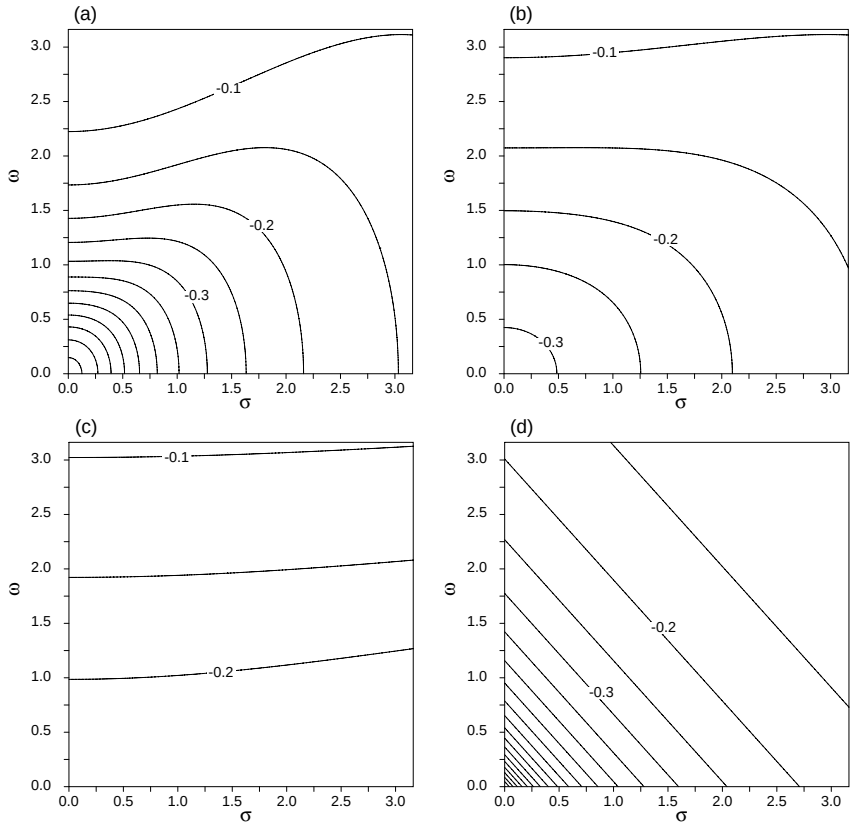

FIGURE 5. The behaviour of the β_1-coefficient in the σ–ω-plane for: (a) the implicit ARSM and the present EARSM, (b) Taulbee[41], (c) Gatski & Speziale[7] and (d) Shih *et al.*[32].

One should of course bear in mind that the underlying approaches are chosen differently in the different models. This only partly explains the different behaviours though. The Taulbee[41] model could, however, be directly compared to the implicit ARSM since the basic approach is the Launder *et al.*[17] model with similar choices of the model coefficients. The classical ARSM assumption is, however, not asymptotically correct for small strain rates and Taulbee thus makes a different approximation in that limit. That difference is clearly seen in the figure. The approximation imposed by Taulbee is motivated by the neglected advection term and gives improved predictions in developing homogeneous shear flows where the advection is important for small times. However, the prediction of fully developed channel flow, where the advection is zero, is also affected by the Taulbee assumption. For that reason this approach is not adopted, even though it improves the predicted shear stresses near the channel centre. A similar effect can be obtained by an approximate inclusion of turbulent diffusion (of a_{ij}) effects, as will be discussed in section 5.

The benefits of a direct, explicit solution of the production to dissipation ratio can be further illustrated by considering rotating plane channel flow. The mean flow is here described by $U(x_2)\,\delta_{i1}$ and the system rotation is taken as $\omega^{\mathrm{s}}\delta_{i3}$. The mean strain rate tensor is unaffected by system rotation, implying that the effective II_S for the calculation of $\mathcal{P}/\varepsilon$ is the same as for a non-rotating channel flow. The 'effective' second invariant of the mean rotation tensor (see equation (14)) becomes

$$II_\Omega^{\mathrm{R}} = \tau^2\left[-\frac{1}{2}\left(U'\right)^2 - 6\left(\frac{13}{4}\right)^2\left(\omega^{\mathrm{s}}\right)^2 + 2\frac{13}{4}\omega^{\mathrm{s}}U'\right]. \tag{28}$$

We note that, whereas the first two terms have the same sign on both sides of the channel, the last term has an alternating sign. For moderate rotation rates the model will, thus, predict a decrease of $\mathcal{P}/\varepsilon$ on the side of the channel where II_Ω is increased, and vice versa. This is in agreement with the observed behaviour of a stabilized and a destabilized side in rotating channel flow. Due to the quadratic term (in ω^{s}) in the expression for II_Ω the model will also predict a global decrease in $\mathcal{P}/\varepsilon$ for very large rates of rotation, as could be expected from comparison with stability theory (see e.g. Matsson & Alfredsson[19]).

2.2. Solution of the simplified ARSM for three-dimensional mean flow. For general three-dimensional mean flows the solution for the β-coefficients can be written as

$$\begin{aligned} \beta_1 &= -\frac{N\left(2N^2 - 7II_\Omega\right)}{Q}, \quad \beta_3 = -\frac{12N^{-1}IV}{Q}, \\ \beta_4 &= -\frac{2\left(N^2 - 2II_\Omega\right)}{Q}, \qquad \beta_6 = -\frac{6N}{Q}, \qquad \beta_9 = \frac{6}{Q}, \end{aligned} \tag{29}$$

where all the other coefficients are identically zero. The denominator

$$Q = \frac{5}{6}\left(N^2 - 2II_\Omega\right)\left(2N^2 - II_\Omega\right) \tag{30}$$

is also here clearly seen always to remain positive since II_Ω always is negative.

The nonlinear equation for N or the corresponding equation for $\mathcal{P}/\varepsilon$ is for example obtained by introducing the above solution (29) for $\mathbf{a}$ into the definition of N. The resulting equation is of sixth order and reads

$$\begin{aligned} N^6 - c_1' N^5 - \left(\frac{27}{10}II_S + \frac{5}{2}II_\Omega\right)N^4 + \frac{5}{2}c_1' II_\Omega N^3 \\ + \left(II_\Omega^2 + \frac{189}{20}II_S II_\Omega - \frac{81}{5}V\right)N^2 - c_1' II_\Omega^2 N - \frac{81}{5}IV^2 = 0. \end{aligned} \tag{31}$$

This equation reduces to the two-dimensional cubic equation by recalling that in two-dimensional mean flows there are only two independent invariants, whereas $III_S = IV = 0$ and $V = II_S II_\Omega/2$. Equation (31) cannot be solved in a closed form but the solution of N for the cubic equation (25) applicable in two-dimensional mean flow, N_c, can be used as a first approximation. A further

improvement of the approximation of N is also possible by making a perturbation solution of the three-dimensional equation. This is done by perturbing the $I\!I\!V$ and V invariants around the two-dimensional solution, that is $I\!I\!V = \sqrt{\phi_1}$ and $V = I\!I_S I\!I_\Omega/2 + \phi_2$, assuming that ϕ_1 and ϕ_2 are independent. Putting this into the three-dimensional equation (31) and sorting in powers of ϕ_1 and ϕ_2 we get

$$N = N_c + \frac{162\left(\phi_1 + \phi_2 N_c^2\right)}{D} + \mathcal{O}\left(\phi_1^2, \phi_2^2, \phi_1\phi_2\right) \tag{32}$$

where the denominator, D, is given by

$$D = 20N_c^4\left(N_c - \frac{1}{2}c_1'\right) - I\!I_\Omega\left(10N_c^3 + 15c_1'N_c^2\right) + 10c_1'I\!I_\Omega^2 \tag{33}$$

where (25) has been used to rewrite the expression for D. From (33) it is obvious that D will always remain positive, since $N_c \geq c_1'$ (see Appendix C).

One could also consider keeping $\mathcal{P}/\varepsilon$ or N implicit during the iteration procedure to a steady-state solution and thus avoid any further approximations. It is, however, not known how this would affect the stability of the numerical method and should be avoided. There could also be problems associated with the existence of multiple roots, especially for three-dimensional cases.

2.2.1. *Example of a three-dimensional mean flow: rotating pipe.* Fully developed turbulent flow in a circular pipe rotating around its length axis is an interesting case, since it represents a three-dimensional flow that can be described with only one spatial coordinate, r in a cylindrical coordinate system ($\hat{\mathbf{r}}$, $\hat{\theta}$, $\hat{\mathbf{z}}$). If the flow is laminar, the tangential velocity, U_θ, varies linearly with the radius, r, like a solid-body rotation. In turbulent flow, on the other hand, the tangential velocity is nearly parabolic, which cannot be described with an eddy-viscosity turbulence model. The fully three-dimensional form of the proposed EARSM is needed to capture this behaviour. Limited forms with only second-order terms is not sufficient, as will be shown below.

The Navier–Stokes equation in the tangential direction can be written as

$$\nu\left(\frac{\mathrm{d}^2U_\theta}{\mathrm{d}r^2} + \frac{1}{r}\frac{\mathrm{d}U_\theta}{\mathrm{d}r} - \frac{U_\theta}{r^2}\right) = \frac{\mathrm{d}}{\mathrm{d}r}\left(Ka_{r\theta}\right) + 2\frac{Ka_{r\theta}}{r}. \tag{34}$$

After two integrations, the tangential velocity can be expressed as

$$U_\theta(r) = U_\theta(R)\frac{r}{R} - \frac{r}{\nu}\int_r^R \frac{Ka_{r\theta}}{u}\mathrm{d}u \tag{35}$$

where R is the radius of the tube. The first term corresponds to the linear U_θ profile while the second term is the correction that may give a parabolic-like profile if the $a_{r\theta}$ anisotropy is positive.

In this particular flow the strain- and rotation-rate tensors are evaluated in an inertial frame and read

$$\mathbf{S} = \frac{1}{2}\tau \begin{bmatrix} 0 & \frac{\mathrm{d}U_\theta}{\mathrm{d}r} - \frac{U_\theta}{r} & \frac{\mathrm{d}U_z}{\mathrm{d}r} \\ \frac{\mathrm{d}U_\theta}{\mathrm{d}r} - \frac{U_\theta}{r} & 0 & 0 \\ \frac{\mathrm{d}U_z}{\mathrm{d}r} & 0 & 0 \end{bmatrix} \tag{36}$$

and

$$\mathbf{\Omega} = \frac{1}{2}\tau \begin{bmatrix} 0 & -\frac{\mathrm{d}U_\theta}{\mathrm{d}r} - \frac{U_\theta}{r} & -\frac{\mathrm{d}U_z}{\mathrm{d}r} \\ \frac{\mathrm{d}U_\theta}{\mathrm{d}r} + \frac{U_\theta}{r} & 0 & 0 \\ \frac{\mathrm{d}U_z}{\mathrm{d}r} & 0 & 0 \end{bmatrix}. \tag{37}$$

The terms that contribute to the $a_{r\theta}$ component in the general expression (18) are the terms associated with the β_1, β_5, β_6 and β_{10}-coefficients. In the case of a linear U_θ profile, $S_{r\theta}$ is zero and the contribution from the β_1-term vanishes. This is consistent with the behaviour for an eddy-viscosity model.

We see from relation (35) that $a_{r\theta}$ should vanish rapidly for increasing Re. To verify that the present EARSM is consistent with such a behaviour we start with the EARSM solution for a flow that may deviate from solid-body rotation. For the present EARSM β_5 and β_{10} are zero, which means that here only the linear term ($\beta_1\mathbf{S}$) and the β_6-term (associated with the $\left(\mathbf{S\Omega}^2 + \mathbf{\Omega}^2\mathbf{S} - \frac{2}{3}I\!V\ \mathbf{I}\right)$-group) contribute to $a_{r\theta}$:

$$\begin{aligned} a_{r\theta} = {} & \frac{1}{2}\beta_1\tau\left(\frac{\mathrm{d}U_\theta}{\mathrm{d}r} - \frac{U_\theta}{r}\right) - \frac{1}{4}\beta_6\tau^3\left(\frac{\mathrm{d}U_\theta}{\mathrm{d}r} - \frac{U_\theta}{r}\right)\left(\frac{\mathrm{d}U_\theta}{\mathrm{d}r} + \frac{U_\theta}{r}\right)^2 \\ & - \frac{1}{4}\beta_6\tau^3\frac{\mathrm{d}U_\theta}{\mathrm{d}r}\left(\frac{\mathrm{d}U_z}{\mathrm{d}r}\right)^2. \end{aligned} \tag{38}$$

For solid body rotation only the third term remains and we see that the $a_{r\theta}$ component will vanish only if the axial mean velocity gradient $\mathrm{d}U_z/\mathrm{d}r$ vanishes. This gradient does indeed vanish in the limit of infinite Reynolds number, but only slowly[1] with increasing Reynolds numbers while the relation (35) indicates a more rapid decay rate ($a_{r\theta} \to 1/Re$).

The β_1 and β_6 coefficients in (38) are both negative, so the term with the axial mean velocity gradient (the last term) gives a positive contribution to $a_{r\theta}$ which drives the azimuthal velocity $U_\theta(r)$ towards a more parabolic-like profile (where $\mathrm{d}U_\theta/\mathrm{d}r > U_\theta/r$). The second term enhances this trend but what is interesting is that the β_1-term (the first term) has the opposite sign and has the possibility of balancing the $a_{r\theta}$ anisotropy component depending on the exact form of the β-coefficients.

[1]The 'two-layer hypothesis' $\Rightarrow$ $(U_{CL} - U_z)/u_\tau = f\left((R-r)/R\right) \Rightarrow (-(R/U_{CL})(\mathrm{d}U_z/\mathrm{d}r))^2 = (-(u_\tau/U_{CL})f')^2 \sim C_f$ where it is also well known that C_f slowly decreases with increasing Reynolds number and that the mean velocity profile in a pipe approaches a top-hat in the infinite Re limit (see e.g. Schlichting[30], chap. 20).

Hence, the required consistency of a rapidly vanishing $a_{r\theta}$ is indeed obtained as a solution to the present EARSM, and is in fact associated with a non-zero deviation from solid-body rotation for large but finite Reynolds numbers.

To clearly see this we may need to take a closer look at (38) by inserting the present EARSM solutions for β_1, β_6. This gives

$$a_{r\theta} \sim \left(7\frac{U_\theta}{r} - \frac{\mathrm{d}U_\theta}{\mathrm{d}r}\right)\left(\frac{\mathrm{d}U_z}{\mathrm{d}r}\right)^2 - \left(\frac{\mathrm{d}U_\theta}{\mathrm{d}r} - \frac{U_\theta}{r}\right)\left[\frac{81}{4\tau^2}\left(C_1 - 1 + \frac{\mathcal{P}}{\varepsilon}\right)^2 + \left(\frac{\mathrm{d}U_\theta}{\mathrm{d}r} + \frac{U_\theta}{r}\right)^2\right] \qquad (39)$$

and balance is obtained for a parabolic-like profile. Hence, the EARSM solution implies an anisotropy that vanishes much more rapidly than $\mathrm{d}U_z/\mathrm{d}r$. As is obvious from (39) we also see that in the limit of infinite Re where $\mathrm{d}U_z/\mathrm{d}r \to 0$ the vanishing $a_{r\theta}$ is associated with an EARSM solution that gives a solid-body rotation.

The rotation also affects the axial velocity component, which becomes less full, i.e. more parabolic. That effect enters mainly through the rotation dependence in the β_1-coefficient and could thus be captured also by a linear eddy-viscosity model where the C_μ-coefficient is dependent on the rotation rate.

A fully developed turbulent rotating pipe flow has been computed using the proposed model. The Reynolds number is 20 000 based on the mean flow velocity and tube diameter. Three different rotation ratios $Z = 0$, 0.5 and 1 were computed where $Z = U_\theta(R)/U_m$, i.e. the wall angular velocity divided by the axial bulk velocity. The results are compared to the experiment by Imao, Itoh & Harada[14]. The turbulence models used are the Chien[1] K–ε model and the proposed EARSM including the near-wall formulation in section 3. The EARSM is based on both the K–ε and K–ω models discussed in section 3.4.

The three-dimensional form of the model has been used and the influence of the approximation of N was assessed by computing the case by using both the zeroth- (N_c) and first-order perturbation solution of N. The former is given by (26) and labelled 'EARSM_0' in the figures while the latter 'EARSM_1' is given by (32).

Figure 6 shows the predicted axial velocity for $Z = 1$ using the Chien K–ε model alone and as the platform for EARSM calculations. The original Chien eddy-viscosity K–ε model is seen to be completely insensitive to rotation, while the EARSM predictions agree well with the experimental results. It is also seen that the different approximations of N only have a minor influence on the predicted velocity profile. In figure 7 predictions for different values of Z are shown for the K–ω model as the platform of the EARSM. The calculated results are seen to capture well the trend with increasing rate of rotation. The EARSM predictions with the K–ε and K–ω platforms are quite similar except in a region close to the wall. The angular velocity (figure 8) is also seen to be reasonably well

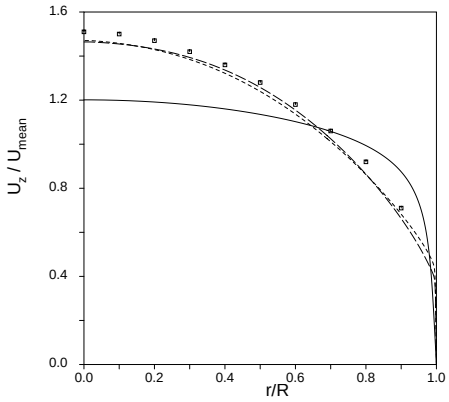

FIGURE 6. Axial velocity in rotating pipe flow for rotation ratio $Z = 1$. Computations with Chien K–ε model (——) and the current EARSM based on Chien K–ε, EARSM_0 (– – –) and EARSM_1 (·····), compared to experiment by Imao *et al.*[14] (▫).

predicted with the different EARSM formulations, among which the differences are small.

The prediction of the velocity could, however, be improved by the inclusion of the neglected other cubic term associated with β_5 (see (18)) and tuning the coefficients for this special case, but it is worth noticing that the results here are obtained without any tuning whatsoever. Moreover, three-dimensional effects driven by turbulence are in most cases quite weak compared to three-dimensional effects driven by mean momentum forces. The rotating pipe is in this case very extreme since the three-dimensional effects are purely turbulence driven.

The zeroth- and first-order solutions of N are only different approximations of the exact solution for N or $\mathcal{P}/\varepsilon$. The error can be investigated by computing the $\mathcal{P}/\varepsilon$ ratio using the different approximations of N from a given flow field. Figure 9 shows $\mathcal{P}/\varepsilon$ with N evaluated from the first- (EARSM_0) and second- (EARSM_1) order solutions of N given by (26) and (32) respectively, compared to the exact solution. The mean flow invariants of these expressions were taken from a fixed mean flow field, which was the solution with EARSM_0 based on K–ε for $Z = 1$. We can see a substantial difference between the zeroth- and first-order solutions and also that the first-order solution is quite close to the exact one. As seen from the previous figures this difference has still a quite small influence on the computed velocity profiles.

2.3. Solution of the general quasi-linear ARSM equation. So far, the explicit solution of the ARSM resulting from the special case of the Launder *et al.*[17] model with $c_2 = 5/9$ has been analysed. The solution procedure described in this section can, however, be applied to any ARSM that has been derived from a linear or quasi-linear pressure–strain model. Quasi-linear here means that the

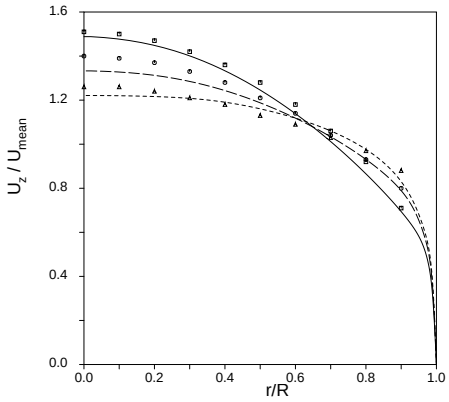

FIGURE 7. Axial velocity in rotating pipe flow for different rotation ratios. Computations with the current EARSM (EARSM_0) based on K–ω (lines) compared to experiment by Imao *et al.*[14] (symbols) for $Z = 1$ (——) (▫), $Z = 0.5$ (– – –) (○) and $Z = 0$ (·····) (△).

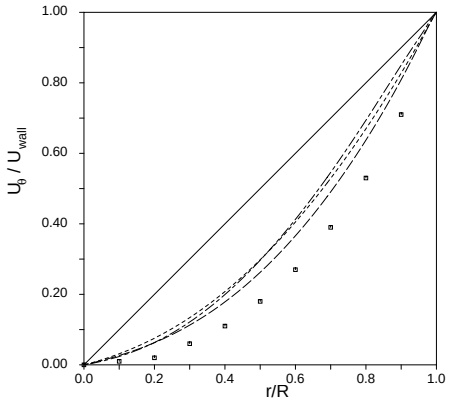

FIGURE 8. Angular velocity in rotating pipe flow for rotation ratio $Z = 1$. Computations with Chien K–ε model (——) and the current EARSM based on Chien K–ε, EARSM_0 (– – –) and EARSM_1 (·····), and the current EARSM (EARSM_0) based on K–ω (– – –) compared to experiment by Imao *et al.*[14] (▫).

pressure–strain model must be tensorially linear in $\mathbf{a}$ but may contain terms like $\mathrm{tr}\{\mathbf{aS}\}\mathbf{a}$. The resulting ARSM may be written

$$N\mathbf{a} = -A_1\mathbf{S} + (\mathbf{a\Omega} - \mathbf{\Omega a}) - A_2\left(\mathbf{aS} + \mathbf{Sa} - \frac{2}{3}\mathrm{tr}\{\mathbf{aS}\}\right) \tag{40}$$

where

$$N = A_3 + A_4\frac{\mathcal{P}}{\varepsilon}. \tag{41}$$

The solution of (40) for three-dimensional mean flow was first derived by Gatski & Speziale[7] where they considered the production to dissipation ratio

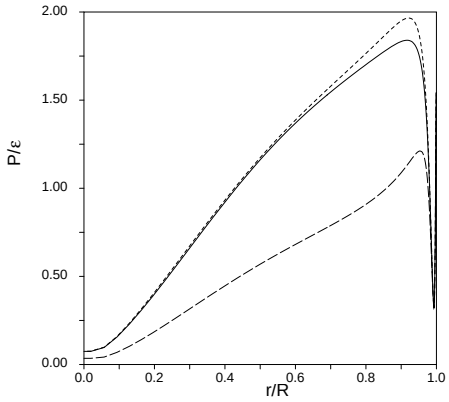

FIGURE 9. Production to dissipation ratio in rotating pipe flow for different approximation levels for N: EARSM_0 (– – –) and EARSM_1 (------) compared to the exact (——) solution. The mean flow from the EARSM_0 K–ε solution for $Z = 1$ was used.

as a universal constant which is equivalent to $A_4 = 0$. The fully consistent solution for two-dimensional mean flow was first derived by Girimaji[8, 9] where the production to dissipation ratio was obtained as part of the solution.

The solution of (40) for three-dimensional mean flow is given in Appendix C. The algebra in that case is considerably more complex than for the simplified ARSM with $c_2 = 5/9$. In this section we restrict our attention to two-dimensional mean flow for which the solution for the β-coefficients is

$$\beta_1 = -\frac{A_1 N}{Q}, \quad \beta_2 = 2\frac{A_1 A_2}{Q} \quad \text{and} \quad \beta_4 = -\frac{A_1}{Q}. \tag{42}$$

The denominator

$$Q = N^2 - 2II_\Omega - \frac{2}{3}A_2^2 II_S \tag{43}$$

for this case consists of both positive and negative terms but it can be shown that it is strictly positive due to the fact that N is a function of II_S and II_Ω (see Appendix C).

The Launder *et al.*[17] model (LRR) is a special case with the A_1 to A_4 coefficients given in table 3. Also, the SSG model by Speziale, Sarkar & Gatski[39] may be expressed in this form if it is linearized according to Gatski & Speziale[7]. The SSG pressure–strain model reads

$$\begin{aligned}\frac{\Pi}{\varepsilon} = &-\left(\frac{C_1}{2} + \frac{C_1^*}{2}\frac{\mathcal{P}}{\varepsilon}\right)\mathbf{a} + \left(C_3 - \frac{C_3^*}{2}\sqrt{II_a}\right)\mathbf{S} \\ &+ \frac{C_4}{2}\left(\mathbf{aS} + \mathbf{Sa} - \frac{2}{3}\mathrm{tr}\{\mathbf{aS}\}\mathbf{I}\right) - \frac{C_5}{2}\left(\mathbf{a\Omega} - \mathbf{\Omega a}\right) + \frac{C_2}{4}\left(\mathbf{a}^2 - \frac{1}{3}II_a\mathbf{I}\right),\end{aligned} \tag{44}$$

where $II_a = \mathrm{tr}\{\mathbf{a}^2\}$ and the coefficients are

$$C_1 = 3.4,\ \ C_1^* = 1.8,\ \ C_2 = 4.2,\ \ C_3 = \frac{4}{5},\ \ C_3^* = 1.30,\ \ C_4 = 1.25,\ \ C_5 = 0.40. \tag{45}$$

The linearized SSG model used by Gatski & Speziale[7] is then obtained by neglecting the quadratic anisotropy term and for the II_a invariant they used the equilibrium value predicted by the SSG model for two-dimensional homogeneous turbulence. This results in the following set of coefficients:

$$C_1 = 3.4,\ \ C_1^* = 1.8,\ \ C_2 = 0,\ \ C_3 = 0.36,\ \ C_3^* = 0,\ \ C_4 = 1.25,\ \ C_5 = 0.40, \tag{46}$$

and A_1 to A_4 are given in table 3. Gatski & Speziale[7] based their EARSM on this linearized SSG pressure–strain model and implied an additional approximation in order to avoid the nonlinearity in the ARSM equation system. The approximation was to use the asymptotic value for the production to dissipation ratio as a universal constant

$$\frac{\mathcal{P}}{\varepsilon} = \frac{C_{\varepsilon 2} - 1}{C_{\varepsilon 1} - 1} \tag{47}$$

which is equivalent to the A_1 to A_4-coefficients given in table 3 for Gatski & Speziale without regularization. The approximation made by Gatski & Speziale[7] is quite severe, especially since the A_4-coefficient is zero which means that the denominator Q given by (43) may become singular. However, in their final expression they have regularized the denominator to avoid the singular behaviour. That form of the model, however, could not exactly be expressed through the A_1 to A_4-coefficients.

The predicted anisotropies in the log-layer and for the asymptotic homogeneous shear flow are listed in tables 4 and 5. The linearized SSG model is able to predict all individual Reynolds stresses fairly well for the two different cases. The Gatski & Speziale[7] model gives the same result for the asymptotic homogeneous shear but fails in the log-layer since the approximation of the production to dissipation ratio used by them is only consistent for asymptotic shear flows. It should be noted here that the regularization in the Gatski & Speziale model does not influence the solution for these two cases.

The proposed model based on the LRR pressure–strain model is a reasonable choice here due to its simplicity in three-dimensional mean flows, and since the most important anisotropies, namely a_{12} and a_{22}, are fairly well predicted for both the log-layer and for the asymptotic homogeneous shear flow. If better predictions of the a_{11} and a_{33} anisotropies are needed, the linearized SSG may be considered as an alternative but one should realize that this model is considerably more complex for three-dimensional mean flows.

TABLE 3. The coefficients in the general ARSM for different models.

	A_1	A_2	A_3	A_4
LRR	$\frac{88}{15(7c_2+1)}$	$\frac{5-9c_2}{7c_2+1}$	$\frac{11(c_1-1)}{7c_2+1}$	$\frac{11}{7c_2+1}$
Current model ($c_1 = 1.8, c_2 = 5/9$)	1.20	0	1.80	2.25
Original LRR ($c_1 = 1.5, c_2 = 0.4$)	1.54	0.37	1.45	2.89
linearized SSG	1.22	0.47	0.88	2.37
Gatski & Speziale w/o regularization	1.22	0.47	5.36	0

TABLE 4. The predicted anisotropy in the log-layer using different models assuming balance between turbulence production and dissipation compared to channel DNS by Kim[16].

	a_{12}	a_{11}	a_{22}	a_{33}	σ
DNS	−0.29	0.34	−0.26	−0.08	1.65
Current model ($c_1 = 1.8, c_2 = 5/9$)	−0.30	0.25	−0.25	0.00	1.69
Original LRR ($c_1 = 1.5, c_2 = 0.4$)	−0.36	0.26	−0.20	−0.06	1.40
Linearized SSG	−0.32	0.36	−0.26	−0.10	1.59
Gatski & Speziale w/o regularization	−0.29	0.22	−0.16	−0.06	1.75
Gatski & Speziale	−0.28	0.22	−0.16	−0.06	1.76

TABLE 5. The predicted anisotropy in homogeneous shear flow using different models with $\sigma = 3.0$ compared to measurements by Tavoularis & Corrsin[43].

	a_{12}	a_{11}	a_{22}	a_{33}	$\mathcal{P}/\varepsilon$
expr	−0.30	0.40	−0.28	−0.12	1.8
Current model ($c_1 = 1.8, c_2 = 5/9$)	−0.30	0.31	−0.31	0.00	1.8
Original LRR ($c_1 = 1.5, c_2 = 0.4$)	−0.38	0.32	−0.25	−0.07	2.3
Linearized SSG	−0.32	0.41	−0.30	−0.11	1.9
Gatski & Speziale w/o regularization	−0.32	0.41	−0.30	−0.11	1.9
Gatski & Speziale	−0.31	0.41	−0.30	−0.11	1.9

3. Near-wall treatments

In the model presented so far no special attention has been given to the very near-wall region. To obtain the correct behaviour in this region it needs to be modified in a similar way to low Reynolds number two-equation turbulence models. An important difference compared to eddy-viscosity models is that the effective C_μ or β_1 in the proposed model is not a constant and, as has been shown by Wallin & Johansson[45], will adjust to the near-wall flow in a more natural way than is possible with eddy-viscosity models.

The turbulence timescale $\tau = K/\varepsilon$, which is used to scale the strain- and rotation-rate tensors goes to zero as the wall is approached. A more appropriate expression for the timescale was proposed by Durbin[4] and reads

$$\tau = \max\left(\frac{K}{\varepsilon}, C_\tau\sqrt{\frac{\nu}{\varepsilon}}\right). \tag{48}$$

This is just the usual timescale with a lower bound given by the Kolmogorov scale. Durbin[4, 4] uses $C_\tau = 6.0$ which will be kept in this study also.

In the very near-wall region of any shear flow the presence of the solid boundary will enforce a nearly parallel flow except in the immediate vicinity of a separation or stagnation point. A fully developed channel flow is exactly parallel and will be used to formulate and calibrate the very near-wall correction. A specific coordinate system will be used in the derivation of the near-wall correction but the final form is invariant to coordinate system.

In a channel flow, as well as in all parallel flows, we can simply express the anisotropy in terms of the two-dimensional β-terms and the non-dimensional shear, σ, which in parallel flow reads

$$\sigma = \frac{1}{2}\frac{K}{\varepsilon}\frac{\mathrm{d}U}{\mathrm{d}y}. \tag{49}$$

The invariants can then simply be expressed as $II_S = 2\sigma^2$ and $II_\Omega = -2\sigma^2$ and the anisotropy becomes

$$a_{12} = \sigma\beta_1, \quad a_{11} = \sigma^2\left(\frac{1}{3}\beta_2 - 2\beta_4\right), \quad a_{22} = \sigma^2\left(\frac{1}{3}\beta_2 + 2\beta_4\right). \tag{50}$$

By letting U in (49) represent the velocity along the limiting streamline at the wall the expressions (50) can also be said to be approximately valid for three-dimensional near-wall boundary layer flows.

The very near-wall behaviour is studied by using channel DNS data by Kim[16] at $Re_\delta \approx 7800$ or $Re_\tau \approx 395$. The mean velocity, K and ε profiles obtained from the DNS data have been used to compute the modelled anisotropy, which is compared to the anisotropy determined directly from the DNS data.

The near-wall asymptotic behaviour can be written as

$$\begin{array}{rcccccc}
u^+_{rms} & = & a_u y^+ & + & b_u {y^+}^2 & + & \cdots, \\
v^+_{rms} & = & a_v {y^+}^2 & + & b_v {y^+}^3 & + & \cdots, \\
w^+_{rms} & = & a_w y^+ & + & b_w {y^+}^2 & + & \cdots, \\
K^+ & = & a_K {y^+}^2 & + & b_K {y^+}^3 & + & \cdots, \\
-\overline{uv}^+ & = & a_{uv} {y^+}^3 & + & b_{uv} {y^+}^4 & + & \cdots.
\end{array} \tag{51}$$

So, Lai & Zhang[36] summarize these near-wall asymptotic coefficients, $a_u, a_v, ...$, for different experimental and numerical near-wall turbulence studies of flat plates, channels and pipes at different Reynolds numbers. These coefficients together with the DNS data by Kim[16] have been used to calibrate the coefficients in the near-wall corrections.

3.1. The shear component of the Reynolds stress. In a channel flow, the mean flow is only directly affected by the Reynolds shear stress, $\overline{uv}$, so let us start by looking at the model of a_{12}.

The modelled a_{12} anisotropy without any near-wall corrections is nearly constant as the wall is approached while DNS data exhibit a behaviour similar to an exponential decay (see figure 10). The obvious choice of 'wall damping function' is of van Driest type

$$f_1 = 1 - \exp\left(-\frac{y^+}{A^+}\right). \tag{52}$$

Also shown in figure 10 is the a_{12} behaviour predicted by a standard K–ε model, without any near-wall damping function, which gives strongly negative values near the wall, almost down to -2. Note that this is well outside the range of physically realizable values, that are limited to be between ± 1. The K–ε model cannot be correctly damped towards the wall as easily as the EARSM and the EARSM is therefore much better suited to be integrated down to the wall. This is due to the fact that the β_1 coefficient is not a constant, as in the eddy-viscosity hypothesis, but a function of the mean flow strain rate. In the very near-wall region the strain, normalized by the turbulent timescale, becomes large but the β_1-coefficient goes to zero for large strain rates giving a balanced a_{12} anisotropy (cf. figure 4).

The slope of the a_{12} anisotropy at the wall can be evaluated from the near-wall asymptotic behaviour to be $\mathrm{d}a_{12}/\mathrm{d}y^+ = -a_{uv}/a_K$. The constant A^+ varies between 18 and 37 in the data summarized by So *et al.*[36]. By choosing $A^+ = 26$, which also is the standard value in the van Driest function, a good fit to the DNS data is obtained according to figure 10, which shows the corresponding $\overline{uv}$ Reynolds stress. The low Reynolds number coefficient can now be determined as

$$\beta_{1,\text{low-Re}} = f_1 \beta_1, \tag{53}$$

where β_1 is the high Reynolds number coefficient obtained from the solution in section 2.

3.2. The normal components of the Reynolds stress. The correct near-wall behaviour for the normal Reynolds stresses is then ensured through a correct behaviour of the β_2- and β_4-coefficients. The near-wall asymptotic behaviour of the a_{11} and a_{22} anisotropy is

$$\begin{aligned} a_{11} &= \frac{\overline{u^2}}{K} - \frac{2}{3} = \frac{{a_u}^2}{a_K} - \frac{2}{3} + \mathcal{O}\left(y^+\right), \\ a_{22} &= \frac{\overline{v^2}}{K} - \frac{2}{3} = \frac{{a_v}^2}{a_K} {y^+}^2 - \frac{2}{3} = -\frac{2}{3} + \mathcal{O}\left({y^+}^2\right). \end{aligned} \tag{54}$$

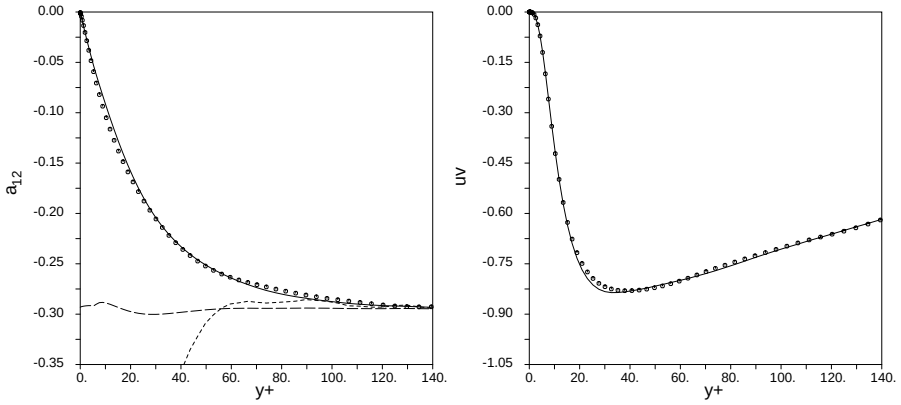

FIGURE 10. a_{12} anisotropy (left) and $\overline{uv}$ stress (right) in channel flow. Comparison of the current EARSM with near-wall correction (——) with DNS data (∘) by Kim[16]. The computed a_{12} anisotropy using the current EARSM without near wall correction (– – –) and the eddy-viscosity model (------) is also shown. The predicted anisotropy was evaluated by use of the DNS data for the $\mathbf{S}$ and $\mathbf{\Omega}$ fields.

The modelled a_{11} and a_{22} anisotropies, without any wall corrections, are limited near the wall, so a blending of the near-wall asymptote and the outer solution can be done. For simplicity, the same blending function, f_2, is used for the both anisotropies, which become

$$\begin{aligned} a_{11,\text{low-Re}} &= f_2 a_{11} + (1-f_2)\left(B_2 - \frac{2}{3}\right), \\ a_{22,\text{low-Re}} &= f_2 a_{22} + (1-f_2)\left(-\frac{2}{3}\right), \end{aligned} \tag{55}$$

where $B_2 = {a_u}^2/a_K$. Equation (54) states that a_{22} has zero slope at the wall so the function f_2 must also have zero slope. A simple choice that satisfies this criterion is $f_2 = {f_1}^2$. The low Reynolds number coefficients then become

$$\beta_{2,\text{low-Re}} = \frac{3B_2 - 4}{2\sigma^2}\left(1 - {f_1}^2\right), \quad \beta_{4,\text{low-Re}} = {f_1}^2\beta_4 - \frac{B_2}{4\sigma^2}\left(1 - {f_1}^2\right), \tag{56}$$

where β_4 is the high Reynolds number coefficient obtained from the solution in section 2.

The constant B_2 can be evaluated using the data summarized by So *et al.*[36] and varies between 1.56 and 1.84. By choosing $B_2 = 1.8$ a good fit to the DNS data is obtained (see figures 11 and 12).

3.3. Extension to general flows. The near-wall correction described so far was obtained for a special case, namely parallel two-dimensional flows, and cannot directly be generalized to three-dimensional mean flows. Some singularities in flows near separation must be considered and the formulation needs to be written in a coordinate-system-invariant form. These additional extensions

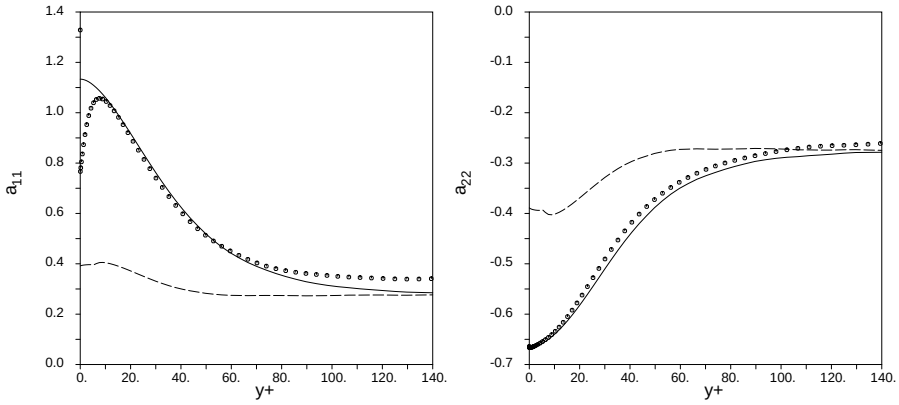

FIGURE 11. a_{11} (left) and a_{22} (right) anisotropies in channel flow. Comparison of the current EARSM with (——) and without (– – –) near-wall correction with DNS data (∘) by Kim[16]. The predicted anisotropy was evaluated by use of the DNS data for the $\mathbf{S}$ and $\mathbf{\Omega}$ fields.

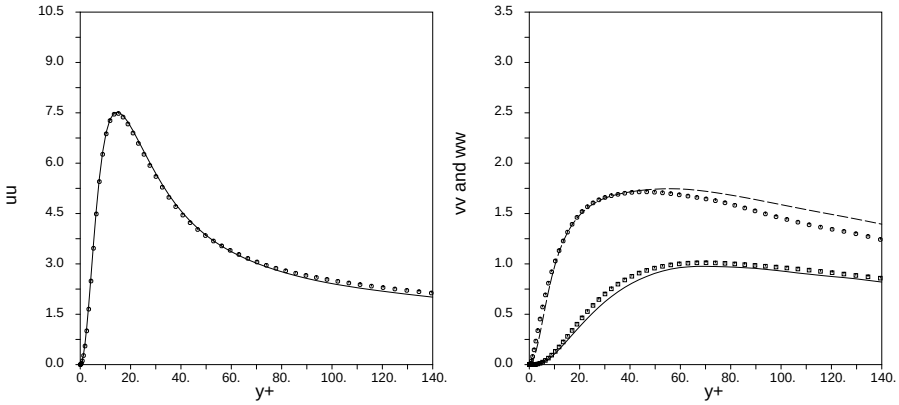

FIGURE 12. Reynolds stresses in channel flow. Comparison of the current EARSM, $\overline{u^2}$ (——) (left) and $\overline{v^2}$ (——), $\overline{w^2}$ (– – –) (right), with DNS data, (▫) and (∘) by Kim[16]. The predicted anisotropy was evaluated by use of the DNS data for the $\mathbf{S}$ and $\mathbf{\Omega}$ fields.

must be formulated such that the original form above is retained for parallel two-dimensional flows.

So far, the near-wall correction is described in terms of σ, which is defined in (49) for a specific coordinate system. By using $II_S = 2\sigma^2$, a coordinate-system-invariant form of the near wall correction can be obtained. In separated flow the shear rate σ may become small, leading to a singular behaviour of the near wall corrections to the β_2- and β_4-coefficients. To avoid this problem, the shear rate in the denominator of the near-wall correction is limited to the equilibrium shear rate where the turbulence production balances the dissipation rate. The

near-wall shear rate is always larger than the equilibrium one in zero pressure gradient flows and the limiter will only be active in flows near separation. The anisotropy model including the near-wall formulation then reads

$$\begin{aligned}\mathbf{a} = & f_1\beta_1\mathbf{S} + \left(1 - {f_1}^2\right)\frac{3B_2 - 4}{\max\left(I\!I_S, I\!I_S^{\mathrm{eq}}\right)}\left(\mathbf{S}^2 - \frac{1}{3}I\!I_S\ \mathbf{I}\right) \\ & + \left({f_1}^2\beta_4 - \left(1 - {f_1}^2\right)\frac{B_2}{2\max\left(I\!I_S, I\!I_S^{\mathrm{eq}}\right)}\right)\left(\mathbf{S\Omega} - \mathbf{\Omega S}\right) \end{aligned} \tag{57}$$

where $I\!I_S^{\mathrm{eq}}$ is the equilibrium value obtained by setting $\mathcal{P} = \varepsilon$ in the two-dimensional solution and reads $I\!I_S^{\mathrm{eq}} = 405c_1^2/\left(216c_1 - 160\right) \approx 5.74$ for $c_1 = 1.8$. The β-coefficients are given by equation (24) and f_1 is given by equation (52). Please observe that even though the high Reynolds number β_2-coefficient is zero the tensor group associated with the β_2-coefficient does not vanish.

The straightforward extension to three-dimensional flow reads

$$\begin{aligned}\mathbf{a} = & f_1\beta_1\mathbf{S} + \left(1 - {f_1}^2\right)\frac{3B_2 - 4}{\max\left(I\!I_S, I\!I_S^{\mathrm{eq}}\right)}\left(\mathbf{S}^2 - \frac{1}{3}I\!I_S\ \mathbf{I}\right) \\ & + f_1^2\beta_3\left(\mathbf{\Omega}^2 - \frac{1}{3}I\!I_\Omega\ \mathbf{I}\right) + \left({f_1}^2\beta_4 - \left(1 - {f_1}^2\right)\frac{B_2}{2\max\left(I\!I_S, I\!I_S^{\mathrm{eq}}\right)}\right)\left(\mathbf{S\Omega} - \mathbf{\Omega S}\right) \\ & + f_1\beta_6\left(\mathbf{S\Omega}^2 + \mathbf{\Omega}^2\mathbf{S} - \frac{2}{3}I\!V\ \mathbf{I}\right) + f_1^2\beta_9\left(\mathbf{\Omega S\Omega}^2 - \mathbf{\Omega}^2\mathbf{S\Omega}\right) \end{aligned} \tag{58}$$

This form reduces to (57) for two-dimensional mean flows.

The near-wall correction is strictly valid only for parallel two-dimensional mean flow but the very near-wall flow is, however, near parallel and two-dimensional also for quite complex three-dimensional flow fields so the equation (58) can be used as a first approximation. The correction can be extended to also be valid for flows near stagnation points like separation and reattachment points, for flows over curved surfaces and also for three-dimensional mean flows. This extension of the near-wall correction is, however, outside the scope of this paper but will be addressed in future studies.

3.4. Lengthscale determining equation. So far, we have proposed a new explicit constitutive relation between the mean flow strain rate and the Reynolds stresses including near-wall treatments. The choice of velocity- and length-scale determining equations has not yet been discussed. The turbulent kinetic energy, K, is a natural choice for determining the turbulent velocity-scale since this equation needs no further modelling. The dissipation of the turbulent kinetic energy, ε, is the most commonly used quantity for determining the turbulent length-scale but other alternatives are also possible like τ and ω.

Common to all length-scale determining equations is that they need a lot of *ad hoc* modelling, substantially more than the K-equation. The different terms are quite empirical and are tuned for specific flow cases. There are many different K–ε models with the major differences in the near-wall modelling in

the ε-equation and in the eddy-viscosity relation. Most of the ε-models are also tuned and calibrated together with the eddy-viscosity assumption, which gives a poor description of the near-wall anisotropy. One should thus not be surprised if the proposed EARSM together with an existing length-scale model does not give any improvements and perhaps also worse capabilities in predicting basic wall-bounded flows.

The correct methodology to obtain a length-scale determining equation is to develop it from scratch together with the proposed EARSM, so that one avoids the risk of inheriting terms that are needed to balance the errors introduced by the eddy-viscosity assumption. This is, however, outside the scope of this paper but will be addressed in future studies. For an illustration of the capability of the proposed model and to obtain an indication of how different length-scale determining equations act, we have tested the proposed model together with the well known Chien[1] K–ε model and the Wilcox[48] K–ω model for the fully developed channel case simulated by Kim[16].

In these computations we did not use the Daly & Harlow model, equation (17), of the diffusion terms in the K and ε (or ω) equations. The approach was to use the standard eddy-viscosity modelling of the diffusion term but with an effective C_μ evaluated from the EARSM such as $C_\mu^{\text{eff}} = -f_1\beta_1/2$. The differences between the Daly & Harlow and the eddy-viscosity approaches were found to be small for the K–ε model as long as the effective C_μ is used rather than a constant. In case of the K–ω model, the turbulent diffusion is complete different compared to that of the K–ε model and thus the Daly & Harlow approach needs to be recalibrated. The eddy-viscosity approach could, however, directly be used also here as long as the effective C_μ (or β^*) is used. In three-dimensional mean flows the effective C_μ is $C_\mu^{\text{eff}} = -f_1(\beta_1 + II_\Omega\beta_6)/2$

Figures 13 to 18 show the result of the computations with the two different two-equation models based on the proposed EARSM as well as with the original eddy-viscosity assumption. The EARSM has been used both with the original and modified ('mod') length-scale equations.

If we first look at the velocity profiles in figure 13 one finds that the additive constant B in the log-law is much too high when the EARSM is used. This clearly illustrates the need for recalibration discussed above. The figure also shows the results when the length-scale equation is tuned or modified to better match the log-law. In the K–ε model the definition of ε in Chien's model has been changed to

$$\varepsilon = \tilde{\varepsilon} + \frac{2\nu K}{y^2}\exp\left(-C_k y^+\right), \tag{59}$$

where the constant $C_k = 0.04$. This means that the original 'wall dissipation' is multiplied by an exponential function to give a more rapid decay of the modification near the wall. In the Wilcox K–ω model, the constant R_β was increased

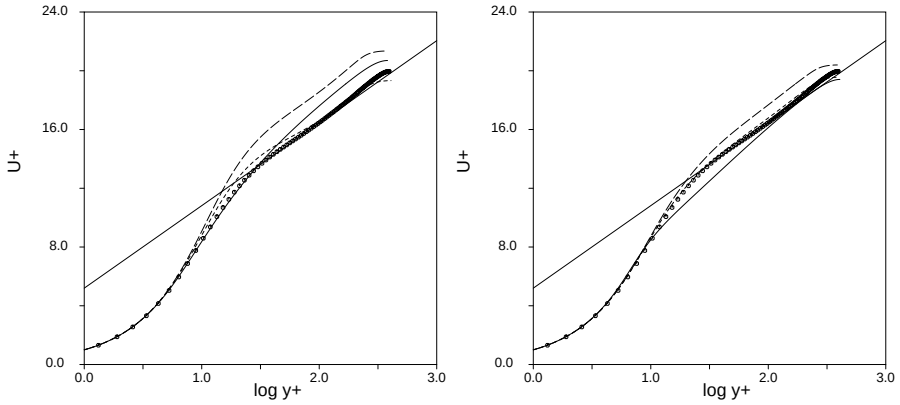

FIGURE 13. The streamwise velocity in channel flow. Computations based on Chien K–ε (left) and K–ω (right) using eddy-viscosity (——) and the current EARSM with the original (– – –) and modified (------) ε and ω equations compared with DNS data (∘) by Kim[16] and the log-law (——).

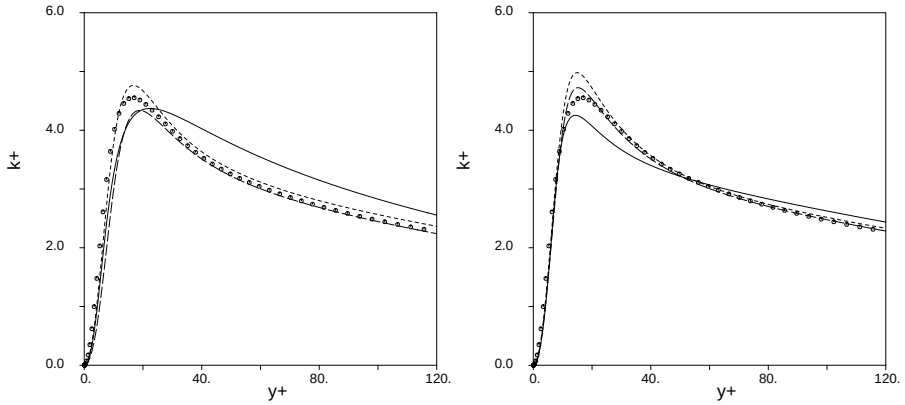

FIGURE 14. The turbulent kinetic energy in channel flow. Computations based on Chien K–ε (left) and K–ω (right) using eddy-viscosity (——) and the current EARSM with the original (– – –) and modified (------) ε and ω equations compared with DNS data (∘) by Kim[16].

from 8 to 10 to obtain the desired behaviour. For a more thorough comparison between K–ε and K–ω models the reader may wish to consult Menter[21].

It is also interesting to note the clear improvement in the K-profiles with the proposed EARSM both for the K–ε and K–ω models in figure 14. The near-wall dissipation ratio shown in figure 15 illustrates the need for a better near-wall modelling of the length-scale equation. In figures 16 to 18 we can see the good near-wall behaviour of the proposed EARSM which seems to be quite insensitive to the choice of basic two-equation model. In figure 16 we can also clearly see how poorly the a_{12} anisotropy is predicted with the eddy-viscosity models.

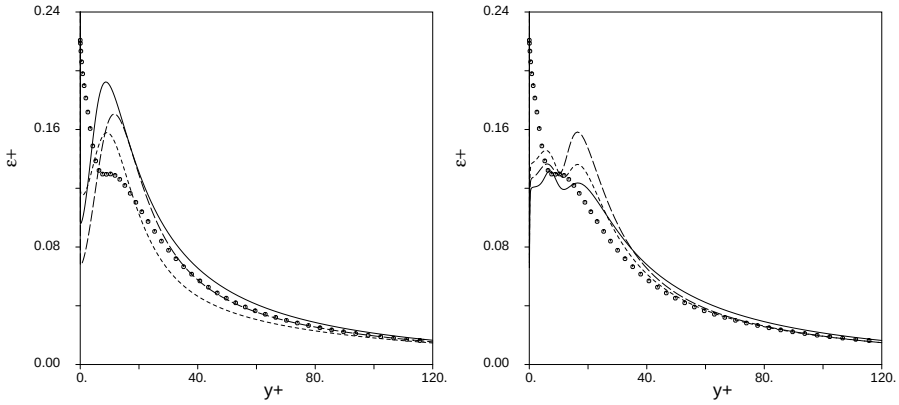

FIGURE 15. The dissipation of turbulent kinetic energy in channel flow. Legend as in figure 14.

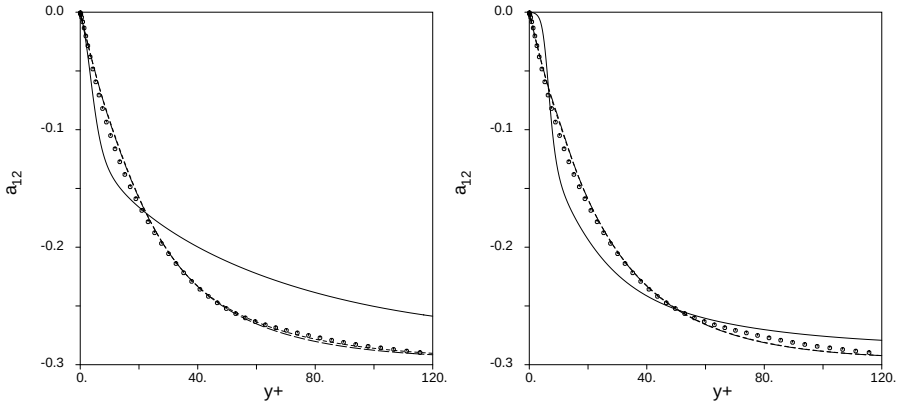

FIGURE 16. The a_{12} anisotropy in channel flow. Legend as in figure 14.

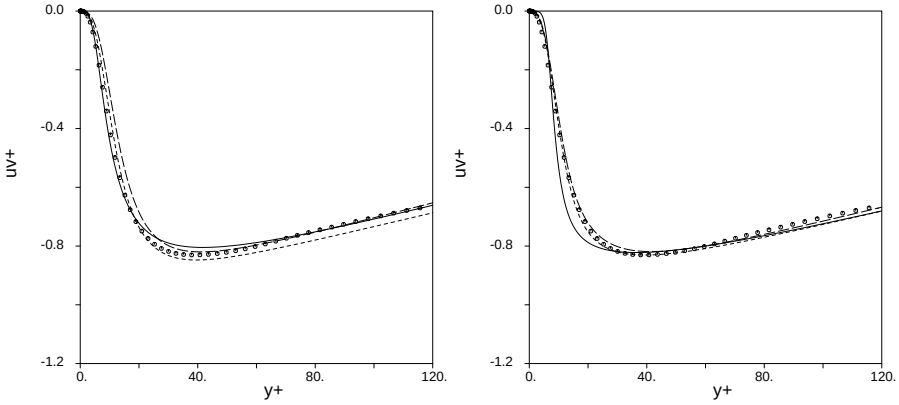

FIGURE 17. The $\overline{uv}$ Reynolds stress in channel flow. Legend as in figure 14.

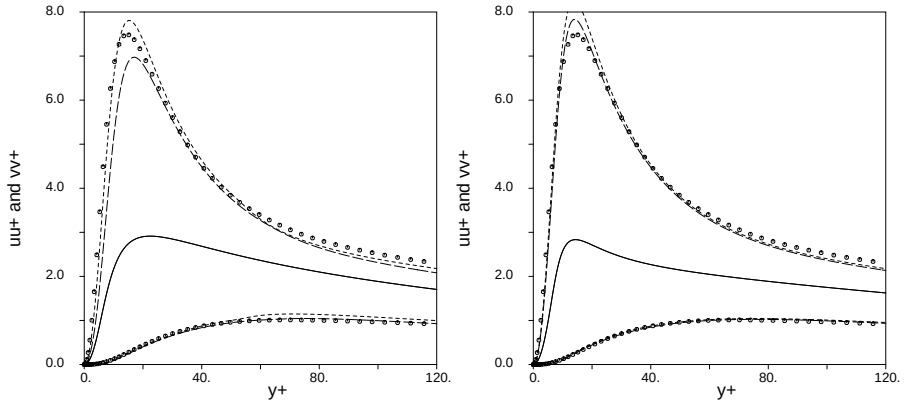

FIGURE 18. The normal Reynolds stresses in channel flow. Legends as in figure 14.

The rotating pipe flow discussed in section 2.2.1 was computed with these two models (K–ε and K–ω) as platforms for EARSM. Figures 6 and 7 show that differences are seen in a region close to the wall, where the K–ε based model shows a higher wall shear stress than the K–ω based model. The latter correctly captures the trend of a decreasing skin friction with increasing rate of rotation, whereas the K–ε based EARSM gives the opposite trend.

3.5. Alternative near-wall scaling. The damping function, f_1 given by equation (52), is formulated in terms of y^+. The scaling with the local wall skin friction is not valid in flows near separation and reattachment. Other possibilities than y^+ are $Re_y \equiv \sqrt{K}y/\nu$ or the turbulent Reynolds number $Re_t \equiv K^2/\nu\varepsilon$ (see e.g. Wilcox[47]).

The approach is here to formulate an alternative scaling y^* in terms of Re_y or Re_t so that $y^* \approx y^+$ for $y^+ \leq 100$ in channel flows. Re_y and Re_t were computed from DNS data at different Reynolds numbers ranging from $Re_\tau = 150$ to 650 in channel flows (Moser, Kim & Mansour[22]) and zero pressure gradient boundary layers (Spalart[37]). It was found that Re_y was increasing from the wall more linearly with less scattering compared to Re_t. Moreover, it should not pose any major problems to compute the wall distance y needed for Re_y if that is defined as the distance to the closest wall point. The following form for y^* is thus proposed:

$$y^* = C_{y1}\sqrt{Re_y} + C_{y2}Re_y^2. \tag{60}$$

The $\sqrt{Re_y}$-term is motivated by the fact that the near-wall asymptotic behaviour for Re_y is $\sim y^2$. The Re_y^2-term is artificially introduced to obtain a near linear relation in the buffer region also. With $C_{y1} = 2.4$ and $C_{y2} = 0.003$ good agreement with y^+ for channel and zero pressure gradient boundary layer flows at different Reynolds numbers is obtained, see figure 19.

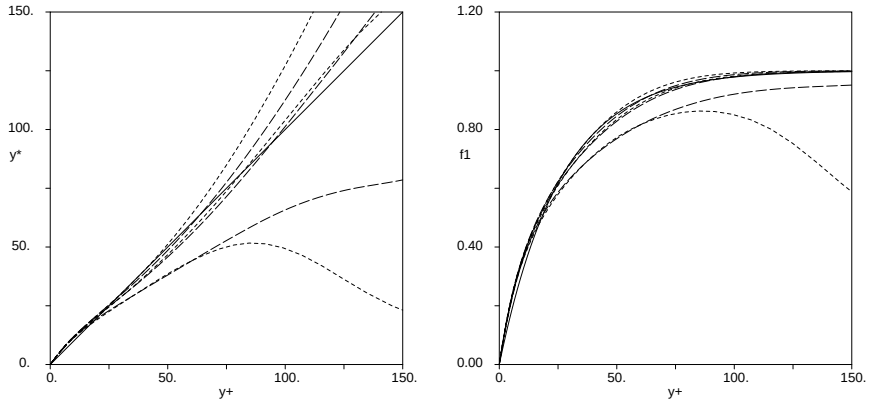

FIGURE 19. (left) The near-wall scaling y^* compared to y^+. (right) The damping function f_1 using y^* or y^+. The original form using y^+ (——) is compared to channel DNS data (Moser *et al.*[22]) at different Reynolds numbers $Re_\tau = 180$, 395 and 590 (– – –) and zero pressure gradient boundary layer DNS data (Spalart[37]) at $Re_\tau = 150$, 325 and 650 (·····). y^* increases with increasing Reynolds number.

In the damping function f_1, y^+ is then replaced by y^*

$$f_1 = 1 - \exp\left(-\frac{y^*}{A^+}\right). \tag{61}$$

In figure 19 the damping function f_1 based on y^* is compared to f_1 based on y^+. The correspondence is good except for the lowest Reynolds numbers.

In some situations the y^+ scaling may worsen the computational results. In a forthcoming study by M. Skote adverse pressure gradient boundary layers are studied by DNS. For the highest pressure gradient studied, with the pressure gradient similarity parameter $m = -0.25$ ($U_\infty \sim x^m$), the difference between the y^+ and y^* approaches are significant here, see figure 20. For this case it is obvious that the y^+ scaling degenerates the model performance and should be avoided.

In other cases, where the Reynolds number is higher, the near-wall scaling is not as critical. Figure 21 shows the computational results for the two-dimensional RAE2822 aerofoil profile using the proposed EARSM compared to the Wilcox[48] K–ω model. The flow in this case is compressible and the formulation is modified in a manner described in section 4. The EARSM approach clearly improves the position of the shock and the results are very much in line with differential Reynolds stress computations by Hellström, Davidsson & Rizzi[12] for exactly the same conditions and geometry.

The damping function in the EARSM is formulated in terms of y^+ as well as y^* and the figure shows no major differences between these approaches except in the separated region where the y^+ formulation gives a somewhat larger negative skin friction. In the figure a computation using the proposed EARSM

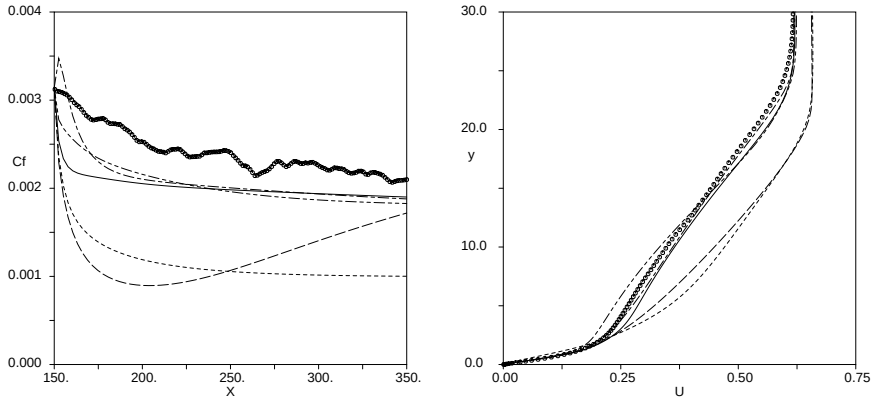

FIGURE 20. (left) The wall skin friction and (right) the velocity profile for an adverse pressure gradient boundary layer ($U_\infty \sim x^{-0.25}$). Computations with standard Wilcox[46] K–ω (– – –), Chien K–ε (———), EARSM based on K–ω and y^+ (·····) or y^* (——) and the Hanjalić[11] RST model (– – –). Comparisons with DNS data (∘), Skote (private communication).

without any damping functions whatsoever is also shown. For that choice, the standard Wilcox[46] K–ω, also without damping functions, must be used as the platform. This combination gives, however, incorrect near-wall behaviour for the turbulence quantities but the mean velocity profiles are well reproduced. That is also seen in the figure where no major differences between the EARSM with or without damping functions are present.

The convergence history is shown in figure 22 where we can see that there are no major differences in convergence rate. Actually, the proposed EARSM converges to a somewhat lower residual than the corresponding eddy-viscosity model for this case. The numerical parameters are the same for these two cases and the computational time for the 5000 iteration steps is 6% higher for the EARSM computation. This case was found to be not completely numerically stationary which results in the residual 'hanging' as for the K–ω model. The fluctuations are, however, very small and could not be seen in the solution. In other cases without separation the convergence curves are even closer to each other, and the convergence rates are in general faster than for the case shown in figure 22. The computational results were obtained using the EURANUS code[25] which is an explicit time-stepping multigrid and multiblock Navier–Stokes solver. The grid convergence was assessed by repeating the computation on a coarser grid.

A further example is a three-dimensional transonic supercritical wing (figure 23). This case is computed using the standard Wilcox[46] K–ω model and the EARSM based on that. Since that K–ω model has no damping functions the EARSM without damping functions must also be used for consistency. Again,

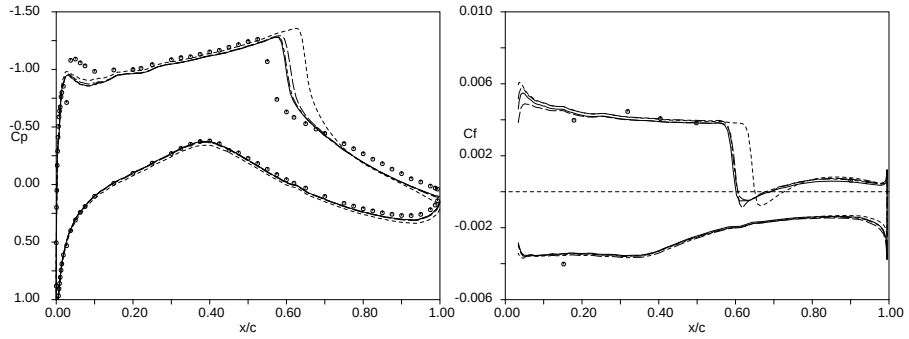

FIGURE 21. Wall pressure and skin friction coefficients for the RAE2822 wing profile ($M = 0.754$, $\alpha = 2.57^\circ$ and $Re = 6.2 \cdot 10^6$). Predictions using Wilcox[48] K–ω (------) and the current EARSM based on K–ω with damping function based on y^+ (– – –), y^* (——) or without any damping functions (–·–·–), compared to experimental data (∘) (Cook *et al.*[2]). The geometry is the measured one including a camber correction.

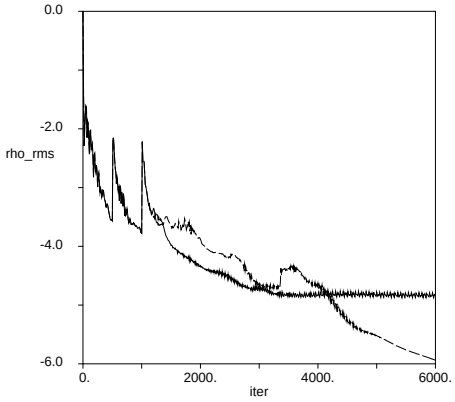

FIGURE 22. Convergence history for the RAE2822 wing profile. Wilcox K–ω (——) compared with the current EARSM based on K–ω (– – –). The computational time is increased by 6% by using EARSM. Three levels of full multigrid is used.

the predicted shock position is improved compared to the eddy-viscosity model. This case illustrates the benefit of the proposed model which is also viable in expensive three-dimensional cases, here with almost one million grid points. Most importantly, there is no substantial increase in the computational cost compared to the, in many cases, robust standard K–ω model.

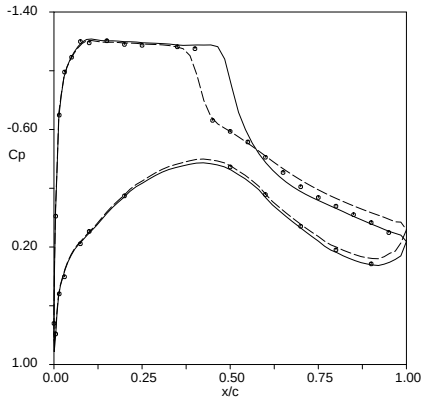

FIGURE 23. Wall pressure coefficient C_p for the LANN-wing ($M = 0.82$, $\alpha = 2.59^\circ$ and $Re = 5.4 \times 10^6$) at the spanwise position of 0.474. Predictions using Wilcox[46] K–ω (——) and the current EARSM (– – –) based on K–ω without wall damping functions. Comparison with experimental data (•) (Horsten *et al.*[13]).

4. Compressibility

Many turbulent flow applications are within the Mach number regime where compressible effects must be considered. Also, in low speed flow compressible effects may be important due to local heating or cooling of the flow. Compressible turbulent flow may be classified according to Friedrich[6] into flows with vanishing compressibility effects due to turbulent fluctuations and flows where such effects play a significant role. Friedrich[6] also states that compressibility effects due to turbulent fluctuations might be important in hypersonic, high Mach number, wall-bounded flows and in mixing layers at high convective Mach numbers. The understanding of such flows is poor and models capable of distinguishing the principal differences between wall-bounded and free shear flows are not well developed. The compressibility effects, due to turbulent fluctuations, increase the anisotropy of the Reynolds stress tensor (see Friedrich[6]) and depend themselves on the anisotropy, which means that algebraic Reynolds stress models are better suited than eddy viscosity models to act as a basis for improving the prediction of compressibility effects.

In wall-bounded flows with Mach numbers below 5 compressibility effects due to turbulent fluctuations may be neglected and the effect of compressibility enters into the problem essentially only through the mean flow compressibility. In this study we will restrict the attention to this class of flows and a straightforward compressibility extension of the incompressible model will be made.

First, the stress anisotropy and the turbulent kinetic energy must be redefined as $a_{ij} \equiv \overline{\rho u_i u_j}/\rho K - 2\delta_{ij}/3$ and $K \equiv \overline{\rho u_i u_i}/2\rho$ where ρ is the local mean density of the fluid. The trace of the strain is not zero for compressible flow. We may

instead use a somewhat redefined normalized strain rate tensor

$$S_{ij} \equiv \frac{\tau}{2}\left(U_{i,j} + U_{j,i}\right) - \frac{\mathcal{D}}{3}\delta_{ij}, \tag{62}$$

where the normalized dilatation of the mean flow is defined as $\mathcal{D} \equiv \tau U_{k,k}$.

The redefinition of $\mathbf{S}$ to have zero trace allows us to make use of the incompressible solution process. The redefinition also implies, however, that the S_{33}-component is non-zero for two-dimensional mean flow in the (x, y)-plane and that the simplifications for two-dimensional mean flow are not strictly valid for compressible flow. This will be addressed as a special case later in this section.

The general linear model of the LRR rapid pressure–strain rate model for incompressible flow does not have zero trace in compressible flow, so the model needs to be generalized according to Vandromme[44] and reads

$$\begin{aligned}\Pi_{ij}^{(r)} \;=\; & -\frac{c_2+8}{11}\left(\mathcal{P}_{ij} - \frac{2}{3}\mathcal{P}\delta_{ij}\right) - \frac{30c_2-2}{55}\rho K\left(U_{i,j} + U_{j,i} - \frac{2}{3}U_{l,l}\delta_{ij}\right) \\ & -\; \frac{8c_2-2}{11}\left(D_{ij} - \frac{2}{3}\mathcal{P}\delta_{ij}\right)\end{aligned} \tag{63}$$

where $\mathcal{P}_{ij} = -\overline{\rho u_i u_k}U_{j,k} - \overline{\rho u_j u_k}U_{i,k}$ and $D_{ij} = -\overline{\rho u_i u_k}U_{k,j} - \overline{\rho u_j u_k}U_{k,i}$. The incompressible models for the slow pressure–strain and the dissipation tensor can also be used here. The general ARSM for compressible flow can now be written as

$$\begin{aligned}\left(c_1 - 1 - \frac{6c_2+4}{11}\mathcal{D} - \mathrm{tr}\{\mathbf{aS}\}\right)\mathbf{a} \;=\; & -\frac{8}{15}\mathbf{S} + \frac{7c_2+1}{11}\left(\mathbf{a\Omega} - \mathbf{\Omega a}\right) \\ & -\; \frac{5-9c_2}{11}\left(\mathbf{aS} + \mathbf{Sa} - \frac{2}{3}\mathrm{tr}\{\mathbf{aS}\}\mathbf{I}\right)\end{aligned} \tag{64}$$

which is identical to the incompressible form, equation (13), except for the dilatation term 0n the left-hand side and the different definitions given above. The same conclusion is valid for the simplified equation obtained by setting $c_2 = 5/9$, which reads

$$\left(c_1 - 1 - \frac{2}{3}\mathcal{D} - \mathrm{tr}\{\mathbf{aS}\}\right)\mathbf{a} = -\frac{8}{15}\mathbf{S} + \frac{4}{9}\left(\mathbf{a\Omega} - \mathbf{\Omega a}\right). \tag{65}$$

The solution of the simplified compressible ARSM equation is the same as the incompressible solution except for the definition of the c_1'-coefficient, which for the compressible case is

$$c_1' = \frac{9}{4}\left(c_1 - 1 - \frac{2}{3}\mathcal{D}\right) \tag{66}$$

bearing in mind that S_{ij} here is defined by (62).

4.1. Compressible two-dimensional mean flow. An approximation of the compressible ARSM equation can be derived by an expansion around a solution obtained by use of the two-dimensional simplification valid in incompressible flow. Let us first define a compressible two-dimensional strain rate as $S_{ij}^{2D} \equiv (\tau/2)\left(U_{i,j} + U_{j,i}\right) - \mathcal{D}\delta_{ij}^{2D}/2$ where $\delta_{ij}^{2D} \equiv \delta_{ij}$ except that $\delta_{33}^{2D} = 0$. The compressible ARSM, equation (65), can now be written as

$$\left(c_1 - 1 - \frac{2}{3}\mathcal{D} - \mathrm{tr}\{\mathbf{a}^{2D}\mathbf{S}^{2D}\}\right)\mathbf{a}^{2D} = -\frac{8}{15}\mathbf{S}^{2D} + \frac{4}{9}\left(\mathbf{a}^{2D}\boldsymbol{\Omega} - \boldsymbol{\Omega}\mathbf{a}^{2D}\right) \tag{67}$$

with the solution $\mathbf{a}^{2D}$, which is derived using the two-dimensional solution process for incompressible flow. The true anisotropy, $\mathbf{a}$, is then related to the solution $\mathbf{a}^{2D}$, as described below.

The difference between $\mathbf{S}$ and $\mathbf{S}^{2D}$ is of $\mathcal{O}(\mathcal{D})$ which can be assumed small except in a shock wave. For the same reason the difference between $\mathbf{a}$ and $\mathbf{a}^{2D}$ can also be assumed to be of $\mathcal{O}(\mathcal{D})$ and with the simplest tensorial form that relates the two-dimensional and three-dimensional anisotropies, leading to the following assumption. Let

$$\mathbf{a} = \mathbf{a}^{2D} + \beta_a \mathcal{D}\left(\mathbf{I}^{2D} - \frac{2}{3}\mathbf{I}\right) + \mathcal{O}\left(\mathcal{D}^2\right), \tag{68}$$

and subtract equation (67) from equation (65). Sorting terms in powers of $\mathcal{D}$ gives us the first-order solution in $\mathcal{D}$

$$\beta_a = -\frac{4}{15\left(c_1 - 1 - \mathrm{tr}\{\mathbf{a}^{2D}\mathbf{S}^{2D}\}\right)}. \tag{69}$$

In obtaining this solution the following relations have been used:

$$\begin{aligned} \mathbf{S}^{2D} &= \mathbf{S} - \frac{\mathcal{D}}{2}\left(\mathbf{I}^{2D} - \frac{2}{3}\mathbf{I}\right) \\ \mathrm{tr}\{\mathbf{a}^{2D}\mathbf{S}^{2D}\} &= \mathrm{tr}\{\mathbf{a}\mathbf{S}\} + \mathcal{O}\left(\mathcal{D}^2\right) \\ \mathbf{a}^{2D}\boldsymbol{\Omega} - \boldsymbol{\Omega}\mathbf{a}^{2D} &= \mathbf{a}\boldsymbol{\Omega} - \boldsymbol{\Omega}\mathbf{a} + \mathcal{O}\left(\mathcal{D}^2\right). \end{aligned} \tag{70}$$

The zeroth-order solution, $\mathbf{a}^{2D}$, is obtained as described for the incompressible case, with the only difference being that c_1' is now given by (66). The full solution is then given by

$$\mathbf{a} = \beta_1\mathbf{S}^{2D} + \beta_4\left(\mathbf{S}^{2D}\boldsymbol{\Omega} - \boldsymbol{\Omega}\mathbf{S}^{2D}\right) + \beta_a\mathcal{D}\left(\mathbf{I}^{2D} - \frac{2}{3}\mathbf{I}\right) + \mathcal{O}\left(\mathcal{D}^2\right) \tag{71}$$

with β_a from (69).

4.2. Shock/boundary layer interaction. The compressible form of the proposed model together with the near-wall formulations has been tested on a shock/boundary layer interaction. A turbulent boundary layer at Mach 5 on a flat plate interacts with an oblique shock from a shock generator above the plate, see figure 24. The flow deflection angle is 10° which gives a strong enough

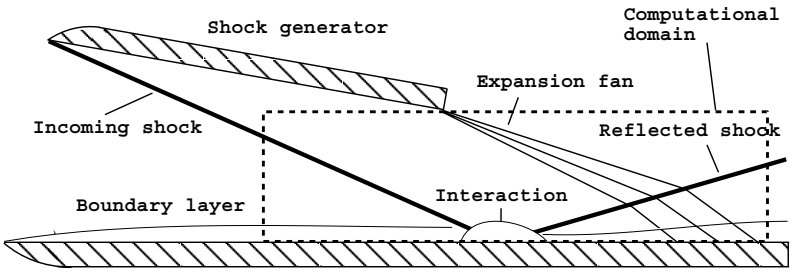

FIGURE 24. Impinging shock at Mach 5. Experimental and computational setup.

shock to cause a boundary layer separation. The experiment by Schülein, Krogmann & Stanewsky[29] was performed at DLR in Göttingen. Figure 25 shows the computed wall pressure and skin friction coefficient along the flat plate compared to the experimental data. The turbulence models used are the Chien[1] K–ε model and the Wilcox[48] K–ω model based on the original eddy-viscosity assumption and also based on the proposed EARSM. The computational results were obtained using the EURANUS code[25]. The grid convergence was assessed by repeating the computation on a coarser grid.

The size of the separated region is underestimated by the two eddy viscosity models whereas a correct separation length is obtained when the models are based on the proposed EARSM. This can be seen both in the skin friction behaviour and in the wall pressure distribution. The computed wall pressure is, however, somewhat shifted downstream.

The Chien K–ε model strongly over-predicts the skin friction downstream of the reattachment point, which is typical for many low Reynolds number K–ε models. This behaviour is inherited by the proposed EARSM based on the Chien K–ε model. The K–ω models give much better skin friction predictions.

5. Diffusion term

In regions of the flow where the production to dissipation ratio is small, the assumption of negligible effects of advection and diffusion of the anisotropy may cause problems, also noticed by Taulbee[41]. In the outer-most part of a boundary layer and in the centre of a turbulent channel flow the magnitude of the β_1 coefficient may thus be too large leading to an overestimation of the $\overline{uv}$ Reynolds stress. The behaviour of the model can be analysed by looking at the effective $C_\mu^{\text{eff}} \equiv -\beta_1/2$ when the strain rate goes to zero, which for the simplified ARSM reads

$$C_\mu^{\text{eff}}\,(\sigma \to 0) = \frac{3}{5c_1'}. \tag{72}$$

For the proposed model constants $C_\mu^{\text{eff}} \approx 0.33$ which is far too high.

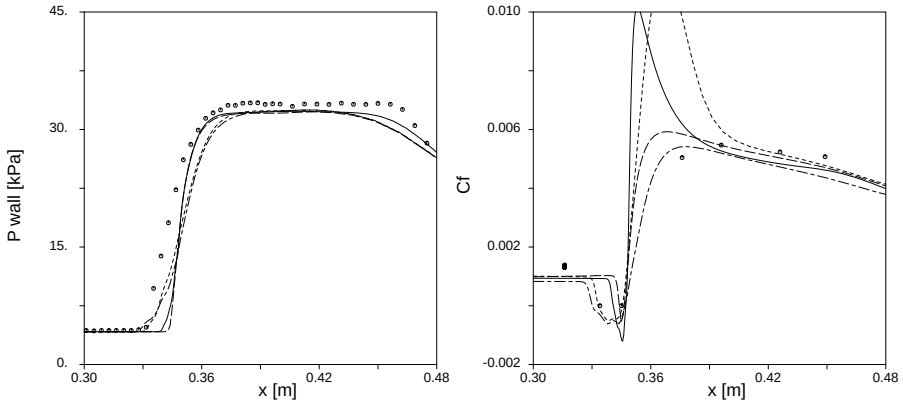

FIGURE 25. (left) Wall pressure and (right) skin friction coefficient for the impinging shock at Mach 5 with the flow deflection angle $\beta = 10^\circ$. Comparison of the predictions using Chien K–ε (——), Wilcox K–ω (– – –) and the current EARSM based on K–ε (------) and K–ω (–·–·) with the experiment by Schülein *et al.*[29] (⊙).

In this section we will discuss the possibility of including a correction to the ARSM equations formulated so that the proposed EARSM solution process can be retained. The transport equation for the Reynolds stress anisotropy is given by (1) where T_{ijl} and $T_l^{(K)}$ are the flux terms for the Reynolds stress tensor and turbulent kinetic energy. A simple model for the neglected diffusion term may be written as

$$\frac{\partial T_{ijl}}{\partial x_l} - \frac{\overline{u_i u_j}}{K}\frac{\partial T_l^{(K)}}{\partial x_l} = C_D a_{ij}\frac{\partial T_l^{(K)}}{\partial x_l}, \tag{73}$$

which gives a modification of the c_1'-coefficient in the simplified ARSM equation (21). The modified coefficient reads

$$c_1' = \frac{9}{4}\left(c_1 - 1 - \frac{C_D}{\varepsilon}\frac{\partial T_l^{(K)}}{\partial x_l}\right). \tag{74}$$

There are, however, numerical problems associated with this form due to the inclusion of the second derivative of K. This could be avoided if the term that balances the turbulent flux term in the K-equation (15) is used to approximate the turbulent flux of K:

$$\frac{\partial T_l^{(K)}}{\partial x_l} \approx \mathcal{P} - \varepsilon. \tag{75}$$

The advection of K is neglected here. Moreover, the extra term worsens the model behaviour for large strain rates and can even lead to a singular behaviour. The correction thus needs to be switched off for $\mathcal{P}/\varepsilon > 1$. The definition of the

c_1'-coefficient then becomes

$$c_1' = \frac{9}{4}\left[c_1 - 1 + C_D \max\left(1 - \frac{\mathcal{P}}{\varepsilon}, 0\right)\right]. \tag{76}$$

The problem with this form is that it is implicit in the $\mathcal{P}/\varepsilon$ ratio and that the max function makes it impossible to solve. The diffusion model will thus be further approximated by using $\mathcal{P}/\varepsilon = -\beta_1 II_S$. If β_1 is approximated with β_1^{eq} where $\mathcal{P} = \varepsilon$, the correction is guaranteed to be zero in the log-layer and for higher strain rates. The definition of the c_1'-coefficient now becomes

$$c_1' = \frac{9}{4}\left[c_1 - 1 + C_D \max\left(1 + \beta_1^{\text{eq}} II_S, 0\right)\right] \tag{77}$$

where

$$\beta_1^{\text{eq}} = -\frac{6}{5}\frac{N^{\text{eq}}}{\left(N^{\text{eq}}\right)^2 - 2II_\Omega} \tag{78}$$

and

$$N^{\text{eq}} = \frac{9c_1}{4}. \tag{79}$$

The constant C_D can now be estimated by looking at the effective C_μ for zero strain rates in (72). With $C_D = 2.2$ the effective C_μ becomes $C_\mu^{\text{eff}} = 0.09$ which is close to what one should expect. The a_{12} anisotropy with the proposed diffusion model is compared to the basic EARSM in figure 26 for parallel flow (cf. figure 4). The inclusion of the diffusion model makes the proposed EARSM behave almost the same as the SST model for this case. In figure 27 we can see an improvement of the a_{12} anisotropy prediction near the centre of the channel simulated by Kim[16]. The actual difference in the predicted mean velocity profile is quite small. This improvement is similar in character to that obtained by the correction introduced by Taulbee[41] although the two approaches are motivated differently.

The derivation of the diffusion correction is based on a number of *ad hoc* arguments and should be seen only as a possible extension of the model to flow situations where diffusion may be of substantial importance.

6. Concluding remarks

For two-dimensional mean flows the new proposed EARSM represents an exact solution of the implicit ARSM relation for the anisotropy tensor, but also a good approximation for three-dimensional mean flows. The fact that it fully accounts for three-dimensional effects gives it a natural predictive capability for complex flows. This was demonstrated here by capturing the correct trends for axially rotating pipe flow. Standard two-equation models predict a solid-body rotation with an unaffected axial velocity profile. In reality the azimuthal velocity has a variation that is close to parabolic and the rotation causes the axial velocity profile to be less full, i.e. more parabolic. To capture these features the model description of the inter-component transfer is crucial. For instance, the simplified

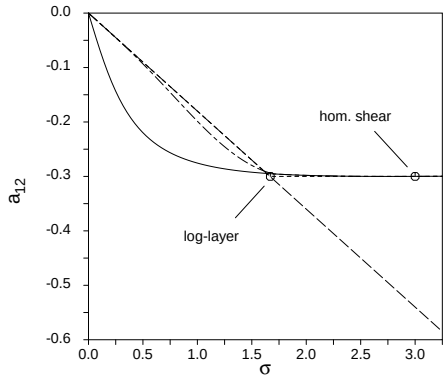

FIGURE 26. The a_{12} anisotropy versus strain rate σ for parallel flow. The current model without (——) and with (– – –) diffusion model compared to an eddy-viscosity model (– – –) and the Menter[20] SST model (·····).

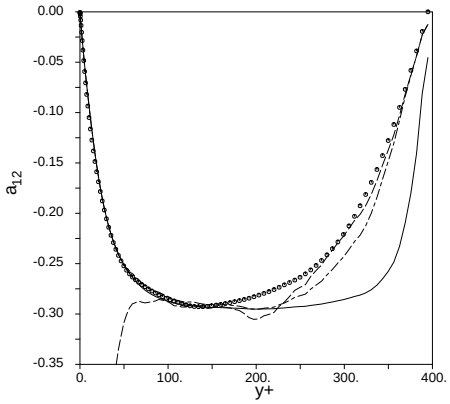

FIGURE 27. The a_{12} anisotropy in channel flow. Comparison of the current EARSM without (——) and with (– – –) diffusion model with the eddy-viscosity model (– – –) and DNS data (◦) by Kim[16].

linear rapid pressure–strain model of Launder *et al.*[17] and Naot, Shavit & Wolfstein[23], usually referred to as the isotropization of production model, does not have the necessary ingredients. The full linear model, on the other hand, together with linear models for the other terms, was demonstrated here to be sufficient to capture the main features of the flow in the axially rotating pipe. In general the predictive capability of the proposed EARSM for rotating flows is substantially better than standard two-equation models and than EARSM formulations including only terms up to second order in $\mathbf{S}$ and $\mathbf{\Omega}$.

The extension to compressible flows is done in a simple way in the present EARSM in which the equations are expressed by use of Favre averages. Compressibility of the mean flow is accounted for, but no explicit compressibility

corrections are added to the 'platform' (K–ε, K–ω ...) equations. With some minor redefinitions the same ARSM relation for a_{ij} as for incompressible flow could be used also here. This approach for wall-bounded turbulent flows is adequate for Mach numbers up to about 5. It was shown to capture the essential features of the complex interaction between an inclined shock and a turbulent boundary layer at Mach 5. In particular it describes the skin friction and separation length much better than standard two-equation models. Compared to the standard two-equation models on which the present EARSM is based it also gives a substantial improvement for the prediction of the skin friction variation in incompressible boundary layers with adverse pressure gradient (detailed results not reported here).

Poor prediction of the effects of rotation and the under-prediction of separation tendency in adverse pressure gradient boundary layers are well known deficiencies of closures based on the eddy-viscosity hypothesis. The present EARSM substantially improves these two aspects, and reduces the need for wall damping. A simple way to obtain the correct near-wall limits of the anisotropies was constructed here on the basis of a van Driest type of damping function. For channel flow this was shown to give a very accurate description, and a simple method to retain numerical stability for situations with separated flows was demonstrated. A form of wall damping function based on $Re_y \equiv \sqrt{K}y/\nu$ was shown to be an attractive alternative to forms based on y^+ in flows with (or near) separation.

The reduced need for wall damping is coupled to the fact that the present EARSM automatically predicts a production to dissipation ratio with correct asymptotic behaviour for large strain rates. For instance, in parallel flows this correctly gives an asymptotically constant shear stress anisotropy component for large strains (shear rates). This behaviour is not a natural part of eddy-viscosity based models, but was incorporated in a somewhat *ad hoc* manner by Menter[21]. In the present model this behaviour emanates naturally from the underlying modelling of the terms in the RST equations and the direct solution of the production to dissipation ratio.

To further illustrate the behaviour for large strain rates the proposed model was tested in homogeneous shear flow at high initial shear rate. The good predictions that was obtained for this case can, however, be regarded as a bit fortuitous in the light of the fact that the basic ARSM approximation is somewhat questionable for a case with a significantly non-zero left-hand side of the a_{ij} transport equation ($\partial a_{ij}/\partial t \neq 0$). Moreover, the Launder *et al.*[17] model does not give accurate predictions of this case when used in a differential form. It is, however, a fact that the self-consistent approach (i.e where the production to dissipation ratio is solved for as part of the total EARSM-solution) gives a model with the correct asymptotic behaviour, which is a pre-requisite for reasonable predictions in the limit of high shear. The present model is not constructed specifically to

incorporate such effects. It is, however, an important step towards a more general engineering model that the model is also able to give reasonable results in extreme flow cases.

Perhaps the most important feature of the proposed model is the numerical behaviour. The computational cost is not significantly increased compared to standard eddy-viscosity two-equation models and the general numerical behaviour is almost the same. Implementation of this model into flow solvers with existing eddy-viscosity two-equation models should not pose major problems. The model may be formulated in terms of an effective eddy viscosity with an additional correction that may be treated fully explicitly (see Appendix A).

The authors would like to thank Dr Torbjörn Sjögren and Dr Magnus Hallbäck for many helpful discussions, especially concerning the treatment of rotating coordinate systems. The first author would also like to thank Dr Sharath Girimaji for many helpful discussions, especially concerning non-equilibrium turbulence. The authors gratefully acknowledge funding of this study from the European Space Agency within a project for improving the modelling of turbulent flows related to hypersonic lifting vehicles and would like to acknowledge Dr Ingemar Lindblad for leading this project.

Appendix A. Summary of the proposed model

The Reynolds stresses may be written in terms of an effective C_μ-coefficient which is mathematically identical with the formulation in section 2:

$$\overline{u_i u_j} = K\left(\frac{2}{3}\delta_{ij} - 2C_\mu^{\text{eff}} S_{ij} + a_{ij}^{(\text{ex})}\right), \tag{80}$$

where the effective C_μ-coefficient is

$$C_\mu^{\text{eff}} = -\frac{1}{2} f_1 \left(\beta_1 + I\!I_\Omega \beta_6\right), \tag{81}$$

and the extra anisotropy $a_{ij}^{(\text{ex})}$ then becomes

$$\begin{aligned}
\mathbf{a}^{(\text{ex})} \;=\; & \left(1 - {f_1}^2\right) \frac{3B_2 - 4}{\max\left(I\!I_S, I\!I_S^{\text{eq}}\right)} + f_1^2 \beta_3 \left(\mathbf{\Omega}^2 - \frac{1}{3} I\!I_\Omega \, \mathbf{I}\right)\left(\mathbf{S}^2 - \frac{1}{3} I\!I_S \, \mathbf{I}\right) \\
& + \left({f_1}^2 \beta_4 - \left(1 - {f_1}^2\right) \frac{B_2}{2\max\left(I\!I_S, I\!I_S^{\text{eq}}\right)}\right)\left(\mathbf{S\Omega} - \mathbf{\Omega S}\right) \\
& + f_1 \beta_6 \left(\mathbf{S\Omega}^2 + \mathbf{\Omega}^2\mathbf{S} - I\!I_\Omega \mathbf{S} - \frac{2}{3} I\!V \, \mathbf{I}\right) + f_1^2 \beta_9 \left(\mathbf{\Omega S \Omega}^2 - \mathbf{\Omega}^2 \mathbf{S \Omega}\right).
\end{aligned} \tag{82}$$

Here $\mathbf{a}$, $\mathbf{S}$ and $\mathbf{\Omega}$ denote second rank tensors, tr$\{\}$ denotes the trace and $\mathbf{I}$ is the identity matrix. The inner product of two matrices is defined as $(\mathbf{SS})_{ij} \equiv \left(\mathbf{S}^2\right)_{ij} \equiv S_{ik} S_{kj}$. The normalized mean strain and rotation tensors are defined

as

$$S_{ij} = \frac{\tau}{2}\left(U_{i,j} + U_{j,i}\right), \qquad \Omega_{ij} = \frac{\tau}{2}\left(U_{i,j} - U_{j,i}\right), \tag{83}$$

where the turbulent timescale is defined by

$$\tau = \max\left(\frac{K}{\varepsilon}, C_\tau\sqrt{\frac{\nu}{\varepsilon}}\right). \tag{84}$$

The invariants are defined by

$$II_S = \mathrm{tr}\{\mathbf{S}^2\}, \quad II_\Omega = \mathrm{tr}\{\mathbf{\Omega}^2\}, \quad IV = \mathrm{tr}\{\mathbf{S\Omega}^2\}, \quad V = \mathrm{tr}\{\mathbf{S}^2\mathbf{\Omega}^2\}, \tag{85}$$

and

$$II_S^{\mathrm{eq}} = \frac{405c_1^2}{216c_1 - 160}. \tag{86}$$

By introducing an effective C_μ-coefficient one can easily introduce this level of modelling into flow solvers with existing two-equation eddy-viscosity models by setting

$$\nu_t = C_\mu^{\mathrm{eff}} K\tau. \tag{87}$$

The contribution from the extra anisotropy $a_{ij}^{(\mathrm{ex})}$ may now be added as fully explicit additional terms in the equations.

The β-coefficients are given by

$$\begin{aligned} \beta_1 &= -\frac{N\left(2N^2 - 7II_\Omega\right)}{Q}, \quad \beta_3 = -\frac{12N^{-1}IV}{Q}, \\ \beta_4 &= -\frac{2\left(N^2 - 2II_\Omega\right)}{Q}, \qquad \beta_6 = -\frac{6N}{Q}, \qquad\quad \beta_9 = \frac{6}{Q}, \end{aligned} \tag{88}$$

with the denominator

$$Q = \frac{5}{6}\left(N^2 - 2II_\Omega\right)\left(2N^2 - II_\Omega\right). \tag{89}$$

For most purposes it is sufficient to take $N = N_c$ where

$$N_c = \begin{cases} \dfrac{c_1'}{3} + \left(P_1 + \sqrt{P_2}\right)^{1/3} + \mathrm{sign}\left(P_1 - \sqrt{P_2}\right) \mid P_1 - \sqrt{P_2} \mid^{1/3}, & P_2 \geq 0 \\ \dfrac{c_1'}{3} + 2\left(P_1^2 - P_2\right)^{1/6} \cos\left(\dfrac{1}{3}\arccos\left(\dfrac{P_1}{\sqrt{P_1^2 - P_2}}\right)\right), & P_2 < 0 \end{cases} \tag{90}$$

with

$$P_1 = \left(\frac{{c_1'}^2}{27} + \frac{9}{20}II_S - \frac{2}{3}II_\Omega\right)c_1', \quad P_2 = P_1^2 - \left(\frac{{c_1'}^2}{9} + \frac{9}{10}II_S + \frac{2}{3}II_\Omega\right)^3 \tag{91}$$

and

$$c_1' = \frac{9}{4}\left(c_1 - 1\right). \tag{92}$$

An additional term can be added to N_c in order to improve the accuracy for three-dimensional mean flows (see section 2.2).

The simplifications for two-dimensional mean flow are

$$\beta_1 = -\frac{6}{5}\frac{N_c}{N_c^2 - 2II_\Omega}, \quad \beta_4 = -\frac{6}{5}\frac{1}{N_c^2 - 2II_\Omega}, \quad \beta_3 = \beta_6 = \beta_9 = 0. \tag{93}$$

The damping function reads

$$f_1 = 1 - \exp\left(-C'_{y1}\sqrt{Re_y} - C'_{y2}Re_y^2\right), \tag{94}$$

where

$$Re_y = \frac{\sqrt{K}y}{\nu}. \tag{95}$$

Finally, the five model constants are

$$C_\tau = 6.0, \quad c_1 = 1.8, \quad B_2 = 1.8, \quad C'_{y1} = \frac{2.4}{26.0}, \quad C'_{y2} = \frac{0.003}{26.0}. \tag{96}$$

Appendix B. The completeness of the $\mathbf{a}(\mathbf{S}, \mathbf{\Omega})$ expression with ten terms

Based on the derivations of Spencer & Rivlin[38] for matrix polynomials Pope[24] concluded that there are ten independent terms in the complete expression $\mathbf{a}(\mathbf{S}, \mathbf{\Omega})$. One should here restrict the meaning of independence to polynomial independence as was also pointed out by Taulbee, Sonnenmeier & Wall[42]. The highest-order term $\left(\mathbf{\Omega S}^2\mathbf{\Omega}^2 - \mathbf{\Omega}^2\mathbf{S}^2\mathbf{\Omega}\right)$ in expression (18) is of order 5 and extension 3.

The $\mathbf{S}$ and $\mathbf{\Omega}$ tensors can appear in powers up to 2. A term $\mathbf{S}^m\mathbf{\Omega}^n$ is then said to be of power $m + n$ and extension 2, etc. Shih & Lumley[34] (see also Shih[33]) also include a term of power 6 and extension 4. They use a notation with the mean velocity gradient tensor and its transpose, but with the present notation such a term can be written as

$$\mathbf{S\Omega}^2\mathbf{S}^2\mathbf{\Omega} - \mathbf{\Omega S}^2\mathbf{\Omega}^2\mathbf{S} - \frac{2}{3}VI\ \mathbf{I}, \tag{97}$$

where the invariant VI equals $\mathrm{tr}\{\mathbf{S\Omega}^2\mathbf{S}^2\mathbf{\Omega}\}$. One may first note that the invariant VI is of third power in $\mathbf{\Omega}$, which means that it cannot be expressed in terms of a polynomial in the other invariants, which are of order zero or two in $\mathbf{\Omega}$. Hence, VI contains sign information that is not contained in the other invariants. We can derive the following relation for its square:

$$VI^2 = \frac{{II_\Omega}^3}{144}\left(9{II_S}^3 + 2{III_S}^2\right) + \frac{{II_\Omega}^2}{6}\left(-3V{II_S}^2 + IV\ II_S\ III_S\right)$$
$$+\frac{II_\Omega}{8}\left(10\,V^2 II_S - 4V\,IV\ III_S - IV^2{II_S}^2\right) - V^3 + \frac{1}{2}V\,IV^2 II_S - \frac{1}{3}IV^3 III_S.$$

In the present modelling the invariant VI will not appear since it would arise from the product of the highest (fifth-order) term and $\mathbf{S}$, and even in the general solution (for $c_2 \neq 5/9$) the coefficient $\beta_{10} = 0$.

We can furthermore express the sixth-order term as the following combination of lower-order terms

$$\mathbf{S\Omega}^2\mathbf{S}^2\mathbf{\Omega} - \mathbf{\Omega}\mathbf{S}^2\mathbf{\Omega}^2\mathbf{S} - \frac{2}{3}VI\ \mathbf{I} = \left(\frac{2}{3}V + \frac{1}{12}II_S II_\Omega\right)(\mathbf{S\Omega} - \mathbf{\Omega S})$$
$$+\tfrac{1}{3}IV\left(\mathbf{S}^2\mathbf{\Omega} - \mathbf{\Omega}\mathbf{S}^2\right) - \tfrac{1}{6}II_\Omega\left(\mathbf{S\Omega}\mathbf{S}^2 - \mathbf{S}^2\mathbf{\Omega}\mathbf{S}\right) + \tfrac{1}{6}II_S\left(\mathbf{\Omega}\mathbf{S}\mathbf{\Omega}^2 - \mathbf{\Omega}^2\mathbf{S}\mathbf{\Omega}\right).$$

By use of the generalized Cayley–Hamilton theorem it is fairly straightforward to show that no other independent sixth- or higher-order term exists (see e.g. Shih & Lumley[34].

Appendix C. Solution of the general quasi-linear ARSM equation

The implicit general quasi-linear ARSM equation is rewritten similarly to the simplified equation (21)

$$N\mathbf{a} = -A_1\mathbf{S} + (\mathbf{a\Omega} - \mathbf{\Omega a}) - A_2\left(\mathbf{aS} + \mathbf{Sa} - \frac{2}{3}\mathrm{tr}\{\mathbf{aS}\}\right), \tag{98}$$

where

$$N = A_3 + A_4\frac{\mathcal{P}}{\varepsilon}. \tag{99}$$

The simplified equation is now a special case of (98) with the coefficients $A_1 = 6/5$, $A_2 = 0$, $A_3 = c_1'$ and $A_4 = 9/4$. For the general case we require that A_1, A_3 and A_4 are positive.

C.1. Solution for two-dimensional mean flow. The solution for two-dimensional mean flow is

$$\beta_1 = -\frac{A_1 N}{Q}, \quad \beta_2 = 2\frac{A_1 A_2}{Q}, \quad \beta_4 = -\frac{A_1}{Q}, \tag{100}$$

where the denominator

$$Q = N^2 - 2II_\Omega - \frac{2}{3}A_2^2 II_S. \tag{101}$$

The equation for N is, for two-dimensional mean flow,

$$N^3 - A_3N^2 - \left(\left(A_1A_4 + \frac{2}{3}A_2^2\right)II_S + 2II_\Omega\right)N + 2A_3\left(\frac{1}{3}A_2^2 II_S + II_\Omega\right) = 0, \tag{102}$$

with the solution

$$N = \begin{cases} \dfrac{A_3}{3} + \left(P_1 + \sqrt{P_2}\right)^{1/3} + \mathrm{sign}\left(P_1 - \sqrt{P_2}\right) \mid P_1 - \sqrt{P_2} \mid^{1/3}, & P_2 \geq 0 \\ \dfrac{A_3}{3} + 2\left(P_1^2 - P_2\right)^{1/6}\cos\left(\dfrac{1}{3}\arccos\left(\dfrac{P_1}{\sqrt{P_1^2 - P_2}}\right)\right), & P_2 < 0 \end{cases} \tag{103}$$

where

$$P_1 = \left(\frac{{A_3}^2}{27} + \left(\frac{A_1A_4}{6} - \frac{2}{9}{A_2}^2\right)II_S - \frac{2}{3}II_\Omega\right)A_3 \tag{104}$$

and

$$P_2 = P_1^2 - \left(\frac{{A_3}^2}{9} + \left(\frac{A_1 A_4}{3} + \frac{2}{9} {A_2}^2 \right) I\!I_S + \frac{2}{3} I\!I_\Omega \right)^3 . \tag{105}$$

Let us investigate whether the denominator in equation (101) can become zero. Equation (102) can be rewritten, by using equation (101), as

$$Q\,(N - A_3) = A_1 A_4 I\!I_S N, \tag{106}$$

which shows that $Q > 0$ if $N > A_3$. The problem is then to show that $N > A_3$. Let us first look at the special case when $I\!I_S = 0$. Equation (102) can then be written

$$(N - A_3)\left(N^2 - 2I\!I_\Omega\right) = 0, \tag{107}$$

with the only real root $N = A_3$. Differentiating equation (102) with respect to $I\!I_S$ gives

$$\frac{\partial N}{\partial I\!I_S} = \frac{\frac{2}{3} A_2^2\,(N - A_3) + A_1 A_4 N}{3\left(N - \frac{2}{3} A_3\right) N - \left(A_1 A_4 + \frac{2}{3} A_2^2\right) I\!I_S - 2I\!I_\Omega}, \tag{108}$$

which is positive if $N \geq A_3$. When $I\!I_S = 0$ (108) can be written as

$$\left.\frac{\partial N}{\partial I\!I_S}\right|_{I\!I_S = 0} = \frac{A_1 A_3 A_4}{A_3^2 - 2I\!I_\Omega} > 0. \tag{109}$$

So far we know that $N = A_3$ for $I\!I_S = 0$ and that N increases until (108) changes sign. By using (102) $I\!I_\Omega$ can be eliminated in (108) which then becomes

$$\frac{\partial N}{\partial I\!I_S} = \frac{\frac{2}{3} A_2^2\,(N - A_3)^2 + A_1 A_4 N\,(N - A_3)}{2N\,(N - A_3)^2 + A_1 A_3 A_4 I\!I_S}. \tag{110}$$

From this form it is obvious that the denominator is strictly positive and that $\partial N / \partial I\!I_S = 0$ for $I\!I_S = 0$ only (where $N = A3$). Hence, the numerator is strictly positive and N increases for all $I\!I_S$, showing that $N \geq A_3$ for all $I\!I_S$. The corresponding relation for the simplified ARSM equation is $N \geq c_1'$.

The denominator Q is thus always positive which guarantees a non-singular solution.

C.2. Solution for three-dimensional mean flow. The solution of the linear equation system where N is assumed as known can be formulated as (see Gatski & Speziale[7])

$$N\beta_\lambda = -A_1 \delta_{1\lambda} + \sum_\gamma J_{\lambda\gamma}\beta_\gamma - A_2 \sum_\gamma H_{\lambda\gamma}\beta_\gamma \tag{111}$$

or in the standard form for linear equation systems

$$\left(N\delta_{\gamma\lambda} - J_{\gamma\lambda} + A_2 H_{\gamma\lambda}\right)\beta_\lambda = -A_1 \delta_{1\gamma} \tag{112}$$

where the matrixes are given below for three-dimensional mean flow

$$\mathbf{H} = \begin{bmatrix} 0 & \frac{1}{3}II_S & -\frac{2}{3}II_\Omega & 0 & 0 & \frac{2}{3}IV & -\frac{1}{3}V & 0 & 0 & 0 \\ 2 & 0 & 0 & 0 & 0 & 2II_\Omega & IV & 0 & 0 & 0 \\ 0 & 0 & 0 & 0 & 0 & II_S & \frac{1}{3}III_S & 0 & 0 & 0 \\ 0 & 0 & 0 & 0 & \frac{1}{2}II_S & 0 & 0 & \frac{1}{3}III_S & -IV & -\frac{1}{3}V - \frac{1}{6}II_S II_\Omega \\ 0 & 0 & 0 & 1 & 0 & 0 & 0 & 0 & -II_\Omega & -\frac{2}{3}IV \\ 0 & 0 & 1 & 0 & 0 & 0 & \frac{1}{2}II_S & 0 & 0 & 0 \\ 0 & 0 & 0 & 0 & 0 & -1 & 0 & 0 & 0 & 0 \\ 0 & 0 & 0 & 0 & -1 & 0 & 0 & 0 & 0 & \frac{1}{3}II_\Omega \\ 0 & 0 & 0 & 0 & 0 & 0 & 0 & 0 & 0 & -\frac{1}{3}II_S \\ 0 & 0 & 0 & 0 & 0 & 0 & 0 & 0 & -2 & 0 \end{bmatrix}, \tag{113}$$

$$\mathbf{J} = \begin{bmatrix} 0 & 0 & 0 & -II_\Omega & 0 & 0 & 0 & 2V - II_S II_\Omega & II_\Omega^2 & 0 \\ 0 & 0 & 0 & 0 & -II_\Omega & 0 & 0 & -2IV & 0 & II_\Omega^2 \\ 0 & 0 & 0 & 0 & -2II_S & 0 & 0 & 0 & -2IV & 2II_S II_\Omega - 2V \\ 1 & 0 & 0 & 0 & 0 & \frac{1}{2}II_\Omega & 0 & 0 & 0 & 0 \\ 0 & 1 & 0 & 0 & 0 & 0 & \frac{1}{2}II_\Omega & 0 & 0 & 0 \\ 0 & 0 & 0 & 3 & 0 & 0 & 0 & II_S & -2II_\Omega & 0 \\ 0 & 0 & 0 & 0 & 3 & 0 & 0 & 0 & 0 & -2II_\Omega \\ 0 & 0 & 0 & 0 & 0 & 0 & 0 & 0 & 0 & 0 \\ 0 & 0 & 0 & 0 & 0 & -1 & 0 & 0 & 0 & 0 \\ 0 & 0 & 0 & 0 & 0 & 0 & -1 & 0 & 0 & 0 \end{bmatrix}. \tag{114}$$

The solution for three-dimensional mean flow is

$$\begin{aligned} \beta_1 &= -\frac{1}{2}A_1 N \left(30A_2 IV - 21N II_\Omega - 2{A_2}^3 III_S + 6N^3 - 3{A_2}^2 II_S N\right)/Q, \\ \beta_2 &= -A_1 A_2 \left(6A_2 IV + 12N II_\Omega + 2{A_2}^3 III_S - 6N^3 + 3{A_2}^2 II_S N\right)/Q, \\ \beta_3 &= -3A_1 \left(2{A_2}^2 III_S + 3N A_2 II_S + 6IV\right)/Q, \\ \beta_4 &= -A_1 \left(2{A_2}^3 III_S + 3{A_2}^2 N II_S + 6A_2 IV - 6N II_\Omega + 3N^3\right)/Q, \\ \beta_5 &= 9A_1 A_2 N^2/Q, \\ \beta_6 &= -9A_1 N^2/Q, \\ \beta_7 &= 18A_1 A_2 N/Q, \\ \beta_8 &= 9A_1 {A_2}^2 N/Q, \\ \beta_9 &= 9A_1 N/Q, \\ \beta_{10} &= 0, \end{aligned} \tag{115}$$

with the denominator

$$Q = 3\,N^5 + \left(-\frac{15}{2}\,II_\Omega - \frac{7}{2}\,{A_2}^2\,II_S \right) N^3 + (\,21\,A_2\,IV - {A_2}^3\,III_S\,)\,N^2$$
$$+ (\,3\,{II_\Omega}^2 - 8\,II_S\,II_\Omega\,{A_2}^2 + 24\,{A_2}^2\,V + {A_2}^4\,{II_S}^2\,)\,N + \frac{2}{3}\,{A_2}^5\,II_S\,III_S$$
$$+ 2\,{A_2}^3\,IV\,II_S - 2\,{A_2}^3\,II_\Omega\,III_S - 6\,IV\,A_2\,II_\Omega. \qquad (116)$$

By substituting $N = 1$, $A_1 = 1$ and $A_2 = 1$ one gets the same ARSM equation as Gatski & Speziale[7] and also an identical solution.

The equation for N can also be derived for three-dimensional mean flow and is a sixth order polynomial equation, as for the simplified case. The expression is, however, complicated and of small practical interest. As for the solution of the simplified ARSM equation, the two-dimensional solution of N can also be used here as a first approximation.

References

[1] Chien, K.Y. 1982 Predictions of channel and boundary-layer flows with a low-Reynolds-number turbulence model. *AIAA J.* **20**, 33–38.

[2] Cook, P.H., MacDonald, M.A. & Firmin, M.C.P. 1979 Aerofoil 2822 - Pressure distributions, boundary layer and wake measurements. *AGARD AR* 138.

[3] Daly, B.J. & Harlow, F.H. 1970 Transport equations in turbulence. *Phys. Fluids* **13**, 2634–2649.

[4] Durbin, P.A. 1993 Application of a near-wall turbulence model to boundary layers and heat transfer. *Int J. Heat Fluid Flow* **14**, 316–323.

[5] Durbin, P.A. 1995 Separated flow computations with the K–ε–v^2 model. *AIAA J.* **33**, 659–664.

[6] Friedrich, R. 1996 Compressibility effects due to turbulent fluctuations. Oral presentation at Sixth European Turbulence Conference, Lausanne, July 1996, submitted to Journal of Appl. Sci. Res.

[7] Gatski, T.B & Speziale C.G. 1993 On explicit algebraic stress models for complex turbulent flows. *J. Fluid Mech.* **254**, 59–78.

[8] Girimaji, S.S. 1996 Fully-explicit and self-consistent algebraic Reynolds stress model *Theor. and Comp. Fluid Dyn.* **8** 387–402 (also *ICASE Report No. 95-82*).

[9] Girimaji, S.S. 1996 Improved algebraic Reynolds stress model for engineering flows In *Engineering Turbulence Modelling and Experiments 3* pp 121–129. Eds W. Rodi and G. Bergeles. Elsevier. Science B.V.

[10] Girimaji, S.S. 1997 A Galilean invariant explicit algebraic Reynolds stress model for turbulent curved flows *Phys. Fluids.* **9** 1067–1077 (also *ICASE Report No. 96-38*).

[11] Hanjalić, K., Jakirlić, S. & Hadžić, I. 1995 Computation of oscillating turbulent flows at transitional *Re*-numbers *Turbulent Shear Flows* **9** pp 323–342. Eds F. Durst, N. Kasagi & B.E. Launder. Springer-Verlag, Berlin.

[12] Hellström, T., Davidson, L. & Rizzi, A. 1994 Reynolds stress transport modelling of transonic flow around the RAE2822 airfoil. *AIAA 94-0309* 32nd Aerospace Sciences Meeting, Reno, Jan 1994.

[13] Horsten, J.J., den Boer, R.G. & Zwaan, R.J. 1983 Unsteady transonic pressure measurements on a semi-span wind tunnel model of a transport-type supercritical wing (LANN model). *AFWAL-TR-83-3039*.

[14] Imao, S., Itoh, M. & Harada, T. 1996 Turbulent characteristics of the flow in an axially rotating pipe *J. Heat Fluid Flow* **17**, 444–451.

[15] Johansson, A.V. & Wallin, S. 1996 A new explicit algebraic Reynolds stress model. Proc. Sixth European Turbulence Conference, Lausanne, July 1996, Ed. P. Monkewitz, 31–34.

[16] Kim, J. 1989 On the structure of pressure fluctuations in simulated turbulent channel flow. *J. Fluid Mech.* **205**, 421–451.

[17] Launder, B.E., Reece, G.J. & Rodi, W. 1975 Progress in the development of a Reynolds-stress turbulence closure. *J. Fluid Mech.* **41**, 537–566.

[18] Lumley, J.L. 1978 Computational modeling of turbulent flows. *Adv. Appl. Mech.* **18**, 123–176.

[19] Matsson, O.J.E. & Alfredsson, P.H. 1990 Curvature- and rotation-induced instabilities in channel flow. *J. Fluid Mech.* **210**, 537–563.

[20] Menter, F.R. 1993 Zonal Two Equation K–ω Turbulence Models for Aerodynamic Flows. *AIAA 93-2906*

[21] Menter, F.R. 1994 Two-equation eddy-viscosity turbulence models for engineering applications. *AIAA J.* **32**, 1598–1604.

[22] Moser, R.D, Kim J. & Mansour N.N. 1998 DNS of Turbulent Channel Flow up to $Re_\tau = 590$. *Phys. Fluids* **11**, 943–945.

[23] Naot, D., Shavit, A. & Wolfstein, M. 1973 Two-point correlation model and the redistribution of Reynolds stresses. *Phys. Fluids* **16**, 738–743.

[24] Pope, S.B. 1975 A more general effective-viscosity hypothesis *J. Fluid Mech.* **72**, 331–340.

[25] Rizzi, A., Eliasson, P., Lindblad, I., Hirsch C., Lacor, C., Haeuser, J. 1993 The engineering of multiblock/multigrid software for Navier–Stokes flows on structured meshes *Computers Fluids* **22**, 341–367.

[26] Rodi, W. 1972 The prediction of free turbulent boundary layers by use of a two equation model of turbulence. *Ph.D. thesis, University of London.*

[27] Rodi, W. 1976 A new algebraic relation for calculating the Reynolds stresses. *Z. angew. Math. Mech.* **56**, T219–221.

[28] Rotta, J.C. 1951 Statistische Theorie nichthomogener Turbulenz. *Z. Phys.* **129**, 547–572.

[29] Schülein, E., Krogmann, P. & Stanewsky, E. 1996 Documentation

of Two-Dimensional Impinging Shock/ Turbulent Boundary Layer Interaction Flow. DLR Report: DLR IB 223 - 96 A 49.

[30] Schlichting, H. 1979 Boundary-Layer Theory, 7th ed., McGraw-Hill, New York.

[31] Shabbir, A. & Shih, T.H. 1992 Critical Assessment of Reynolds Stress Turbulence Models Using Homogeneous Flows NASA TM 105954, ICOMP-92-24, CMOTT-92-12.

[32] Shih, T.H., Zhu, J. & Lumley, J.L. 1992 A Realizable Reynolds Stress Algebraic Equation Model NASA TM 105993, ICOMP-92-27, CMOTT-92-14.

[33] Shih, T.-H. 1996 Constitutive relations and realizability of single-point turbulence closures Chapter 4 of **Turbulence and Transition Modelling**, Eds. M. Hallback, D.S. Henningson, A.V. Johansson and P.H. Alfredsson. Kluwer.

[34] Shih, T.-H. & Lumley, J.L. 1993 Remarks on turbulent constitutive relations *Math. Comput. Modelling*, **18**, 9–16.

[35] Sjögren, T. 1997 Development and Validation of Turbulence Models Through Experiment and Computation Doctoral thesis, Dept. of Mechanics, KTH, Stockholm, Sweden.

[36] So, R.M.C., Lai, Y.G. & Zhang, H.S. 1991 Second-Order Near-wall Turbulence Closures: A Review. *AIAA J.* **29**, 1819–1835.

[37] Spalart P.R. 1988 Direct simulation of a turbulent boundary layer up to $R_\theta = 1410$. *J. Fluid Mech.* **187**, 61–98.

[38] Spencer, A.J.M. & Rivlin, R.S. 1959 The theory of matrix polynomials and its application to the mechanics of isotropic continua *Arch. Rat. Mech. Anal.* **2**, 309–336.

[39] Speziale, C.G., Sarkar, S. & Gatski, T.B. 1991 Modelling the pressure–strain correlation of turbulence: an invariant dynamical systems approach. *J. Fluid Mech.* **227**, 245–272.

[40] Speziale, C.G. & Xu, X.-H. 1996 Towards the development of second-order closure models for nonequilibrium turbulent flows *Int. J. Heat and Fluid Flow* **17**, 238–244.

[41] Taulbee, D.B. 1992 An improved algebraic Reynolds stress model and corresponding nonlinear stress model. *Phys. Fluids A* **4**, 2555–2561.

[42] Taulbee, D.B., Sonnenmeier, J.R. & Wall, K.M. 1994 Stress relation for three-dimensional turbulent flows *Phys. Fluids* **6**, 1399–1401.

[43] Tavoularis, S. & Corrsin, S. 1981 Experiments in nearly homogeneous turbulent shear flow with a uniform mean temperature gradient. Part I. *J. Fluid Mech.* **104**, 311–347.

[44] Vandromme, D. 1992 Introduction to the Modeling of Turbulence *von Karman Institute for Fluid Dynamics, Lecture Series 1991-02.*

[45] Wallin, S. & Johansson, A.V. 1996 A new explicit algebraic Reynolds stress turbulence model including an improved near-wall treatment. Proc. Flow Modeling and Turbulence Measurements VI, Tallahassee FL, Chen, Shih,

Lienau & Kung (eds), 399–406.
[46] Wilcox, D.C. 1988 Reassessment of the scale-determining equation for advanced turbulence models. *AIAA J.* **26**, 1299–1310.
[47] Wilcox, D.C. 1993 Turbulence modeling for CFD. *DCW Industries Inc., La Cañada, California*.
[48] Wilcox, D.C. 1994 Simulation of transition with a two-equation turbulence model. *AIAA J.* **32**, 247–255.

2

Paper 2

A PREDICTION METHOD FOR HIGH SPEED TURBULENT SEPARATED FLOWS WITH EXPERIMENTAL VERIFICATION

I. A. A. Lindblad (Head Comp. aerodynamics dept.), S. Wallin (Research Scientist)
The Aeronautical Research Institute of Sweden (FFA), Bromma, Sweden

A. V. Johansson, (Professor)
The Royal Institute of Technology (KTH), Stockholm, Sweden

R. Friedrich (Professor), R. Lechner (PhD student)
Technische Universität München (TUM), Garching, Germany

P. Krogmann (Senior Research Scientist), E. Schülein (Research Scientist)
Deutsches Zentrum für Luft- und Raumfahrt (DLR), Göttingen, Germany

J.-C. Courty (Senior Research Scientist), M. Ravachol (Research Scientist)
Dassault Aviation (DAA), St Cloud, Paris, France

D. Giordano (ESA Technical Project Officer)
ESA/ESTEC, Noordwijk, The Netherlands

Abstract. It is well known that the level of current engineering computational aerodynamic analysis for turbulent hypersonic separated flows is not satisfactory. Computations using standard two-equation turbulence models do not give sufficiently accurate predictions. Existing compressibility corrections do not provide general improvements. In fact, they seem to render predictions worse, at least for Mach numbers up to five. Possible improvements using Explicit Algebraic Turbulence Models (EARSM) have been investigated. This class of models allow for a more general coupling between the mean field and the turbulent Reynolds stresses, compared to the standard two-equation models based on the Boussinesq hypothesis. A new class of EARSMs is proposed and compared to results of existing standard models. It is demonstrated that the new proposed EARSM gives improved prediction over standard two-equation models and previously published EARSMs for validation cases relevant for high speed separated flows. A new complete EARSM turbulence model based on the k-ω two-equation model is recommended as giving the overall best prediction of the validation test cases. As part of the project a new series of detailed validation experiments, with turbulent boundary layer-shock wave interaction on a flat plate at Mach 5, with different degree of flow separation, have been performed.

1. Introduction

1.1. Problems in hypersonic aerodynamics. Future space transportation systems, in particular reusable vehicles, will have to be more aerodynamically optimised than current designs. Currently novel space transportation concepts are under consideration, in Europe and elsewhere. The detailed evaluation of the technical feasibility and economy of the concepts as well as technical development of a selected design must be

done to a large extent by CFD methods, in part because full scale flight conditions cannot in general be reproduced in ground based experimental facilities.

External as well as internal flows are of importance. Heat loads of complex attached and separated flows must be determined with sufficient accuracy. Current industrial standard CFD methods in some cases fall short of supplying a reliable solution to the given analysis problem. In many instances the shortcomings are related to the turbulence modeling in Reynolds Averaged Navier-Stokes methods. In the current project we have mainly dealt with the problem of predicting turbulent flow separation in high-speed flows. Typical applications are air intakes of hypersonic airbreathing vehicles or flow over control surfaces, with hinge line flow separation.

1.2. Project description. Turbulence modeling in high-speed flows is a vast subject. Our approach has been that a more general modeling, including the necessary flow physics, will be able to treat a wider range of flow problems, also in areas of 'extrapolation' beyond the regime of calibration of the model. With this general idea turbulence modeling has been reviewed (Lindblad et al., 1995, chs 3-4). As a result of this review a class of turbulence models, Explicit Algebraic Reynolds Stress Models (EARSMs) was selected for further study and development.

The EARSM is formulated together with a base-line two equation turbulence model. In the project three partners (FFA, TUM, DAA) used different base-line models, which were all modified to be EARSM. To compare results and to judge the most promising route of development the codes were first tested on common schematic test cases (Wallin et al., 1996). In order to ensure that the codes gave the same results with the same models and assumptions, test cases assuming laminar flow or using a simple algebraic turbulence model were computed. The results using the different base-line models were subsequently compared. All base-line models were modified, to include published EARSMs.

Based on the experiences of implementation and validation of existing EARSMs a new anisotropy formulation was developed (Johansson and Wallin, 1996; Wallin & Johansson, 1997). This model was implemented in the codes on the basis of the different two-equation turbulence models and tested. One variant was selected as giving the overall best results.

A set of test cases was selected for the project, after an extensive review of suitable flow cases for the validation of turbulence models for the selected classes of target problems (Lindblad et al. 1995; Wallin et al. 1996). These were mainly schematic two-dimensional cases related to the selected target problems, used for model development and validation. A three-dimensional test case (Rodi & Dolling, 1992) was selected for the demonstration of the generality of the model development and implementation.

One project goal was to contribute to the database of validation data for turbulence models at high speed. In the literature survey a lack of schematic test cases for hypersonic shock wave-turbulent boundary layer interaction was identified. A set of test

experiments, with a shock wave incident on flat plate boundary layer at Mach 5 was conducted by DLR (Krogmann & Schülein, 1996). This was used as the main validation case in the project. The results are summarised in section 4.

Selected project computational results, demonstrating the main findings, are analysed in section 5. The main conclusions of the turbulence model development and validation, as well as the lessons learned from the experimental campaign are summarised in section 6.

2. Problems in turbulence modeling for high speed flows

2.1. The required level of modeling. In the review of turbulence modeling for high speed flows (Lindblad et al., 1995, ch. 4) the specific problems of turbulence models for compressible flows were investigated. It was concluded that intrinsic compressibility effects on the turbulence had a significant influence on free shear flows. In wall bounded flows the main influence of compressibility (for Mach numbers less than five) lies in the interaction between the turbulence and the compressible mean field. The importance of the intrinsic compressibility effects on turbulence is measured by a turbulent Mach number. Recent evidence (Sarkar, 1995, Blaisdell et al. 1991) points to the gradient Mach number $M_g = S(\lambda/\bar{c})$ as the representative compressible parameter. Here S is the mean shear rate, λ is a representative integral length scale and c is the mean speed of sound.

In cases where the turbulent Mach number (or gradient Mach number) is large, explicit compressibility terms should be added to the turbulence model equations. Attempts have been made at modeling pressure-dilatation correlation and dilatational dissipation rate for compressible flows (e.g. Sarkar et al., 1991; Zeman, 1990). However, these do in general not agree well with experimental or DNS results, in particular not for wall-bounded flows.

As noted above the main target applications in the current project feature flow separation of wall bounded flows. We have concluded that the most fruitful direction of development is to improve on incompressible turbulence models, formulated for compressible flow by applying Favre averaging to the equations. A survey of incompressible turbulence models was performed, aimed at the question of prediction of separated flows. It was concluded that in order to seek a general improvement in prediction of a wide class of separated flows in complex configurations, it is necessary to work with Reynolds Stress turbulence models. In general prediction of complex, separated flows requires a realistic model for the anisotropy of the Reynolds stress tensor, appearing in the averaged Navier-Stokes equations. In principle it would be advantageous to derive a transport equation for the independent stress components, leading to a differential Reynolds Stress Model (DRSM). The practical application of DRSM is still in early stages. The implementation and calibration of DRSM models are quite complex for the types of target problems envisioned for the current project. The computational cost and prob-

lems with numerical robustness precludes the use of DRSM models for engineering purposes in the near future.

In two-equation models the transport equations for individual Reynolds stresses are replaced by a simple algebraic proportionality between the Reynolds Stress anisotropy, a_{ij} and the mean flow strain rate S_{ij} (Boussinesq's hypothesis). This is a quite simplistic model for the Reynolds stress components and is formally valid only for the shear stress component, $\overline{uv}$, in near parallel flows in equilibrium. Despite this, the standard two-equation turbulence models work quite well in many engineering flow problems, attesting to the fact that these are often close to equilibrium. A possible route for improving on the known deficiencies of two-equation models in prediction e.g. flow separation, is to generalise the relation between the Reynolds stress anisotropy and the mean flow strain and rotation rate

$$f(a_{ij}, S_{ij}, \Omega_{ij}) = 0 \tag{1}$$

This is the idea of the Algebraic Reynolds Stress Models (ARSM), pioneered by Rodi (1972, 1976). The first of these models were formulated as implicit relations to be solved as part of the iteration process. The use of ARSM has been slowed by the numerical difficulties, as serious as for DRSMs, which are due to the implicit and non-linear algebraic relations to be solved in the ARSM case. This has motivated the development of Explicit Algebraic Reynolds Stress Models (EARSM) in which the Reynolds Stress anisotropy is expressed as an explicit function of the mean flow strain and rotation rate tensors,

$$a_{ij} = a_{ij}(S_{ij}, \Omega_{ij}) \,. \tag{2}$$

The EARSM formulation allows a direct evaluation of the Reynolds stress terms once the mean field is known. This is quite amenable to the numerical procedures of flow solvers and makes EARSM models as robust as two-equation turbulence models.

2.2. Development of an EARSM anisotropy model. In the current project EARSMs have been reassessed and a novel development has been made. Published models (Shih, Zhu & Lumley, 1992; Gatski & Speziale, 1993) were implemented and tested for reference. The EARSM concept has been reassessed and a new model developed (Johansson & Wallin, 1996; Wallin & Johansson, 1996). The following main developments have been made.

- The development of the complete explicit expression a_{ij} from (2) in terms of a series of nonlinear combinations of S_{ij} and Ω_{ij}. The coefficients of this series have been determined to make the EARSM anisotropy model an exact solution of the ARSM equations for two-dimensional flows and an approximate solution for three-dimensional flows.

- A calibration of the near wall behaviour of the new EARSM. A low Reynolds number formulation has been created in which it has been attempted to allow the Reynolds stress anisotropy to behave according to evidence from experimental and DNS results.

The classical algebraic Reynolds stress model (ARSM) developed by Rodi (1976) based on the general linear pressure strain model by Launder *et.al.* (1975) was the starting point for the new anisotropy model, which is described in detail by Wallin & Johansson (1997). The ARSM is a non-linear relation between the Reynolds stress anisotropy tensor, $a_{ij} = \overline{\rho u_i u_j}/\rho k - 2\delta_{ij}/3$, and the mean velocity strain and rotation rate tensors, S_{ij} and Ω_{ij}. By making reasonable choices of constants of the rapid pressure strain model the resulting ARSM is simplified and reads

$$\left(C_1 - 1 - \frac{2}{3}D - a_{kl}S_{lk}\right)a_{ij} = -\frac{8}{15}S_{ij} + \frac{4}{9}(a_{ik}\Omega_{kj} - \Omega_{ik}a_{kj})\,. \tag{3}$$

where C_1 is the Rotta constant. Several attempts have been made at solving this equation to obtain an explicit relation between the anisotropy tensor and the mean flow field which is an explicit algebraic Reynolds stress model (EARSM), see *e.g.* Pope (1975), Taulbee (1992) and Gatski & Speziale (1993). The non-linearity in a_{ij} forms a major obstacle in the solution process but recently it has independently been shown by Johansson & Wallin (1996) and Girimaji (1995) that this equation can be solved exactly for two-dimensional mean flows and also that good approximations exists also for three-dimensional mean flows (Wallin & Johansson 1996 and 1997). The correct treatment of the non-linear term is of crucial importance for the asymptotic model behaviour for large strain rates and represents a substantial improvement with this type of modeling. The resulting EARSM has been found to be well suited for integration to the wall. The new model development includes a new near wall treatment ensuring realizability for the individual stress components which can be well predicted by introducing one simple wall damping function of 'van Driest' type.

A two-equation turbulence model is used as the basis on which to build the EARSM. The basis for the two-equation models is the derivation of transport equations which give an estimate of the turbulent velocity and length scales. The selection of the dependent variables is somewhat arbitrary. The equation for the turbulent kinetic energy, k, gives an estimate for the velocity scale. The formulation of the length scale equation is less obvious and formulations based on the dissipation, ε, or on another quantity such as $\omega \sim \varepsilon/k$ or $\tau \sim k/\varepsilon$ have been developed. In principle these formulations are equivalent. Different detailed modeling, calibration of constants and near wall modifications make the respective formulations show different behaviour, in particular in regions of separated flow. This nonuniqueness in the formulation carries over to the EARSMs. In the project we have taken the modest route of implementing and testing the new EARSM based on the different two-equation formulations of the project partners. In this way it was possible to quantify the effect of the EARSM modification of

different formulations of the length scale equation. Also the different grid and numerical methods strategies used have been utilized to increase the experience in using the new models. Based on the experience of the implementation of the new EARSM based on the different base-line two-equation models a recommended choice of complete model was made.

3. Models used for validation

3.1. Codes and base-line turbulence models. We here present a summary of the codes and base-line turbulence models used as a basis for the development of an improved prediction methodology. The codes and turbulence models used in the project are described in detail in Wallin et. al (1996).

FFA has used the EURANUS code (Rizzi et al., 1993), which is a multi-block structured three-dimensional Navier-Stokes solver. The governing equations of compressible flow are in Favre averaged form. The base-line two-equation turbulence model used is the $k-\varepsilon$ model of Chien (1982). The dependent variables are stored in cell centers and the code employs, in this project, second order upwind symmetric TVD scheme with Van Leer limiters for the convective terms and purely central approximation for the viscous fluxes. The equations are converged with a Runge-Kutta time stepping procedure with multigrid acceleration.

TUM has used the structured NSFLEX code (Eberle, 1985 and Schmatz, 1989), in a two-dimensional version. The governing equations are Favre averaged. As a base-line model TUM has implemented the $k-\omega$ model of Wilcox (1991) with low-Reynolds number corrections proposed by Wilcox (1993), (1994). The dependent variables are stored in cell centers. The equations are transformed to nonorthogonal, curvilinear coordinates. The convective fluxes are approximated by a hybrid local characteristic (Eberle, 1985) and a Steger-Warming scheme (Schmatz et al., 1991). Viscous fluxes are approximated by central differences. The time-stepping is first order implicit employing a point Gauss-Seidel relaxation technique.

DAA uses the unstructured FEM Navier-Stokes solver VIRGINI. The governing equations are expressed in terms of entropy variables. The base-line two-equation turbulence model is the $k-\varepsilon$ model (Launder & Spalding, 1974). The near wall region is treated by the two-layer model of Patel and Chen (1991). The equations are solved using the Galerkin least-squares method. The equations are converged to steady state using an implicit iterative method using the GMRES algorithm.

3.2. Validation procedure. The development and validation procedure was made in a step-by-step fashion, described in detail in Wallin et al. (1996). The different Navier-Stokes codes were first compared on a laminar flow case (flat plate at Mach 2) to ensure that the numerical errors of the methods and the grids used were under control. As a second step results using the same turbulence model (Baldwin-Lomax) were compared

to ensure that a simple turbulence model did not introduce errors. In a third step results using the different base-line two-equation models were compared. The differences between the results using different base-line models were judged to be in line with known differences in predictions using the models. These differences carry over to the main computational phase of the project (section 5).

4. The validation experiment

4.1. Wind Tunnel Facility. For the validation of numerical computations the Ludwieg Tube Tunnel Facility RWG of DLR Göttingen with Mach number five was chosen because of its high Reynolds number capability (maximum unit Reynolds number of $50x10^6$ m^{-1}) and documented flow quality. The RMS fluctuations of mass flow and pitot pressure are of the order of 1%.

4.2. Experimental model and test setup. As test case the zero pressure gradient flat plate turbulent boundary layer interfering with an impinging two-dimensional oblique shock wave of different shock strength at Mach five and a freestream unit Reynolds number of approximately $40x10^6$ m^{-1} was defined.

The test set-up, shown in Figure 1, consisted of a basic flat plate 400 mm wide and 500 mm in length with sharp leading edge and rows of static pressure tabs in axial direction close to the center-line and in lateral direction immediately upstream of the anticipated shock impingement location. As shock generator served a second flat plate at incidence mounted above the basic plate such that for all incidences tested the inviscid shock/boundary layer interaction occurred at the same position at x = 350 mm downstream of the leading edge ($Re_x \approx 14x10^6$ m^{-1}). This Reynolds number was considered to be high enough to guarantee a fully developed turbulent boundary layer at the shock impingement position. The plate incidences tested were ß = 0°, 6°, 8°, 10°, 12° and 14°, giving an extensive database of shock-boundary layer interaction at varying shock strength. For the project the 0°, 6°, 10° and 14° cases were mainly used.

Initially, some preliminary qualitative oil flow visualizations were conducted on the basic plate at the shock interaction location in order to demonstrate the two-dimensionality of the flow in this region, the shock generator being at ß = 10°. A straight separation line caused by the impinging shock could be observed over a considerable distance across the flat plate center line, verifying the anticipated two-dimensional turbulent flow field.

Furthermore, the basic plate was equipped in the axial direction with ten and laterally with three additional ports for mounting a miniature flattened pitot pressure probe for boundary layer profile measurements. The three lateral ports were applied in the course of the experiments in order to demonstrate that the mean flow in the interaction region was really two-dimensional.

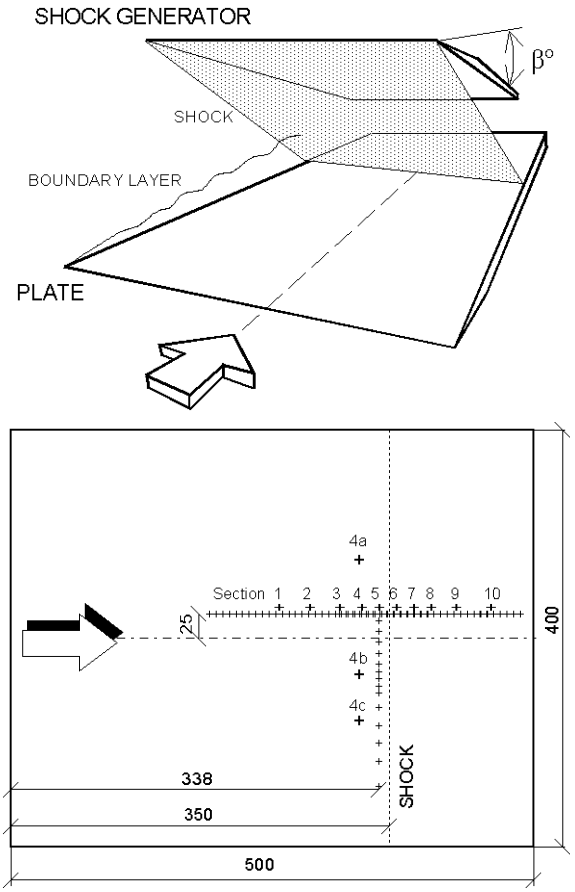

FIGURE 1: A schematic of the test model with measurement stations on the flat plate.

4.3. Experimental results. The first boundary layer profile measurements upstream and downstream of the anticipated shock impingement location as well as static pressure distribution measurements were performed on the basic plate without the shock generator installed, $\beta = 0^{\circ}$. The velocity profiles show self-similarity and fit well to the wall-wake law. From the measured velocity profiles the relevant boundary layer properties, thickness d, displacement thickness d^*, momentum thickness q and skin friction coefficient C_f are determined. Figure 2 shows the boundary layer parameters together with skin friction and static pressure distribution. The accuracy of determining the thickness parameters of the boundary layer may be demonstrated by the four points taken laterally at $x = 316$ mm.

At the end of all measurements a newly developed oil film interferometry measurement technique for determining the local skin friction was applied for the first time in RWG. The results (marked as Optic/LISF) are compared in Figure 2 with those values

derived from the velocity profile measurements. It is seen that at $x \approx 100$ mm the skin friction increase due to transition is completed and that downstream the boundary layer may be considered as turbulent.

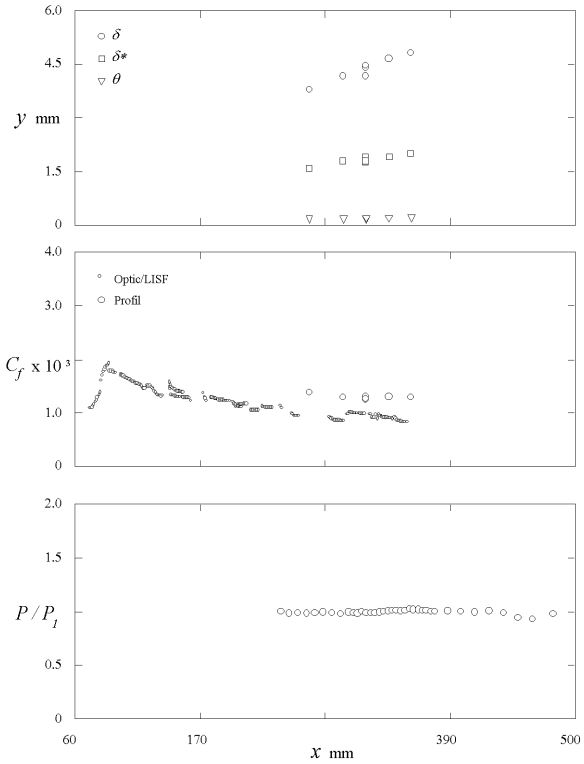

FIGURE 2: Boundary layer on the flat plate.

The static pressure distribution is fairly constant at the level of freestream pressure within an uncertainty of less than 1 % up to a distance of $x = 425$ mm. Only on the rear of the plate the pressure drops somewhat below the freestream pressure which may be attributed to an upstream influence of the expansion at the trailing edge over the subsonic part of the relatively thick boundary layer.

With the impinging shock generated by the shock generating plate set to an incidence of $\beta = 6^\circ$ no separation is observed. The static pressure starts slightly upstream of the inviscid shock impingement position to rise up to the inviscid level.

The case of an impinging shock generated by the shock generator at $\beta = 10^\circ$ incidence was defined as the main test case for the numerical computations. The results of boundary layer and pressure distribution measurements are shown in Figure 3. The impinging shock causes a moderate separation zone which is marked in the skin friction coefficient distribution by the two solid symbols "S" and "R" for separation and reattachment position. The static pressure increase up to the inviscid pressure level occurs

over an enlarged distance in this case. The pressure drop at the rear of the plate is caused by the expansion fan built up at the trailing edge of the shock generator. In Figure 4 a sketch of the flow field obtained from the measurements is compared with the corresponding shadowgraph. The boundary layer development, the incoming shock and the separation and reattachment shocks were clearly discerned in the measurements.

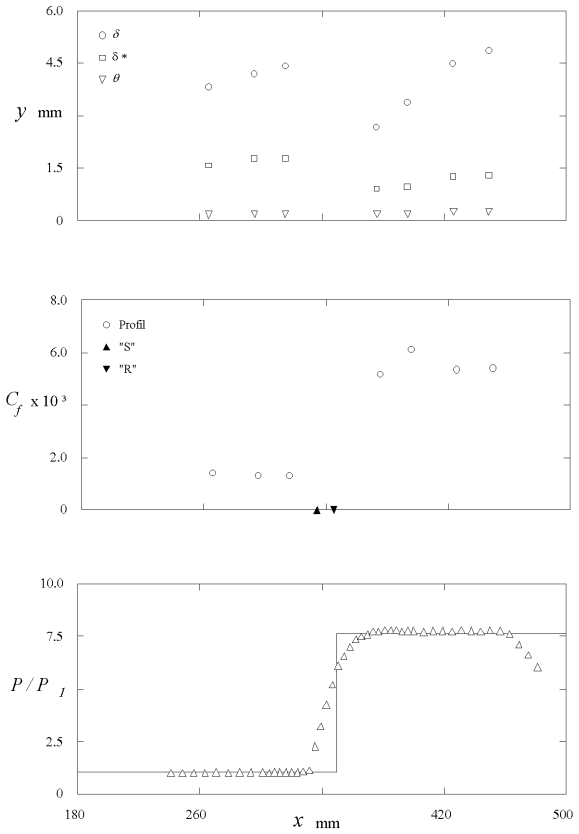

FIGURE 3: Impinging shock/boundary layer interaction at $\beta = 10°$.

Finally, the strength of the impinging shock was increased by setting the shock generator to an incidence of $\beta = 14°$. The impinging shock, thus generated, causes a more severe separation. A small plateau appears over the separated region before it rises to the theoretical inviscid level. After reattachment the skin friction coefficient is drastically increased. The flow in the separated region is severely disturbed by the impinging shock.

5. Computational results

The computations of the DLR experiment described in the previous section give a clear picture of the differences in prediction using different classes of turbulence modeling

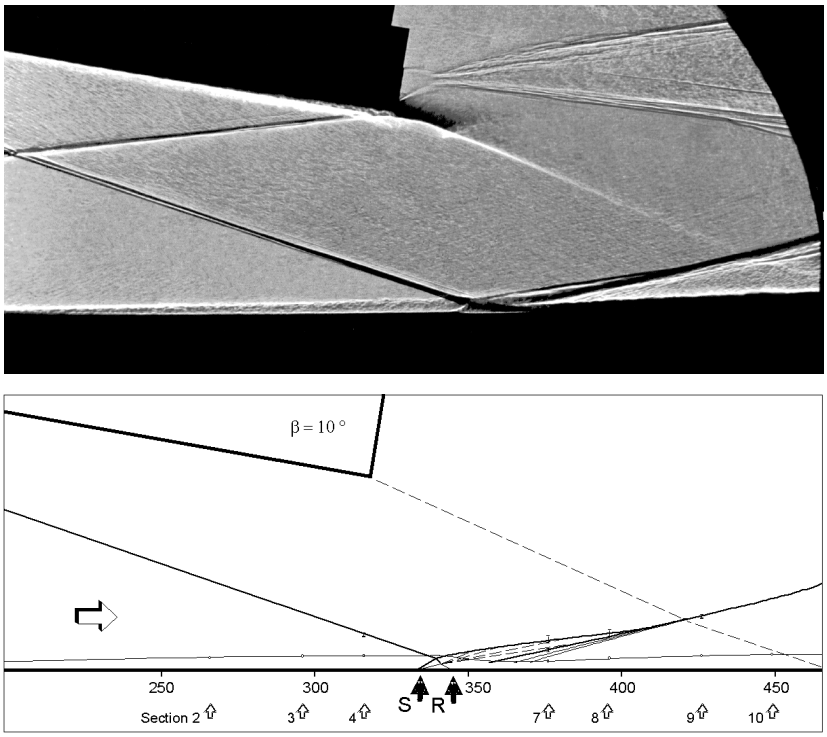

FIGURE 4: Impinging shock/boundary layer interaction at $\beta = 10°$.

for high speed separated flows and will be used for illustration of the project results. The conclusions drawn from the other test cases were in line with these results.

5.1. The DLR experiment of shock wave-boundary layer interaction. The three shock generator plate angles $\beta = 6°$, $10°$ and $14°$ were computed using different turbulence models. The emphasis was put on the $10°$ case, where moderate separation occurs. The computational grid used in this study consists of 80x80 cells, providing in most flow regions well resolved results. The grid points are clustered around the incoming shock, in the boundary layer and around the shock wave-boundary layer interaction, with the use of different grids for the varying strength of the incoming shock.

5.1.1. *Comparison of results using different levels of turbulence modeling.* In order to illustrate the improvement of flow prediction with more complex turbulence models, computations were performed with a range of models, from an algebraic mixing length model to a DRSM. The results in terms of skin friction are shown in Figure 5. The Baldwin-Lomax (1978) mixing length model (FFA_BL in the figure legend), was designed for attached boundary layers and gives for this case a much too large separa-

tion length with a separation onset somewhat downstream the experimental one. The two-equation Wilcox (1994) $k-\omega$ model (TUM_k-w) underestimates the separation length, in a way typical for two-equation eddy viscosity models without further corrections for separated flows. The separation lengths predicted with the Reynolds stress models represented by the recommended EARSM, built on the $k-\omega$ model, (TUM_EARSM_k-w) and the SSG (Speziale, *et.al.* 1991) DRSM (TUM_SSG_k-w) are almost equal. The predicted skin friction peaks (maximum and minimum) are somewhat higher using DRSM compared to EARSM.

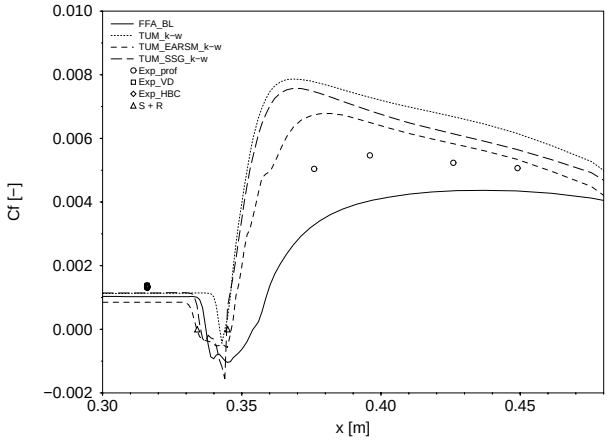

FIGURE 5: Different level of modeling. Impinging shock at Mach 5, $\beta = 10°$, Experiment by Krogmann & Schülein (1996).

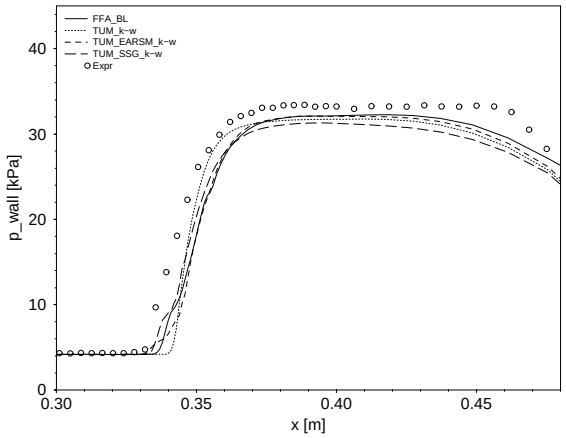

FIGURE 6: Different level of modeling. Impinging shock at Mach 5, $\beta = 10°$, Experiment by Krogmann & Schülein (1996).

Figure 6 shows the computed wall pressure for the same case. The underprediction of the separation length by the eddy-viscosity model gives a too steep pressure rise. The

slope of the pressure rise computed with the Reynolds stress models better matches the experimental data. We can se a small difference between the algebraic and differential Reynolds stress models in the beginning of the separation zone, where the DRSM shows a somewhat steeper pressure rise compared to the EARSM and also that there is a tendency of a 'pressure plateau' in the DRSM results. This can be interpreted as the DRSM predicting a thicker separation bubble than EARSM. However, no pressure plateau could be seen in the experiment for this case. The computed pressure rise is shifted somewhat downstream and the experimental pressure level downstream of the interaction is not completely reached due to approximate inflow conditions used for the computations.

The computed velocity profiles are compared to the measured values at different cross sections in Figure 7. Sections 2 to 4 are located upstream of the interaction while the sections 7 to 10 are downstream. The position of the measured velocity profiles corresponds to the position of the skin friction measurements where sections 4 and 7 to 10 are seen in Figure 5. There are only minor differences among the computed velocity profiles before the interaction and a consistent difference between the computed and measured velocity profiles. This difference is also consistent with the underpredicted skin friction coefficient before the interaction in Figure 5. The reason is that the inflow profile used in the computations at $x = 0.2$ m could not be perfectly matched to the experimental profile. After the interaction, stations 7 to 10, the differences among the computed velocity profiles are much larger and it is quite clear that the computed profiles using the two different Reynolds stress models are closest to the experiments. There are only minor differences between the algebraic and differential Reynolds stress models. Overall the recommended EARSM model gives substantially improved predictions of this case compared to standard two-equation models.

5.1.2. *Computations using different EARSMs.* In order to investigate the difference between the EARSM formulation developed in the current project and previously published versions, the new EARSM was compared to the Shih, Zhu & Lumley (1992) (SZL) model, both built on the $k-\omega$ two-equation model. The SZL model was modified with respect to its near wall treatment. The computed skin friction is shown in Figure 8. The modified Shih *et.al.* model gives results similar to those using the $k-\omega$ model upstream of the separation while it is closer to the new EARSM downstream of the separation. The modified Shih *et.al.* model is, however, did not predict the correct separation length.

In order to select the best two-equation basis for the EARSM, results using different two-equation models were compared (see Figure 9). Here we can see that all models give the correct separation length besides the EARSM based on the Patel & Chen $k-\varepsilon$ model (DAA_EARSM_k-e) where the flow reattaches too far downstream. The behaviour of the different models downstream of the reattachment point is similar to that of the same models with the original eddy-viscosity hypothesis. The overpredicted skin

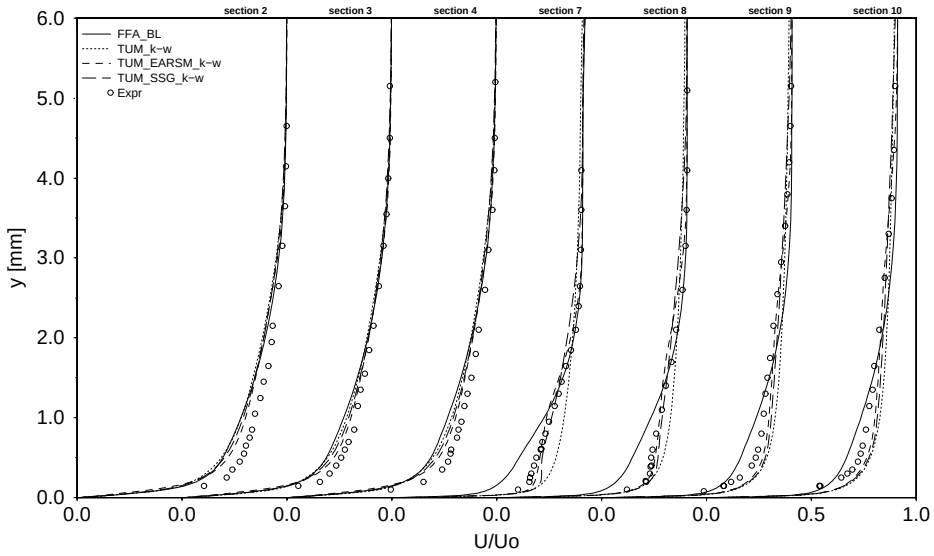

FIGURE 7: Different level of modeling. Impinging shock at Mach 5, $\beta = 10°$, Experiment by Krogmann & Schülein (1996).

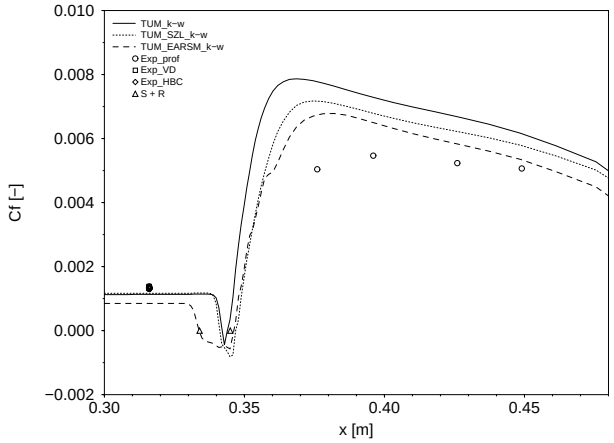

FIGURE 8: Different EARSM. Impinging shock at Mach 5, $\beta = 10°$, Experiment by Krogmann & Schülein (1996).

friction using the Chien $k-\varepsilon$ model basis (FFA_EARSM_k-e) and the underpredicted skin friction with the Patel & Chen $k-\varepsilon$ model are present also in the original two-equation formulations. The overall best results are obtained using the $k-\omega$ model as the basis. This conclusion was also drawn from computing the other test cases and that version was chosen as the recommended model.

There are noticable differences between the two different EARSM computations based on the $k-\omega$ model (FFA_EARSM_k-w and TUM_EARSM_k-w) in Figure 10.

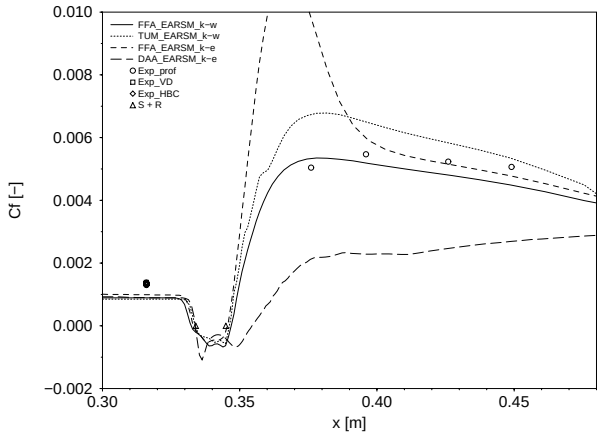

FIGURE 9: Newly developed EARSM using different two-equation model basis. Impinging shock at Mach 5, $\beta = 10°$, Experiment by Krogmann & Schülein (1996).

These are similar to the differences between the two computations with the same model based on the eddy-viscosity assumption. The differences are probably due to differences in the FFA and TUM implementations of the wall boundary conditions and also in the definition of the effective eddy viscosity which is used in the Modeling of the turbulent diffusion of k and ω. This demonstrates that near wall and boundary condition formulations are quite important and merit further study.

5.1.3. *Shock strength.* The major effort has been in computing the $10°$ case where the results are presented above but also the $6°$ and $14°$ cases have been computed. The stronger shock in the $14°$ case induces a much larger separation compared to the $10°$ case, see Figure 10. The different turbulence models show the same characteristic deviations. It is worth noting that the proposed EARSM based on the $k-\omega$ model (FFA_EARSM_k-w) predicts the separation length and skin friction behaviour after reattachment correctly. The good result at $10°$ was not a coincidence.

6. Discussion and recommendations

Our main conclusions from the literature survey, development and computations with regards to the requirements on turbulence modelling for high speed separated flows may be summarised

- Two-equation eddy viscosity models do not include the relevant physics involved in separated flows without ad-hoc modifications. This class of models did not give accurate predictions for the chosen test cases.

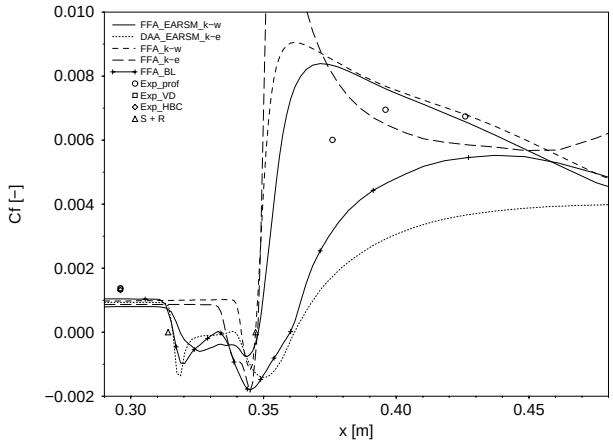

FIGURE 10: Computed skin friction. Impinging shock at Mach 5, $\beta = 14°$, Experiment by Krogmann & Schülein (1996).

- Differential Reynolds stress models (DRSMs) are more general in the sense that the intercomponent transfer in the Reynolds stress tensor can be considered. The numerical treatment and computational effort in complex flow situations is a major disadvantage of these models.
- By developing a suitable explicit algebraic Reynolds stress model to replace the eddy viscosity hypothesis of the standard two-equation models, we were able to obtain results which showed the correct trends for the chosen test cases, closer to experimental values. In a limited comparative study the EARSM produced results closer to DRSM results than two-equation results.

The three different two-equation models with the original eddy viscosity hypothesis give quite similar results in zero pressure gradient flows but different results in flows with nonzero pressure gradient. These differences are inherited when the two-equation models are used together with the EARSM. One of the main short-comings of the Chien $k-\varepsilon$ model is the large overprediction of C_f after reattachment. The $k-\omega$ model has a more regular behaviour in the separation region and the ω equation performs better in pressure gradient flows than the Chien ε equation. For these reasons the $k-\omega$ model was selected as the recommended basis.

The new EARSM anisotropy model has been found to be well suited for integration to the wall. It includes a near wall treatment ensuring realizability for the individual stress components which can be well predicted by introducing one simple wall damping function of 'van Driest' type. When the proposed EARSM is used together with an existing two-equation eddy viscosity model, it was found by Wallin *et.al.* (1997) that the additive constant B in the log-law is slightly overpredicted for both the Chien $k-\varepsilon$ and Wilcox low Reynolds number $k-\omega$ models for zero pressure gradient flows. The near wall corrections within the different length-scale determining equations must thus be modified in order to give the correct near wall behaviour. The near wall behaviour is

improved if the effect of the near wall modification in the original ε or ω equation is reduced which indicates that the inclusion of the proposed EARSM reduces the need for ad hoc modifications in the length-scale determining equation.

There are deficiences in the prediction of the presented models which are not clearly understood. One is the lag in prediction of the pressure rise in cases like the DLR experiment, also known from two-equation models. One must also keep in mind that the EARSM with its algebraic anisotropy model is not able to predict strongly nonequilibrium turbulent situations. In conclusion, however, it seems that the model class gives improvements in engineering prediction of a large set of important complex flows.

The new recommended model is one of the first in a new class of models, and not a final step. A thorough testing of the model in different parameter regimes must be made in order to assess the range of validity for the recommended model. Moreover, a number of new possible extensions are now within reach with the proposed model class as the platform for further developments.

The numerical behaviour of the new recommended model has been found to be similar to the basic two-equation model used. The numerical efficiency and robustness could be further improved by analysing the numerical behaviour of the basic two-equation model together with the proposed EARSM.

One of the results from this study is that the length-scale equation has a major impact on the prediction capability of the EARSM model. The recommendation of using the $k-\omega$ model as the basis gives limitations known from the model in standard form. As already mentioned, the choice of the dependent variable has an impact on the near wall treatment and wall boundary conditions as well as far-field boundary conditions and far-field behaviour. A new lengthscale determining equation should be developed with the use of the proposed EARSM to avoid the risk of inheriting terms that are needed to balance the errors introduced by the eddy viscosity hypothesis.

Our understanding of the features and behaviour of truly compressible turbulent flows is quite limited. General models to describe compressibility effects due to turbulent fluctuations are not yet available. A critical review in this topic was performed in this project which pointed out limitations and lack of generality of the models currently available. More basic research in this area is needed to increase the understanding of this phenomena through numerical simulations of compressible turbulence and novel experiments, see also Friedrich and Bertolotti (1997). One interesting observation made in the review is that intrinsic compressibility is affected by the Reynolds stress anisotropy. One necessary condition to be able to catch this behaviour is the possibility to correctly represent the individual Reynolds stresses. This makes the EARSM class of models an interesting platform for future compressibility correction models.

The experimental test cases available for the validation of high speed separated flows were reviewed as part of the project. A substantial set of generic cases relevant for high speed air intake and control surface flows are available in different databases. A gap in the available set was identified, which could be filled by the DLR experiment performed in the current project. Closer scrutiny of the existing high speed test cases with

separated flows reveal uncertanties which often limits the usefulness of the data for validation of turbulence models.

- Flow definition
  - External, in particular inflow, conditions are often uncertain. Either because they are not measured carefully enough or disturbed by transition effects with the turbulence in a nonequilibrium state. An obvious need for turbulence model validation is that the inflow turbulence data has been measured, in particular turbulent kinetic energy profiles. There is also a difficulty in keeping external conditions, such as pressure gradients or flow homogeneity under full control.
  - In situations with stronger interactions the simple flow geometry assumed in the generic geometry of e.g. a two-dimensional test case is strongly modified by three-dimensional flow.
- The well proven measurement techniques available at high speed are limited. The main tool is pitot pressure measurement, calibrated to generate velocity profiles in a way which becomes questionable near separation regions. Alternative techniques such as the optical measurement technique, used to determine skin friction directly in the DLR experiment, may give useful additional data.

The data from the DLR experiment was obtained with great care. There were some differenences between experiments and boundary layer computations of the inflow conditions, which were not fully resolved during the project. The deviations from the expected conditions were however limited and systematic and we may conclude from the work that this is a very valuable contribution to the database of high speed validation test cases.

As seen in the current project also numerical experiments, using Direct Numerical Simulation have a useful role in the development of advanced turbulence models. In particular the near wall behaviour and the anisotropy of the Reynolds stress tensor are difficult to obtain in any other way.

Future experimental work should be developed with the requirements for validation and calibration of Reynolds stress turbulence models in mind. There is a need for further refined experiments, where the emphasis is put on obtaining a well defined flow situation also with regard to turbulent data, in creating experimental series with variation in interaction strength parameters and in measuring turbulent data.

The DLR experiment should be complemented with quantitative measurements in the separated zone and if possible also by obtaining turbulent data. New experimental techniques, such as the optical interferometry measurement of skin friction should be applied through the interaction region.

We have concluded that the main problems in the predicition of high speed wall bounded turbulent separated flows more lie in the formulation of the basic turbulence model, than in specific high speed effects. Also, the more advanced Reynolds stress turbulence models of the class developed here require more turbulent data, under different conditions (pressure gradients etc) for their calibration and validation. It is thus reasonable to use experimental test cases at lower speed where there are more experimental

techniques available, in particular hot wire and LDV techniques, giving turbulence data. Still there is a severe problem both having high enough Reynolds numbers to obtain equilibrium turbulent inflow conditions and at the same time measuring with high resolution in the boundary layers and separated flow regions.

We also recommend that a strong effort is put on generating high quality DNS data for the calibration of Reynolds stress turbulence models. This will probably be the most reasonable way of getting enough detail about all the Reynolds stress components. DNS computations should be done in simple geometries and e.g. with variation in streamwise pressure gradients to allow the calibration of models suitable for separated flows.

Acknowledgements

The current project was funded by ESA/ESTEC within the TRP programme under contract no. 11018/94/NL/FG/(SC). The support of ESA is gratefully acknowledged.

References

[1] Blaisdell, G.A., Mansour, N.N., Reynolds W.C. 1991: Numerical simulations of compressible homogeneous turbulence. Dept. of Mechanical Engineering, Stanford University, Report No. TF-50.

[2] Friedrich, R. and Bertolotti, F. 1997 ”Compressibility effects due to turbulent fluctuations”, To appear in Applied Scientific Research.

[3] Gatski, T. B., Speziale, C. G., “On explicit algebraic stress models for complex turbulent flows”, J. Fluid Mech., vol. 254, 1993.

[4] Girimaji, S.S., 1995, “Fully-Explicit and Self-Consistent Algebraic Reynolds Stress Model”, ICASE Report No. 95-82.

[5] Johansson, A. V., Wallin, S., 1996, “A new explicit algebraic Reynolds stress model”, Proc. Sixth European Turbulence Conference, Lausanne, P. Monkewitz (ed).

[6] Krogmann, P. & Schülein E., 1996, ”Documentation of Two-dimensional Impinging Shock/Turbulent boundary Layer Interaction Flow”, DLR IB 223- 96 A 49.

[7] Launder, B. E., & Spalding, D. B., 1974 ”The Numerical Computation of turbulent Flows”, Computer Methods in Applied Mechanics and Engineering, **3**, 269-289.

[8] Launder, B. E., Reece, G. J., Rodi, W., 1975, “Progress in the development of a Reynolds-stress turbulence closure”, J. Fluid Mech., vol. 41.

[9] Lindblad, I. A. A., Wallin S., Courty J.-C., Stanewsky, E., Friedrich, R. & Johansson, A. V., 1995, ’Critical Review of Prediction Methods for Compressible Turbulent Attached and Separated Flows’, FFA TN 1995-43.

[10] Patel, V. C., Chen, H. C., 1991, “Near wall turbulence models for complex flows including separation”, AIAA J., Vol. 29, No. 6.

[11] Pope, S.B., 1975, “A more general effective-viscosity hypothesis”, J. Fluid Mech., vol. 72, part 2.

[12] Rizzi, A., Eliasson, P., Lindblad I., Hirsch, C., Lacor C. & Häuser, J., 1993, “The engineering of multiblock/multigrid software for Navier-Stokes flows on structured meshes”, Comp. Fluids., Vol. 22, pp 341-367.

[13] Rodi, P.E., Dolling, D.S., 1992, “An Experimental/ Computational Study of Sharp Fin Induced Shock Wave/Turbulent Boundary Layer Interactions at Mach 5: Experimental Results”, AIAA-92-0749.
[14] Rodi, W., 1972, ”The prediction of free turbulent boundary layers by use of a two equation model of turbulence”, *Ph.D. thesis*, University of London.
[15] Rodi, W., 1976, “A new algebraic relation for calculating the Reynolds stresses”, Z. angew. Math. Mech. 56, T219-221.
[16] Sarkar, S., Erlebacher, G., Hussaini, M.Y., Kreiss H.O. 1991: The analysis and modelling of dilatational terms in compressible turbulence. J. Fluid Mech., 227, pp.473-493.
[17] Sarkar, S. 1995: The stabilizing effect of compressibility in turbulent shear flow. J. Fluid Mech., 282, pp. 163-186.
[18] Schmatz, M. A., 1989, ”NSFLEX - An Implicit Relaxation Method for the Navier-Stokes Equations for a Wide Range of Mach Numbers”, MBB Internal report MBB/ FE122/S/PUB/366.
[19] Schmatz, M.A., Höld, R.K., Monnoyer, FF., Mundt, Ch., Wanni, K.M. 1991, ”Numerical Methods for Aerodynamic Design II”. *Space Course Aachen* 1991.
[20] Shih, T. H., Zhu, J., Lumley, J. L., “A Realizable Reynolds Stress Algebraic Equation Model”, NASA TM 105993, ICOMP-92-27, CMOTT-92-14, 1992.
[21] Taulbee, D. B., “An improved algebraic Reynolds stress model and corresponding nonlinear stress model”, Phys. Fluids A 4 (11), Nov., 1992.
[22] Wallin, S., Krogmann, P., Stanewsky, E. Shülein, E., Lechner, R., Ravachol, M. & Courty, J.-C., 1996, “Preparatory Activities for Theoretical and Experimental Tasks in Turbulence Modeling of Hypersonic Air Intake Flows”, FFA TN 1996-46.
[23] Wallin, S. & Johansson, A. V., 1996, A New Explicit Algebraic Reynolds Stress Turbulence Model Including an Improved Near-wall Treatment”, Proc. 6th Int. Symp. Flow Mod. and Turb. Meas., Tall. Fl., Sept 8-10, 1996, Ed. Chen, C.-J., Shih, C., Lienau, J. & Kung, R.
[24] Wallin, S.,Lechner, R. Ravachol, M., 1997, “Validation of Improved Turbulence Model”, FFA TN 1997-14.
[25] Wallin, S. & Krogmann, P., 1997, “Validation of Improved Methodology”, FFA TN 1997-15.
[26] Wallin, S, Johansson, A. V., 1997, “A complete explicit algebraic Reynolds stress turbulence model for incompressible and compressible flows”,FFA TN 1997-51.
[27] Wilcox, D. C., 1991, ”Progress in Hypersonic Modeling”, AIAA paper 91-1785.
[28] Wilcox, D. C., 1993, ”Turbulence Modeling for CFD, DCW Industries Inc., La Canada, USA.
[29] Wilcox, D. C., 1994, ”Simulation of Transition with a Two-equation Turbulence Model, AIAA J. **32** no. 2, 247-255.
[30] Zeman, O., 1990, ”Dilatational Dissipation: The Concept and Application in Modeling Compressible Mixing Layers”, *Phys. of Fluids A*, **2**, 178-188.

Paper 3

3

EVOLUTION OF AN ISOLATED TURBULENT TRAILING VORTEX

Stefan Wallin
The Aeronautical Research Institute of Sweden (FFA)
Box 11021, SE-16111 Bromma, Sweden

Sharath S. Girimaji
Institute for Computer Applications in Science and Engineering (ICASE)
NASA Langley Research Center, Hampton, VA 23681

Abstract. The long time development of an isolated wing tip turbulent vortex has been studied by Reynolds averaged Navier-Stokes computations. The vortex is assumed to extend to infinity and to be axisymmetric and homogeneous in the axial direction, and the axial velocity is assumed to be negligible. The validity of different turbulence models, ranging from Reynolds stress transport models to eddy-viscosity K-ε models, has been assessed and qualitative comparisons with field measurements are made. Reynolds stress transport models correctly predict strong suppression of the turbulence in the rotation-dominated vortex core and a reasonable decay rate of the vortex. Outside of the core, the different Reynolds stress models differ significantly. The standard eddy-viscosity K-ε model is insensitive to rotation and, thus, overpredicts the vortex decay rate. Computations using explicit algebraic Reynolds stress models that are strictly based on Reynolds stress transport models show that the algebraic form compares reasonably well with the full transport form. It is, however, important that the curved flow algebraic assumption is invoked when deriving the explicit algebraic model.

1. Introduction

The long time development of wing tip vortices is of major interest in determining the safe distance between airplanes at takeoff and landing. The vortices persist for long times because the turbulence in the vortex core is strongly suppressed by the rotation. The vortex decays from the outer parts leaving the core more or less unaffected for long times, and thus, the radius of the maximum swirl velocity does not change much in time.

The decay mechanism for aircraft trailing vortices evolving in atmospheric turbulence is complex and involves several different processes. It is believed (Proctor [1], Sarpkaya and Daly [2], Sarpkaya [3], and others) that the decay mechanism is influenced by ambient atmospheric turbulence and stratification, three-dimensional vortex pair dynamic instabilities, and ground effects, as well as self-generated turbulence in the vortex. Each of these effects may be important at different conditions and should not be excluded in a complete analysis.

Coherent Doppler laser radar (LIDAR) measurements of trailing vortices of aircraft at takeoff and landing have been analyzed by Proctor [1], and the overall conclusion is that there exist strong correlations between the vortex decay rates and ambient conditions. That suggests that the self-generated turbulence within the vortex is of secondary importance, especially during daytime when the atmospheric dissipation rates are high. The vortex dissipation mechanisms are complex, are not fully understood, and involve many different aspects that will not be addressed within this study. In a typical wake vortex, the Reynolds number is of the order of 10^7, which means that molecular diffusion is of lesser importance compared to turbulent diffusion.

Measurements of the near-field vortex rollup process [4] [5] show that the vortex is initially fully turbulent. The source of turbulence is primarily the highly unstable shear layer from the wing trailing edge that winds up around the core. The winding of the vortex sheet generates a wakelike deficit in the axial velocity. That is another strong source of turbulence, shown by Ragab and Sreedhar [6] using large-eddy simulations. The turbulence in the vortex core is, however, strongly suppressed. It has been observed, experimentally as well as numerically, that the Reynolds shear stresses and turbulence production tend to zero approaching the vortex core. The reason for that is that the flow in the core is close to solid body rotation, which is strongly stabilizing. Because the Reynolds number is large, the core expands very little in time.

Further downstream, the winding vortex sheet and the axial velocity deficit have been diffused by the turbulence, and any strong sources of turbulence do not exist any more. In this study, we will focus on this later stage of the vortex development. Because physical or numerical experimental data are rare for far-field vortices, we must rely on field observations and measurements. From field measurements the following features of trailing vortices have been established: 1) The core persists for a reasonable long period of time as the decay begins at the outer edges of the vortex and propagates inward. 2) there is no discernible overshoot in the circulation profile.

In a previous study by Zeman [7] of an isolated single vortex, it is reported that two-equation eddy-viscosity models, such as the K-ε model, 1) strongly overpredict the decay rate of the vortex and 2) predict massive overshoots in circulation. The results obtained using a Reynolds stress transport (RST) model were in fact almost laminar. The turbulence shear stress $\overline{uv}$ was much lower than the molecular stress all over the vortex. The observed vortex decay is, however, much faster than laminar decay for the high Reynolds number vortices from a typical aircraft.

In an accompanying ongoing study by Wallin and Girimaji, single finite and infinite vortices using more advanced RST models are studied. Their results are more in line with observed trailing vortex behavior as they capture all of the qualitative aspects quite accurately. The objective of this study is to determine

if a two-equation explicit algebraic Reynolds stress model (EARSM) is indeed capable of capturing the observed features of the trailing vortex. This study is motivated by our ultimate goal of developing a three-dimensional unsteady Reynolds averaged Navier-Stokes (RANS) capability for detailed investigation of trailing vortices. Clearly, for such an effort a two-equation EARSM is more viable than the more expensive RST models.

We will later show the importance of the pressure-strain model in this highly rotating flow and that models based on the Speziale–Sarkar–Gatski (SSG) [8] model give results in line with observations whereas models based on the Launder–Reece–Rodi (LRR) [9] model give lower turbulence levels and, thus, a vortex decay rate slower than observed. This will explain the laminar solution that Zeman [7] obtained with the so-called isotropization of production model, which is close to the LRR model.

We will also show that explicit algebraic Reynolds stress models are capable of predicting the qualitative behavior if 1) the model is fully self-consistent, 2) the model is based on SSG, and 3) the weak equilibrium assumption is made in an appropriate curvilinear coordinate system (see Girimaji [10]).

2. Modeling assumptions

We will consider the wing-tip vortex in the farwake after any three-dimensional and time-dependent disturbances have vanished. The axial velocity component and the axial derivatives are assumed to be negligible. The vortex may, thus, be considered as axisymmetric, homogeneous in the axial direction, and developing in time [11]. It is, therefore, natural to express the flow in the vortex in a cylindrical coordinate system where $\hat{\mathbf{e}}_i = [\hat{\mathbf{r}}, \hat{\boldsymbol{\theta}}, \hat{\mathbf{z}}]$.

We define the spatial differentiation operator as

$$\nabla \equiv \hat{\mathbf{e}}_i \frac{\partial}{\partial x_i} \tag{1}$$

where

$$\frac{\partial}{\partial x_i} \equiv \left[\frac{\partial}{\partial r}, \frac{1}{r}\frac{\partial}{\partial \theta}, \frac{\partial}{\partial z} \right] \tag{2}$$

in a cylindrical coordinate system. In the problem considered, $\partial/\partial z \equiv 0$ because the axial direction is homogeneous. The problem is also homogeneous in the azimuthal direction, but the $\hat{\boldsymbol{\theta}}$ derivative may not be excluded from the nabla operator because the $\hat{\boldsymbol{\theta}}$ derivative of the unit vectors $\hat{\mathbf{r}}$ and $\hat{\boldsymbol{\theta}}$ are nonzero. Let us define the derivative of the unit vectors as follows:

$$\frac{\partial \hat{\mathbf{e}}_i}{\partial x_j} = \Gamma_{ijk} \hat{\mathbf{e}}_k \tag{3}$$

where Γ_{ijk} is all zero except $\Gamma_{122} = 1/r$ and $\Gamma_{221} = -1/r$. By the use of this definition, one may expand the gradient operating on any tensor of any rank

simply by the use of the chain rule, that is, the gradient of the velocity expands to

$$\nabla \mathbf{U} = \hat{\mathbf{e}}_i \frac{\partial}{\partial x_i} (\hat{\mathbf{e}}_j U_j) = \hat{\mathbf{e}}_i \hat{\mathbf{e}}_j \left(\frac{\partial U_j}{\partial x_i} + \Gamma_{kij} U_k \right). \tag{4}$$

By the use of the preceding assumptions, the Reynolds averaged velocity may be written as $\mathbf{U} = \hat{\boldsymbol{\theta}} V(r)$, and the Reynolds averaged momentum equation in the $\hat{\boldsymbol{\theta}}$ direction reads

$$\frac{\partial V}{\partial t} = \frac{1}{r^2} \frac{\partial}{\partial r} \left[r^3 \nu \frac{\partial}{\partial r} \left(\frac{V}{r} \right) - r^2 \overline{uv} \right] \tag{5}$$

To close the momentum equation one needs an expression for $\overline{uv}$, which is the $\hat{\mathbf{r}}\hat{\boldsymbol{\theta}}$ component of the Reynolds stresses, $\overline{\overline{\tau}} = \hat{\mathbf{r}}\hat{\mathbf{r}}\overline{u^2} + \hat{\boldsymbol{\theta}}\hat{\boldsymbol{\theta}}\overline{v^2} + \hat{\mathbf{z}}\hat{\mathbf{z}}\overline{w^2} + (\hat{\mathbf{r}}\hat{\boldsymbol{\theta}} + \hat{\boldsymbol{\theta}}\hat{\mathbf{r}})\overline{uv}$.

2.1. Reynolds stress transport modeling. Strong rotational and streamline curvature effects are present in the vortex. The stabilizing effects are in fact so strong that any preexisting turbulence in the core of the vortex is almost completely suppressed. It is, thus, believed that RST closures are needed in order to capture the turbulence physics properly. The transport equation for the Reynolds stress tensor in an inertial frame of reference may be written in symbolic form as

$$\frac{\mathrm{D}\,\tau_{ij}}{\mathrm{D}t} - \mathcal{D}_{ij} = \mathcal{P}_{ij} + \Pi_{ij} - \varepsilon \left(e_{ij} + \frac{2}{3}\delta_{ij} \right) \tag{6}$$

The molecular and turbulent diffusion $\mathcal{D}_{ij}$ the pressure-strain term Π_{ij}, and the dissipation rate anisotropy e_{ij} need to be modeled because they contain higher-order correlations. The production term is, however, explicit and reads

$$\mathcal{P}_{ij} = -\left(\tau_{ik} S_{kj} + S_{ik} \tau_{kj}\right) + \left(\tau_{ik} \Omega_{kj} - \Omega_{ik} \tau_{kj}\right) \tag{7}$$

where the mean flow strain and rotation rate tensors are

$$\begin{aligned} \mathbf{S} &= \frac{1}{2} \left[(\nabla \mathbf{U})^T + \nabla \mathbf{U} \right] = \frac{1}{2} \left(\frac{\partial V}{\partial r} - \frac{V}{r} \right) \left(\hat{\mathbf{r}}\hat{\boldsymbol{\theta}} + \hat{\boldsymbol{\theta}}\hat{\mathbf{r}} \right) \\ \boldsymbol{\Omega} &= \frac{1}{2} \left[(\nabla \mathbf{U})^T - \nabla \mathbf{U} \right] = \frac{1}{2} \left(\frac{\partial V}{\partial r} + \frac{V}{r} \right) \left(\hat{\boldsymbol{\theta}}\hat{\mathbf{r}} - \hat{\mathbf{r}}\hat{\boldsymbol{\theta}} \right) \end{aligned} \tag{8}$$

The standard form of the transport equation for the dissipation rate ε is adopted. For the vortex considered, the advection of ε, as well as the advection of any scalar quantity, is zero, and the equation for ε reads

$$\frac{\partial \varepsilon}{\partial t} - \mathcal{D}^{(\varepsilon)} = \left(C_{\varepsilon 1} \mathcal{P} - C_{\varepsilon 2} \varepsilon \right) \frac{\varepsilon}{K} \tag{9}$$

where the production $\mathcal{P} \equiv \mathcal{P}_{ii}/2$ and $\mathcal{D}^{(\varepsilon)}$ is the molecular and turbulent diffusion of ε. $C_{\varepsilon 1} = 1.45$ and $C_{\varepsilon 2} = 1.90$ is used.

The assumptions made for the vortex are that both the $\hat{\mathbf{z}}$ and $\hat{\boldsymbol{\theta}}$ directions are homogeneous. Moreover, the $\hat{\mathbf{r}}$ component of the mean velocity vanishes. The advection of the Reynolds stresses then only contain algebraic (nondifferential)

TABLE 1. The values of the C coefficients for different linear pressure-strain models

	C_1^0	C_1^1	C_2	C_3	C_4
Linearized SSG (L-SSG)	3.4	1.8	0.36	1.25	0.40
Original LRR	3.0	0	0.8	1.75	1.31
Re-calibrated LRR (LRR)	3.6	0	0.8	2	1.11

terms that originate from the $\hat{\boldsymbol{\theta}}$ derivatives of the unit vectors. The material derivative in cylindrical coordinates, thus, becomes

$$\frac{\mathrm{D}\,\tau_{ij}}{\mathrm{D}t} = \frac{\partial \tau_{ij}}{\partial t} - \left(\tau_{ik}\Omega_{kj}^{(r)} - \Omega_{ik}^{(r)}\tau_{ki}\right) \tag{10}$$

where

$$\boldsymbol{\Omega}^{(r)} = \frac{V}{r}\left(\hat{\boldsymbol{\theta}}\hat{\mathbf{r}} - \hat{\mathbf{r}}\hat{\boldsymbol{\theta}}\right) \tag{11}$$

that is, the advection does not contain any spatial derivatives. With $V/r = \omega^R$, this term is actually half of the Coriolis term that appears in the Reynolds stress equation written in a rotating frame of reference, where ω^R is the (constant) rotation rate of the system. The other half of the Coriolis term originates from a similar transformation of the production term.

The modeling of the pressure-strain term is an important issue, especially in rotation-dominated flows. Models that are linear in the Reynolds stress anisotropy have been widely used due to the simplicity and general good behavior in a number of benchmark flows of engineering interest. Recently more attention has been placed on non-linear models, for example, the SSG model [8], which has been found to be superior to linear models in many aspects. In this study, we will focus on the performance of EARSMs where only linear pressure-strain models may be considered.

The pressure-strain and dissipation rate anisotropy are usually lumped together into the general linear form, for example see Girimaji [12],

$$\begin{aligned}\frac{\Pi_{ij}}{\varepsilon} - e_{ij} = -\frac{1}{2}\left(C_1^0 + C_1^1\frac{\mathcal{P}}{\varepsilon}\right)a_{ij} + C_2\frac{K}{\varepsilon}S_{ij} \\ +\frac{C_3}{2}\frac{K}{\varepsilon}\left(a_{ik}S_{kj} + S_{ik}a_{kj} - \frac{2}{3}a_{kl}S_{lk}\delta_{ij}\right) - \frac{C_4}{2}\frac{K}{\varepsilon}\left(a_{ik}\Omega_{kj} - \Omega_{ik}a_{kj}\right)\end{aligned} \tag{12}$$

where the Reynolds stress anisotropy a_{ij} is defined as

$$a_{ij} \equiv \frac{\tau_{ij}}{K} - \frac{2}{3}\delta_{ij} \tag{13}$$

and $K \equiv \tau_{ii}/2$ is the turbulent kinetic energy. The classical LRR model [9] and the SSG model [8] linearized around equilibrium homogeneous shear may be included in this general form where the C coefficients are given in Table 1 (for example, see Gatski and Speziale [13] for linearization of the SSG model).

The original calibration of the LRR model have not been optimal in all situations, and more recent calibrations of the LRR model imply that the Rotta coefficient $c_1 \approx 1.8$ and the coefficient in the rapid pressure strain model $c_2 \approx 5/9$, for example, see Taulbee [14], Lumley [15], Shabbir and Shih [16], and Wallin and Johansson [17] [18]. All LRR computations in this study were made using the recalibrated set of coefficients. The SSG model, also in the linearized form, is known to be superior to the LRR model in rotation-dominated flows, for example, see Gatski and Speziale [13], where the SSG model, the differential as well as its algebraic form, performs well for homogeneous rotating shear flows. In this study we will investigate the differences between these models for the vortex flow.

The term that remains to be modeled in the Reynolds stress transport equation (6) is the turbulent transport term. The molecular and turbulent diffusion of the Reynolds stresses, $\mathcal{D}_{ij}$, is

$$\hat{\mathbf{e}}_i \hat{\mathbf{e}}_j \mathcal{D}_{ij} = \nabla \cdot \left(\nu \nabla \overline{\overline{\tau}} - \mathbf{T} \right) \tag{14}$$

where $\mathbf{T}$ is the turbulent flux of Reynolds stresses. In the present computation we will adopt the Daly and Harlow [19] model that reads

$$\mathbf{T} = -c_s \frac{K}{\varepsilon} \overline{\overline{\tau}} \cdot \nabla \overline{\overline{\tau}} \tag{15}$$

where $c_s = 0.25$. With the assumptions we have made for the vortex, the diffusion becomes

$$\mathcal{D}_{ij} = \frac{1}{r} \frac{\partial}{\partial r} \left[r \left(\nu + c_s \frac{K}{\varepsilon} \overline{u^2} \right) \frac{\partial \tau_{ij}}{\partial r} \right] + \mathcal{D}_{ij}^{(ex)} \tag{16}$$

where the extra diffusion $\mathcal{D}_{ij}^{(ex)}$ consists of all terms that emanate from the nonzero $\hat{\boldsymbol{\theta}}$ derivatives of the unit vectors. The nonzero components of the extra diffusion read

$$\begin{aligned}
\mathcal{D}_{uv}^{(ex)} &= \frac{1}{r} \frac{\partial}{\partial r} \left[c_s \frac{K}{\varepsilon} \overline{uv} \left(\overline{u^2} - \overline{v^2} \right) \right] + c_s \frac{K}{\varepsilon} \frac{\overline{uv}}{r} \left[\frac{\partial}{\partial r} \left(\overline{u^2} - \overline{v^2} \right) - 4 \frac{\overline{v^2}}{r} \right] - 4\nu \frac{\overline{uv}}{r^2} \\
\mathcal{D}_{uu}^{(ex)} &= -\mathcal{D}_{vv}^{(ex)} = \frac{1}{r} \frac{\partial}{\partial r} \left[-2 c_s \frac{K}{\varepsilon} \overline{uv}^2 \right] \\
&\quad - 2 c_s \frac{K}{\varepsilon} \left[\frac{\overline{uv}}{r} \frac{\partial \overline{uv}}{\partial r} + \frac{\overline{v^2} \left(\overline{u^2} - \overline{v^2} \right)}{r^2} \right] - 2\nu \frac{\overline{u^2} - \overline{v^2}}{r^2}
\end{aligned} \tag{17}$$

Finally, the Daly and Harlow model for the dissipation reads

$$\mathcal{D}^{(\varepsilon)} = \frac{1}{r} \frac{\partial}{\partial r} \left[r \left(\nu + c_\varepsilon \frac{K}{\varepsilon} \overline{u^2} \right) \frac{\partial \varepsilon}{\partial r} \right] \tag{18}$$

where $c_\varepsilon = 0.15$.

2.2. Algebraic Reynolds stress modeling. An alternative of writing the system of equations in terms of the Reynolds stresses is to reformulate the equations in terms of the Reynolds stress anisotropy and the turbulent kinetic energy. In flows where the anisotropy varies slowly in time and space, the transport equation for the Reynolds stress anisotropy tensor reduces to an implicit algebraic relation. Also in many inhomogeneous flows of engineering interest, the flow is steady and the advection and diffusion of the Reynolds stress anisotropy may be neglected [20] [21]. This is equivalent to assuming that the advection and diffusion of the individual Reynolds stresses scale with those of the turbulent kinetic energy.

The advection of the Reynolds stress tensor is, however, dependent on the coordinate system and would, thus, lead to an algebraic relation and a model that is dependent of the choice of coordinate system. This could be of major importance in flows with strong streamline curvature, such as strongly rotating flows. In circular flows it is, therefore, most appropriate to neglect the advection of the anisotropy following a streamline, which is similar to neglecting the rate of change of the anisotropy following a fluid particle. For the vortex flow considered in this study, this is fulfilled exactly by including the algebraic terms in (10). In a more general flow it is possible to define a Galilean invariant curvilinear coordinate system based on the acceleration vector [10].

By the use of the general linear pressure-strain model in (12), the transport equation for the Reynolds stress anisotropy tensor reads

$$\frac{K}{\varepsilon}\left(\frac{\partial a_{ij}}{\partial t}-\mathcal{D}_{ij}^{(a)}\right)=-\left(L_1^0+\frac{L_1^1}{2}\frac{\mathcal{P}}{\varepsilon}\right)a_{ij}+2L_2\frac{K}{\varepsilon}S_{ij}$$
$$+L_3\frac{K}{\varepsilon}\left(a_{ik}S_{kj}+S_{ik}a_{kj}-\frac{2}{3}a_{kl}S_{lk}\delta_{ij}\right)-L_4\frac{K}{\varepsilon}\left(a_{ik}\Omega_{kj}^*-\Omega_{ik}^*a_{kj}\right) \quad (19)$$

The advection of the Reynolds stress anisotropy is, for the vortex, exactly included in the modified rotation rate tensor

$$\mathbf{\Omega}^*=\mathbf{\Omega}-\frac{\mathbf{\Omega}^{(r)}}{L_4} \quad (20)$$

where $\mathbf{\Omega}^{(r)}$ is given by (11). The L coefficients are related to the C coefficients in (12) through

$$L_1^0=\frac{C_1^0}{2}-1,\quad L_1^1=C_1^1+2,\quad L_2=\frac{C_2}{2}-\frac{2}{3},\quad L_3=\frac{C_3}{2}-1,\quad L_4=\frac{C_4}{2}-1 \quad (21)$$

The transport equation for the turbulent kinetic energy is obtained by taking half of the trace of the equation for the Reynolds stress tensor

$$\frac{\partial K}{\partial t}-\mathcal{D}^{(K)}=\mathcal{P}-\varepsilon \quad (22)$$

where the diffusion of turbulent kinetic energy is

$$\mathcal{D}^{(K)} = \frac{1}{2}\mathcal{D}_{ii} = \frac{1}{r}\frac{\partial}{\partial r}\left[r\left(\nu + c_s\frac{K}{\varepsilon}\overline{u^2}\right)\frac{\partial K}{\partial r}\right] \tag{23}$$

Neglecting the time dependency and the molecular and turbulent diffusion of the Reynolds stress anisotropy $\mathcal{D}_{ij}^{(a)}$, the left-hand side of (19), leads to an algebraic relation

$$\begin{aligned} 0 = &-\left(L_1^0 + \frac{L_1^1}{2}\frac{\mathcal{P}}{\varepsilon}\right)a_{ij} + 2L_2\frac{K}{\varepsilon}S_{ij} \\ &+ L_3\frac{K}{\varepsilon}\left(a_{ik}S_{kj} + S_{ik}a_{kj} - \frac{2}{3}a_{kl}S_{lk}\delta_{ij}\right) - L_4\frac{K}{\varepsilon}\left(a_{ik}\Omega_{kj}^* - \Omega_{ik}^*a_{kj}\right) \end{aligned} \tag{24}$$

Also in the algebraic equation, advection of the Reynolds stress anisotropy is exactly included through the modified rotation rate tensor $\mathbf{\Omega}^*$ (20). Thus, the importance of the advection may be investigated by excluding the $\mathbf{\Omega}$ correction.

2.3. Explicit algebraic Reynolds stress modeling. Using representation theory, Pope [22] proposed that the implicit relation (24) may be solved so that an explicit relation for the anisotropy is obtained. The scalar nonlinearity in $\mathcal{P}/\varepsilon$, because $\mathcal{P} = -Ka_{ij}S_{ji}$, may be expressed as a cubic polynomial that has an explicit solution [12] [23]. That will result in a fully explicit and self-consistent algebraic relation for the Reynolds stress anisotropy tensor that may be written as

$$a_{ij} = \beta_1\frac{K}{\varepsilon}S_{ij} + \beta_2\left(\frac{K}{\varepsilon}\right)^2\left(S_{ik}S_{kj} - \frac{2}{3}I\!I_S\delta_{ij}\right) + \beta_4\left(\frac{K}{\varepsilon}\right)^2\left(S_{ik}\Omega_{kj}^* - \Omega_{ik}^*S_{kj}\right) \tag{25}$$

where

$$\beta_1 = -\frac{A_1N}{Q} \quad \beta_2 = 2\frac{A_1A_2}{Q} \quad \beta_4 = -\frac{A_1}{Q} \tag{26}$$

and

$$Q = N^2 - 2\left(\frac{K}{\varepsilon}\right)^2 I\!I_{\Omega^*} - \frac{2}{3}A_2^2\left(\frac{K}{\varepsilon}\right)^2 I\!I_S \tag{27}$$

The invariants $I\!I_S \equiv S_{ik}S_{kj}$ and $I\!I_{\Omega^*} \equiv \Omega_{ik}^*\Omega_{kj}^*$, and $N \equiv A_3 + A_4\mathcal{P}/\varepsilon$. The solution to the cubic equation for $\mathcal{P}/\varepsilon$ or N reads

$$N = \begin{cases} \dfrac{A_3}{3} + \left(P_1 + \sqrt{P_2}\right)^{1/3} + \left(P_1 - \sqrt{P_2}\right)^{1/3} & , P_2 \geq 0 \\ \dfrac{A_3}{3} + 2\left(P_1^2 - P_2\right)^{1/6}\cos\left(\dfrac{1}{3}\arccos\left(\dfrac{P_1}{\sqrt{P_1^2 - P_2}}\right)\right) & , P_2 < 0 \end{cases} \tag{28}$$

where

$$P_1 = \left[\frac{{A_3}^2}{27} + \left(\frac{A_1 A_4}{6} - \frac{2}{9}{A_2}^2\right)\left(\frac{K}{\varepsilon}\right)^2 II_S - \frac{2}{3}\left(\frac{K}{\varepsilon}\right)^2 II_{\Omega^*}\right] A_3$$

$$P_2 = {P_1}^2 - \left[\frac{{A_3}^2}{9} + \left(\frac{A_1 A_4}{3} + \frac{2}{9}{A_2}^2\right)\left(\frac{K}{\varepsilon}\right)^2 II_S + \frac{2}{3}\left(\frac{K}{\varepsilon}\right)^2 II_{\Omega^*}\right]^3 \quad (29)$$

When computing the third root, one need to make sure that the real root is returned even for negative arguments, and the arccos function should return an angle between 0 and π. The A coefficients are related to the L coefficients in (19) through

$$A_1 = 2\frac{L_2}{L_4}, \quad A_2 = \frac{L_3}{L_4}, \quad A_3 = -\frac{L_1^0}{L_4}, \quad A_4 = -\frac{1}{2}\frac{L_1^1}{L_4} \quad (30)$$

Thus, the Reynolds stress anisotropy is fully explicitly expressed in terms of the mean flow gradient and the turbulent time scale (K/ε). This replaces the transport equation for the anisotropy tensor and is used together with the transport equations for the turbulent kinetic energy (22) and the dissipation rate (9). The Reynolds stresses are directly related to the anisotropy through definition (13). The Daly and Harlow modeling of the transport of K and ε, (23) and (18), is also kept at this level of modeling.

The formal reduction of the full Reynolds stress transport model results in a two-equation turbulence model where the standard eddy-viscosity assumption is replaced with a more complete constitutive relation. This can be compared to the eddy-viscosity assumption that relates the Reynolds stresses linearly to the mean flow strain rate tensor

$$a_{ij} = -2C_\mu \frac{K}{\varepsilon} S_{ij} \quad (31)$$

where the coefficient $C_\mu = 0.09$. Even the first term in (25) gives a much better description of the anisotropy since the effective $C_\mu^{\text{eff}} = -\beta_1/2$ is not a constant but is dependent on the local flow state. Moreover, the eddy-viscosity assumption does not give realistic values of the normal Reynolds stress components, and thus, the Daly and Harlow diffusion model could not be used. The diffusion terms in the K and ε equations, for the standard eddy-viscosity K-ε model, are thus modeled using a simple gradient diffusion model that reads

$$\mathcal{D}^{(K)} = \frac{1}{r}\frac{\partial}{\partial r}\left[r\left(\nu + \frac{C_\mu}{\sigma_K}\frac{K^2}{\varepsilon}\right)\frac{\partial K}{\partial r}\right]$$

$$\mathcal{D}^{(\varepsilon)} = \frac{1}{r}\frac{\partial}{\partial r}\left[r\left(\nu + \frac{C_\mu}{\sigma_\varepsilon}\frac{K^2}{\varepsilon}\right)\frac{\partial \varepsilon}{\partial r}\right] \quad (32)$$

where the standard values $\sigma_K = 1.0$ and $\sigma_\varepsilon = 1.3$ are used.

3. Numerical methods and boundary conditions

The system of equations is integrated in time using a first-order implicit method (backward Euler) from a prescribed initial condition. For every time step, the system of equations is iterated until convergence by reducing the residual 6 decades. Second-order central differences on a staggered grid is used for the spatial discretization.

Typically, 1000 time steps for two-equation computations and 2000 time steps for full Reynolds stress computations were used in the computations. Decreasing the time step did not influence the result here. 100 computational points in the radial direction were used, 20 points with an equidistant distribution within $r = 2R_c$ and the other points smoothly stretched towards the outer boundary. Doubling the number of grid points alters the computed circulation by less than 1%.

To keep the symmetry for the velocity components in the cylindrical coordinate system, the tangential velocity as well as the Reynolds shear stress component must be zero. Moreover, the normal Reynolds stress components as well as K and ε should have zero spatial derivatives. The boundary conditions at $r = 0$ are

$$V = \frac{\partial \overline{u^2}}{\partial r} = \frac{\partial \overline{v^2}}{\partial r} = \frac{\partial \overline{w^2}}{\partial r} = \frac{\partial K}{\partial r} = \frac{\partial \varepsilon}{\partial r} = \overline{uv} = 0 \tag{33}$$

The outer edge of the computational domain is situated far away from the vortex. The boundary condition for the tangential velocity is obtained by assuming that the flow is inviscid, and thus, the vortex circulation Γ approaches a constant. The boundary condition for the turbulence quantities are set in such a way that an initial freestream turbulence level would properly decay in time. This requires, however, that the computational domain is large enough so that the production and diffusion at the outer boundary, R_{max}, are negligible. In this study $R_{max} \approx 100$ core radii. The boundary conditions at $r = R_{max}$ are

$$\frac{\partial}{\partial r}(rV) = \frac{\partial \overline{u^2}}{\partial r} = \frac{\partial \overline{v^2}}{\partial r} = \frac{\partial \overline{w^2}}{\partial r} = \frac{\partial K}{\partial r} = \frac{\partial \varepsilon}{\partial r} = \frac{\partial \overline{uv}}{\partial r} = 0. \tag{34}$$

The system of equation and the boundary conditions are specified in a differential form using the symbolic manipulation tool MAPLE. FORTRAN subroutines that compute the discrete system matrix are then automatically generated with the aid of routines written in MAPLE. The sources of programming errors are then reduced to the much more limited number of lines of the MAPLE code compared to the final Fortran code.

4. The test case and computational results

In the test case adopted for this study we will eliminate all effects of ambient influence, such as atmospheric turbulence, stratification, or the other vortex, to study the isolated effect of vortex decay subjected to self-generated turbulence.

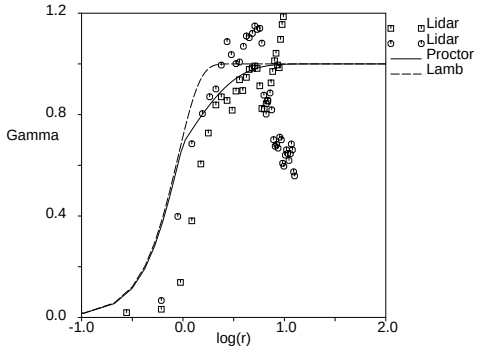

FIGURE 1. Different initial circulation profiles, Proctor and Lamb, compared to measured profiles at $t = 5$s.

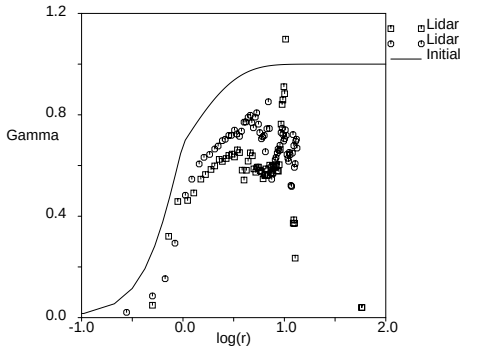

FIGURE 2. Measured circulation profiles at $t = 55s$ compared to the initial profile (Proctor).

The outer edge boundary condition is, thus, put far away, and the vortex is initiated assuming that it extends to infinity. LIDAR measurements of an aircraft trailing vortex at the Memphis airport, case 1252 [24] [25], will be used for a qualitative comparison with the computations. The case is characterized by low ambient turbulence during nighttime and slow vortex decay rate. Despite the low turbulence levels, it is still believed that the ambient conditions are of importance for the vortex decay rate. Comparisons with the observed vortex decay rate are, thus, not fully relevant because these effects are not present in the computations. Nevertheless, the measured circulation profile at $t = 5$s will be used as initial conditions for the computations, and the computational results will be compared to profiles measured at $t = 55$s, shown in Figures 1 and 2.

4.1. Initial conditions. The vortex circulation, defined as $\Gamma \equiv 2\pi r V$, increases from zero at the core center and levels up to a fairly constant level, Γ_0, outside of the vortex core. The vortex strength Γ_0 is typically around $350\text{m}^2/\text{s}$ and the core radius R_c, defined as the position of the peak tangential velocity, is typically around 1.8m. That gives a Reynolds number based on Γ_0 of about $20 \cdot 10^6$.

The problem is made nondimensional based on $\Gamma_0 = 350\text{m}^2/\text{s}$ and $R_c = 1.8\text{m}$. That means that all lengths are normalized by R_c, time by R_c^2/Γ_0, velocity by Γ_0/R_c, turbulent kinetic energy and Reynolds stresses by Γ_0^2/R_c^2, and dissipation rate by Γ_0^3/R_c^4.

Laminar vortices where the viscosity is constant are self-similar in time with the normalized vortex circulation given by

$$\Gamma = 1 - \exp\left[-\alpha r^2\right] \tag{35}$$

This is referred to as a Lamb vortex (see Saffman [26], p. 253). The coefficient α is usually around 1.26, which gives a maximal normalized velocity $V_{max} \approx 0.11$.

Measurements of aircraft wing-tip trailing vortices over airfields show that the typical circulation distribution is somewhat different from a Lamb vortex. By considering a large set of data from vortex measurements, Proctor [1] proposed an alternative form that better matches the data

$$\Gamma = \begin{cases} 1.4\left(1 - \exp\left[-10\left(\dfrac{1}{B}\right)^{3/4}\right]\right)\left(1 - \exp\left[-1.2527r^2\right]\right) & , r < 1 \\ 1 - \exp\left[-10\left(\dfrac{r}{B}\right)^{3/4}\right] & , r \geq 1 \end{cases} \tag{36}$$

where B is the (normalized) span width of the airplane that generates the vortex. This gives the normalized maximal velocity $V_{max} \approx 0.11$. The initial circulation profiles, Lamb and Proctor, are compared to measured data in Figure 1. The vortex is initially prescribed according to (36) using the normalized span width $B = 17.7$. The initial profile does not perfectly match the data, but the initial core radius was fit to a large number of measurements and the data in Figure 1 are only one set of measurements.

The initialization of the turbulence is, however, not obvious because turbulence field measurements within the vortex are rare. The measured atmospheric turbulence could, however, act as a lower limit for the initial vortex turbulence. For the low turbulence case considered (Dallas 1997 Wake Vortex Data Set CD-ROM, personal communication with Proctor, Flight Dynamics and Control Division, NASA Langley Research Center), the turbulent kinetic energy $K \sim 0.02\text{m}^2/\text{s}^2$ and the dissipation rate $\varepsilon \sim 10^{-5}\text{m}^2/\text{s}^3$. That corresponds to a normalized turbulence level of the order of $K \sim 10^{-7}$ and $\varepsilon \sim 10^{-12}$. The integral length scale is of the order of 10^2 (core radius) which may be unrealistically high for the self-generated turbulence in the vortex. The dissipation rate is, however, universal over all turbulent scales, and by assuming a length scale of the vortex self-generated turbulence in the order of unity, one obtains $K \sim 10^{-8}$ and $\varepsilon \sim 10^{-12}$. At these low initial levels the growth rate is so slow that the flow remains nearly laminar in the RANS computations.

The rollup of a wing-tip vortex takes place in the very near-wake region, and a fully developed and nearly symmetric vortex is formed within the near wake. In the experiment by Chow et al. [4], rollup happened within less than one chord

length from the trailing edge of the wing, whereas Devenport et al. [5] observed a much more extended rollup of the near wake. The vortex is fully turbulent, although the turbulence shear stress in the core is strongly suppressed. The turbulence level at the most downstream measured section is of the order of 10% of the axial freestream velocity, and the maximum swirl velocity was of the same order as the axial freestream velocity. By assuming that the turbulence length scale is of the order of the core radius, one obtains the normalized $K = 10^{-4}$ and $\varepsilon = 10^{-6}$. Using that as initial condition, one found that the turbulence levels quickly decrease to some asymptotic level that is about one order of magnitude lower, shown in Figure 3 (a). During that process, the high-intensity turbulence diffuses the tangential velocity before the decay rate settles down to some asymptotic level. The transient behavior of the circulation is seen in Figure 4 (a). By the setting of the initial turbulence level to the order of that asymptotic state, the initial transient is eliminated and the computed time history becomes somewhat independent of small initial variations and the exact form of the initial profiles.

The turbulence is initially assumed homogeneous, or uniform, with the normalized $K_0 = 10^{-5}$ and $\varepsilon_0 = 10^{-8}$, which gives a freestream turbulence level of 2% of V_{max} and the turbulent macro lengthscale $\Lambda = K^{3/2}/\varepsilon \approx 3.2$. In the differential Reynolds stress computations, the normal Reynolds stress anisotropy is prescribed to be zero, and the normalized Reynolds stress shear component $\overline{uv} = K_0 V(r)$. Figure 4 (b) shows a typical time evolution of a computation initiated with these conditions.

The vortex flow was integrated for a time period of $50s$, which corresponds to 600 vortex turnover times defined as R_c/V_{max}. The computed results may then be compared to the measured data at $t = 55s$. Sarpkaya and Daly [2] introduced an alternative timescale based on the downsweep of the vortex pair and the initial vortex separation $t^* = V_0 t/B$, where $V_0 = \Gamma_0/(2\pi B)$. Note that 55s corresponds to $t^* = 3.0$.

4.2. Reynolds stress transport models. The flow in the core of the vortex approaches solid body rotation, and thus, the production of the turbulence is suppressed. In the outer part of the vortex, the flow gradually changes from rotation-dominated to completely strain dominated. It is well known that standard eddy-viscosity two-equation models, such as the K-ε model, are unable to describe the turbulence in rotation-dominated flows satisfactorily. Also the response of different RST models are known to be substantially different in rotation-dominated flows.

The results using the different RST models are shown in Figure 5. The SSG model is known to perform better than the LRR model in rotation-dominated flows, and the results show that the linear SSG compares well with the measurements in this case whereas the LRR model predicts a decay rate slower than observed. Moreover, no overshoot in circulation could be seen, which is in line

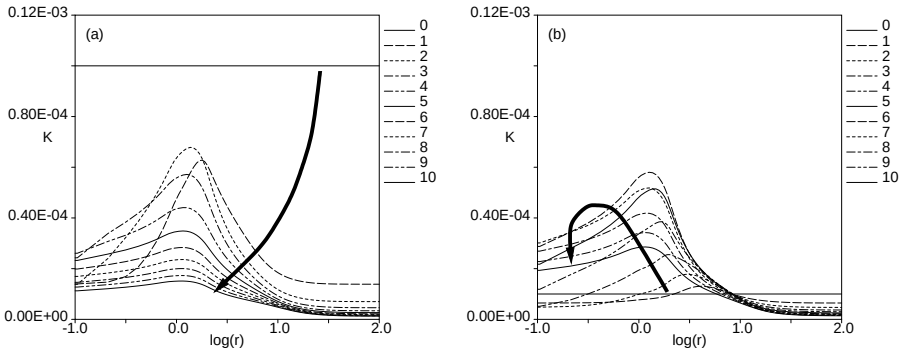

FIGURE 3. The evolution of the computed turbulent kinetic energy subjected to different initial turbulent levels using EARSM based on SSG. (a): High levels where $K = 10^{-4}$ and $\varepsilon = 10^{-6}$. (b): Nominal levels where $K = 10^{-5}$ and $\varepsilon = 10^{-8}$. The spacing between each line is 5s.

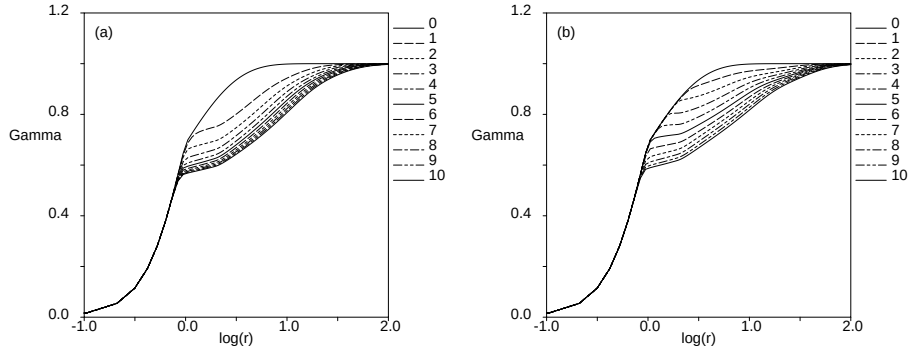

FIGURE 4. The evolution of the computed circulation subjected to different initial turbulent levels using EARSM based on SSG. (a): High levels where $K = 10^{-4}$ and $\varepsilon = 10^{-6}$. (b): Nominal levels where $K = 10^{-5}$ and $\varepsilon = 10^{-8}$. The spacing between each line is 5s.

with observations. A further discussion about a possible overshoot is given in section 4.5.

Figure 5 also shows the Reynolds shear stress for the different RST models. The models correctly predict the strong damping of the turbulence in the vortex core, but in the outer part of the vortex the two models predict very different turbulence shear stresses. The low $\overline{uv}$-values predicted using LRR are consistent with the slow vortex decay rate. Figure 6 shows the turbulent kinetic energy, which, opposite to $\overline{uv}$, do not approach zero in the vortex core. This has also been observed by Devenport et al. [5] experimentally and was explained as influence from the surrounding turbulence.

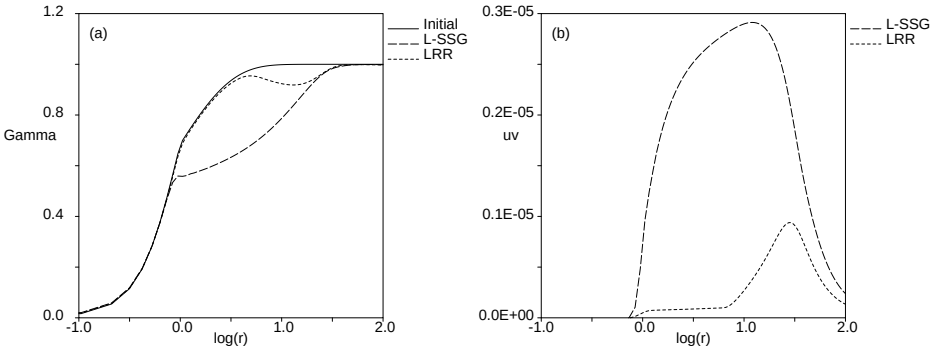

FIGURE 5. The computed vortex circulation (a) and shear stress (b) profiles at $t = 55$s using different RST models. The flow is initiated using the Proctor profile.

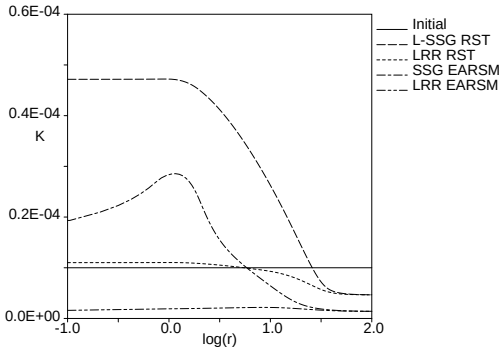

FIGURE 6. The computed turbulent kinetic energy profiles at $t = 55$s using different models. The flow is initiated using the Proctor profile.

4.3. Algebraic Reynolds stress models. Reynolds stress transport models are still not widely used in engineering methods, and so an interesting question is, is it possible to obtain computational results similar to the full SSG by means of much simpler two-equation models?

Self-consistent EARSMs are the most consistent approximations of the basic RST models at a two-equation level. In Figure 7, computational results using EARSM based on both the linearized SSG and the LRR are shown. The EARSM level of modeling follows the behavior of the full Reynolds stress models they are based on. The EARSM based on the LRR predicts a low decay rate of the vortex whereas the EARSM based on the linearized SSG predicts a vortex decay rate in line with observations. For comparison, the result from using the standard K-ε eddy-viscosity model is also shown in Figure 7. As expected, the vortex decay rate is very much overpredicted, and there is a massive overshoot in the circulation profile.

An important difference between the differential and algebraic form of the linearized SSG is the prediction of the Reynolds shear stress and the turbulent kinetic energy (Figure 6). In the outer parts of the vortex the EARSM predicts a much lower $\overline{uv}$ compared to the full RST. However, this has just a small implication on the mean swirl velocity as long as the shear stress in and near the vortex core is reasonably predicted.

In the EARSM computations, the weak equilibrium assumption is made in a Galilean invariant curvilinear coordinate system. The importance of that is investigated by computing one case, EARSM based on SSG, where the weak equilibrium assumption is made in an inertial system. That is equivalent of letting $\mathbf{\Omega}^* = \mathbf{\Omega}$ in (24). The results are labeled (SSG no rot) in Figure 7 and show a vortex decay rate that is complete in error. This result demonstrates the importance of the correct treatment of the advection term in algebraic modeling of turbulent strongly curved flows. Neglecting this effect makes EARSM as bad as standard eddy-viscosity models.

The EARSM approach taken for this study is that the explicit solution is fully self-consistent. That means that the implicit algebraic relation is exactly solved without further assumptions. The importance of this approach is assessed by computing the case using the EARSM based on the linearized SSG model, but without considering the solution for $\mathcal{P}/\varepsilon$ or N in (28), but rather to use the equilibrium value in homogeneous shear. This is similar to the Gatski and Speziale model [13], but in this study we do not consider the regularization of the denominator to avoid singular behavior that is a part of the Gatski and Speziale model, and thus, the only difference between the models is the consistency condition. This model is labeled (G&S) in Figure 8. The G&S model gives a similar vortex decay rate compared to the SSG, but the circulation profile is distorted just outside of the core, and the decay rate is somewhat lower in the outermost regions of the core. It is, however, possible that the regularization would cure this behavior, but that is not considered in this study.

The turbulent diffusion of K and ε in the EARSM computations are determined using the Daly and Harlow model, which relates the diffusivity to the u fluctuations, equations (23) and (18). The importance of the diffusion modeling is determined by using the standard eddy-viscosity gradient diffusion model of the diffusion (32) as a comparison. To obtain somewhat realistic values on the diffusivity, the C_μ coefficient is not taken as a constant, but is related to β_1 in (26), $C_\mu = -\beta_1/2$. Figure 8 shows this comparison for the EARSM based on the linearized SSG model, where (SSG) and (SSG nut) labels the computations using the Daly and Harlow, and eddy-viscosity modeling of the diffusion, respectively. There are only minor differences between the two modeling approaches indicating that the turbulent diffusion modeling is not a critical issue.

The LRR and SSG models gave very different behavior for this flow, and one important difference between the two models is the C_2 coefficient before the S_{ij}

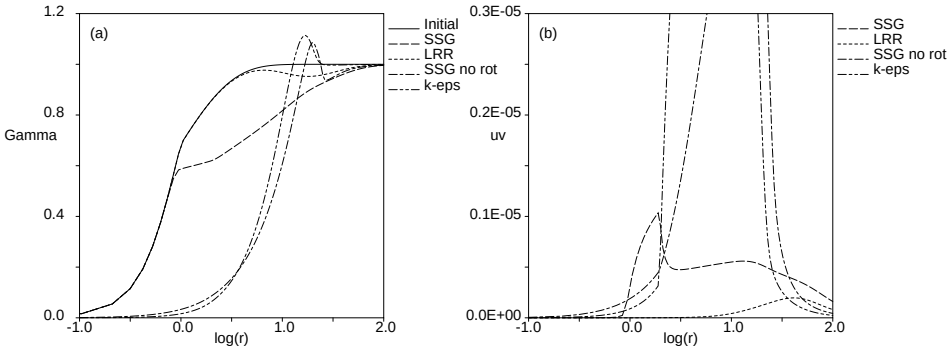

FIGURE 7. The computed vortex circulation (a) and shear stress (b) profiles at $t = 55$s using different two-equation models, different EARSM's and the standard eddy-viscosity K-ε model (k-eps). The flow is initiated using the Proctor profile.

term in (12). In the linearized SSG model, the equilibrium value $C_2 = 0.36$ is used whereas $C_2 = 0.8$ in the LRR model, which corresponds to rapid distortion theory. The algebraic form of the LRR model (using the newly re-calibrated coefficients) is especially attractive because the complexity of the algebra in three-dimensional mean flows is very reduced [14] [23]. It is possible to keep exactly the same algebraic form by changing the L coefficients in (21) so that the A coefficients in (30) remain unchanged and the C_2 coefficient takes the value of 0.36 rather than 0.8. That leads to the alternative set of C coefficients where $C_1^0 = 4.92$, $C_1^1 = 1.65$, $C_2 = 0.36$, $C_3 = 2$ and $C_4 = 0.378$. Because the A coefficients remain unchanged compared to the LRR model, the basic EARSM remains unchanged, and the simple algebraic form is preserved. The only difference enters through the modified rotation rate tensor to account for the advection. The computational result from using this model, (mix) in Figure 8, is much closer to the SSG model than the LRR model. Thus, it is reasonable to believe that this mechanism is the most important difference between the SSG and LRR models for this flow and that the decay rate of the vortex is much controlled by the C_2 coefficient. This mixed model is, however, not yet another proposal of a linear pressure-strain model, but only constructed to assess the differences between the SSG and LRR models and the importance of the C_2 coefficient.

4.4. Variation of the initial circulation profile. The observations in the preceding sections are made using an initial circulation profile that corresponds to observed trailing vortices. That initial circulation profile deviates somewhat from the Lamb vortex that has been used in previous studies of trailing vortices, for example, see Zeman [7]. The two different initial profiles are shown in Figure 1. The computations with this alternative (Lamb) initial profile follows the previous computations, see Figure 9. The SSG-based models, in differential

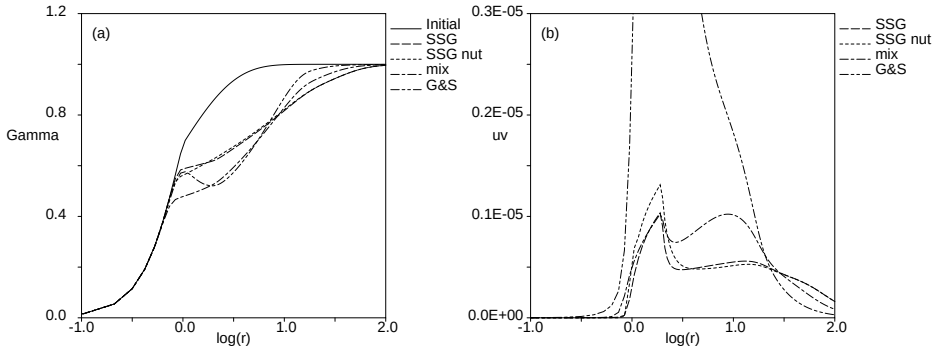

FIGURE 8. The computed vortex circulation (a) and shear stress (b) profiles at $t = 55$s using different EARSM's based on the linearized SSG model. The flow is initiated using the Proctor profile.

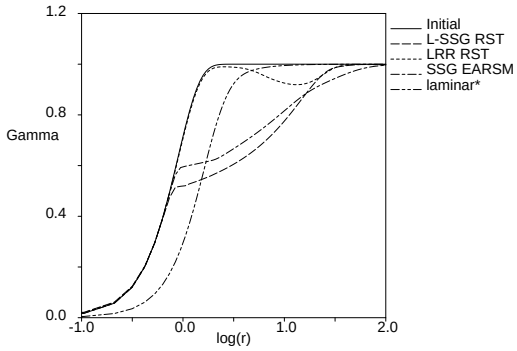

FIGURE 9. The computed vortex circulation profiles at $t = 55$s using different models. The laminar results was obtained at a lower Reynolds number, $Re = 10^4$. The flow is initiated using the Lamb profile.

form as well as in algebraic form, give reasonable results whereas the LRR-based models strongly underpredict the vortex decay rate. Also here one may observe that the algebraic modeling assumption gives results comparable to the full RST models.

Also shown in Figure 9 are the laminar results where the Reynolds number has been decreased from $20 \cdot 10^6$ to 10^4; otherwise there would have been almost no difference between the initial and final profiles. The laminar result shows a complete different nature where the vortex decays mostly from the core and outwards giving an increased vortex radius while leaving the exterior part of the vortex unaffected. The laminar decay rate is also much slower than the turbulent decay rate.

4.5. Comments on the obtained results. There are some questions concerning the obtained results that need to be further discussed. The vortices studied here are linearly stable according to Rayleigh's [27] stability criterion.

The model computations show an initial growth of turbulence that saturates and starts to decrease slowly (Figure 3b). The level at which the turbulence saturates is, however, fairly low, $K \sim 10^{-5}$ (normalized by Γ_0 and R_c). This could be compared to the large-eddy simulations by Ragab and Sreedhar [6], where the computations were interrupted when $K \sim 10^{-4}$, or the measurements by Devenport et al. [5], where the maximal level at the final streamwise position was $K \sim 10^{-4}$.

If the initial turbulence level in the model computations is prescribed much higher than the saturation level, no initial growth could be seen. The turbulence rapidly decreases to about the saturation level (Figure 3a). If the initial turbulence level is prescribed to be very low, the initial growth is very weak, but still positive, and the saturation level will not be reached within the time period investigated here.

The same principal behavior could be observed using models based on SSG, as well as LRR, but the saturation level is much lower when using the LRR model.

The question is if this behavior, predicted by the models, is physically reasonable or not. We know that the vortex is linearly stable (at least if we ignore that the mean flow is not stationary), and thus, we do not have exponential growth of any of the eigenmodes. Also if the eigenmodes are orthogonal, we would expect an overall exponential decay of any disturbances. However, the eigenmodes are not orthogonal, and thus, there exists a mechanism for disturbances to grow. The perhaps most classical example of this is plane Couette flow that is linearly stable for all Reynolds numbers [28] but transient growth nevertheless could lead to turbulence.

Schmid et al. [29] studied the eigenvalue sensitivity for the Batchelor vortex, for example, which is linearly unstable due to an axial velocity deficit. Large sensitivity is closely connected to the possibility of transient growth. For this case they found strong transient growth that was not related to the most unstable mode but rather due to large sensitivities of stable or weakly unstable modes. From this, it is not unrealistic to expect similar behavior for other types of vortices, even if they are linearly stable, and that an alternative growth mechanism may exist.

To our knowledge it is not clear whether the Lamb type of vortex could sustain turbulence or not. Numerical experiments (for example, large-eddy simulation by Ragab and Sreedhar [6]) did not show any evidence of sustained turbulence for the linearly stable case. However, the saturated turbulence level could be quite low without any large structures, which is typical for cases with a highly unstable mode, and may be overlooked if not explicitly searched for. These computations were interrupted when $K \sim 10^{-4}$, which is one order of magnitude larger than

the saturated level predicted by our SSG model computations. Moreover, the stable case computed by Ragab and Sreedhar shows an initial behavior that could be interpreted as transient growth.

An other question concerns a possible overshoot in the circulation profile. The angular momentum must be conserved, and Govindaraju and Saffman [11] showed that a vortex that entrains the ambient at a rate greater than that due to molecular diffusion must develop a circulation overshoot. However, no overshoot could be seen in our computational results, except for the strongly diffusive eddy-viscosity K-ε model. In the analysis by Govindaraju and Saffman, the Reynolds shear stress $\overline{uv}$ was assumed to decrease with increasing radius at a rate faster than r^{-2}. That means that an effective eddy viscosity must decrease with increasing radius. In our computations we have initiated the turbulence with a uniform K and ε field, which gives an effective eddy viscosity that far exceeds the molecular viscosity also at the outer boundary of the computational domain. The angular momentum or circulation will, thus, be transported out of the computational domain without developing any overshoot of circulation within the domain.

The assumption of an initially uniform turbulent field is not unreasonable when studying vortices in atmospheric conditions because the atmospheric turbulence level may act as a lower limit on the eddy viscosity at increasing radius. This could actually be the reason for the lack of experimentally observed circulation overshoots.

5. Conclusions

The turbulent vortex flow investigated is strongly affected by rotation, and even at the Reynolds stress transport modeling level, there are important differences between different models. All models based on the Reynolds stress transport equations, differential as well as algebraic, predict the strong suppression of the turbulence within the vortex core, consistent with observations. However, models based on the LRR pressure-strain model predict that the turbulence is almost completely suppressed also in the exterior part of the vortex, and the predicted vortex decay rate is much lower than observed. In that sense, models based on SSG perform more in line with observations. Computations show a fully turbulent vortex outside of the stabilized vortex core, and the vortex decay rate is of the same order as observed decay rates during low turbulent ambient conditions. The computations were made by assuming a vortex that extends to infinity, and thus, any real influence from ambient conditions are not included. The comparison with measured data is therefore not fully relevant because strong correlations between ambient conditions and vortex decay rates has been observed and direct comparisons should be avoided. For the idealized case of an isolated vortex, it is not obvious which of the SSG or LRR models give the most physically reasonable results, nor if the isolated vortex is capable

of sustaining turbulence at all. However, the particular observation used in this study was one of the slowest decaying ones, and thus, it would be somewhat surprising if the idealized case would substantially deviate from the observed one.

EARSMs are attractive due to reduced complexity and computational effort compared to full RST models. The computational results using EARSM closely follow the results obtained with the full RST models. It is, however, important that the algebraic assumption is made in a streamline based coordinate system. Neglecting this effect makes the model as bad as the eddy-viscosity K-ε model, which strongly overpredicts the vortex decay rate. Moreover, it is important that the EARSM is based on a self-consistent approach where the implicit algebraic relation is exactly solved without further assumptions. The modeling of the diffusion terms in the K-ε equations is not very important in this flow. The anisotropy diffusivity approach by Daly and Harlow [19] gives results comparable to the standard eddy-diffusivity approach as long as the eddy diffusivity is based on an effective C_μ determined from the EARSM relations rather than a universal constant (usually 0.09).

Acknowledgments

The authors gratefully acknowledge funding for this study from the Aeronautical Research Institute of Sweden (FFA) and from the Flight Dynamics and Control Division at NASA Langley Research Center. This study was performed at the Institute for Computer Applications in Science and Engineering, NASA Langley Research Center, during a visit by the first author. The authors would like to thank F. Proctor for introducing us to this problem and sharing with us his experience in this field.

References

[1] Proctor, F.H. 1998 The NASA-Langley Wake Vortex Modeling Effort in Support of an Operational Aircraft Spacing System. Invited paper, 35th Aerospace Sciences Meeting & Exhibit, 12-15 January, Reno, NV AIAA Paper No. 98-0589, 19 pp.

[2] Sarpkaya, T. & Daly J.J. 1987 Effect of Ambient Turbulence on Trailing Vortices. *J. Aircraft* **24** (6) 399–404.

[3] Sarpkaya, T. 1998 Decay of Wake Vortices of Large Aircraft. *AIAA J.* **36** (9) 1671–1679.

[4] Chow, J.S., Zilliac, G.G. & Bradshaw, P. 1997 Mean and Turbulence Measurements in the Near Field of a Wingtip Vortex. *AIAA J.* **35** (10) 1561–1567.

[5] Devenport, W.J., Rife, M.C., Liapis, S.I. & Follin, G.J. 1996 The structure and development of a wing-tip vortex. *J. Fluid Mech.* **312**, 67–106.

[6] Ragab, S. & Sreedhar, M. 1995 Numerical simulation of vortices with axial velocity deficits. *Phys. Fluids* **7** (3) 549–558.

[7] Zeman O. 1994 The persistence of trailing vortices: A modeling study. *Phys. Fluids* **7** (1) 135–143.

[8] Speziale, C.G., Sarkar, S. & Gatski, T.B. 1991 Modelling the pressure-strain correlation of turbulence: an invariant dynamical systems approach. *J. Fluid Mech.* **227**, 245–272.

[9] Launder, B.E., Reece, G.J. & Rodi, W. 1975 Progress in the development of a Reynolds-stress turbulence closure. *J. Fluid Mech.* **41**, 537–566.

[10] Girimaji, S.S. 1997 A Galilean invariant explicit algebraic Reynolds stress model for turbulent curved flows *Phys. Fluids.* **9** (4) 1067–1077.

[11] Govindaraju, S.P. & Saffman, P.G. 1971 Flow in a Turbulent Trailing Vortex. *Phys. Fluids* **14** (10) 2074–2080.

[12] Girimaji, S.S. 1996 Fully explicit and self-consistent algebraic Reynolds stress model *Theor. and Comp. Fluid Dyn.* **8** (6) 387–402.

[13] Gatski, T.B & Speziale C.G. 1993 On explicit algebraic stress models for complex turbulent flows. *J. Fluid Mech.* **254**, 59–78.

[14] Taulbee, D.B. 1992 An improved algebraic Reynolds stress model and corresponding nonlinear stress model. *Phys. Fluids A* **4** (11) 2555–2561.

[15] Lumley, J.L. 1978 Computational modeling of turbulent flows. *Adv. Appl. Mech.* **18** 123–176, Academic Press, New York.

[16] Shabbir, A. & Shih, T.H. 1992 Critical Assessment of Reynolds Stress Turbulence Models Using Homogeneous Flows NASA TM 105954, ICOMP-92-24, CMOTT-92-12.

[17] Wallin, S. & Johansson, A.V. 1996 A new explicit algebraic Reynolds stress turbulence model including an improved near-wall treatment. In Proc. Flow Modeling and Turbulence Measurements VI, Tallahassee FL, C.-J. Chen, C. Shih, J. Lienau & R.J. Kung (eds), 399–406.

[18] Wallin, S. & Johansson, A.V. 1999 An explicit algebraic Reynolds stress model for incompressible and compressible turbulent flows. To appear in J. Fluid Mech. (Also FFA TN 1997-51).

[19] Daly, B.J. & Harlow, F.H. 1970 Transport equations in turbulence. *Int. Phys. Fluids* **13** (11) 2634–2649.

[20] Rodi, W. 1972 The prediction of free turbulent boundary layers by use of a two-equation model of turbulence. *Ph.D. thesis, Imperial College of Science and Technology, Dept. of Mechanical Engineering*; HTS/72/24.

[21] Rodi, W. 1976 A new algebraic relation for calculating the Reynolds stresses. *Z. angew. Math. Mech.* **56** (3) T219–221.

[22] Pope, S.B. 1975 A more general effective-viscosity hypothesis *J. Fluid Mech.* **72**, 331–340.

[23] Johansson, A.V. & Wallin, S. 1996 A new explicit algebraic Reynolds stress model. In Proc. Sixth European Turbulence Conference, Lausanne, July

1996, Eds. S. Gavrilakis, L. Machiels & P.A. Monkewitz, Kluwer, 31–34.

[24] Campbell, S.D., Dasey, T.J., Freehart, R.E., Heinrichs, R.M., Matthews, M.P. & Perras, G.H. 1996 Wake Vortex Field Measurement Program at Memphis, TN. 34th Aerospace Sciences Meeting & Exhibit, Reno, NV, AIAA Paper No. 96-0399, January 1996.

[25] Campbell, S.D., Dasey, T.J., Freehart, R.E., Heinrichs, R.M., Matthews, M.P., Perras, G.H. & Rowe, G.S. 1997 Wake Vortex Field Measurement Program at Memphis, TN Data Guide. Project Report: NASA/L-2, January 1997.

[26] Saffman, P.G. 1992 Vortex Dynamics. *Cambridge University Press, New York*.

[27] Rayleigh, Lord 1916 On the dynamics of revolving fluids. *Proc. R. Soc. A* **93** 148–154.

[28] Herron, I.H. 1991 Observations on the role of vorticity in the stability theory of wall bounded flows. *Stud. Appl. Math.* **85** (3) 269–286.

[29] Schmid, P.J., Henningson, D.S., Khorrami, M.R. & Mujeeb, R.M. 1993 A study of eigenvalue sensitivity for hydrodynamic stability operators. *Theoret. Comput. Fluid Dyn.* **4** (5) 227–240.

Paper 4

4

A COMPUTATIONAL STUDY OF UNSTEADY TURBULENT BUFFET AERODYNAMICS

Dieqian Wang, Stefan Wallin, Martin Berggren and Peter Eliasson
The Aeronautical Research Institute of Sweden (FFA)
Box 11021, SE-16111 Bromma, Sweden

Abstract. The periodic self-excited turbulent flow around an 18-percent thick circular-arc airfoil at transonic speeds has been computed by solving the unsteady Reynolds-averaged Navier-Stokes equations. Three different turbulence models were used: an algebraic model, an eddy-viscosity $K-\omega$ model, and an explicit algebraic Reynolds stress model (EARSM). Grid and time-step studies were performed to assess the numerical accuracy. The EARSM is a fully self-consistent approximation of a Reynolds stress transport model in the weak-equilibrium limit and behaves reasonable well also in non-equilibrium flows. Moreover, the model has the correct near-wall asymptotic behavior for all individual Reynolds stresses with a near-wall damping function formulated without use of the wall skin friction (or y^+). Computational results indicate that the EARSM predicts the unsteadiness due to shock and boundary-layer separation better than the two-equation model based on the Boussinesq hypothesis and the algebraic turbulence model. The EARSM predicts the frequency of self-exited unsteady transonic flow to high accuracy and the motion of the shock agrees well with the experimental data.

1. Introduction

Flows around blunt bodies, airfoils near and in stall, flows around turbine blades and shock induced separation on airfoils are some examples of unsteady turbulent flows of engineering interest. The unsteadiness may be forced or self-induced due to flow instabilities, and interaction with the structure (aeroelasticity) may be present in the examples above.

In this study we focus on buffet aerodynamics. Transonic flow over an airfoil may result in a periodic motion of the shock over the surface of the airfoil. The unsteadiness is driven by the interaction between the shock, boundary layer and the vortex shedding in the wake. The reduced frequency is usually less than one which means that the time scale of the wall-bounded turbulence is much smaller than the periodic unsteadiness which motivates a quasi-steady approach.

The 18% bicircular-arc airfoil has been excessively studied experimentally and numerically with respect to the buffet behavior and was chosen as the validation case in this study. Previous computational studies using Reynolds averaged Navier-Stokes methods were performed by Levy[2], Steger[3], Seegmiller et al.[4], Edwards and Thoms[5]. All employed algebraic turbulence models. In all of these studies the self-excited oscillations were reproduced, but the reduced frequencies

were predicted about 20 percent lower than in the experiment of McDevitt[6]. The same case was also computed in the context of the ETMA[7] research program where the partners employed algebraic or two-equation turbulence models. The general conclusion from ETMA is that the principal flow characteristics are predictable, even for the simple algebraic turbulence models, since an important part of the complex physical process is contained in the periodic motion, which is resolved by the phase-averaging approach. But also here, the predicted frequencies are lower than in the experiment.

In the paper of Rumsey[8], results with the algebraic Baldwin–Lomax[9] (B-L) and the one-equation Spalart–Allmaras[10] (S-A) turbulence models. The S-A turbulence model calculations predict the experimental reduced frequency of the oscillations as well as the Mach number range within which hysteresis takes place. But the motion of the shock toward and ahead of the mid chord is not predicted by the S-A model.

In this study, which is a continuation of earlier work[1], we will identify the general requirements on a turbulence model for unsteady turbulent flows and make a choice of suitable models to test. The numerical method used for accurate time integration will be described and the accuracy assessed before we will present computational results on the bicircular arc airfoil.

2. Modelling of unsteady periodic turbulence

Modelling of unsteady turbulence very much resembles the modelling of statistically steady turbulence. The main difference is the definition of the averaging operation. In steady turbulence an instantaneous flow variable ϕ is decomposed into a mean part $\overline{\phi}$ and a fluctuating part ϕ', that is $\phi = \overline{\phi} + \phi'$. The mean is typically defined as the time or ensemble average. Averaging the momentum equation results in the Reynolds averaged Navier-Stokes (RANS) equation for the mean flow quantities. The Reynolds stress tensor $\overline{u_i u_j}$ is an additional stress term that appear in the RANS equations and needs to be modelled in terms of the mean flow quantities.

The mean flow is considered as unsteady when the time scale of the mean flow unsteadiness is much larger than the characteristic integral time scale of the turbulence. In that case the turbulence energy spectrum is well separated from the unsteadiness. The turbulence may, thus, be modelled while the mean flow unsteadiness is left to be resolved in the unsteady RANS solution. This is known as the quasi-steady approach where a standard RANS turbulence model, with the time derivatives included, may be used. No additional modification of the turbulence model is in principal needed due to the unsteadiness.

If there is no clear separation between the turbulence scales and the unsteadiness, then standard RANS turbulence models cannot be used. This class of problems needs to be tackled using large eddy simulations (LES) where subgrid-scale models are used to represent the unresolved stresses. The Reynolds averaged

and the LES-filtered Navier-Stokes equations are in principal similar but the unknown correlation $\overline{u_i u_j}$ is modelled completely different in RANS and LES.

When the unsteady turbulent flow is, by nature or forced to be, periodic, the mean is conveniently defined as a phase average, see *e.g.* Jin & Braza[13]. The flow variables are then decomposed into three parts, $\phi = \overline{\phi} + \phi" + \phi'$, where $\overline{\phi}$ is the time-averaged value, $\phi"$ is the periodic component and ϕ' the turbulent fluctuations. The phase-averaged variable is then defined as $\langle\phi\rangle \equiv \overline{\phi} + \phi"$.

In the quasi-steady approach RANS turbulence models will be used without any explicit modifications due to the unsteadiness. However, the unsteadiness of the mean flow poses some additional requirements on the turbulence model, or will stress existing requirements on models for steady flows even further. This will be discussed in the following.

2.1. Requirements on RANS models for unsteady turbulence. Fan & Lakshminarayana[11] and Mankbadi & Mobark[12] consider unsteady boundary layers where either the wall or the free stream fluctuates. The flow is characterized by a near-wall flow that fluctuates in phase with the wall and an outer region with a substantial phase shift. An instantaneous log-law does not in general exist and near-wall formulations based on the log-law and the equilibrium assumption are not appropriate, according to Fan & Lakshminarayana. This disqualifies algebraic eddy-viscosity models and two-equation models with log-law boundary conditions or with near-wall damping functions based on the wall friction (such as y^+). Moreover, it is believed that the correct near-wall representation of the Reynolds stresses is important in representing unsteady near-wall turbulence.

When the frequency of the unsteadiness increases and approaches the turbulence characteristic frequency, the turbulence becomes more directly affected by the fluctuating mean flow. That means that non-equilibrium effects become more important. The most extreme kind of unsteady turbulence is rapid distorted turbulence where the turbulence is far from the equilibrium state. Turbulence models that are well behaved in non-equilibrium turbulence may thus be supposed to be suitable for unsteady turbulent flows. This has also been briefly discussed by Mankbadi & Mobark[12].

One application of unsteady turbulent flows is the unsteady flow around transonic airfoils. The shock may induce boundary layer separation that may be unsteady in some parameter regimes. In such flows it is crucial that the turbulence model is able to predict separated flows accurately. This aspect is discussed by Jin & Braza[13] who show that reasonable predictions are obtained if the model is able to predict the boundary layer separation.

The following general requirements on a two-equation model for unsteady wall-bounded flows can thus be identified: (i) No y^+ or log-law dependency, (ii) correct near-wall asymptotic behavior, (iii) good prediction of non-equilibrium turbulence and (iv) good prediction of boundary layer separation.

2.2. Choice of turbulence model. The self-consistent explicit algebraic Reynolds stress model (EARSM) by Wallin & Johansson[14] based on $K-\omega$ matches well the requirements above and has been found to be able to predict flow cases where standard eddy-viscosity models fail. This model has been shown to give results that in many aspects are similar to those of full Reynolds stress transport models but for a computational effort that is comparable with standard two-equation models; an issue of major importance, especially in three-dimensional unsteady computations.

The EARSM is solved together with a low-Reynolds number $K-\omega$ model, and has a near-wall damping function that gives the correct near-wall behavior for all individual Reynolds stresses. The near-wall damping in the EARSM formulation is expressed in terms of $Re_y \equiv \sqrt{K}y/\nu$ while the $K-\omega$ model has damping functions in terms of the turbulent Reynolds number, $Re_t \equiv K^2/\nu\varepsilon$.

The proposed model is fully self-consistent, which means that the model represents an exact solution of the Reynolds stress transport model in the weak-equilibrium limit where the advection and diffusion of the Reynolds stress anisotropies are neglected. This gives a model that has the correct asymptotic behavior for large strain rates. Wallin & Johansson[14] show that the model behaves reasonable well even for the highly non-equilibrium homogeneous rapid sheared flow where the initial $SK/\varepsilon = 50$.

The prediction of boundary layer separation is important for capturing the unsteady flow around transonic airfoil. The eddy-viscosity assumption fails to correctly predict the production of the turbulent kinetic energy which is overestimated in strong adverse pressure gradients and near separation or reattachment points. Improvements can be obtained by an empirically based limiter on the eddy viscosity or production, as in the Menter SST $K-\omega$ model[19]. A similar effect is obtained from the proposed EARSM which in a natural way decreases the turbulent shear stress in such flows. Transonic highly loaded wings and supersonic impinging shocks were computed by Wallin & Johansson[14] and they found that the shock position, separation length and skin friction was considerably improved compared to standard eddy-viscosity models. The reduced frequency for the case adopted in this study is, however, not very high and thus accurate prediction of the shock position and boundary layer separation is the most important requirement here.

To assess the results from EARSM together with the low-Reynolds number $K-\omega$ model, the Wilcox eddy-viscosity low-Reynolds number $K-\omega$ model[20] and the Baldwin & Lomax algebraic model[9] are applied for the study, and the results are compared with experiment[6] and other computational results.

3. Numerical method

The 2D/3D structured multi-block, cell-centered finite-volume code Euranus[15] is used for the study. The code solves the Euler or Navier–Stokes equations

for steady as well as unsteady flow problems, and has numerous options concerning numerical schemes, convergence acceleration, and options for reacting gas in equilibrium or non equilibrium. Algebraic as well as several two-equation turbulence models are implemented in the code.

Euranus can be used for time-accurate computations with explicit Runge–Kutta time marching or implicit time integration with pseudo-time relaxation[16, 17]. In this study, an implicit second-order backward-difference scheme for time advancement is employed. This scheme yields a nonlinear system of equations at each time step which is resolved by pseudo-time marching combined with multigrid and local time stepping. The spatial discretization are treated with a second-order upwind scheme with symmetric TVD and van Leer limiters[18].

4. Computational Results

We consider the 18% bicircular-arc airfoil in free space at $M_\infty = 0.76$, $\alpha = 0$ and $Re = 11{\times}10^6$. Experimental data[6] as well as previous computations are available for comparison.

The baseline grid, generated by FFANET[21], is of C-type with 193×65 points and with 129 points on the airfoil. The first layer over the airfoil surface is located at about unit y^+. The outer boundary is about 25 chords away. A close-up of the grid near the airfoil is shown in figure 1. The grid is symmetric around the symmetric airfoil. A finer grid with 385×129 grid points is also used for assessing grid convergence. The solution on the baseline grid was found to be somewhat grid dependent.

4.1. Convergence Investigation. The reason for introducing fully implicit temporal discretizations is that these are expected to allow significantly larger time steps than the ones dictated by explicit scheme's stability conditions. The time step can then be chosen solely according to the time scale of the physical problem. The use of dual time stepping introduces, however, the complication of deciding how many multigrid cycles that are needed in the subiterations each time step. It is reasonable to expect a trade-off; longer time steps advances the computation faster but will need more iterations each time step. We study these issues below, concentrating on following questions.

- How small time steps are needed for this problem?
- How many multigrid iterations are needed in the subiterations for each time step?
- Does it pay off to increase the time step?

For all convergence investigations results reported here, we used the 193×65 mesh and the Wallin & Johansson EARSM[14].

4.1.1. *Effects of changing time step and convergence criterion.* For two different time steps, corresponding to 165 and 350 time steps per period, respectively, figure 2 shows the lift coefficient C_l as a function of reduced time $t^* = t/(c/U_\infty)$;

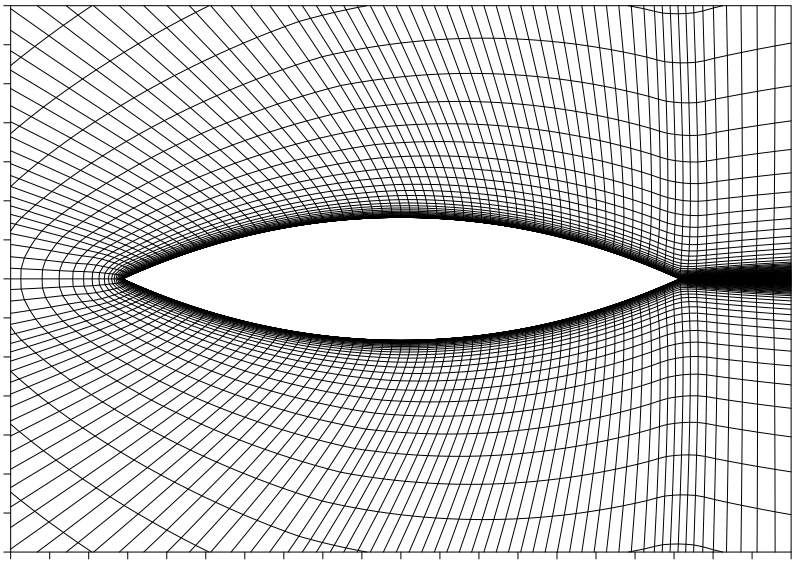

FIGURE 1. Close up of the baseline computational grid.

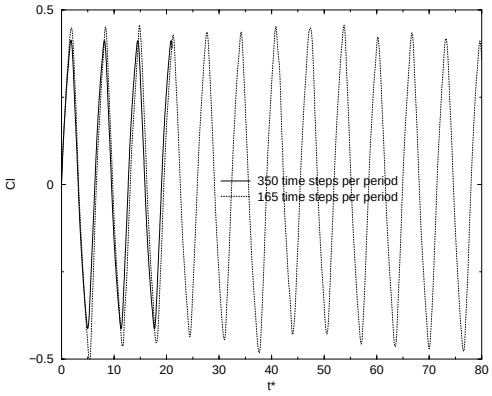

FIGURE 2. Effect of changing the time step size on the lift coefficient.

c is the airfoil chord and U_∞ the free-stream speed. Note that the longer time step lowers the buffet frequency somewhat and introduces a low-frequency modulation of the amplitude. Thus, at least 350 time steps per period seems necessary for an accurate prediction of the lift.

Figure 3 shows the effect on C_l versus t^* when relaxing the convergence criterion for the subiterations; instead of requiring one order-of-magnitude residual reduction, we prescribe a small, fixed number (10) of iterations. The latter leads to a residual reduction which is much less than one order of magnitude and a

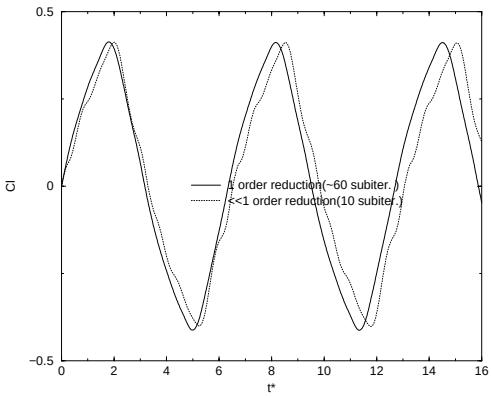

FIGURE 3. Effect of the convergence criterion, one order and less than one order reduction on the lift coefficient.

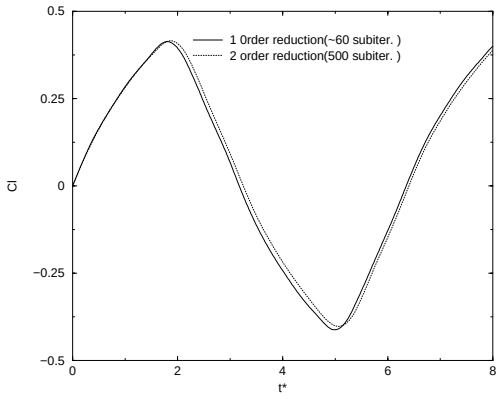

FIGURE 4. Effect of the convergence criterion, one order and two order reduction, on the lift coefficient.

reduced frequency for the buffet around $k = 0.481$, whereas the stricter convergence criterion yields $k = 0.493$. The residual is here defined as the maximum of the density residuals in the domain and the reduction of the residual is measured within one time step. Figure 4 shows the effect on C_l versus t^* when sharpening the convergence criterion for the subiterations from one order-of-magnitude residual reduction to two. The reduced frequency using the sharpened convergence criterion is still around $k = 0.49$. We conclude that one order-of-magnitude residual reduction seems to be a sufficient for this case. The time step in figures 3 and 4 corresponds to about 350 time steps per period.

Regarding the last of the three questions above, we performed several runs with different time steps and recorded the number of subiterations needed to achieve the same residual reduction, one order of magnitude. Table 1 shows the

TABLE 1. Effect of changing the time step size while keeping one order of magnitude residual reduction.

No. of Δt per period	50	100	165	350
No. of iteration/Δt	~ 260	~ 200	~ 120	~ 60
Iterations/period (10^3)	~ 13	~ 20	~ 20	~ 21

result. We make the somewhat surprising observation that it does not pay off to reduce the number of time step from 350 to 165 per period; the number of subiterations doubles approximately. A small improvement in efficiency can be noted for the larger time steps in table 1. However, these longer time steps yield an inaccurate solution; see the remarks above on the time-step selection. Fixing the number of subiterations to 500, we are able to achieve more than two orders-of-magnitude residual reduction when using 350 time steps per period, whereas less then two orders-of-magnitude is achieved when using 165 time steps per period.

4.1.2. *The main conclusion from the convergence investigation.*

- The time step should be small enough to get a good solution. About 350 time steps per period seems appropriate for the grid and model used.
- Larger time step does *not* save time when using the same convergence criterion (keeping a reasonable resolution in time).
- Using one or two order of magnitude residual reduction yield very similar solutions and, thus, one order of magnitude reduction was found to be sufficient in this case.
- Using a small (10) number of iterations per time step yields smaller reduced frequency and slightly wavy C_l curves.

Note that the temporal resolution that is needed, 350 time steps per period, is much higher than the smooth behavior of the C_l-versus-time curve would suggest. Even if our interest only lies in a slowly-varying integrated quantity such as C_l, this suggests that it seems important to capture accurately the time history of the flow on a faster time scale. This differs from our experience with unsteady Euler calculation of forced airfoil pitching at transonic speeds [17, 22], where accurate results were obtained with quite large time steps, say 24 time steps per period.

4.2. Turbulence modelling effects. To assess the performance of the Wallin–Johansson EARSM model described above, we compare with results obtained using the Wilcox $K-\omega$ [20] and the Baldwin–Lomax [9] model, with other computations from the literature, and with experiments. Free-stream conditions are used as initial conditions in the time accurate calculations. All of the computations are performed using the baseline grid 193×65 and ~ 350 time steps per period (but ~ 490 time steps per period when using the Baldwin–Lomax model).

TABLE 2. Computed reduced frequency compared to experiment by McDevitt[6].

model	$EARSM$	$K-\omega$	$B-L$	Exp.
k	0.493	0.441	0.461	~ 0.49

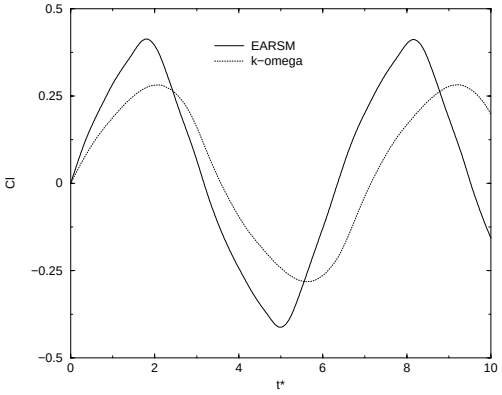

FIGURE 5. Computed lift coefficient using EARSM and $K-\omega$.

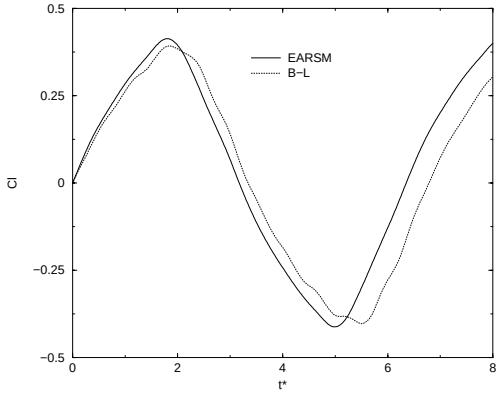

FIGURE 6. Computed lift coefficient using EARSM and Baldwin-Lomax.

4.2.1. *Reduced frequency and the C_l evolution.* Table 2 compares the experimental reduced frequency [6] with the ones obtained using the different turbulence models. Rumsey [8] obtained $k = 0.492$ using the Spalart–Allmaras model and a 165×65 mesh.

The lift coefficients as a function of reduced time for the different turbulence models are given in figures 5 and 6.

We are thus able to predict accurately the reduced frequency only when using the Wallin–Johansson EARSM. Both the Baldwin–Lomax and the Wilcox $K-\omega$ model yield too low frequency. It should also be noted that the turbulence models

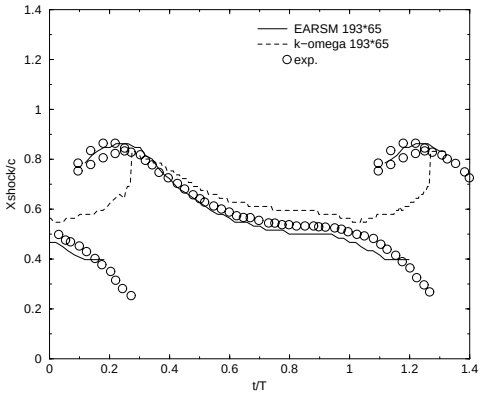

FIGURE 7. Computed shock position using EARSM and $K-\omega$ compared to experiment[6].

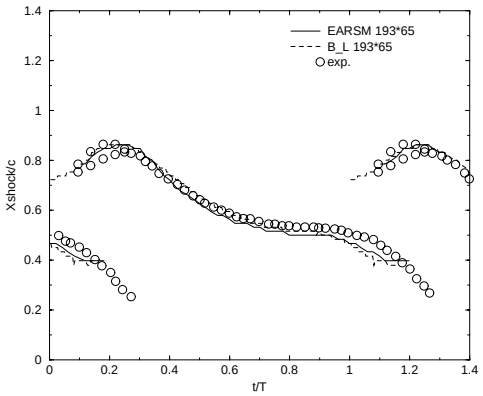

FIGURE 8. Computed shock position using EARSM and Baldwin-Lomax compared to experiment[6].

differ with respect to how long time it take to initiate the buffeting from the initial, free-stream state. The time it takes to reach a periodic state corresponds to about 0.5, 3, and 7.5 periods for the Baldwin–Lomax, the EARSM, and the Wilcox $K-\omega$ models, respectively. The Wilcox $K-\omega$ model appears to give too high turbulence levels for this application, damping the natural unsteadiness and thus both the frequency and amplitude are underpredicted.

4.2.2. *Instantaneous shock position.* Figures 7 8 and 9 depicts the shock position versus time in the experiments [6], in our calculations using the different turbulence models, and the results from Rumsey [8] using the Spalart–Allmaras turbulence model. In these pictures, the shock position at the airfoil is nondimensionalized by the chord c, and the time by the period of oscillation T. In the

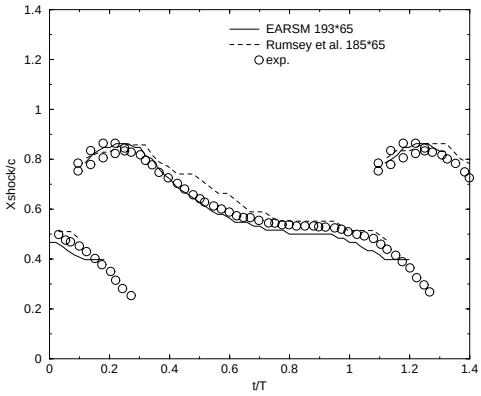

FIGURE 9. Computed shock position using EARSM compared to computations by Rumsey[8] using Spalart-Allmaras and experiment[6].

experiment, the time $t/T = 0$ is taken to be the time when the shock is at mid chord. However, this is not a convenient definition for the computational results, since some models do not predict motion of the shock forward of mid chord. In the computational results of Rumsey[8], $t/T = 0$ is the time when the shock is closest to mid chord. In our calculations, $t/T = 0$ is defined as the time when $C_l = 0$ and $\partial Cl/\partial t > 0$, since there are several time instants when the shock is positioned at mid chord in our calculations.

The best prediction of the shock position is obtained when using the EARSM. The Baldwin–Lomax model predicts the shock position well, whereas the Wilcox $K - \omega$ model gives a poor prediction.

4.2.3. *Instantaneous pressure distribution.* Figure 10 shows instantaneous pressure distributions on the upper airfoil surface at $t/T = 0$, 0.1, ... , 0.9. Computations using the EARSM on two different grid levels are compared to measurements. Also here we define time $t/T = 0$ as the instant when $C_l = 0$ and C_l is increasing. With respect to pressure distribution, the computational results agree rather well with the experimental results upstream of the shock but the pressure recovery in the separated region downstream of the shock is not well predicted. Note that the weak secondary shock appearing in the experiment at times $t/T = 0.2$ and 0.3 is not present in the computational results. The most upstream computed shock position is at $x/c = 0.42$ while the shock is present further upstream in the experiment, which is also clear from Figures 7, 8 and 9.

4.3. Grid convergence. The influence from grid refinement in studied from computational results using the EARSM on two different grids; 385×129 and 193×65. Figure 11 shows the lift and drag coefficients, C_l and C_d, versus reduced time. The reduced frequency for the finer and baseline grids differ

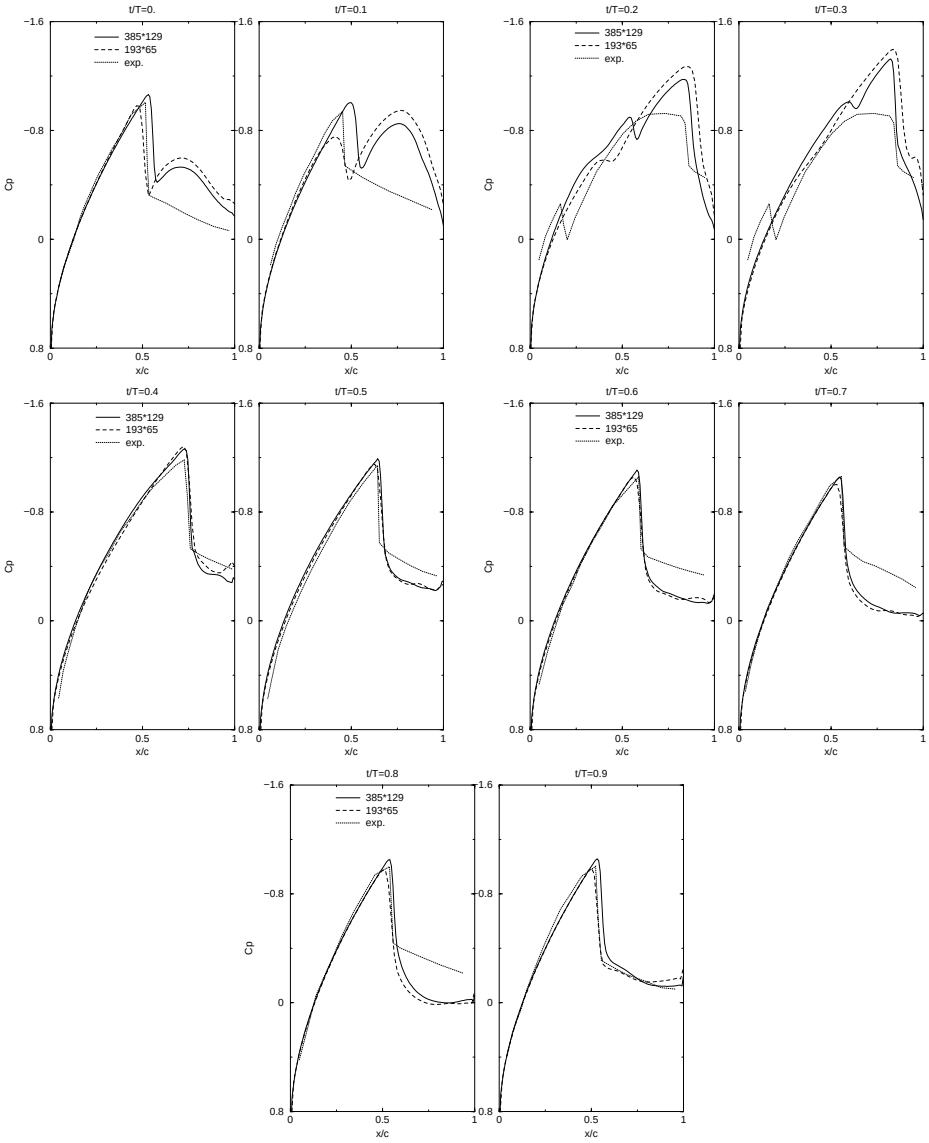

FIGURE 10. Computed pressure distribution at different times using EARSM on different grids compared to experiment[6].

only in the third digit; $k = 0.497$ for the finer grid and $k = 0.493$ for the baseline grid. However, the difference in the amplitude of the lift oscillations is large. Figure 12 shows that the prediction of the temporal evolution of the shock position improves for the finer mesh. The amplitude of C_l is strongly correlated to the time variation of the shock position and thus it may be reasonable to believe that also the C_l amplitude is more accurate predicted on the finer grid.

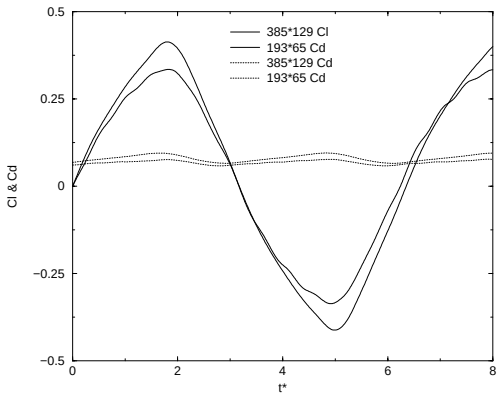

FIGURE 11. Computed lift and drag coefficients using EARSM on different grids.

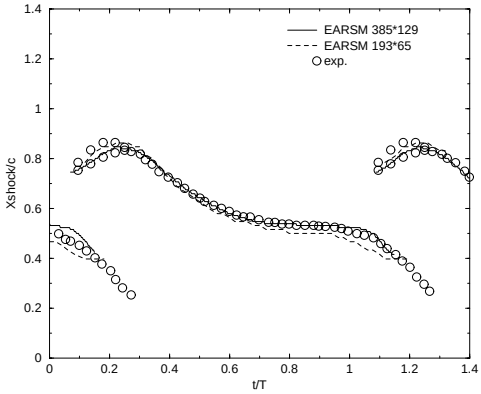

FIGURE 12. Computed shock position using EARSM on different grids.

5. Conclusions

The implicit time integration procedure used in this study was found to be robust and efficient. The overall computational time was not very sensitive to the size of the time step within the range studied, 50–350 time steps per cycle. The reason for this was that the number of pseudo-time relaxation steps could be reduced as the size of the time step decreased, keeping the same reduction of the residual.

Small time steps were needed for accuracy reasons and at least 350 time steps per cycle was recommended which is much higher than the smooth behavior of the C_l-versus-time curve would suggest. Even if our interest only lies in a slowly-varying integrated quantity such as C_l, this suggests that it seems important to capture accurately the time history of the flow on a faster time scale.

The solution was, however, not very sensitive to the number of subiterations as long as the residual was reduced at least one order of magnitude. Grid convergence could not be demonstrated completely, The differences between the baseline, 193x65, grid and a fine, 385x129, grid was small with respect to the frequency, whereas the differences in shock position and the amplitude of the lift oscillations were larger.

Three different turbulence models were studied and the influence of and differences between the models were significant. The more physically complete model, the explicit algebraic Reynolds stress model (EARSM) proposed by Wallin & Johansson[14], significantly improved the computational results over the Baldwin-Lomax[9] and Wilcox $K-\omega$[20] models. Both the shock position and the frequency of the periodic motion were predicted to a high accuracy using the EARSM. The Baldwin-Lomax model gave a reasonable shock position but underpredicted the frequency. The $K-\omega$ model failed in both these respects. Compared with the experimental pressure distribution, EARSM still can not correctly predict the flow recovery downstream of the shock induced separation, especially when the shock is positioned ahead of mid chord. The inability to correctly predict the flow recovery downstream of separation seems to be a general problem with turbulence models.

Four general requirements on a turbulence model for unsteady mean flows has been identified: (i) No y^+ or log-law dependency, (ii) correct near-wall asymptotic behavior, (iii) good prediction of non-equilibrium turbulence, and (iv) good prediction of boundary layer separation. The Wallin & Johansson EARSM was chosen for this study since that model reasonable well fulfills these requirements. It is, however, reasonable to believe that accurate prediction of boundary layer separation is the most important quality for a turbulence model in this case.

Acknowledgment

This research was performed as a part of the UNSI project (Unsteady Viscous Flow in the Context of Fluid–Structure Interaction), a collaboration between Alenia, BAe, CASA, Dasa–M (Coordinator), Dassault, DERA, DLR, FFA, IMFT, IRPHE, NUMECA, ONERA, Saab, TUB, and UMIST. The project is funded by the European Commission, DG XII, Brite/EuRam, under the IMT initiative (Project Ref: BRPR-CT97-0583). Partial funding was also provided by NUTEK, the Swedish National Board for Industrial and Technical Development.

References

[1] Grønland, T. A., Eliasson, P., and Nordström, J., "Accuracy of Unsteady Transonic Flow Computations," ICAS-98, 1998.

[2] Levy, Jr., L., "Experimental and Computational Steady and Unsteady Transonic Flow about a Thick Airfoil," *AIAA Journal*, Vol. 16, No. 6, 1978, pp. 564–572.

[3] Steger, J., "Implicit Finite-Difference Simulation of Flow about Arbitrary Two-Dimensional Geometries," *AIAA Journal*, Vol. 16, No. 7, 1978, pp.679-686.

[4] Seegmiller, H. L., Marvin, J. G., and Levy L. L., "Steady and Unsteady Transonic Flow," *AIAA Journal*, Vol. 16, No. 12, 1978, pp.1461-1471.

[5] Edwards, J., and Thomas, J., "Computational Methods for Unsteady Transonic Flows," Unsteady Transonic Aerodynamics, AIAA Progress in Astronautics and Aeronautics, Nixon, D. (ed.), Vol. 120, 1989, pp.211-261.

[6] McDevitt, J., "Supercritical Flow about a Thick Circular-Arc Airfoil," NASA TM-78549, 1979.

[7] "Unsteady airfoil flow." In *Computation and Comparison of Efficient Turbulence Models for Aeronautics – European Research Project ETMA*, pp. 535–572. (ed. by A. Dervieux, M Braza & J.-P. Dussauge) Vieweg 1998. Notes on Numerical Fluid Mechanics, Vol. 65.

[8] Rumsey, C. L., Sanetrik, M. D., Biedron, R. T., Melson, N. D. and Parlette, E. B., "Efficiency and Accuracy of Time-Accurate Turbulent Navier-Stokes Computations," AIAA-95-1835, 1995.

[9] Baldwin, B., and Lomax, H., "Thin Layer Approximation and Algebraic Model for Separated Turbulent Flow," AIAA-78-257, 1978.

[10] Spalart, P., and Allmaras, S., "A One-Equation Turbulence Model for Aerodynamic Flows," AIAA-92-0439, 1992.

[11] Fan, S., and Lakshminarayana, B., "Low-Reynolds-Number $k-\varepsilon$ Model for Unsteady Turbulent Boundary-Layer Flows," *AIAA Journal*, Vol. 31, No. 10, 1993, pp. 1777-1784.

[12] Mankbadi, R. R., and Mobark, A., "Quasi-steady Turbulence Modeling of Unsteady Flows," *Int. J. Heat and Fluid Flow*, Vol. 12, 1991, pp. 122-129.

[13] Jin, G., and Braza, M., "Two-Equation Turbulence Model for Unsteady Separated Flows around Airfoils," *AIAA Journal*, Vol. 32, 1994, pp. 2316-2320.

[14] Wallin, S., and Johansson A. V., "An explicit algebraic Reynolds stress model of incompressible and compressible flows," *Accepted for publication in J. Fluid Mech.* 1999.

[15] Rizzi, A., Eliasson, P., Lindblad, I., , Hirsch, C., Lacor, C., and Häuser, S., "The Engineering of Multiblock/Multigrid Software for Navier-Stokes Flows on Structured Meshes," *Computers & Fluids*, vol. 22, 1993, pp. 341-367.

[16] Jameson, A., "Time Dependent Calculations using Multigrid, with Applications to Unsteady Flows past Airfoils and Wings," AIAA-91-1596, 1991.

[17] Eliasson, P., and Nordström, J., "The Development of an Unsteady Solver for Moving Meshes," FFA TN 1995-39, 1995.

[18] Lacor, C., Zhu, Z.W., and Hirsch, C., "A New Family of Limiters Within the Multigrid/Multiblock Navier-Stokes code Euranus," AIAA/DGLR 5th Int. Aerospace Planes and Hypersonics Conf., Munich. 1993.

[19] Menter, F. R., "Zonal Two-Equation $k-\omega$ models for Aerodynamic Flow," AIAA-93-2906, 1993.

[20] Wilcox, D.C., "Simulation of transition with a two-equation turbulence model," *AIAA Journal* Vol. 32, 1994, pp. 247–255.

[21] Tysell, L, and Hedman, S. G., "Towards a general three-dimensional grid generation system," ICAS Paper 88-4.7.4. 1988.

[22] Berggren, M., "Geometric conservation for structured moving meshes," Technical Report TN 1998-28, FFA, the Aearonautical Research Institute of Sweden, P. O. Box 11021, S-161 11 Bromma, Sweden, 1998.

Paper 5

5

DERIVATION AND INVESTIGATION OF A NEW EXPLICIT ALGEBRAIC MODEL FOR THE PASSIVE SCALAR FLUX

Petra M. Wikström
Department of Mechanics, KTH, SE-100 44 Stockholm, Sweden

Stefan Wallin
The Aeronautical Research Institute of Sweden (FFA)
Box 11021, SE-16111 Bromma, Sweden

Arne V. Johansson
Department of Mechanics, KTH, SE-100 44 Stockholm, Sweden

Abstract. An algebraic relation for the scalar flux, in terms of mean flow quantities, is formed by applying an equilibrium condition in the transport equations for the normalized scalar flux. This modelling approach is analogous to explicit algebraic Reynolds stress modelling (EARSM) for the Reynolds stress anisotropies. The assumption of negligible advection and diffusion of the normalized passive scalar flux gives, in general, an implicit, nonlinear set of algebraic equations. A method to solve this implicit relation in a fully explicit form is proposed, where the nonlinearity in the scalar-production-to-dissipation ratio is considered and solved. The nonlinearity, in the algebraic equations for the normalized scalar fluxes, may be eliminated directly by using a nonlinear term in the model of the pressure scalar-gradient correlation and the destruction and thus results in a much simpler model for both two- and three-dimensional mean flows. The performance of the present model is investigated in three different flow situations. These are homogeneous shear flow with an imposed mean scalar gradient, turbulent channel flow and the flow field downstream a heated cylinder. The direct numerical simulation data are used to analyse the passive scalar flux in the homogeneous shear and channel flow cases and experimental data are used in the case of the heated cylinder wake. Sets of parameter values giving very good predictions in all three cases are found.

1. Introduction

Proper modelling of the passive scalar flux is important in many engineering applications. The passive scalar quantity may, for example, be temperature, species concentrations in combustion flows, or pollutant in atmospheric or ocean flows.

In analogy with the eddy viscosity concept for the Reynolds stresses, the passive scalar flux, $\overline{u_i\theta}$, is commonly modelled through a simple gradient diffusion assumption,

$$\overline{u_i\theta} = -\frac{\nu_t}{\mathrm{Pr}_t}\frac{\partial \Theta}{\partial x_i}, \tag{1}$$

where u_i and θ represents the fluctuating parts of the velocity and scalar, respectively. Here Θ is the mean scalar value, and ν_t is the turbulent (eddy) viscosity. In a zero equation model the turbulent Prandtl number, Pr_t (or turbulent Schmidt number) is assumed to be constant. In models without the assumption of a constant turbulent Prandtl number, the scalar variance, $\overline{\theta^2}$, and the dissipation rate of half the scalar variance, ε_θ, are usually needed to be solved for in analogy with $K-\varepsilon$ modelling. Still the eddy diffusivity approach, using a scalar eddy diffusivity, is unable to predict realistic values of all components of $\overline{u_i\theta}$, since it predicts the scalar flux to be aligned with the mean scalar gradient.

A tensor eddy diffusivity proportional to the Reynolds stresses was introduced by Daly & Harlow [1] giving the following model for the scalar fluxes,

$$\overline{u_i\theta} = -c_\theta \tau_\theta \overline{u_i u_j} \frac{\partial \Theta}{\partial x_j}, \tag{2}$$

where c_θ is a model parameter and τ_θ is an appropriate time scale. In the case that the mean scalar gradient exists only in the y direction, the ratio of the scalar fluxes, $\overline{u\theta}/\overline{v\theta}$, is then given by the Reynolds stress ratio $\overline{uv}/\overline{v^2}$. In the near-wall region of wall-bounded shear flows θ correlates more strongly with u than with v and (2) underpredicts the scalar flux ratio, see for example Kim & Moin [2] and Abe & Suga [3]. The following model was therefore proposed by Abe *et al.* [3],

$$\overline{u_i\theta} = -c_\theta \tau_\theta \overline{u_i u_k} \frac{\overline{u_k u_j}}{K} \frac{\partial \Theta}{\partial x_j}, \tag{3}$$

which instead gives a scalar flux ratio approximately proportional to $\overline{u^2}/\overline{uv}$ in the near-wall region when the mean scalar gradient exists only in the y direction. For this quadratic form much better predictions were obtained than with those of (2), in wall bounded shear flows, see [3].

In transport-equation modelling, of the passive scalar flux, the transport equations for, $K_\theta \equiv \overline{\theta^2}/2$, its destruction rate, ε_θ, and the passive scalar flux, $\overline{u_i\theta}$, are modelled. The former two ($K_\theta,\ \varepsilon_\theta$) are only needed for the construction of the decay time scale $K_\theta/\varepsilon_\theta$ for the passive scalar. Information about this timescale may be particularly important in situations when it differs significantly from K/ε. The set of transport equations is solved together with transport equations for the Reynolds stresses and the dissipation rate of the turbulent kinetic energy. This level of modelling is supposed to capture most of the relevant phenomena involved in engineering flows, but it is not very attractive in complicated geometries since it leads to 12 transport equations for the turbulence quantities in three-dimensional mean flows.

There is a renewed interest in algebraic models which are obtained from the transport equations using some equilibrium assumption. The most common approach is the weak equilibrium assumption, where the advection and diffusion of the normalized scalar flux $\overline{u_i\theta}/\sqrt{K K_\theta}$ is neglected, rather than the scalar flux itself, see *e.g.* Adumitroaie *et al.* [4], Girimaji & Balachandar [5], Abe

et al. [6], Shih & Lumley [7] and Shih [8]. This is equivalent to that used to formulate algebraic Reynolds stress models (ARSMs). A different approach is taken by Shabany & Durbin [9] where the advection and diffusion of the normalized dispersion tensor are neglected.

The equilibrium assumption for the normalized scalar flux results in an algebraic relation for $\overline{u_i\theta}$ that is implicit and nonlinear in the scalar flux. The nonlinearity forms a major obstacle for deriving a relation that is fully explicit and self-consistent, *i.e.* an expression that fulfills the basic implicit algebraic equation. Adumitroaie *et al.* [4] leave this nonlinearity to be implicitly solved as a part of the solution procedure. Explicit forms of the models are, however, attractive since this leads to decreased numerical problems and computational efforts. Abe *et al.* [6] obtain a fully explicit expression by modelling the nonlinear part in terms of known quantities and thus self-consistency is not fulfilled. The model proposed by Girimaji & Balachandar [5] is both fully explicit and self-consistent but is restricted to a special case, Rayleigh–Bernard convection with vanishing mean flow gradients.

In the present paper a new explicit algebraic scalar flux model is presented which is fully explicit and self-consistent. The approach is similar to that of Girimaji & Balachandar [5] but extended to be valid for general flows. The present modelling approach for the scalar fluxes, $\overline{u_i\theta}$, is thus analogous to that of an self-consistent explicit algebraic Reynolds stress model (EARSM) for the Reynolds stresses, see Johansson & Wallin [10] and Girimaji [11]. An implicit algebraic equation for $\overline{u_i\theta}$ is constructed as an algebraic approximation of the modelled transport equation for the scalar fluxes. The implicit system of equations is inverted and the scalar production to dissipation ratio is determined to obtain an explicit formulation. Both the dynamical time-scale, K/ε, and the scalar time-scale, $K_\theta/\varepsilon_\theta$, are present in the formulation. For a complete model of the scalar fluxes, models of the transport equations for K, K_θ, ε and ε_θ are therefore to be included. This explicit algebraic scalar flux model (EASFM) for $\overline{u_i\theta}$ is suitably used together with an EARSM for $\overline{u_iu_j}$, such as that of Wallin & Johansson [12] and [13].

In section 2 the concept of second-order moment closures for the scalar fluxes is considered as well as the equilibrium assumption needed to obtain algebraic forms. The solution of the algebraic relation for the normalized scalar fluxes, derived in section 2, is obtained in section 3. A method to solve this implicit relation in a fully explicit form is proposed where the nonlinearity in the scalar production to dissipation ratio is considered and solved. The solution is exact in two-dimensional mean flows. In three-dimensional mean flows the tensorial form is exact, but an approximation for the scalar production to dissipation ratio needs to be introduced for a general set of model parameters. However, the nonlinearity, in the algebraic equations for the normalized scalar fluxes, may be

eliminated directly by using a nonlinear term in the model of the pressure scalar-gradient correlation and the destruction. This special case, which results in a much simpler model for both two- and three-dimensional mean flows, is proposed as a particularly interesting and practically useful model. In section 4 a set of test cases is described and in section 5 data from these are compared to the present EASFM predictions. It is also investigated how appropriate the equilibrium assumption is for each of the test cases. Some conclusions and summarizing comments are given in section 6.

2. Scalar flux modelling

Transport-equation models for the Reynolds-stress tensor and passive scalar flux vector contains substantially more of the underlying physics than standard two-equation models based on, *e.g.*, $K-\varepsilon$ and $K_\theta-\varepsilon_\theta$, respectively. A considerable part of this improvement can be retained also on algebraic approximations of the Reynolds-stress and scalar flux transport equations. The modelling level for the scalar fluxes should not be higher than that of the Reynolds stresses, since the scalar transport predictions heavily rely on the velocity field description.

We first describe a second-order modelling approach for the passive scalar fluxes analogous to Reynolds stress transport models for $\overline{u_i u_j}$. The Reynolds averaged transport equation for the mean scalar, Θ, for incompressible flows reads

$$\frac{\mathrm{D}\Theta}{\mathrm{D}t} = \frac{\partial}{\partial x_j}\left(\alpha\frac{\partial\Theta}{\partial x_j} - \overline{u_j\theta}\right), \tag{4}$$

where $\mathrm{D}/\mathrm{D}t(\equiv \partial/\partial t + U_j\partial/\partial x_j)$ implies the substantial derivative and α is the molecular diffusivity. The scalar flux vector, $\overline{u_i\theta}$, appears as an unknown quantity, which originates from the averaging of the nonlinear term in the transport equation of the total scalar field. This is analogous to the Reynolds averaged Navier-Stokes (RANS) equations. Also in analogy with the transport equations for the Reynolds stresses, a transport equation of the scalar-flux vector can be written in symbolic form as

$$\frac{\mathrm{D}\overline{u_i\theta}}{\mathrm{D}t} - \mathcal{D}_i = \mathcal{P}_{\theta i} + \Pi_{\theta i} - \varepsilon_{\theta i}, \tag{5}$$

where the production term is given by

$$\mathcal{P}_{\theta i} = -\overline{u_i u_j}\frac{\partial\Theta}{\partial x_j} - \overline{u_j\theta}\frac{\partial U_i}{\partial x_j}. \tag{6}$$

The molecular and turbulent diffusion, $\mathcal{D}_i$, the pressure scalar-gradient correlation, $\Pi_{\theta i}$, and the destruction rate tensor, $\varepsilon_{\theta i}$, contain unknown and higher-order correlations, and the system of equations is not closed. A scalar flux transport (SFT) model is obtained by modelling these unknowns in terms of the gradients of the mean velocity and scalar fields, $\partial U_i/\partial x_j$ and $\partial\Theta/\partial x_j$, the Reynolds

stresses, $\overline{u_i u_j}$, and the passive scalar fluxes, $\overline{u_i\theta}$. Also, the turbulent kinetic energy $K \equiv \overline{u_i u_i}/2$, the half-scalar variance $K_\theta \equiv \overline{\theta^2}/2$, and their dissipation rates ε and ε_θ, respectively, may be involved in this modelling.

An equivalent alternative to (5) is to form a transport equation for the normalized scalar flux,

$$\xi_i \equiv \frac{\overline{u_i\theta}}{\sqrt{K K_\theta}}, \tag{7}$$

which reads

$$\frac{\mathrm{D}\xi_i}{\mathrm{D}t} - \mathcal{D}_i^{(\xi)} = -\frac{1}{2}\xi_i\left(\frac{\mathcal{P}_\theta - \varepsilon_\theta}{K_\theta} + \frac{\mathcal{P}_K - \varepsilon}{K}\right) + \frac{\mathcal{P}_{\theta i} - \varepsilon_{\theta i} + \Pi_{\theta i}}{\sqrt{K K_\theta}}. \tag{8}$$

This corresponds to the transport equation for the Reynolds stress anisotropy tensor, defined as

$$a_{ij} \equiv \frac{\overline{u_i u_j}}{K} - \frac{2}{3}\delta_{ij}, \tag{9}$$

The transport equation for a_{ij} together with the equation for the turbulent kinetic energy represents an alternative to formulating an equation for the Reynolds stress tensor.

The K and K_θ transport equations are given by

$$\begin{aligned} \frac{\mathrm{D}K}{\mathrm{D}t} - \mathcal{D}^{(K)} &= \mathcal{P}_K - \varepsilon \\ \frac{\mathrm{D}K_\theta}{\mathrm{D}t} - \mathcal{D}^{(\theta)} &= \mathcal{P}_\theta - \varepsilon_\theta, \end{aligned} \tag{10}$$

where the production terms are

$$\mathcal{P}_K = -\overline{u_i u_j}\frac{\partial U_i}{\partial x_j} \qquad \mathcal{P}_\theta = -\overline{u_i\theta}\frac{\partial \Theta}{\partial x_i}. \tag{11}$$

The term $\mathcal{D}_i^{(\xi)}$ in (8) is the molecular and turbulent diffusion of ξ_i and reads

$$\mathcal{D}_i^{(\xi)} = \frac{\mathcal{D}_i}{\sqrt{K K_\theta}} - \frac{1}{2}\left(\frac{\mathcal{D}^{(K)}}{K} + \frac{\mathcal{D}^{(\theta)}}{K_\theta}\right)\xi_i. \tag{12}$$

To close the system of equations for the normalized scalar flux, transport equations for ε and ε_θ are needed. Moreover, the Reynolds stresses, $\overline{u_i u_j}$ need to be modelled in a way such that the individual anisotropy components are accounted for. This disqualifies eddy-viscosity models.

The modelled transport equation for the normalized scalar flux vector, ξ_i, may be written in the following symbolic form,

$$\mathrm{Trans}\left(\xi_i\right) = f_i^{\xi}\left(a_{mn}, S_{mn}, \Omega_{mn}, \Theta_m, r\right), \tag{13}$$

where the strain- and rotation-rate tensors, normalized with the turbulent time scale, are

$$S_{ij} \equiv \frac{1}{2}\frac{K}{\varepsilon}\left(\frac{\partial U_i}{\partial x_j} + \frac{\partial U_j}{\partial x_i}\right) \quad \Omega_{ij} \equiv \frac{1}{2}\frac{K}{\varepsilon}\left(\frac{\partial U_i}{\partial x_j} - \frac{\partial U_j}{\partial x_i}\right). \tag{14}$$

The last argument in f_i^ξ is the ratio of the scalar to dynamical time-scales,

$$r \equiv \frac{K_\theta/\varepsilon_\theta}{K/\varepsilon}. \tag{15}$$

Transport terms, advection and diffusion, are included in $\mathrm{Trans}\,(\xi_i)$ and the redistribution terms are lumped into f_i^ξ. In the modelling this is taken to be a function of the stress anisotropy, S_{mn}, Ω_{mn} and the normalized mean scalar gradient defined as

$$\Theta_i \equiv \frac{K}{\varepsilon}\sqrt{\frac{K}{K_\theta}}\frac{\partial\Theta}{\partial x_i}. \tag{16}$$

2.1. The equilibrium assumption for the scalar flux. In nearly homogeneous steady flows the advection and diffusion of the nondimensional scalar flux may be neglected, see *e.g.* Adumitroaie *et al.* [4], Abe *et al.* [6] and Girimaji *et al.* [5]. This is in many engineering flows a reasonable approximation especially if the driving forces (the velocity and scalar gradients) are large. By using the equilibrium assumption, for which the left-hand side of (8) is zero, the following implicit algebraic equation system is obtained:

$$\frac{1}{2}\xi_i\left(\frac{\mathcal{P}_\theta-\varepsilon_\theta}{K_\theta}+\frac{\mathcal{P}_K-\varepsilon}{K}\right)=\frac{\mathcal{P}_{\theta i}-\varepsilon_{\theta i}+\Pi_{\theta i}}{\sqrt{KK_\theta}}. \tag{17}$$

This is in direct analogy with the equilibrium assumption for the Reynolds stresses where the advection and diffusion of the Reynolds stress anisotropy is neglected, introduced by Rodi (1972, 1976). Equation (17) may also be rearranged using (15) to

$$\frac{1}{2}\xi_i\left[\frac{\mathcal{P}_\theta}{\varepsilon_\theta}-1+r\left(\frac{\mathcal{P}_K}{\varepsilon}-1\right)\right]=\frac{1}{\varepsilon_\theta}\sqrt{\frac{K_\theta}{K}}\left(\mathcal{P}_{\theta i}+\Pi_{\theta i}-\varepsilon_{\theta i}\right) \tag{18}$$

The modelling needed is of the form

$$\Pi_{\theta i}-\varepsilon_{\theta i}=\varepsilon_\theta\sqrt{\frac{K}{K_\theta}}F_i\left(a_{mn},\xi_m,S_{mn},\Omega_{mn},\Theta_m,r\right), \tag{19}$$

where F_i is a nondimensional function of the six nondimensional arguments. The equation (18) together with the modelling expression (19) can be seen as a system of equations for the nondimensional scalar flux, ξ_i. Since the scalar flux is included in the expression for the production of the scalar variance, $\mathcal{P}_\theta$, according to (11), the algebraic equation system has a scalar nonlinearity in $\overline{u_i\theta}$ (or, equivalently, ξ_i) which needs to be considered in a solution that is fully self-consistent, *i.e.*, that the ratio of scalar production and dissipation, $\mathcal{P}_\theta/\varepsilon_\theta$, used in the *lhs* of (17) is identical to that of (11).

A similar nonlinearity arises in the algebraic Reynolds stress equations that needs to be considered for a fully self-consistent explicit algebraic Reynolds stress model, see Johansson & Wallin [10] and Girimaji [11]. The self-consistent approach for the Reynolds stresses results in a polynomial equation for the production to dissipation ratio, $\mathcal{P}_K/\varepsilon$, and is crucial in flows far from equilibrium and

ensures, *e.g.*, that the solution has the correct asymptotic behaviour for large strain rates.

The equation system (18) may in principal be solved by forming the most general tensorial form for the scalar flux as a function of the nondimensional mean scalar gradient, the normalized mean flow strain and rotation rate tensors, as well as the Reynolds stress anisotropy, a_{ij}, *i.e*,

$$\xi_i = \xi_i \left(a_{mn}, S_{mn}, \Omega_{mn}, \Theta_m, r \right). \tag{20}$$

The next step would then be to solve for the coefficients of the linearly independent vector groups. By using an explicit algebraic Reynolds stress model the anisotropy may be written in terms of the strain and rotation rate tensors, S_{ij} and Ω_{ij}, and thus the scalar flux is then of the following form:

$$\xi_i = \xi_i \left(S_{mn}, \Omega_{mn}, \Theta_m, r \right). \tag{21}$$

Since the exact transport equation of $\overline{u_i\theta}$ only involves linear terms of Θ_m, it is natural to restrict the relation to

$$\xi_i = -\mathcal{D}_{ij} \left(S_{mn}, \Omega_{mn}, r \right) \Theta_j. \tag{22}$$

The dispersion tensor, $\mathcal{D}_{ij}$, also introduced by Shabany & Durbin [9], has no symmetry properties and is not, in general, traceless, so the general tensor form of $\mathcal{D}_{ij}$ in terms of S_{ij} and Ω_{ij} consists of 17 linearly independent tensor groups. Shih & Lumley [7] and Shih [8] include also an 18th, sixth-order term, which actually may be expressed in the other terms. Due to the complexity this approach is of minor practical use in three-dimensional mean flows. In section 3 a solution to the implicit algebraic ξ_i-relation given by (17)–(19) in a fully explicit form will instead be derived.

An alternative to neglecting the advection and diffusion of the nondimensional scalar flux was proposed by Shabany & Durbin [9]. They form a transport equation for the dispersion tensor. The alternative equilibrium assumption is then to neglect the advection and diffusion of the nondimensional dispersion tensor. The two different approaches are similar in flows where the direction of the mean scalar gradient varies only slowly in the mean flow direction. In cases where the direction of the mean scalar gradient varies rapidly in the mean flow direction, the nondimensional dispersion tensor may be nearly constant while the direction of the nondimensional scalar flux varies with the mean scalar gradient. Neglecting the advection and diffusion of the nondimensional dispersion tensor may thus be more appropriate than neglecting the advection and diffusion of the nondimensional scalar flux. The algebraic equation associated with the Shabany & Durbin [9] equilibrium assumption is, however, not as conveniently solved in three-dimensional flows since the general form with the 17 linearly independent tensor groups cannot be avoided in that approach.

2.2. Modelling $\Pi_{\theta i}$ and $\varepsilon_{\theta i}$. The dissipation vector, $\varepsilon_{\theta i}$, and the pressure scalar-gradient correlation, $\Pi_{\theta i}$, need to be modelled in terms of the dependent variables, according to (19). A model form that has been widely used, see, *e.g*, Shabany & Durbin [9] and also Launder [16], can be written as

$$\Pi_{\theta i} - \varepsilon_{\theta i} = -c_{\theta 1}\frac{\varepsilon}{K}\overline{u_i\theta} + c_{\theta 2}\overline{u_j\theta}\frac{\partial U_i}{\partial x_j} + c_{\theta 3}\overline{u_j\theta}\frac{\partial U_j}{\partial x_i} + c_{\theta 4}\overline{u_iu_j}\frac{\partial \Theta}{\partial x_j}. \tag{23}$$

This is the most general linear form, conserving the superposition principle for passive scalars. A time scale consisting of both the dynamical timescale, K/ε, and the scalar timescale, $K_\theta/\varepsilon_\theta$, could be used, though, instead of K/ε in the $c_{\theta 1}$ term. More generally, one could allow the four model parameters to depend on r. This would lead to a violation of the superposition principle for passive scalars, but an analogous violation is made, *e.g.*, when modelling the pressure-strain rate tensor. A model for the pressure-strain rate tensor that is nonlinear in the Reynolds stress tensor violates the superposition principle of Reynolds stress spectrum tensors.

From a formal solution of the Poisson equation for the rapid pressure a linear model for $\Pi^r_{\theta i} \equiv \overline{(p^r/\rho)(\partial\theta/\partial x_j)}$ may be derived. This model contains only rapid terms involving mean velocity gradients, that is, the second and third terms of (23), (see, *e.g.*, Shih [8]). In (23) also a fourth term is added, which is a composite model of dissipative and redistributive terms in the scalar flux equation. To capture effects of mean scalar gradients, an alternative to the $c_{\theta 4}$ term would be to include the nonlinear term $-c_{\theta 5}(1/K_\theta)\overline{u_k\theta}(\partial\Theta/\partial x_k)\overline{u_i\theta}$, which would give the following model, $-\left(c_{\theta 1} + c_{\theta 5}(K/\varepsilon K_\theta)\overline{u_k\theta}(\partial\Theta/\partial x_k)\right)(\varepsilon/k)\overline{u_i\theta}$, for the sum of slow pressure scalar-gradient correlation and the destruction. (Also this term gives a violation of the superposition principle). The mean scalar gradient has been included in a nonlinear term in a model of the slow term, in a similar manner by Craft & Launder [17]. The following model for $\Pi_{\theta i} - \varepsilon_{\theta i}$,

$$\begin{aligned}\Pi_{\theta i} - \varepsilon_{\theta i} \;=\; &-\left(c_{\theta 1} + c_{\theta 5}\frac{K}{\varepsilon K_\theta}\overline{u_k\theta}\frac{\partial\Theta}{\partial x_k}\right)\frac{\varepsilon}{K}\overline{u_i\theta} + c_{\theta 2}\overline{u_j\theta}\frac{\partial U_i}{\partial x_j}\\ &+\; c_{\theta 3}\overline{u_j\theta}\frac{\partial U_j}{\partial x_i} + c_{\theta 4}\overline{u_iu_j}\frac{\partial\Theta}{\partial x_j},\end{aligned} \tag{24}$$

will here be used, where effects of the mean scalar gradients are to be captured by the $c_{\theta 4}$ or the $c_{\theta 5}$ terms.

3. Solution of the implicit algebraic equation for ξ_i

The algebraic scalar-flux equation system (17) and (24) can be solved by direct inversion, which gives the scalar fluxes on an explicit form. Adumitroaie *et al.* [4] have proposed a solution method which is quite simple and compact also for three-dimensional flows. That model is, however, not fully explicit since the production to dissipation ratios, $\mathcal{P}_K/\varepsilon$ and $\mathcal{P}_\theta/\varepsilon_\theta$ are left implicit. We will follow the solution method proposed by Adumitroaie *et al.* [4] to obtain a formal

solution of the scalar fluxes in general three-dimensional mean flows, where $\mathcal{P}_\theta/\varepsilon_\theta$ is left as an unknown.

The formal solution is then used to formulate an equation for $\mathcal{P}_\theta/\varepsilon_\theta$. This equation has a closed solution for general two-dimensional mean flows in which the solution becomes fully explicit and self-consistent. Moreover, this solution is a reasonable approximation for three-dimensional mean flows. This approach follows the ideas proposed by Girimaji *et al.* [5] for the special case of Rayleigh–Bernard convection where the mean flow shear vanishes. Here, these methods will be extended to general mean flow fields. The associated difficulties will be discussed and a fully explicit model will be proposed. It will be shown that a drastic algebraic simplification, and full self-consistency, is obtained for the parameter value choice of $c_{\theta 5} = 1/2$.

The nondimensional system of equations for the scalar flux (17) and (24) is given by

$$N_\theta \xi_i = -(1 - c_{\theta 4})\left(a_{ij} + \frac{2}{3}\delta_{ij}\right)\Theta_j - [(1 - c_{\theta 2} - c_{\theta 3})\, S_{ij} + (1 - c_{\theta 2} + c_{\theta 3})\, \Omega_{ij}]\xi_j, \tag{25}$$

where

$$N_\theta = G + \frac{1}{r}\frac{\mathcal{P}_\theta}{\varepsilon_\theta}\left(\frac{1}{2} - c_{\theta 5}\right) = G - \left(\frac{1}{2} - c_{\theta 5}\right)\xi_l \Theta_l$$
$$G = \frac{1}{2}\left(2c_{\theta 1} - 1 - \frac{1}{r} + \frac{\mathcal{P}_k}{\varepsilon}\right).$$

For $c_{\theta 5} \neq 1/2$ the equation system (25) is nonlinear due to the term $\xi_l \Theta_l$ in N_θ that multiplies ξ_i. Equation (25) may be rewritten as

$$A_{ij}\xi_j = -c'_4\left(a_{ij} + \frac{2}{3}\delta_{ij}\right)\Theta_j, \tag{26}$$

where the matrix A_{ij} is given by

$$A_{ij} = N_\theta \delta_{ij} + c_S S_{ij} + c_\Omega \Omega_{ij}, \tag{27}$$

and

$$c_S = 1 - c_{\theta 2} - c_{\theta 3} \qquad c_\Omega = 1 - c_{\theta 2} + c_{\theta 3} \qquad c'_4 = 1 - c_{\theta 4}. \tag{28}$$

For $c_{\theta 5} \neq 1/2$ the formal solution of the system (26), where N_θ is not yet determined reads

$$\xi_i = -c'_4 A^{-1}_{ij}\left(a_{jk} + \frac{2}{3}\delta_{jk}\right)\Theta_k. \tag{29}$$

It is obtained by using the inverse of the matrix A_{ij}. One interesting observation is that the influences from the mean velocity gradient through A^{-1}_{ij}, the Reynolds stress anisotropy, and the mean scalar gradient are tensorially separated.

3.1. Solution for three-dimensional flows. In the following, bold face denotes a second rank tensor, *e.g.* $\mathbf{A} \equiv A_{ij}$. The matrix $\mathbf{A}$ is conveniently inverted analytically, as proposed by Adumitroaie *et al.* [4], with the aid of the Cayley–Hamilton theorem. Any general matrix satisfies its own characteristic polynomial equation, which for a 3×3 matrix reads

$$\mathbf{A}^3 - \mathrm{tr}\{\mathbf{A}\}\mathbf{A}^2 + \frac{1}{2}\left(\mathrm{tr}\{\mathbf{A}\}^2 - \mathrm{tr}\{\mathbf{A}^2\}\right)\mathbf{A} - \det(\mathbf{A})\mathbf{I} = 0, \tag{30}$$

where $\det(\mathbf{A})$ is the determinant of $\mathbf{A}$, $\mathrm{tr}\{\}$ denotes the trace, $\left(\mathbf{A}^2\right)_{ij} \equiv A_{ik}A_{kj}$, and $\mathbf{I}$ is the identity matrix. By multiplying (30) with $\mathbf{A}^{-1}$ the inverse of $\mathbf{A}$ is obtained as

$$\mathbf{A}^{-1} = \frac{\frac{1}{2}\left(\mathrm{tr}\{\mathbf{A}\}^2 - \mathrm{tr}\{\mathbf{A}^2\}\right)\mathbf{I} - \mathrm{tr}\{\mathbf{A}\}\mathbf{A} + \mathbf{A}^2}{\det(\mathbf{A})}. \tag{31}$$

The inverse of $\mathbf{A}$ exists only if the determinant of $\mathbf{A}$ is nonzero. Using the definition (27), the inverse of $\mathbf{A}$ may be written in terms of $\mathbf{S}$ and $\mathbf{\Omega}$ as

$$\mathbf{A}^{-1} = \frac{\left(N_\theta^2 - \frac{1}{2}Q_1\right)\mathbf{I} - N_\theta\left(c_S\mathbf{S} + c_\Omega\mathbf{\Omega}\right) + \left(c_S\mathbf{S} + c_\Omega\mathbf{\Omega}\right)^2}{N_\theta^3 - \frac{1}{2}N_\theta Q_1 + \frac{1}{2}Q_2}, \tag{32}$$

where

$$Q_1 \equiv c_S^2 I\!I_S + c_\Omega^2 I\!I_\Omega \qquad Q_2 \equiv \frac{2}{3}c_S^3 I\!I\!I_S + 2c_S c_\Omega^2 I\!V \tag{33}$$

and the invariants of the mean flow gradients are

$$I\!I_S \equiv \mathrm{tr}\{\mathbf{S}^2\} \qquad I\!I_\Omega \equiv \mathrm{tr}\{\mathbf{\Omega}^2\} \qquad I\!I\!I_S \equiv \mathrm{tr}\{\mathbf{S}^3\} \qquad I\!V \equiv \mathrm{tr}\{\mathbf{S}\mathbf{\Omega}^2\}. \tag{34}$$

For arbitrary $c_{\theta 5}$, the quantity N_θ depends on the scalar-variance production to dissipation ratio, $\mathcal{P}_\theta/\varepsilon_\theta$, and may be determined by using some iteration procedure. The relation is, however, strongly nonlinear and the iteration procedure is thus not guaranteed to converge towards the physical, correct root. Moreover, the iteration procedure, for N_θ might influence the convergence rate, to a steady state solution, and it is preferable to have a fully explicit relation.

A self-consistent solution is obtained if N_θ may be determined without making any assumptions about the scalar-variance production to dissipation ratio, $\mathcal{P}_\theta/\varepsilon_\theta$. A self-consistent and explicit model is thus obtained by using the formal solution for the scalar flux, (29), in the definition of N_θ to obtain an explicit relation for N_θ. This is similar to the model proposed by Girimaji *et al.* [5] for the special case of Rayleigh–Bernard convection.

Following these ideas, a polynomial equation for N_θ is obtained by inserting (32) into the definition (26), that is

$$N_\theta = G - \left(\frac{1}{2} - c_{\theta 5}\right)\xi_l\Theta_l = G + \left(\frac{1}{2} - c_{\theta 5}\right)c_4' A_{ij}^{-1}\left(a_{jk} + \frac{2}{3}\delta_{jk}\right)\Theta_k\Theta_i. \tag{35}$$

The equation for N_θ is in general a fourth-order polynomial equation, of which the solution may be found in any mathematical textbook,

$$2N_\theta^4 - 2GN_\theta^3 - (Q_1 + R_1)\, N_\theta^2 + (GQ_1 + R_2 + Q_2)\, N_\theta \\ -R_3 - GQ_2 + \frac{1}{2}Q_1R_1 = 0 \tag{36}$$

where

$$\begin{aligned} R_1 &= 2\left(\frac{1}{2} - c_{\theta 5}\right) c_4' \mathrm{tr}\left\{\left(\mathbf{a} + \frac{2}{3}\mathbf{I}\right)\Theta^2\right\}, \\ R_2 &= 2\left(\frac{1}{2} - c_{\theta 5}\right) c_4' \mathrm{tr}\left\{\left(c_S\mathbf{S} + c_\Omega\mathbf{\Omega}\right)\left(\mathbf{a} + \frac{2}{3}\mathbf{I}\right)\Theta^2\right\}, \\ R_3 &= 2\left(\frac{1}{2} - c_{\theta 5}\right) c_4' \mathrm{tr}\left\{\left(c_S\mathbf{S} + c_\Omega\mathbf{\Omega}\right)^2\left(\mathbf{a} + \frac{2}{3}\mathbf{I}\right)\Theta^2\right\} \end{aligned} \tag{37}$$

and $\left(\Theta^2\right)_{ij} \equiv \Theta_i\Theta_j$. The problem of determining the physical, correct root is, however, not considered here. For two-dimensional mean flows the equation for N_θ is cubic and has a reasonably simple closed solution. This solution may be used as a first approximation for N_θ in three-dimensional mean flows.

3.2. Solution for two-dimensional flows. The tensor $\mathbf{A}$ and the anisotropy tensor $\mathbf{a}$ are 3x3 matrices in general three-dimensional mean flows as well as in two-dimensional (2D) mean flows. In the latter case, when the third direction is the homogeneous one, the components $A_{\alpha 3} = A_{3\alpha} = a_{\alpha 3} = a_{3\alpha} = \Theta_3 = 0$ for $\alpha \neq 3$. (The $a_{\alpha 3}$ components may be nonzero in 2D mean flows only if the initial conditions of $a_{\alpha 3}$ are nonzero). The A_{33} and a_{33} components are nonzero, but they do not influence any of the ξ_i components, which is obvious by inspecting (26). The tensor $\mathbf{A}$ may thus be considered as a 2x2 matrix, denoted $\mathbf{A}^{2D}$, during the inversion of $\mathbf{A}$. The inverse of the matrix $\mathbf{A}^{2D}$ in two-dimensional mean flows is somewhat simpler than for three-dimensional mean flows and reads

$$\left(\mathbf{A}^{2D}\right)^{-1} = \frac{2N_\theta\mathbf{I}^{2D} - \mathbf{A}^{2D}}{\mathrm{d}et(\mathbf{A}^{2D})}, \tag{38}$$

where the determinant is given by

$$\mathrm{d}et(\mathbf{A}^{2D}) = N_\theta^2 - \frac{1}{2}Q_1. \tag{39}$$

The 3x3 form of the inverse of $\mathbf{A}$ defined by (27) may now be written in terms of $\mathbf{S}$ and $\mathbf{\Omega}$ as

$$\mathbf{A}^{-1} = \frac{N_\theta\mathbf{I} - \left(c_S\mathbf{S} + c_\Omega\mathbf{\Omega}\right)}{\mathrm{d}et(\mathbf{A}^{2D})} - \left(\frac{N_\theta}{\mathrm{d}et(\mathbf{A}^{2D})} - \frac{1}{N_\theta}\right)\left(\mathbf{I} - \mathbf{I}^{2D}\right). \tag{40}$$

The last term in (40) contributes only to the A_{33}^{-1} term and may be dropped in the expression for the scalar flux according to the discussion earlier.

The equation for N_θ is obtained from the relation (35) or from the equation for N_θ in three-dimensional flows, (36), by considering that $Q_2 = 0$ and $R_3 =$

$Q_1 R_1/2$ in two-dimensional flows. The equation for N_θ in two-dimensional flows is then given by

$$2N_\theta^3 - 2GN_\theta^2 - (Q_1 + R_1)N_\theta + GQ_1 + R_2 = 0. \tag{41}$$

This equation has three roots and at least one of them is real.

The physical, correct root is identified by looking at the special case when the mean scalar gradient, Θ_i, is zero. A local, or algebraic, model should then predict a scalar flux, $\xi_i = 0$, which can be seen from (26). $\Theta_i = 0$ gives $R_1 = R_2 = 0$ and the equation for N_θ can be written as

$$det(\mathbf{A}^{2D})\,(N_\theta - G) = 0 \tag{42}$$

with the aid of (39). This equation has three roots. The root $N_\theta = G$ is the physical, correct root since the other two roots, $\det(\mathbf{A}^{2D}) = 0$, implies that a solution to (26) does not exist. It is also easily seen in (26) that $N_\theta = G$ is the physical, correct root for zero mean scalar gradients. The solution to the cubic equation is then formulated so that the correct root is obtained for the special case of vanishing scalar gradient. The solution for general two-dimensional mean flows reads

$$N_\theta = \frac{G}{3} + \begin{cases} \operatorname{sgn}\left(P_{\theta1}+\sqrt{P_{\theta2}}\right)|P_{\theta1}+\sqrt{P_{\theta2}}|^{1/3} + \operatorname{sgn}\left(P_{\theta1}-\sqrt{P_{\theta2}}\right)|P_{\theta1}-\sqrt{P_{\theta2}}|^{1/3}, & P_{\theta2} \geq 0 \\ 2\left(P_{\theta1}^2 - P_{\theta2}\right)^{1/6}\cos\left(\frac{1}{3}\arccos\left(\frac{P_{\theta1}}{\sqrt{P_{\theta1}^2-P_{\theta2}}}\right)\right), & P_{\theta2} < 0,\ P_{\theta1} \geq 0 \\ 2\left(P_{\theta1}^2 - P_{\theta2}\right)^{1/6}\cos\left(-\frac{1}{3}\arccos\left(\frac{-P_{\theta1}}{\sqrt{P_{\theta1}^2-P_{\theta2}}}\right) + \frac{\pi}{3}\right), & P_{\theta2} < 0,\ P_{\theta1} < 0 \end{cases} \tag{43}$$

where

$$\begin{aligned} P_{\theta1} &= \frac{G^3}{27} - \frac{1}{6}GQ_1 + \frac{1}{12}GR_1 - \frac{1}{4}R_2 \\ P_{\theta2} &= P_{\theta1}^2 - \left(\frac{G^2}{9} + \frac{1}{6}Q_1 + \frac{1}{6}R_1\right)^3. \end{aligned} \tag{44}$$

For arbitrary parameter values the solution is not continuous in $P_{\theta1}$ and $P_{\theta2}$ since there is a discontinuity when $P_{\theta1} < 0$ and $P_{\theta2}$ changes sign. A parameter choice leading to this discontinuity should be avoided. One possibility is to use the parameter choice $c_{\theta5} = 1/2$, for which this problem is eliminated since then $N_\theta = G$ is the only solution for any value of the mean scalar gradient.

3.2.1. *The determinant of A in 2D flows and realizability constraints.* The explicit relation (29) becomes singular if the determinant of $\mathbf{A}$ is zero. In that case no solution of the implicit relation (17) exists and it is reasonable to suspect that there would be numerical problems associated with the solution of the corresponding transport model. If the determinant of $\mathbf{A}$ is zero for some parameter

regime, the solution is valid only outside of that regime. The determinant of $\mathbf{A}$ may be written as

$$\det(\mathbf{A}^{2D}) = N_\theta^2 - \frac{1}{2}Q_1 = N_\theta^2 - \frac{1}{2}\left(c_S^2 II_S + c_\Omega^2 II_\Omega\right). \tag{45}$$

The obvious problem is that the determinant consists of both positive and negative terms and it is not possible from this form to judge if the determinant has the possibility to become zero. Since N_θ is strongly coupled to the parameters II_S and II_Ω it is not obvious whether the determinant may become zero for some set of parameters. One possibility would be to choose the coefficient $c_S = 0$, which gives a strictly positive determinant since $II_\Omega < 0$ by definition. c_S, however, can not be neglected for arbitrary choices of model constants ($c_{\theta 2}$ and $c_{\theta 3}$).

Let us study the cubic equation (41) which may be rewritten as

$$2\det(\mathbf{A}^{2D})\left(N_\theta - G\right) = R_1 N_\theta - R_2, \tag{46}$$

where $\det(\mathbf{A}^{2D})$ is given by (45). The only possibility for the determinant to become zero is if the rhs term, $R_1 N_\theta - R_2$, is zero. Since the physical correct root then is $N_\theta = G$, it is thus sufficient to investigate whether the determinant can become zero for the special case $N_\theta = G$. In that case the determinant is

$$4\det(\mathbf{A}^{2D}) = 4G^2 - 2Q_1 = \left(2c_{\theta 1} - \frac{r+1}{r} + \frac{\mathcal{P}_K}{\varepsilon}\right)^2 - 2c_S^2 II_S - 2c_\Omega^2 II_\Omega. \tag{47}$$

The determinant is strictly positive if

$$c_{\theta 1} > \frac{1}{2}\left(1 + \frac{1}{r}\right) \tag{48}$$

and

$$c_S^2 < \frac{1}{2II_S}\left(2c_{\theta 1} - \frac{r+1}{r} + \frac{\mathcal{P}_K}{\varepsilon}\right)^2 - c_\Omega^2 \frac{II_\Omega}{II_S}. \tag{49}$$

$\mathcal{P}_K/\varepsilon$ becomes negative only in rare conditions. This behaviour is not caught by algebraic Reynolds stress models and thus not considered here. The limitation on the $c_{\theta 1}$ coefficient could always be violated for sufficiently small time-scale ratios, r. The only possibility to avoid this is by letting $c_{\theta 1}$ depend on r such that $c_{\theta 1}$ is nearly constant for reasonable flows but that the asymptotic behaviour is $c_{\theta 1} \sim 1/r$ for small time-scale ratios, r.

A suitable form is

$$c_{\theta 1} = c'_{\theta 1}\frac{r+1}{r}, \tag{50}$$

where $c'_{\theta 1}$ is a constant. The limitation (48) then gives $c'_{\theta 1} > 1/2$. For all practical cases that approximately fulfill the equilibrium condition assumed here, the time-scale ratio should be roughly constant and of order unity. Inclusion of this time-scale dependence, though, could give better model predictions in flows

with moderate deviations from equilibrium. This will be illustrated later for the case of a heated cylinder wake.

The limitation on the c_S coefficient may not be that severe since all terms on the *rhs.* of (49) are positive. For large strain rates, II_S, the term $(\mathcal{P}_K/\varepsilon)^2/II_S$ on the *rhs.* should asymptotically approach a positive constant when using an anisotropy model with a correct asymptotic behaviour. The limitation on the constant c_S depends on the particular choice of the other model parameters as well as on the particular choice of the Reynolds stress anisotropy model. For instance, the explicit algebraic Reynolds stress model by Wallin & Johansson [10], [12] and [13] does have the correct asymptotic behaviour for large strain rates. For $II_\Omega = 0$ and $II_S \to \infty$ that model gives the following limitation:

$$c_S < \sqrt{\frac{4}{15}} \approx 0.52. \tag{51}$$

In parallel mean flows $II_S = -II_\Omega$, and (49) is then automatically satisfied if, *e.g.*, we choose $c_S = c_\Omega$ (and satisfy (48)). It is, however, possible to construct extreme flow cases for which $c_S = 0$ is the only possible choice that avoids the singularity. One could thus also here consider some weak flow-field dependency in c_S.

The limitations obtained for the $c_{\theta 1}$ and c_S coefficients should also be considered when using an implicit algebraic model or a transport model for the scalar flux to prevent odd numerical behaviour.

3.3. A Daly & Harlow-type model. The parameter choice $c_{\theta 2} = 1$ and $c_{\theta 3} = 0$ implies that both c_S and c_Ω are zero. This special choice of parameters gives a drastically simplified model. The last term in equation (25) then vanishes and the model reduces to

$$\xi_i = -\frac{1 - c_{\theta 4}}{N_\theta}\left(a_{ij} + \frac{2}{3}\delta_{ij}\right)\Theta_j. \tag{52}$$

This simplified model is very similar to the model of Daly & Harlow [1], given in (2). For both models the dispersion tensor, $\mathcal{D}_{ij}$, is proportional to the Reynolds-stress tensor.

The equation for N_θ is in this case given by

$$2N_\theta\left(N_\theta - G\right) = R_1 \tag{53}$$

with the physical solution

$$N_\theta = \frac{1}{2}G + \sqrt{\frac{1}{4}G^2 + \frac{1}{2}R_1} \tag{54}$$

valid for arbitrary three-dimensional mean flows. From (29) it is evident that the restriction $c_4' > 0$, that is $c_{\theta 4} < 1$, has to be made. Then (54) has only real roots. For $R_1 = 0$ the solution $N_\theta = G$ is the physical one, see (26) and (37).

Hence, no singularity will occur as long as the condition

$$c_{\theta 1} > \frac{1}{2}\left(1 + \frac{1}{r}\right) \quad \Leftrightarrow \quad c'_{\theta 1} > \frac{1}{2} \tag{55}$$

is satisfied.

There is actually some theoretical support for a value of $c_{\theta 2}$ close to unity and a value of $c_{\theta 3}$ close to zero (see section 2.2). Basic mathematical constraints (see e.g. Shih [8]) give $c_{\theta 2} = 4/5$ and $c_{\theta 3} = -1/5$. In the present case a fourth term is also added in (24), which is a composite model of dissipative and redistributive terms in the scalar flux equation.

3.4. A new simple, fully explicit model. Models where the dispersion tensor is proportional to the Reynolds-stress tensor, such as the simplified model in the previous section, have not proven to be successful. It was pointed out in the introduction that such models fail in *e.g.* the near-wall region of wall bounded flows.

The general solution could also be cumbersome due to the complex algebra even i two-dimensional mean flows, and it is not obvious how to treat fully three-dimensional mean flows.

For the special choice

$$c_{\theta 5} = \frac{1}{2} \tag{56}$$

the simple solution

$$N_\theta = G, \tag{57}$$

valid for arbitrary three-dimensional mean flows is obtained. Hence, no equation for N_θ needs to be solved, and a fully explicit, self-consistent model

$$\mathbf{A}^{-1} = \frac{\left(G^2 - \frac{1}{2}Q_1\right)\mathbf{I} - G\left(c_S\mathbf{S} + c_\Omega\mathbf{\Omega}\right) + \left(c_S\mathbf{S} + c_\Omega\mathbf{\Omega}\right)^2}{G^3 - \frac{1}{2}GQ_1 + \frac{1}{2}Q_2} \tag{58}$$

to be inserted in (29), is automatically obtained. The simplicity is here retained for any choice of the model parameters $c_{\theta 1}$-$c_{\theta 3}$, and thus the dispersion tensor is not necessary directly proportional to the Reynolds-stress tensor. The calibration of the model parameters will be considered later. A restriction is also here that they should be chosen such that the denominator of (58) is guaranteed to be nonzero.

4. The test cases

4.1. Homogeneous shear flow. We will here use data from a direct numerical simulation (DNS) of homogeneous shear flow with mean scalar gradients in each of the three orthogonal directions made by Rogers *et al.* [18]. The simulations were performed with 128×128×128 spectral modes and a mesh spacing of $(\Delta x, \Delta y, \Delta z)$=(0.07792, 0.03896, 0.03896). In the comparisons, in section 5, data from the simulations with a Prandtl number 0.7 and a turbulence Reynolds

number, $4K^2/\nu\varepsilon$, of 847 are used. The shear rate, S, will be used to nondimensionalize the time.

4.2. Turbulent channel flow. A DNS of a turbulent channel flow with a passive scalar and a Prandtl number of 0.71 has been performed by Wikström & Johansson [19]. The Reynolds number based on the centerline mean velocity and the channel half-width, δ, is 5000, and the Reynolds number based on the wall friction velocity, u_τ, and the channel half-width is 265. The simulation code uses spectral methods, with Fourier representation in the streamwise (x) and spanwise (z) directions and Chebyshev polynomials in the wall-normal (y) direction. The computational domain is 12.56δ, 2δ, and 5.5δ in the streamwise, wall-normal, and spanwise directions, respectively, and the number of spectral modes is 256×193×192. This gives a resolution in the x-, y and z directions of 13.0, 2.7(on average), and 7.6 wall units, respectively. The boundary conditions used for the scalar field, with $\delta = 1$, are

$$\Theta'(x,-1,z,t) = -1, \qquad \Theta'(x,1,z,t) = 1 \tag{59}$$

where Θ' is the dimensionless total scalar field, $\Theta + \theta$. The scalar value, *e.g.*, temperature, at each wall is thus kept constant (*i.e.*, the scalar fluctuations on the walls are zero) with a higher temperature of the upper wall. This boundary condition, which represents a case where the passive scalar is introduced at the upper wall ($y = 1$) and removed from the lower wall ($y = -1$), results in an antisymmetric mean scalar profile in the channel. The DNS data presented in the following consist of averages of 24 statistically independent fields.

4.3. The heated cylinder wake. Measurements in the self-similar region of a heated cylinder wake has been made by Wikström *et al.* [20]. The experiments were performed in the MTL wind tunnel at KTH, Stockholm, which has a 7.0 m long test section of 1.2×0.8 m^2 cross section and a free stream turbulence level less than 0.05%. The diameter of the wake-generating cylinder was 6.4 mm and all the measurements were made at a velocity, U_0, of 10.1 m/s giving a maximum mean velocity deficit of 0.5 m/s at $x/d = 400$. The present Reynolds number, $U_0 d/\nu = 4300$, is about three times higher than that of Browne & Antonia [21]. The cylinder was electrically heated, giving a maximum mean temperature excess, Θ_s, of 0.8 °C above the ambient air temperature at $x/d = 400$.

Simultaneous measurements of velocity and temperature statistics were made using a three-wire probe configuration consisting of an X-probe for velocity measurements and a single cold wire for temperature detection, located 0.5 mm in front of the X-wire mid-point. The hot wires had a length of 0.5 mm and a diameter of 2.5 μm. The corresponding dimensions for the cold wire were 1.0 mm and 0.63 μm. Voltages from the constant temperature and constant current circuits were filtered at 5 kHz and sampled at 10 kHz.

Cross-stream derivatives of measured quantities were obtained by using cubic-spline smoothing. Derivatives in the streamwise direction, needed to determine

TABLE 1. The different combinations of the parameter values in the model of $\Pi_{\theta i} - \varepsilon_{\theta i}$ given by (24).

model	$c_{\theta 1}$	$c_{\theta 2}$	$c_{\theta 3}$	$c_{\theta 4}$	$c_{\theta 5}$
(a)	3.2	0	0	0	0
(b)	3.2	0.5	0	0	0
(c)	3.2	1	0	0	0
(d)	3.2	0.5	0.5	0	0
(e)	2.5	0	0	0.35	0
(a^r)	$1.2\,(r+1)/r$	0	0	0	0
(b^r)	$1.2\,(r+1)/r$	0.5	0	0	0
(e^r)	$1.0\,(r+1)/r$	0	0	0.35	0
(a^{WWJ})	$1.6\,(r+1)/r$	0	0	0	0.5

advective terms, were obtained by assuming self-similarity. It was demonstrated that this assumption was valid at $x/d = 400$. The thermal dissipation, ε_θ, was determined from the transport equation of K_θ and ε was determined from the transport of K by neglecting pressure diffusion.

The results presented below are obtained from data at $x/d = 400$, where the turbulent Reynolds number, $4K^2/\nu\varepsilon$, is about 3200 at the location of maximum production.

5. Model comparison

In the following, model predictions with the present explicit algebraic scalar flux model (EASFM), for different choices of the set of parameter values, are compared to data for the three different flow situations described in the previous section. In this comparison the Reynolds stresses are taken directly from DNS or experimental data and not obtained from any model. The different model parameters used are presented in Table 1. Model (a) represents a model for $\Pi_{\theta i} - \varepsilon_{\theta i}$ aligned with the scalar flux vector and model (b) is that of Launder [16]. Model (c) is the Daly–Harlow-type model, with $c_{\theta 1}$=3.2 and $c_{\theta 4}$=0 as in the two previous cases, and in model (d) $c_S = 0$, *i.e.*, singularities are guaranteed not to occur for any flow situation. For model (e) $c_{\theta 1}$=2.5, $c_{\theta 2}$=$c_{\theta 3}$=0, $c_{\theta 4}$=0.35 and the coefficients of this model are tuned for a good performance in the channel flow case.

In the first four models the $c_{\theta 1}$ parameter value is the same (that of Launder [16]) to be able to compare the effects of the $c_{\theta 2}$ and $c_{\theta 3}$ terms. In models (a^r), (b^r), (e^r) and (a^{WWJ}) the time-scale dependence on the $c_{\theta 1}$-term, discussed in section 3.2.1, is taken into account. Apart from this modification, models (a^r), (b^r), and (e^r) are equivalent to models (a), (b), and (e) respectively.

In the last case, model ($\mathrm{a}^{\mathrm{WWJ}}$), the mean scalar-gradient correction of the $c_{\theta 1}$ term is included. For $c_{\theta 5} = 1/2$, the nonlinear terms in (25) vanishes. This very attractive parameter choice is adopted here and $c_{\theta 2}$–$c_{\theta 4}$ are set to zero.

Note that for all of the last four models, $c'_{\theta 1} > 1/2$, hence, satisfying the condition (48), necessary to avoid singular behaviour for small time-scale ratios.

Also, comparisons with the models of Rogers *et al.* [22] and Abe *et al.* [6] are made. The model of Rogers *et al.* [22] is given by

$$C_D \frac{\varepsilon}{2K} \overline{u_i \theta} = -\overline{u_i u_j} \frac{\partial \Theta}{\partial x_j} - \overline{u_j \theta} \frac{\partial U_i}{\partial x_j}, \tag{60}$$

where

$$C_D = 18 \left(1 + \frac{130}{\mathrm{PrRe}_T}\right)^{0.25} \left(1 + \frac{12.5}{{Re_T}^{0.48}}\right)^{-2.08}, \quad Re_T = \frac{4K^2}{\varepsilon \nu} \tag{61}$$

is an empirically determined function calibrated against the homogeneous shear flow data by Rogers *et al* [18], [22]. This model is an implicit algebraic approximation of the $\overline{u_i \theta}$ transport equation. The right-hand side of (60) is the production term $\mathcal{P}_{\theta i}$.

5.1. Homogeneous shear flow. In Table 2 the models for $\Pi_{\theta i} - \varepsilon_{\theta i}$ are compared to the DNS data of homogeneous shear flow, described in the previous section. In Case 1 the mean scalar gradient is imposed in the streamwise (x) direction and in Case 2 it is imposed in the cross-stream (y) direction. The best predictions are given by models (a), (a^r), and ($\mathrm{a}^{\mathrm{WWJ}}$). Models (e) and ($\mathrm{e}^r$) also give reasonably good predictions. Models (b) and (b^r), for which $c_{\theta 2} = 0.5$, somewhat overpredict the amplitude of the $\Pi_{\theta 1} - \varepsilon_{\theta 1}$-values, and for the Daly–Harlow-type model, (c), for which $c_{\theta 2} = 1$, this tendency is even worse. Model (d) gives severe overpredictions of the $\Pi_{\theta 2} - \varepsilon_{\theta 2}$-values.

In the simulation of Rogers *et al.* [18] the normalized scalar flux becomes approximately constant for large simulation times. The equilibrium assumption is thus quite appropriate in this flow case. In Table 3 the predictions of the scalar flux ratio $\overline{u\theta}/\overline{v\theta}$ are given. Good predictions are given by models (a), (a^r), ($\mathrm{a}^{\mathrm{WWJ}}$), (e), ($\mathrm{e}^r$), and the model of Rogers *et al.* [22].

Models (b) and (b^r) somewhat underpredict the amplitude of the scalar-flux ratios and for the Daly–Harlow-type model, (c), this is more accentuated. Model (d) gives predictions that both qualitatively and quantitatively deviate severely from the DNS data. The model of Abe *et al.* [6] gives a quite large overprediction of the amplitude of the flux-ratio in Case 1.

Only the models that behave reasonable well in homogeneous shear flow will be kept in the following. In Table 4 the predictions of models (a), (e), (a^r), (e^r), ($\mathrm{a}^{\mathrm{WWJ}}$), and the models of Rogers *et al.* [22], and Abe *et al.* [6], for the individual flux components are given. In Case 3 the mean scalar gradient is imposed in the spanwise (z) direction. The simple model (a^{WWJ}) gives a very good compromise for both components of the scalar fluxes in all three cases. The

TABLE 2. The predictions of the components of $\Pi_{\theta i} - \varepsilon_{\theta i}$ of models (a)-(a$^{\mathrm{WWJ}}$) compared to the DNS data of Rogers et al. [18], case C128U, Pr = 0.7, at St=12.

	Case 1 $\Pi_{\theta 1} - \varepsilon_{\theta 1}$	Case 1 $\Pi_{\theta 2} - \varepsilon_{\theta 2}$	Case 2 $\Pi_{\theta 1} - \varepsilon_{\theta 1}$	Case 2 $\Pi_{\theta 2} - \varepsilon_{\theta 2}$
DNS data	33.1	−6.90	−15.9	7.14
(a)	39.1	−7.31	−15.3	5.84
(b)	45.6	−7.31	−20.4	5.84
(c)	52.0	−7.31	−25.6	5.84
(d)	45.6	−41.4	−20.4	19.1
(e)	30.6	−5.71	−11.9	4.57
(a^r)	42.0	−7.85	−15.0	5.74
(b^r)	48.5	−7.85	−20.2	5.74
(e^r)	45.6	−9.52	−15.6	7.87
(a$^{\mathrm{WWJ}}$)	38.6	−7.21	−14.7	5.62

TABLE 3. The predictions of the scalar flux ratio of models (a)-(a$^{\mathrm{WWJ}}$), the model of Rogers *et al.* [22], and the model of Abe *et al.* [6], compared to the DNS data of Rogers et al. [18], case C128U, Pr = 0.7, at St=12.

	$\overline{u\theta}/\overline{v\theta}$, Case 1	$\overline{u\theta}/\overline{v\theta}$, Case 2
DNS data	−5.37	−2.57
(a)	−4.96	−2.33
(b)	−4.27	−1.65
(c)	−3.53	−0.97
(d)	2.30	−51.6
(e)	−5.35	−2.73
(a^r)	−4.90	−2.35
(b^r)	−4.24	−1.66
(e^r)	−5.21	−2.68
(a$^{\mathrm{WWJ}}$)	−4.92	−2.45
Rogers *et al.*	−4.89	−2.33
Abe *et al.*	−6.92	−2.17

model predictions of (a$^{\mathrm{WWJ}}$) and those of the model by Rogers *et al.* [22] attain approximately the same values in all cases.

The model of Abe *et al.* [6] underpredicts the amplitudes of all components in all cases, whereas the predictions for $\overline{v\theta}$ in Case 2 and $\overline{w\theta}$ in Case 3 are somewhat better. In the investigation of the model performance by Abe *et al.* [6] only information of $\overline{v\theta}$ in the cross-stream direction (*i.e.*, two-direction) was needed.

TABLE 4. The predictions of the scalar fluxes of models (a), (b), (e), (a^r)-(a^{WWJ}), the model of Rogers *et al.* [22], and the model of Abe *et al.* [6], compared to the DNS data of Rogers et al. [18], case C128U at St=12.

	Case 1		Case 2		Case 3
	$\overline{u\theta}$	$\overline{v\theta}$	$\overline{u\theta}$	$\overline{v\theta}$	$\overline{w\theta}$
DNS data	−2.41	0.45	0.94	−0.36	−0.67
(a)	−2.13	0.43	0.99	−0.42	−0.41
(b)	−1.90	0.44	0.67	−0.42	−0.41
(e)	−1.90	0.36	0.97	−0.35	−0.35
(a^r)	−2.02	0.41	1.01	−0.43	−0.37
(b^r)	−1.80	0.42	0.71	−0.43	−0.37
(e^r)	−1.71	0.33	0.92	−0.34	−0.30
(a^{WWJ})	−2.05	0.42	1.13	−0.46	−0.70
Rogers *et al.*	−2.00	0.41	0.98	−0.42	−0.71
Abe *et al.*	−1.12	0.16	0.53	−0.24	−0.42

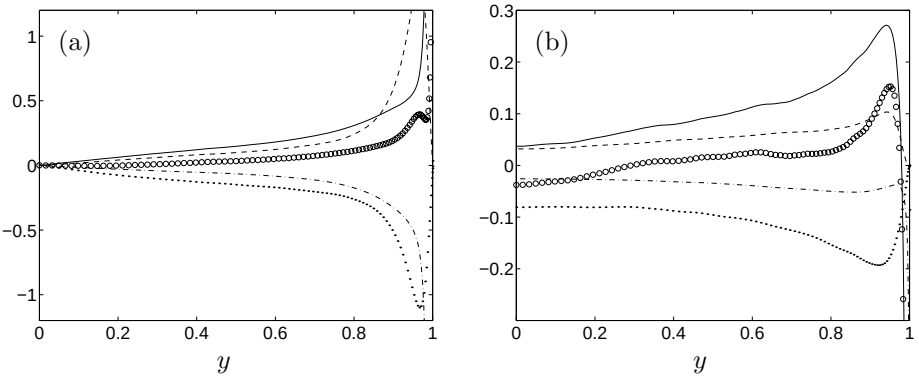

FIGURE 1. Validity of the equilibrium assumption, in the channel flow. (a): ξ_1: - - -, $-\xi_1\left(\mathcal{P}_\theta/(2K_\theta)+\mathcal{P}_K/(2K)\right)$; - · -, $\xi_1\left(\varepsilon_\theta/(2K_\theta)+\varepsilon/(2K)\right)$; ·, $\mathcal{P}_{\theta 1}/\sqrt{KK_\theta}$; —, $\left(\Pi_{\theta 1}-\varepsilon_{\theta 1}\right)/\sqrt{KK_\theta}$; ○, the sum. (b): ξ_2: - - -, $-\xi_2\left(\mathcal{P}_\theta/(2K_\theta)+\mathcal{P}_K/(2K)\right)$; - · -, $\xi_2\left(\varepsilon_\theta/(2K_\theta)+\varepsilon/(2K)\right)$; ·, $\mathcal{P}_{\theta 2}/\sqrt{KK_\theta}$; —, $\left(\Pi_{\theta 2}-\varepsilon_{\theta 2}\right)/\sqrt{KK_\theta}$; ○, the sum

5.2. The turbulent channel flow. In Fig. 1 the validity of the equilibrium assumption, in the present channel flow, is investigated. According to this assumption the sum of all the terms on the right hand side of (8), that is, $\mathrm{D}\xi_i/\mathrm{Dt}-\mathcal{D}_i^{(\xi)}$, should vanish, *i.e.*, be negligible in comparison with characteristic magnitudes of individual terms on the right-hand side. Since the advective terms, $\mathrm{D}\xi_i/\mathrm{Dt}$, are zero in the channel flow, the sum of all the terms on the right-hand side of (8) equals $-\mathcal{D}_i^{(\xi)}$. For the ξ_1-component the equilibrium assumption is appropriate

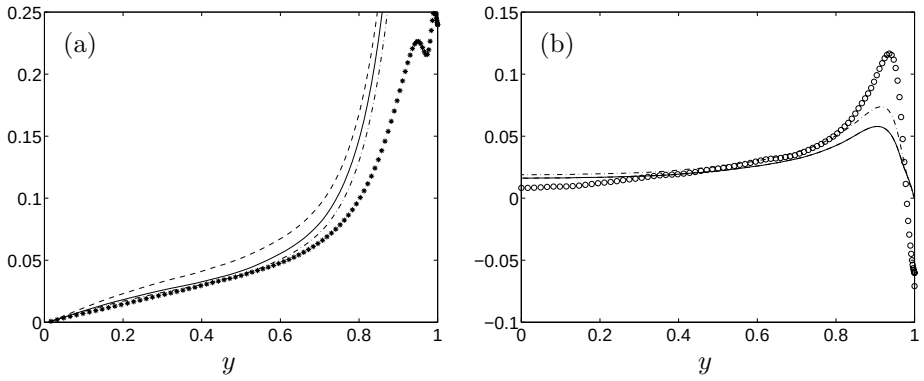

FIGURE 2. Model predictions of $\Pi_{\theta i} - \varepsilon_{\theta i}$ in the channel flow, using the parameter combinations given in Table 1. (a): —, (a); - - -, (b); - · -, (e); ∗, $\Pi_{\theta 1} - \varepsilon_{\theta 1}$ from DNS. (b): —, (a), (b); - · -, (e); ∘, $\Pi_{\theta 2} - \varepsilon_{\theta 2}$ from DNS.

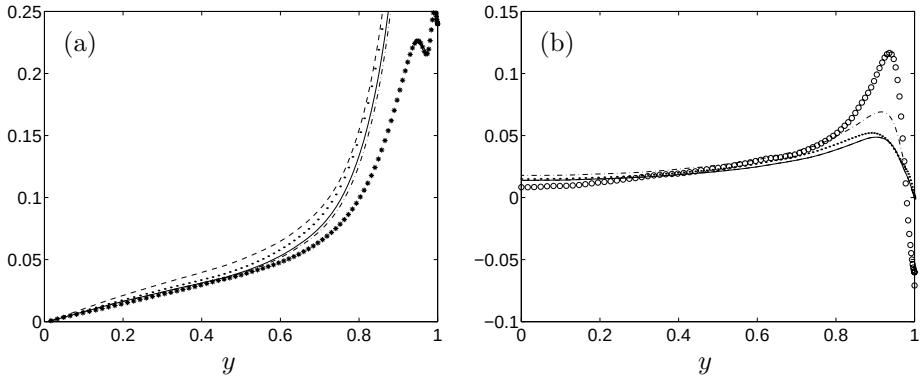

FIGURE 3. Model predictions of $\Pi_{\theta i} - \varepsilon_{\theta i}$ in the channel flow, using the parameter combinations given in Table 1. (a): —, (a^r); - - -, (b^r); - · -, (e^r); · · ·, (a^{WWJ}); ∗, $\Pi_{\theta 1} - \varepsilon_{\theta 1}$ from DNS. (b): —, (a^r), (b^r); - · -, (e^r); · · ·, (a^{WWJ}); ∘, $\Pi_{\theta 2} - \varepsilon_{\theta 2}$ from DNS.

except near the wall. This is also the case for the ξ_2-component except in the center of the channel where $\mathcal{D}_2^{(\xi)}$ may be said to be non-negligible.

In Figs. 2 and 3 the two components of $\Pi_{\theta i} - \varepsilon_{\theta i}$ are shown together with the model predictions of (24) using the different parameter choices given in Table 1 except for (c) and (d). All terms are normalized by $\alpha\,(\partial U/\partial y)_{\mathrm{wall}}\,(\partial \Theta/\partial y)_{\mathrm{wall}}$, where α is the molecular diffusivity. Let us first consider models (a) and (b), where the $c_{\theta 1}$ parameter is taken to be 3.2. Since the $c_{\theta 2}$ parameter only affects the $\Pi_{\theta 1} - \varepsilon_{\theta 1}$- component, in the present case, these two models give the same predictions of the $\Pi_{\theta 2} - \varepsilon_{\theta 2}$-component. Of these models, *i.e.*, $c_{\theta 1} = 3.2$, the aligned model, (a), gives the best agreement and the discrepancy in the $\Pi_{\theta 1} - \varepsilon_{\theta 1}$-component prediction increases as $c_{\theta 2}$ increases. Models (a) and (e) give

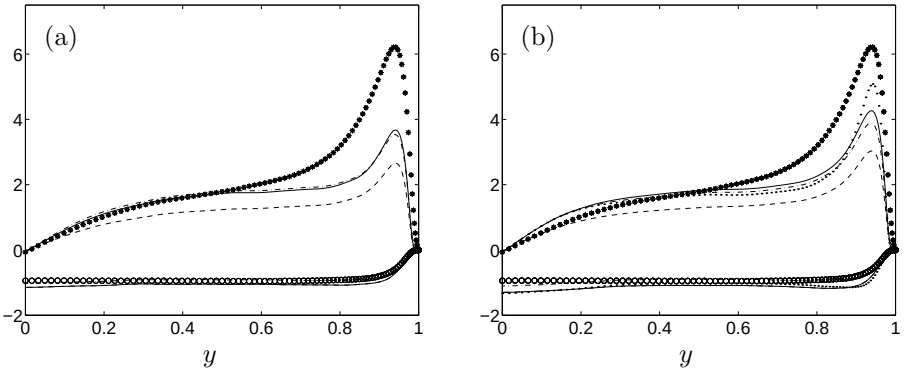

FIGURE 4. Model predictions of the scalar flux components, in the channel flow, using the parameter combinations given in Table 1. (a): —, (a); - - -, (b); - · -, (e). (b): —, (a^r); - - -, (b^r); - · -, (e^r); · · ·, (a^{WWJ}). ∗, $-\overline{u\theta}$; ∘, $\overline{v\theta}$ from DNS.

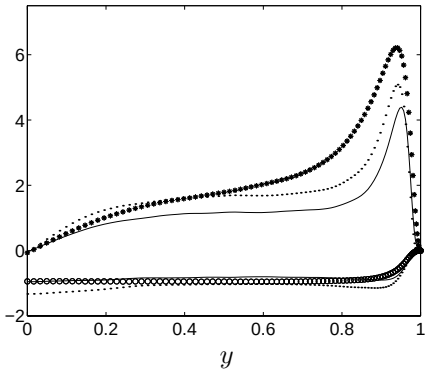

FIGURE 5. Comparison of model (a^{WWJ}) and the model of Rogers *et al.* [22], in the channel flow. —, Rogers *et al.*; · · ·, (a^{WWJ}); ∗, $-\overline{u\theta}$ from DNS; ∘, $\overline{v\theta}$ from DNS.

the best agreement for both components, but also the simple model (a^{WWJ}) gives encouragingly good results. All models slightly overpredict the $\Pi_{\theta 2} - \varepsilon_{\theta 2}$-component in the center of the channel.

It is evident that the model, given by (24), is unable to capture the behaviour of $\Pi_{\theta i} - \varepsilon_{\theta i}$ near the wall. Since it is linear (without the $c_{\theta 5}$-term) and thereby not realizable, there is a need for damping functions, in analogy with, *e.g.*, the EARSM by Wallin & Johansson [12], [13]. It could also be considered to add wall-reflection terms to the model to obtain better predictions of $\Pi_{\theta i} - \varepsilon_{\theta i}$ near the wall. From Fig. 3 it is seen that inclusion of the time-scale dependency in the $c_{\theta 1}$-term slightly improves the prediction abilities of (24). The difference, though, is quite small since the timescale-ratio variation is small in the present channel flow.

Figure 4 shows the model predictions of the scalar fluxes, using the model parameters given in Table 1 except for (c) and (d). The terms are normalized by $\alpha\,(\partial\Theta/\partial y)_{\rm wall}$. Increasing the $c_{\theta 2}$ parameter results in a decrease of the model prediction of the amplitude of the $\overline{u\theta}$-component. An increase of $c_{\theta 1}$ or $c_{\theta 4}$ results in a decrease of the predictions of the amplitudes of both the scalar-flux components.

Models (a), (a^r) and (a$^{\rm WWJ}$) capture the behaviour of the scalar-flux components quite well. This was also the case in the homogeneous shear flow. A perfect prediction of $\Pi_{\theta 2}-\varepsilon_{\theta 2}$ for $|y|\leq 0.2$ results in an underprediction of $\overline{v\theta}$ in this region. This is due to the fact that the equilibrium assumption, $\mathcal{D}_2^{(\xi)}$=0, is not quite fulfilled here. All the models discussed here give a much more realistic description of the scalar fluxes than a standard eddy diffusivity model, which predicts a zero $\overline{u\theta}$-component throughout the channel.

In Fig. 5 a comparison of the prediction of model (a$^{\rm WWJ}$) and that of Rogers *et al.* [22] is made. By decreasing the $c'_{\theta 1}$ value in model (a$^{\rm WWJ}$) (and also in model (a^r)), the prediction of the scalar fluxes are very similar to that of the model of Rogers *et al.* [22]. The $c'_{\theta 1}$ parameter is here tuned to give the best performance in the homogeneous shear-flow case and with that value the predictions of the scalar fluxes, in the channel-flow case, are very good in the region where the equilibrium assumption is approximately satisfied.

5.3. The heated cylinder wake. In Fig. 6 the validity of the equilibrium assumption, in the present wake flow, is investigated. For the ξ_2-component the equilibrium assumption is quite appropriate except near the free-stream. This is also the case for the ξ_1-component except in the center of the wake where $\mathrm{D}\xi_1/\mathrm{D}t-\mathcal{D}_1^{(\xi)}$ is of importance. The relative magnitude of the terms neglected in the equilibrium assumption are somewhat larger in this case than in the channel case. Applying the equilibrium assumption is thus slightly more appropriate in the channel case. For $\eta>2$ there is a large deviation from equilibrium, but since the scalar fluxes approach zero for $\eta>2$ this is actually of minor importance.

In Fig. 7 the two components of $\Pi_{\theta i}-\varepsilon_{\theta i}$ are shown together with the model predictions of (24) using the parameter choices given in Table 1 except for (c) and (d). All terms are normalized by $U_s^2\Theta_s/l$, where U_s and Θ_s are the maximum mean velocity defect and mean temperature excess respectively and l is the mean velocity defect half-width. Since the $c_{\theta 2}$ parameter only affects the $\Pi_{\theta 1}-\varepsilon_{\theta 1}$-component, in the present case, models (a) and (b) give the same prediction of the $\Pi_{\theta 2}-\varepsilon_{\theta 2}$-component. The aligned model, (a), and model (e) give a severe underprediction of the $\Pi_{\theta 1}-\varepsilon_{\theta 1}$-component. The Launder model, (b) gives an improvement compared to these. The importance of the rapid terms when modelling $\Pi_{\theta i}-\varepsilon_{\theta i}$ in the heated cylinder wake has been investigated by Wikström *et al.* 1998 [20].

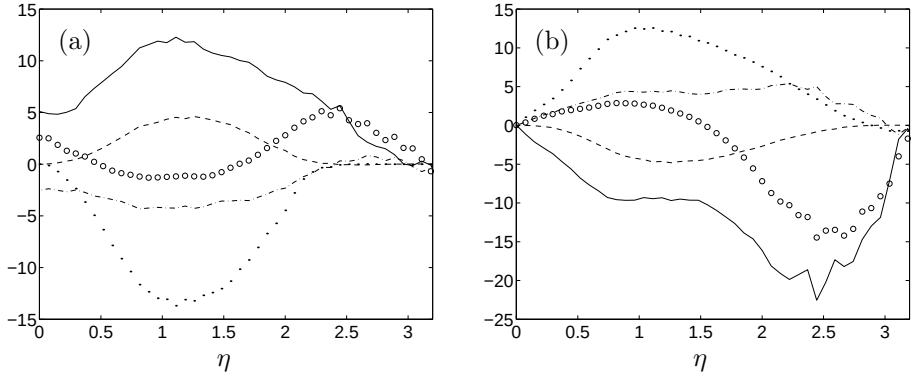

FIGURE 6. Validity of the equilibrium assumption, in the cylinder wake. (a): ξ_1: - - -, $-\xi_1\left(\mathcal{P}_\theta/(2K_\theta)+\mathcal{P}_K/(2K)\right)$; - · -, $\xi_1\left(\varepsilon_\theta/(2K_\theta)+\varepsilon/(2K)\right)$; ·, $\mathcal{P}_{\theta 1}/\sqrt{KK_\theta}$; —, $\left(\Pi_{\theta 1}-\varepsilon_{\theta 1}\right)/\sqrt{KK_\theta}$; ∘, the sum. (b): ξ_2: - - -, $-\xi_2\left(\mathcal{P}_\theta/(2K_\theta)+\mathcal{P}_K/(2K)\right)$; - · -, $\xi_2\left(\varepsilon_\theta/(2K_\theta)+\varepsilon/(2K)\right)$; ·, $\mathcal{P}_{\theta 2}/\sqrt{KK_\theta}$; —, $\left(\Pi_{\theta 2}-\varepsilon_{\theta 2}\right)/\sqrt{KK_\theta}$; ∘, the sum

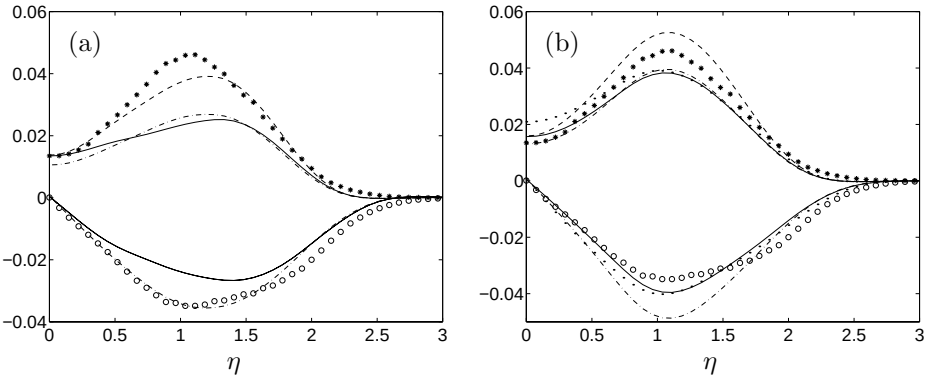

FIGURE 7. Model predictions of the components of $\Pi_{\theta i}-\varepsilon_{\theta i}$, in the cylinder wake, using the parameter combinations given in Table 1. (a): —, (a); - - -, (b); - · -, (e). (b): —, (a^r); - - -, (b^r); - · -, (e^r); · · ·, (a^{WWJ}). ∗, $\Pi_{\theta 1}-\varepsilon_{\theta 1}$; ∘, $\Pi_{\theta 2}-\varepsilon_{\theta 2}$.

From Fig. 7, it is seen that inclusion of the time scale dependency in the $c_{\theta 1}$-term improves the prediction abilities of (24), especially for the $\Pi_{\theta 1}-\varepsilon_{\theta 1}$-component. The effects of this inclusion is here larger than in the channel flow case, since the time-scale-ratio variation is larger in the wake flow.

Figure 8 shows the model predictions of the scalar fluxes, using the model parameters given in Table 1 except for (c) and (d). The terms are normalized by $U_s\Theta_s$. The aligned model, (a), and model (e) give a severe overprediction of the amplitude of the $\overline{u\theta}$-component, whereas they gave good predictions in both the homogeneous shear-flow and the channel cases. One interesting observation is that models (a) and (e) give approximately the same predictions, of the scalar

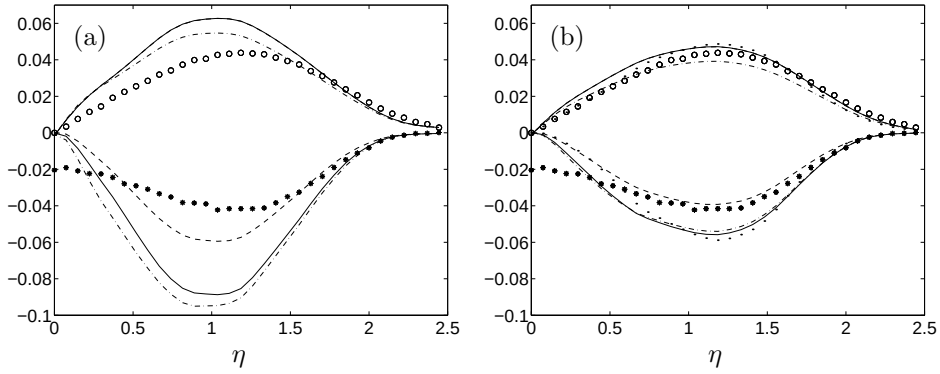

FIGURE 8. Model predictions of the scalar flux components, in the cylinder wake, using the parameter combinations given in Table 1. (a): —, (a); - - -, (b); - · -, (e). (b): —, (a^r); - - -, (b^r); - · -, (e^r); · · ·, (a^{WWJ}). ∗, $\overline{u\theta}$; ∘, $\overline{v\theta}$.

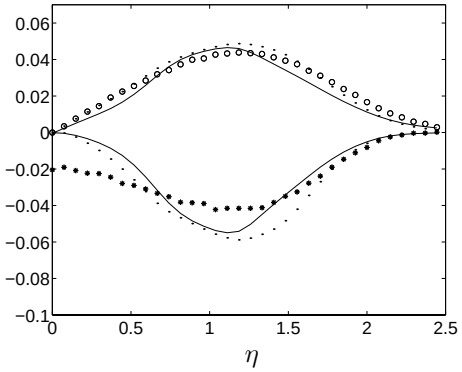

FIGURE 9. Comparison of model (a^{WWJ}) and the model of Rogers *et al.* [22], in the cylinder wake. —, Rogers *et al.*; · · ·, (a^{WWJ}); ∗, $\overline{u\theta}$; ∘, $\overline{v\theta}$.

fluxes, in both the channel flow and the cylinder wake. Increasing the $c_{\theta 2}$ parameter results in a decrease of the model prediction of the amplitude of $\overline{u\theta}$. From Fig. 8 it is also seen that inclusion of the time scale dependency in the $c_{\theta 1}$-term significantly improves the prediction abilities of (24). The effect of this inclusion on the scalar fluxes (and the sum of pressure scalar-gradient correlation and destruction) is much larger here than in the channel-flow case. These types of models all give a reasonably good agreement with the experimental data. Model (b^r), for which $c_{\theta 2} = 0.5$, gives an excellent agreement here. This was not the case for the homogeneous shear flow and the channel flow.

Models (a^r) and (a^{WWJ}), though, give a very good agreement in all three test cases. Since no equation for the scalar quantity N_θ has to be solved when using

the parameter choice $c_{\theta 5} = 1/2$, model ($\mathrm{a}^{\mathrm{WWJ}}$) appears particularly attractive and can be recommended for a wide class of situations.

By using a model with the time-scale-ratio dependence of models (a^{r})-($\mathrm{a}^{\mathrm{WWJ}}$), numerical problems associated with extreme values of the time-scale ratio are also avoided. As in the previous case, all models in Table 1 give a more realistic description of the scalar fluxes than a standard eddy diffusivity model, which, *e.g.*, predicts a zero value of the $\overline{u\theta}$-component throughout the wake. The consequences of applying the equilibrium assumption, in the present case, may be seen in Figs. 7 and 8. Model (e) gives an excellent prediction of $\Pi_{\theta 2} - \varepsilon_{\theta 2}$ for $|\eta| \leq 1.5$, whereas $\overline{v\theta}$ is overpredicted in this region. This is due to the fact that the equilibrium assumption, $\mathrm{D}\xi_1/\mathrm{Dt} - \mathcal{D}_1^{(\xi)} = 0$, is not quite fulfilled in this region. Since all mean scalar gradients are zero at the center line, a zero prediction of $\overline{u\theta}$ is obtained. To be able to give a nonzero prediction at the center line, nonlocal effects have to be taken into account and the equilibrium assumption should not be applied. In Fig. 6 it is seen that the transport terms are important in the region near the center line.

In Fig. 9 a comparison of the prediction of model ($\mathrm{a}^{\mathrm{WWJ}}$) and that of Rogers *et al.* [22] is made. As in the homogeneous shear flow, and in the channel flow, the model predictions are very similar for each component of the scalar flux.

5.4. Comparison with the model of Rogers *et al.* When comparing the ($\mathrm{a}^{\mathrm{WWJ}}$) model with that of Rogers *et al.* [22] there are several things that should be pointed out.

First, the model of Rogers *et al.* is an implicit model, which for large Reynolds numbers becomes a Daly & Harlow type of model and thus in this limit will underpredict the scalar flux ratio. See Abe *et al.* [3] and model (c) in Table 3. This model involves an empirically determined parameter, C_D, a function of the turbulence Reynolds number and the turbulence Peclet number, which is calibrated against homogeneous shear flow DNS data. Model ($\mathrm{a}^{\mathrm{WWJ}}$) is, on the other hand, an explicit model which involves a function of the time-scale ratio, r. This function is obtained directly from the modeled equations to avoid singularities.

Second, and perhaps the most important issue, is that the model of Rogers *et al.*, which is formed by considering homogeneous shear flows, and neglecting the diffusion terms in the transport equation of the dimensional scalar flux. Also the time evolution of the scalar flux, $\partial\overline{u_i\theta}/\partial t$, is assumed to be proportional to the flux itself. This last term is then combined with the model of $\Pi_{\theta i} - \varepsilon_{\theta i}$, and together they are modelled by $\Pi_{\theta i} - \varepsilon_{\theta i} - \partial\overline{u_i\theta}/\partial t = -C_D(\varepsilon/2K)\overline{u_i\theta}$. For general flows exactly the same model formulation is obtained by applying the equilibrium assumption in the transport equation for the nondimensional scalar flux, (8), adding and subtracting $\left(\partial\overline{u_i\theta}/\partial t\right)/\sqrt{KK_\theta}$ to the right-hand side of,

(8), using the model $\Pi_{\theta i} - \varepsilon_{\theta i} - \partial\overline{u_i\theta}/\partial t = -C_D(\varepsilon/2K)\overline{u_i\theta}$, and finally assuming

$$-\frac{\partial\overline{u_i\theta}}{\partial t}/\sqrt{KK_\theta} = -\frac{1}{2}\xi_i\left(\frac{\mathcal{P}_\theta - \varepsilon_\theta}{K_\theta} + \frac{\mathcal{P}_K - \varepsilon}{K}\right). \tag{62}$$

For statistically stationary (nonhomogeneous) flows exactly the same model formulation is thus obtained by assuming

$$-\frac{1}{2}\xi_i\left(\frac{\mathcal{P}_\theta - \varepsilon_\theta}{K_\theta} + \frac{\mathcal{P}_K - \varepsilon}{K}\right) = 0, \tag{63}$$

and using the model $\Pi_{\theta i} - \varepsilon_{\theta i} = -C_D(\varepsilon/2K)\overline{u_i\theta}$, since $\partial\overline{u_i\theta}/\partial t = 0$. In the present non homogeneous test cases, where diffusion terms are present, *i.e*, the channel flow and the cylinder wake, (63) is approximately satisfied, which may be seen in Figs.1 and6. This explains why there are no major differences between the model predictions of the model of Rogers *et al.*, (a^r), and ($\mathrm{a}^{\mathrm{WWJ}}$), which all are based on models for $\Pi_{\theta i} - \varepsilon_{\theta i}$ that are aligned with the scalar flux, whereas models (a^r) and ($\mathrm{a}^{\mathrm{WWJ}}$) do not include the assumption (63). (In the case of ($\mathrm{a}^{\mathrm{WWJ}}$) the mean scalar gradient is invoked in the model of the slow term, see (24)). Model ($\mathrm{a}^{\mathrm{WWJ}}$) is obtained by neglecting the advection and diffusion terms in the transport equation of the nondimensional scalar flux and keeping the first term on the right-hand side of (8), that is, not making the assumption (63), and would in general do a much better job in nonhomogeneous flows where (63) is not valid (and the equilibrium assumption is appropriate).

6. Conclusions

An algebraic relation for the scalar flux in terms of mean flow quantities has been formed by applying an equilibrium assumption in the transport equation for the scalar flux. The resulting set of algebraic equations is implicit and nonlinear unless the model parameter $c_{\theta 5} = 1/2$ is used in the model of the sum of the pressure scalar-gradient correlation and the destruction. A solution to the general implicit relation for the normalized scalar flux in a fully explicit form is proposed. The solution is exact in two-dimensional mean flows. In three-dimensional mean flows the tensorial form is exact but an approximation for the scalar production to dissipation ratio is introduced.

The Daly–Harlow-type model, $c_{\theta 2} = 1$ and $c_{\theta 3} = 0$, can readily be transformed into a formulation of a model for the dispersion tensor, $\mathcal{D}_{ij}$ (see *e.g.* (22)), which inserted into the implicit algebraic equation for ξ_i, yields

$$\mathcal{D}_{ij} = \frac{1 - c_{\theta 4}}{N_\theta}\frac{\overline{u_iu_j}}{k}, \tag{64}$$

where N_θ is given by (54). Hence, for this simplified model we have a dispersion tensor (in two-dimensional as well as in three-dimensional mean flows) that is proportional to the Reynolds stress tensor. The dependency of the mean flow gradients here enters through the scalar N_θ. For this model the distribution of the relative dispersion is proportional to the relative turbulence intensities in

the different directions. This is analogous to the Daly & Harlow [1] model for turbulent diffusion of the Reynolds stresses. As a comparison one may note that the simplest eddy-diffusivity approach implicitly assumes an isotropic dispersion tensor.

From the general model formulation, it is seen that for model parameters that deviate from $c_{\theta 2} = 1$ and $c_{\theta 3} = 0$, a dispersion tensor with principal axes different from those of the Reynolds stress tensor is obtained.

With the parameter choice $c_{\theta 5} = 1/2$, the equation system (25) for the scalar fluxes becomes explicit without any need for solving an equation for N_θ. This is the case for both two- and three-dimensional mean flows. The parameter choice $c_{\theta 5} = 1/2$ is thus very attractive. The present EASFM is then given by

$$\xi_i = -(1 - c_{\theta 4})\, A_{ij}^{-1} \left(a_{jk} + \frac{2}{3}\delta_{jk} \right) \Theta_k, \tag{65}$$

where the inverse of the matrix $\mathbf{A}$ is given by

$$\mathbf{A}^{-1} = \frac{\left(G^2 - \frac{1}{2}Q_1\right)\mathbf{I} - G\left(c_S\mathbf{S} + c_\Omega\mathbf{\Omega}\right) + \left(c_S\mathbf{S} + c_\Omega\mathbf{\Omega}\right)^2}{G^3 - \frac{1}{2}GQ_1 + \frac{1}{2}Q_2} \tag{66}$$

Predictions of the present EASFM have been compared to data for three different types of flow situations. These are homogeneous shear flow, turbulent channel flow, and the flow behind a heated cylinder. With the Daly–Harlow-type model, *i.e.*, $c_{\theta 2} = 1$ and $c_{\theta 3} = 0$, an underprediction of the $\overline{u\theta}$-component compared to the $\overline{v\theta}$-component is obtained in all cases. Using model ($\mathrm{a}^{\mathrm{WWJ}}$) in Table 1 (given by (65) and (66) with $c_S = c_\Omega = 1$ and $c_{\theta 4} = 0$), for which $c_{\theta 5} = 1/2$, very good predictions are obtained for all test cases. Since no equation for the scalar quantity N_θ has to be solved when using the parameter choice $c_{\theta 5} = 1/2$, model ($\mathrm{a}^{\mathrm{WWJ}}$) is strongly recommended.

By using a model with the time-scale-ratio dependence of models (a^r)-($\mathrm{a}^{\mathrm{WWJ}}$), numerical problems associated with extreme values of the time-scale ratio are also avoided. In the wake flow where the largest variations of the time-scale ratio are present, compared to the other two cases, the inclusion of this time-scale dependence is shown to be of significant importance. This time-scale ratio dependence in the $c_{\theta 1}$-parameter is necessary to obtain good predictions in the heated cylinder wake, using the model parameters that give good model predictions in the present homogeneous shear and channel-flow cases.

In a comparison of the prediction of model ($\mathrm{a}^{\mathrm{WWJ}}$) and that of Rogers *et al.* [22] it is found that the model predictions are very similar for each component in all test cases of the scalar flux. Model ($\mathrm{a}^{\mathrm{WWJ}}$), which is obtained by neglecting the advection and diffusion terms in the transport equation of the nondimensional scalar flux and keeping the first term on the right-hand side of (8), that is, not making the assumption (63), would in general do a much better job in nonhomogeneous flows where (the equilibrium assumption is appropriate and) (63) not is valid.

An explicit algebraic scalar flux model as proposed here ((65) and (66)) should suitably be used together with an appropriate EARSM for the Reynolds stresses. To make the model complete model equations for $\overline{\theta^2}$ and ε_θ are needed to be able to determine the time-scale ratio r.

References

[1] Daly, B. J. & Harlow, F. H. 1970 Transport equations in turbulence. *Phys. Fluids* **13**, 2634–2649.

[2] Kim, J., & Moin, P. 1989 Transport of passive scalars in a turbulent channel flow. in proc. *Turbulent Shear Flows 6*, Toulouse Sept. 7-9 1987, Springer, 85–96

[3] Abe, K., & Suga, K. 1998 Large eddy simulation of passive scalar fields under several strain conditions. in proc. Turbulent Heat Transfer II, Manchester May 31 – June 5, **2**, 8-15–8-30.

[4] Adumitroaie, V., Taulbee, D. B. & Givi, P. 1997 Explicit Algebraic Scalar-Flux Models for Turbulent Reacting Flows. *A. i. ch. e. J.* **43**, 1935–2147.

[5] Girimaji, S. S. & Balachandar, S. 1998 Analysis and modeling of boyancy-generated turbulence using numerical data. *Int. J. Heat Mass Transfer* **41**, 915–929.

[6] Abe, K., Kondoh, T. & Nagano, Y. 1996 A two-equation heat transfer model reflecting second-moment closures for wall and free turbulent flows. *Int. J. Heat and Fluid Flow* **17**, 228–237.

[7] Shih, T. H. & Lumley, J. L. 1993 Remarks on Turbulent Constitutive Relations. *Mathl. Comput. Modelling* **18**(2), 9–16.

[8] Shih, T. H. 1996 Constitutive relations and realizability of single-point turbulence closures. Turbulence and Transition Modelling, M. Hallbäck, D.S. Henningson, A.V. Johansson & P.H. Alfredsson (eds), Vol 2, Kluwer.

[9] Shabany, Y. & Durbin, P. A. 1997 Explicit Algebraic Scalar Flux Approximation. *AIAA J.* **35**, 985–989.

[10] Johansson, A. V. & Wallin, S. 1996 A new explicit algebraic Reynolds stress model. Proc. Sixth European Turbulence Conference, Lausanne, July 1996, Ed. P. Monkewitz, 31–34.

[11] Girimaji, S. S. 1995 Fully explicit and self-consistent algebraic Reynolds stress model. *Theor. Comp. Fluid Dyn.* **8**, 387.

[12] Wallin, S. & Johansson, A. V. 1996 A complete explicit algebraic Reynolds stress turbulence model including an improved near-wall treatment. Proc. Flow Modeling and Turbulence Measurements VI, Tallahassee FL, C.-J. Chen, C. Shih, J. Lienau & R.J. Kung (eds), 399–406, Balkema, Rotterdam.

[13] Wallin, S. & Johansson, A. V. 2000. An explicit algebraic Reynolds stress model for incompressible and compressible turbulent flows. To appear in *J. Fluid Mech.* **403**, 89–132.

[14] Rodi, W. 1972 The prediction of free turbulent boundary layers by use of a two equation model of turbulence. *Ph.D. thesis, University of London.*

[15] Rodi, W. 1976 A new algebraic relation for calculating the Reynolds stresses. *Z. angew. Math. Mech.* **56**, T219–221.

[16] Launder, B. E. 1978 Heat and mass transport. In Turbulence, P. Bradshaw (ed.), Springer, Berlin, 231–287.

[17] Craft, T. J., Launder, B. E. 1996 Recent developments in second-moment closure for boyancy-affected flows. *Dynamics of Atmospheres and Oceans* **23**, 99–114.

[18] Rogers, M.M., Moin, P. & Reynolds, W.C. 1986 The structure and modeling of the hydrodynamic and passive scalar fields in homogeneous turbulent shear flow. Dept. Mech. Engng. Rep. TF-25, Stanford University, Stanford, California.

[19] Wikström, P. M. and Johansson, A. V. 1998 DNS and scalar-flux transport modelling in a turbulent channel flow. in proc. Turbulent Heat Transfer II, May 31-June 5, Manchester, 1998.

[20] Wikström, P. M., Hallbäck, M., and Johansson, A. V. 1998 Measurements and heat-flux transport modelling in a heated cylinder wake. *Intl. J. Heat Fluid Flow* **19**, 556–562.

[21] Browne, L. W. B., & Antonia, R. A. 1986 Reynolds shear stress and heat flux measurements in a cylinder wake. *Phys. Fluids A.* **29**, 709–713.

[22] Rogers, M.M., Mansour, P. & Reynolds, W.C. 1989 An algebraic model for the turbulent flux of a passive scalar. *J. Fluid Mech.* **203**, 77–101.

Paper 6

6

AN EFFICIENT EXPLICIT ALGEBRAIC REYNOLDS STRESS k-ω MODEL (EARSM) FOR AERONAUTICAL APPLICATIONS

Stefan Wallin
The Aeronautical Research Institute of Sweden (FFA), Bromma, Sweden

Abstract. The self-consistent explicit algebraic Reynolds stress model (EARSM) proposed by Wallin & Johansson (1997) with the k-ω wo-equation transport model as platform was the starting point for some further developments. The original near-wall damping function was reformulated in terms of $Re_y \equiv \sqrt{k}y/\nu$ and an additional alternative without any damping functions whatsoever was introduced. The EARSM approach clearly improves the shock position for transonic wings without significal increase in computational cost. The EARSM may be expressed as an extension to an eddy-viscosity model and thus no major problems should be expected in implementing EARSM into a flow solver with existing two-equation eddy-viscosity models.

1. Introduction

Standard two-equation models based on the eddy-viscosity assumption are still dominating in the context of industrial flow computations. In flows with strong effects of streamline curvature, adverse pressure gradients, flow separation or system rotation, such models fail to give accurate predictions. Turbulence models based on the transport equations for the individual Reynolds stresses have the natural potential for dealing with, *e.g.*, the associated complex dynamics of intercomponent transfer. The eddy-viscosity hypothesis may in this context be said to be replaced by transport equations for the individual Reynolds stress anisotropies. As yet, there are non-trivial numerical aspects of flow computations with such models in complex flow situations. This represents an active area of research. In parallel with such efforts there has been a considerable renewed interest in various forms of explicit algebraic approximations of the anisotropy transport equations, see *e.g.* Pope (1975), Gatski & Speziale (1993), Girimaji (1995), Johansson & Wallin (1996) and Wallin & Johansson (1997).

The model proposed by Wallin & Johansson has been proven to give important improvements over standard two-equation models based on the eddy-viscosity assumption in flows with strong effects of streamline curvature, adverse pressure gradients, flow separation or system rotation. The near-wall formulation in the model is, however, based on y^+ which may cause problems in some situations.

In the present work the near-wall formulation in the model proposed by Wallin & Johansson will be revised in terms of the wall distance which replaces the y^+-dependency. Moreover, a simplified version is proposed without near-wall damping functions whatsoever which may be attractive for computation of complicated 3D flows.

2. Description of the models

The turbulence models that will be described here are variations of the explicit algebraic Reynolds stress model (EARSM) described in detail by Wallin & Johansson (1997). That model is based on a recalibrated Launder, Reece & Rodi (1975) model which is a differential Reynolds stress model. A self-consistent and fully explicit algebraic relation for the Reynolds stresses in terms of the mean flow field is then obtained by applying the so-called 'equilibrium assumption', Rodi (1972 & 1976), where the advection and diffusion of the Reynolds stress anisotropy is neglected.

The model is based on transport equations for the turbulent kinetic energy k and the specific dissipation rate ω and we are recommending two options: (i) EARSM based on the Wilcox (1988) standard $k-\omega$ model denoted 'WJ_skw' and (ii) EARSM based on the Wilcox (1994) low-Reynolds number $k-\omega$ model denoted 'WJ_kw'. There is actually a third option that is an eddy-viscosity model obtained from further simplification of (i). That is (iii) Linear EARSM based on the Wilcox (1988) standard $k-\omega$ model denoted 'LWJ_kw'.

A well known problem with these options is that the $k-\omega$ model is unphysically sensitive to the free-stream turbulence level. That has recently been resolved by Kok (1999) by adding a cross-diffusion term in the ω-equation. An interesting, but not thoroughly tested alternative is thus EARSM based on Kok $k-\omega$, alternative (iv).

Which of these options that should be recommended depends on the application. The following may be used as a guide:

(i) EARSM based on standard $k-\omega$ is more simple to implement and needs no wall-distance information. The turbulent kinetic energy and the Reynolds stress profiles are qualitatively wrong in the near-wall region, $y^+ < 100$, but the velocity profiles and skin friction are correct. This alternative is thus most suitable as an engineering tool for complicated 3D flows where detailed information of the near-wall turbulence is not needed.

(ii) EARSM based on low-Reynolds number $k-\omega$ is somewhat more complex and needs the distance to the closest wall. The model is, however, independent of the local wall skin friction or y^+. The influence by the near-wall damping functions are limited to the very near-wall region and are practically zero for $y^+ > 100$. For this reason, it should not be an important issue how multiple walls and corners are treated. The turbulent kinetic energy and the Reynolds stress profiles are well predicted also in the near-wall region. This alternative should thus be used if detailed information of the near-wall turbulence is needed.

(iii) Linear EARSM based on standard $k-\omega$ model is only motivated from the somewhat simplified implementation. The model is actually an eddy-viscosity model and thus only the routine that computes the eddy viscosity needs to be modified. Some of the prediction capabilities of the full EARSM, (i) or (ii), is lost but this alternative is still better than the more ad-hoc standard eddy-viscosity models with constant C_μ.

(iv) EARSM based on Kok $k-\omega$ is similar to alternative (i) regarding implementation and prediction capabilities since the only difference is a cross-diffusion term added to the ω-equation. The advantage with this alternative is that the unphysical free-stream dependency in the standard $k-\omega$ is eliminated. However, this model is not thoroughly tested yet.

These three models will be described with special emphasis on the extension to an EARSM.

2.1. EARSM based on standard k-ω

2.1.1. *Transport equations.* The transport equations for k and ω read

$$\begin{aligned}\frac{D}{Dt}(\rho k) &= \mathcal{P}-\rho\varepsilon+\frac{\partial}{\partial x_j}\left[\left(\mu+\frac{\mu_T}{\sigma_k}\right)\frac{\partial k}{\partial x_j}\right]\\ \frac{D}{Dt}(\rho\omega) &= \alpha\frac{\omega}{k}\mathcal{P}-\beta\rho\omega^2+\frac{\partial}{\partial x_j}\left[\left(\mu+\frac{\mu_T}{\sigma_\omega}\right)\frac{\partial\omega}{\partial x_j}\right]\end{aligned} \tag{1}$$

where

$$\frac{D}{Dt}\equiv\frac{\partial}{\partial t}+U_j\frac{\partial}{\partial x_j}. \tag{2}$$

The production of the turbulent kinetic energy is defined as

$$\mathcal{P}\equiv-\overline{\rho u_i u_j}\frac{\partial U_i}{\partial x_j} \tag{3}$$

and the dissipation rate

$$\varepsilon\equiv\beta^*\omega k. \tag{4}$$

$\alpha = 5/9$, $\beta = 3/40$, $\beta^* = 9/100$, $\sigma_k = 2.0$ and $\sigma_\omega = 2.0$ are the model constants.

In the original eddy-viscosity model the Reynolds stresses are obtained from

$$\overline{\rho u_i u_j} = \frac{2}{3}\rho k\delta_{ij}-2\mu_T S^*_{ij} \text{ where } S^*{}_{ij} = \frac{1}{2}\left(\frac{\partial U_i}{\partial x_j}+\frac{\partial U_j}{\partial x_i}-\frac{2}{3}\frac{\partial U_k}{\partial x_k}\delta_{ij}\right) \tag{5}$$

and the turbulent viscosity is given by

$$\mu_T = \frac{\rho k}{\omega}. \tag{6}$$

2.1.2. *Reynolds stresses.* The Reynolds stresses $\overline{\rho u_i u_j}$ expressed by EARSM may be written in terms of an effective turbulent viscosity μ_T and an extra anisotropy $a^{(\mathrm{ex})}_{ij}$

$$\overline{\rho u_i u_j} = \frac{2}{3}\rho k\delta_{ij}-2\mu_T S^*_{ij}+\rho k a^{(\mathrm{ex})}_{ij}. \tag{7}$$

The effective turbulent viscosity then reads

$$\mu_T = -\frac{1}{2}(\beta_1 + I\!I_\Omega \beta_6)\rho k\tau \tag{8}$$

and the extra anisotropy

$$\begin{aligned} \boldsymbol{a}^{(\mathrm{ex})} &= \beta_3\left(\Omega^2 - \frac{1}{3}I\!I_\Omega \mathbf{I}\right) + \beta_4(\boldsymbol{S}\Omega - \Omega\boldsymbol{S}) \\ &+ \beta_6\left(\boldsymbol{S}\Omega^2 + \Omega^2\boldsymbol{S} - I\!I_\Omega\boldsymbol{S} - \frac{2}{3}I\!V\,\mathbf{I}\right) + \beta_9(\Omega\boldsymbol{S}\Omega^2 - \Omega^2\boldsymbol{S}\Omega) \end{aligned} . \tag{9}$$

The invariants are

$$I\!I_S = \mathrm{tr}\{S^2\}\,,\ I\!I_\Omega = \mathrm{tr}\{\Omega^2\} \text{ and } I\!V = \mathrm{tr}\{S\Omega^2\}\,. \tag{10}$$

Here $\boldsymbol{a}$, $\boldsymbol{S}$ and Ω denotes second rank tensors. tr{ } denotes the trace and $\mathbf{I}$ (or δ_{ij}) is the identity matrix. The inner product of two matrices is defined as $(\boldsymbol{SS})_{ij} \equiv (\boldsymbol{S}^2)_{ij} \equiv S_{ik}S_{kj}$. The normalized mead strain- and rotation rate tensors are defined as

$$S_{ij} = \tau S^*_{ij} \text{ and } \Omega_{ij} = \tau\Omega^*_{ij} \tag{11}$$

where τ is the turbulent time-scale. The dimensional strain- and rotation rate tensors are

$$S^*_{ij} = \frac{1}{2}\left(\frac{\partial U_i}{\partial x_j} + \frac{\partial U_j}{\partial x_i} - \frac{2}{3}\frac{\partial U_k}{\partial x_k}\delta_{ij}\right) \text{ and } \Omega^*_{ij} = \frac{1}{2}\left(\frac{\partial U_i}{\partial x_j} - \frac{\partial U_j}{\partial x_i}\right). \tag{12}$$

In the near-wall region, viscous effects become important and the turbulent time-scale in (11) need to be limited by the Kolmogoroff time scale as proposed by Durbin (1993)

$$\tau = \max\left(\frac{k}{\varepsilon}, C_\tau\sqrt{\frac{\mu}{\rho\varepsilon}}\right) \tag{13}$$

where $C_\tau = 6.0$ is a model constant.

The β-coefficients in (8) and (9) are given by

$$\begin{aligned} \beta_1 &= -\frac{N(2N^2 - 7I\!I_\Omega)}{Q} \qquad \beta_3 = -\frac{12N^{-1}I\!V}{Q} \\ \beta_4 &= -\frac{2(N^2 - 2I\!I_\Omega)}{Q} \qquad \beta_6 = -\frac{6N}{Q} \qquad \beta_9 = \frac{6}{Q} \end{aligned} \tag{14}$$

with the non-singular denominator

$$Q = \frac{5}{6}(N^2 - 2I\!I_\Omega)(2N^2 - I\!I_\Omega)\,. \tag{15}$$

N is given by

$$N = \begin{cases} \frac{C_1'}{3} + (P_1 + \sqrt{P_2})^{1/3} + (P_1 - \sqrt{P_2})^{1/3} & , P_2 \geq 0 \\ \frac{C_1'}{3} + 2(P_1^2 - P_2)^{1/6} \cos\left(\frac{1}{3}\arccos\left(\frac{P_1}{\sqrt{P_1^2 - P_2}}\right)\right) & , P_2 < 0 \end{cases} \tag{16}$$

where

$$P_1 = \left(\frac{C_1'^2}{27} + \frac{9}{20}I\!I_S - \frac{2}{3}I\!I_\Omega\right)C_1', \; P_2 = P_1^2 - \left(\frac{C_1'^2}{9} + \frac{9}{10}I\!I_S + \frac{2}{3}I\!I_\Omega\right)^3 \tag{17}$$

and

$$C_1' = \frac{9}{4}(c_1 - 1). \tag{18}$$

When computing the third root one need to make sure that the real root is returned even for negative arguments and the arccos function should return an angle between 0 and π. $c_1 = 1.8$ is a model constant.

In 2D mean flows the β-coefficients are

$$\beta_1 = -\frac{6}{5}\frac{N}{N^2 - 2I\!I_\Omega} \qquad \beta_4 = -\frac{6}{5}\frac{1}{N^2 - 2I\!I_\Omega}$$
$$\beta_3 = 0 \qquad \beta_6 = 0 \qquad \beta_9 = 0 \tag{19}$$

and the relation (9) simplifies significantly.

2.2. EARSM based on low-Re k-ω. The transport equation for k and ω are given by (1) to (3) and the dissipation rate ε is given by (4) as for the standard $k - \omega$ model. The differences enter through the model coefficients that in the case of low-Reynolds number $k - \omega$ are functions of the turbulent Reynolds number Re_T.

These functions read:

$$\beta^* = \frac{9}{100}\frac{5/18 + (Re_T/R_\beta)^4}{1 + (Re_T/R_\beta)^4}$$
$$\alpha = \frac{5}{9}\frac{\alpha_0 + Re_T/R_\omega}{1 + Re_T/R_\omega} \cdot (\alpha^*)^{-1} \tag{20}$$
$$\alpha^* = \frac{\beta/3 + Re_T/R_k}{1 + Re_T/R_k}$$

where the turbulent Reynolds number is defined as

$$Re_T = \frac{\rho k}{\omega\mu}. \tag{21}$$

$R_\beta = 8$, $R_\omega = 2.7$, $R_k = 6$, $\alpha_0 = 1/10$, and $\beta = 3/40$ are the model constants.

2.2.1. *Reynolds stresses.* The Reynolds stresses $\overline{\rho u_i u_j}$ is also here written in terms of the effective turbulent viscosity μ_T and the extra anisotropy $a_{ij}^{(\mathrm{ex})}$ as in (7) but here a near-wall damping function needs to be introduced. The effective turbulent viscosity then reads

$$\mu_T = -\frac{1}{2} f_1 (\beta_1 + I\!I_\Omega \beta_6) \rho k \tau \tag{22}$$

and the extra anisotropy

$$\begin{aligned} \boldsymbol{a}^{(\mathrm{ex})} = {} & (1 - f_1^2) \frac{3B_2 - 4}{\max(I\!I_S, I\!I_S^{\mathrm{eq}})} \left(\boldsymbol{S}^2 - \frac{1}{3} I\!I_S \mathbf{I} \right) \\ & + f_1^2 \beta_3 \left(\Omega^2 - \frac{1}{3} I\!I_\Omega \mathbf{I} \right) + \left(f_1^2 \beta_4 - (1 - f_1) \frac{B_2}{2\max(I\!I_S, I\!I_S^{\mathrm{eq}})} \right) (\boldsymbol{S\Omega} - \boldsymbol{\Omega S}) \\ & + f_1 \beta_6 \left(\boldsymbol{S\Omega}^2 + \boldsymbol{\Omega}^2 \boldsymbol{S} - I\!I_\Omega \boldsymbol{S} - \frac{2}{3} I\!V \mathbf{I} \right) + f_1^2 \beta_9 (\boldsymbol{\Omega S \Omega}^2 - \boldsymbol{\Omega}^2 \boldsymbol{S \Omega}) \end{aligned} \tag{23}$$

where

$$I\!I_S^{\mathrm{eq}} = \frac{405 c_1^2}{216 c_1 - 160} \tag{24}$$

and $B_2 = 1.8$ is an additional model constant.

The near-wall damping function f_1 in (22) and (23) was original defined in terms of y^+ by Wallin & Johansson (1997) but has later been redefined in terms of Re_y. The near-wall damping is needed when EARSM is used together with low-Reynolds number two-equation models with correct near-wall asymptotic behaviour.

$$f_1 = 1 - \exp(-C_{yA} \sqrt{Re_y} - C_{yB} Re_y^2) \tag{25}$$

where

$$Re_y \equiv \frac{\rho \sqrt{k} y}{\mu}. \tag{26}$$

$C_{yA} = 0.092$ and $C_{yB} = 1.2 \cdot 10^{-4}$ are model constants. The β-coefficients in (22) and (23) are defined as previous in (14) to (17) or in (19) for 2D mean flows.

2.3. Linear EARSM based on standard k-ω. An alternative to EARSM based on standard $k - \omega$ that is even more simple to implement, since it actually is an eddy-viscosity model, is here described. The approach is to keep only the eddy-viscosity part of the relation (7) which means that $a_{ij}^{(\mathrm{ex})} = 0$. Some of the physics covered of the full EARSM is naturally missing in this approach and it cannot be motivated from increased robustness or decreased computational cost. However, as an eddy-viscosity model this approach is based on a more sound basis compared to standard eddy-viscos-

ity models with constant C_μ. The only motivation for this approach is that only the routine that computes the eddy-viscosity needs to be modified.

2.4. EARSM based on Kok k-ω. The dependenc on free-stream ω-values in the $k-\omega$ model has been resolved by Kok (1999) by adding a cross-diffusion term in the ω-equation and modifying the diffusion coefficients.

This model is identical to EARSM based on standard $k-\omega$ (see section 2.1) except a few details. The transport equation for ω reads

$$\frac{D}{Dt}(\rho\omega) = \alpha\frac{\omega}{k}\mathcal{P} - \beta\rho\omega^2 + \frac{\partial}{\partial x_j}\left[\left(\mu + \frac{\mu_T}{\sigma_\omega}\right)\frac{\partial\omega}{\partial x_j}\right] + \sigma_d\frac{\rho}{\omega}\max\left(\frac{\partial k}{\partial x_j}\frac{\partial\omega}{\partial x_j}, 0\right) \tag{27}$$

where the diffusion coefficients are $\sigma_\omega = 2.0$ and $\sigma_d = 0.5$. The diffusion coefficient in the k-equation (1) is modified to $\sigma_k = 1.5$.

3. Implementation

3.1. Formulation in terms of an effective viscosity. The Reynolds stresses expressed by EARSM is written in terms of an effective turbulent viscosity μ_T and an extra anisotropy $a_{ij}^{(\mathrm{ex})}$. The reason for this is that many CFD solvers already have different eddy-viscosity two-equation models implemented and that many routines may be reused when the model is formulated in terms of an effective turbulent viscosity μ_T. Our experience is that it is sufficient only to consider the effective turbulent viscosity μ_T when determining the stability limit for explicit methods or the system Jacobian for implicit methods. The extra terms associated with the extra anisotropy $a_{ij}^{(\mathrm{ex})}$ may be treated as a fully decoupled source term without loss of performance of the solution method.

3.2. Terms to be modified. 3.2.1. *Production of the turbulent kinetic energy.* The production of the turbulent kinetic energy is defined as

$$\mathcal{P} \equiv -\overline{\rho u_i u_j}\frac{\partial U_i}{\partial x_j} \tag{28}$$

and needs no further modelling since the Reynolds stresses are explicitly known. In an eddy-viscosity two-equation model, this term is modelled as

$$\mathcal{P}^{(\mathrm{EVM})} = \left(2\mu_T S_{ij}^* - \frac{2}{3}\rho k\delta_{ij}\right)\frac{\partial U_i}{\partial x_j}. \tag{29}$$

Many important physical aspects are lost through this assumption, like effects of streamline curvature and local and global rotation and this term is thus the most important to modify. By using the effective turbulent viscosity μ_T in (29) and by adding the

contribution from the extra anisotropy the original definition of the production of the turbulent kinetic energy is preserved

$$\mathcal{P} = \mathcal{P}^{(\mathrm{EVM})} - \rho k a_{ij}^{(\mathrm{ex})} \frac{\partial U_i}{\partial x_j}. \tag{30}$$

3.2.2. *The turbulent transport of momentum.* The second most important term to modify is the turbulent transport of momentum in the momentum equation. This term is also exactly defined in terms of the Reynolds stresses and reads

$$T_i \equiv \frac{\partial}{\partial x_j}(-\overline{\rho u_i u_j}) . \tag{31}$$

In an eddy-viscosity two-equation model, this term is modelled as

$$T_i^{(\mathrm{EVM})} = \frac{\partial}{\partial x_j}\left(2\mu_T S_{ij}^* - \frac{2}{3}\rho k \delta_{ij}\right). \tag{32}$$

Also for this term many important physical aspects are lost through this assumption, like turbulence induced secondary motions. By using the effective turbulent viscosity μ_T in (29) and by adding the contribution from the extra anisotropy the original definition of turbulent transport of momentum is preserved

$$T_i = T_i^{(\mathrm{EVM})} - \frac{\partial}{\partial x_j}(\rho k a_{ij}^{(\mathrm{ex})}) . \tag{33}$$

3.2.3. *Turbulent transport terms.* There are also a number of other turbulent transport terms, but these terms needs to be modelled even in terms of the Reynolds stresses. In eddy-viscosity two-equation models, these terms are most commonly modelled using gradient diffusion where the diffusion coefficients are related to the turbulent viscosity. Also here the effective turbulent viscosity should be used, but no further modifications of these terms are necessary.

It is, however, possible to adopt some more elaborate modelling in terms of the Reynolds stresses also for these terms, but in that case one must use the near-wall correct EARSM including near wall damping functions.

3.3. Wall boundary conditions. The physical wall boundary conditions on k and ω are

$$k = 0 , \frac{\partial k}{\partial y} = 0 \text{ and } \omega \to \frac{6\mu}{\beta \rho y^2} \tag{34}$$

where y is the wall distance in the wall-normal direction. In a cell centred FVM, the boundary condition should result in a correct wall flux. That is obtained by setting

$k_0 = -k_1$ for the convective fluxes and $k_0 = k_1$ for the viscous fluxes. Index $_0$ indicates the dummy cell value while index $_1$ indicates the first interior cell.

The boundary condition on ω is $\omega_0 = 2\omega_{\text{wall}} - \omega_1$ where the wall value is given by

$$\omega_{\text{wall}} = C_{\omega\text{-w}} \frac{6\mu}{\beta\rho y_{1/2}^2} \tag{35}$$

where $y_{1/2}$ is the wall normal distance to the first cell centre (for a cell centred scheme) and $C_{\omega\text{-w}}$ is a constant. Menter (1994) originally chosen that constant to 10 but later Hellsten (1998) suggested a value of 1.5 which minimizes the influence of the near-wall grid spacing. The approach of Hellsten was adopted here, thus $C_{\omega\text{-w}} = 1.5$.

3.4. General numerical discretization. The numerical treatment of standard two-equation turbulence models described by Eliasson (1999), concerning *e.g.* multigrid, positiveness, second order upwind scheme, was adopted also for the EARSM approach.

4. Shock - turbulence interaction

A shock may cause problems in computations using standard eddy-viscosity two-equation models. The problem is that the turbulence may grow at the shock and the growth increases typically with increasing grid density. This problem do not occur in the boundary layer and if EARSM is used. This phenomena is here analysed.

Let us consider a model problem, a one-dimensional moving shock. The shock velocity is V, the velocity jump over the shock ΔV and the shock thickness Δx. The thickness of the shock is in high Reynolds number flows a function of the numerical resolution of the shock.

Following the shock, the equation for the turbulent kinetic energy becomes, if the diffusion and dissipation are neglected

$$V\frac{\partial}{\partial x}(\rho K) = \mathcal{P} \tag{36}$$

and by integrating once

$$\Delta(\rho K) = \int \frac{\mathcal{P}}{V} dx \approx \mathcal{P}\frac{\Delta x}{V}. \tag{37}$$

We have here assumed that the production may be considered as constant over the shock.

The production is

$$\mathcal{P} = -\overline{\rho u_i u_j}\frac{\partial U_i}{\partial x_j} = -\rho K\left(a_{ij} + \frac{2}{3}\delta_{ij}\right)\frac{\partial U_i}{\partial x_j} = -\rho K\left(a_{11} + \frac{2}{3}\right)\frac{\partial U}{\partial x} \sim \rho K\frac{\Delta V}{\Delta x} \tag{38}$$

since the anisotropy is limited to around unity. The integrated K-equation then becomes

$$\Delta(\rho K) \sim \rho K \frac{\Delta V}{V}. \tag{39}$$

The turbulence growth over the shock is thus independent of the shock thickness, *i.e.* the resolution of the shock.

In an eddy-viscosity model the production is modelled as

$$\mathcal{P}^{(\mathrm{EVM})} = \left(2\mu_T S^*_{ij} - \frac{2}{3}\rho K \delta_{ij}\right)\frac{\partial U_i}{\partial x_j} \sim \mu_T \left(\frac{\Delta V}{\Delta x}\right)^2 \tag{40}$$

and the integrated K-equation becomes

$$\Delta(\rho K) \sim \mu_T \frac{(\Delta V)^2}{V \Delta x} \tag{41}$$

and the turbulence growth over the shock increases with decreasing shock thickness. For high Reynolds numbers, the turbulence may grow almost unbounded and thus generates unphysical high turbulence levels downstream of the shock. In fact also in subsonic flows, any small disturbance in the velocity field or grid may generate unphysical growth of free stream turbulence.

To avoid that effect in eddy-viscosity models the production may be limited. One often used form is to limit the production by the dissipation rate $\mathcal{P} < C\rho\varepsilon$ where C is some sufficiently high number. The problem with this form is that in rapidly growing turbulence the production rate is, and should be, independent of the dissipation rate. A more appropriate form is obtained by considering the relation (38)

$$|\mathcal{P}| = \left|-\rho K\left(a_{ij} + \frac{2}{3}\delta_{ij}\right)\frac{\partial U_i}{\partial x_j}\right| \le \rho K \left\|a_{ij}\right\| \left\|S^*_{ij}\right\| < \rho K \left\|S^*_{ij}\right\| = \rho K \sqrt{S^*_{ij} S^*_{ji}} \tag{42}$$

which could serve as an upper limit for $\mathcal{P}$. This limit is related to the realizability constraint that the norm of the anisotropy should be limited. The limit could also be expressed in terms of the eddy-viscosity production as

$$\mathcal{P}^{(\mathrm{lim})} = \rho K \sqrt{\frac{\mathcal{P}^{(\mathrm{EVM})}}{\mu_T}} \tag{43}$$

and the limited production is obtained by $\mathcal{P} = \min(\mathcal{P}^{(\mathrm{EVM})}, \mathcal{P}^{(\mathrm{lim})})$ which is easily implemented. $\mathcal{P}^{(\mathrm{EVM})} < \mathcal{P}^{(\mathrm{lim})}$ for $\mathcal{P}^{(\mathrm{EVM})} < \varepsilon/(C_\mu f_\mu)$ which implies that the limit would not be active for $\mathcal{P}/\varepsilon < 10$. The limitor should thus not interfere with the prediction capability of the model.

This problem does not occur for the proposed EARSM since the production is here not modelled using the eddy-viscosity hypothesis. Even the linear EARSM described previous does not have this deficiency. The reason for this is that the effective turbulent viscosity, or the effective C_μ, is a function of the strain rate such that $C_\mu \to 1/\sqrt{S^*_{ij} S^*_{ji}}$ for large strain rates.

5. Test cases

5.1. RAE2822: 2D transonic wing profile. The two-dimensional transonic wing profile RAE2822, case10 illustrates the behaviour of the proposed model. The wing is highly loaded and a boundary layer separation occurs at the shock impingement. Figure 1 shows the wall pressure and skin friction coefficients, C_p and C_f. Standard eddy-viscosity models, like the Wilcox (1988) standard $k-\omega$ model denoted 'std_kw', predict a shock position downstream of the observed one. The proposed EARSM approach clearly improves the shock position and the results are very much in line with differential Reynolds stress computations by Hellström *et al.* (1994). For this case there are no major difference in computational results between EARSM based on standard or low-Reynolds number $k-\omega$, 'WJ_skw' or 'WJ_kw'. The eddy-viscosity version 'LWJ_kw' gives, however, a shock position downstream of the EARSM's. Also the computational results using the Menter (1994) SST model, 'SST_kw', is shown in the figure. That model gives a somewhat better shock position. The best prediction of the shock position is, however, obtained with EARSM based on the Kok $k-\omega$ model. Figure 3 shows the velocity profiles at different x-positions.

There are still some deviations from the experimental data and there are other computations published on this case that have better agreements. The reason for this is that there exists a number of different geometries for this case, the measured or design geometry with or without an additional camber correction. For this case the measured geometry with the camber correction was used.

The $\mathrm{RMS}(\rho)$-residual convergence history is shown in figure 2. The eddy-viscosity $k-\omega$ model has the best convergence rate but the different EARSM's have similar convergence rates. The EARSM approach increases the computational time with less that 10% and the different computations were obtained by using the same numerical settings (CFL, multigrid levels, upwind discretization, et.c.). In flows without separation the convergence curves are even closer to each other.

5.2. LANN: 3D transonic wing. A further example for illustrating the model in three-dimensional flows is the transonic LANN-wing, measured by Horsten *et al.* (1983). Figure 4 shows the pressure coefficient distribution at different spanwise positions and figure 5 shows the surface pressure distribution as well as the computed skin friction lines. Also here the EARSM approach ('WJ_skw') improves the predicted shock position compared to the Wilcox (1988) standard $k-\omega$ model ('std_kw').

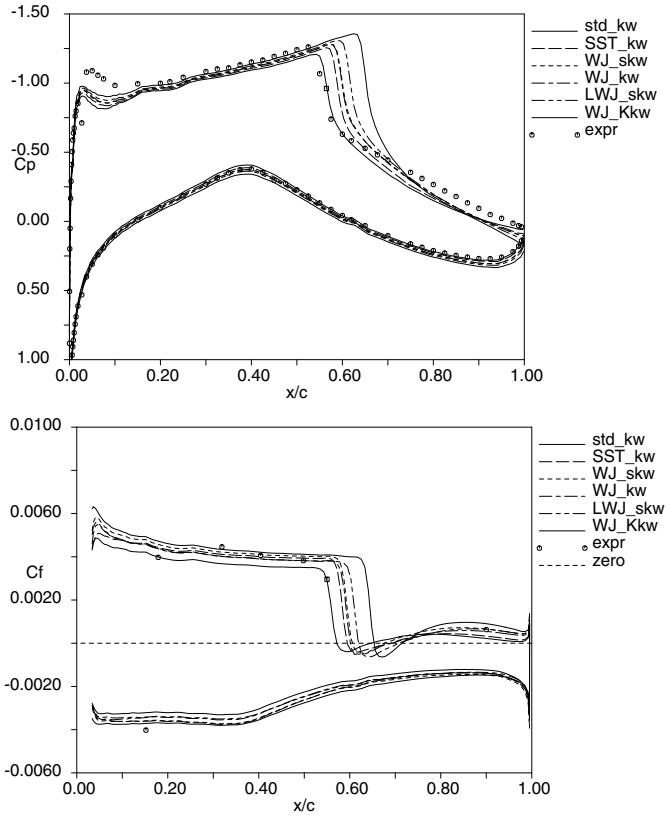

FIGURE 1: Predicted C_p and C_f distributions compared to measurements for the RAE2822 wing profile at $Ma = 0.754$, $\alpha = 2.57$ and $Re = 6.2 \cdot 10^6$ (Case 10). The standard eddy-viscosity $k-\omega$ model (std_kw) and Menter SST $k-\omega$ (SST_kw) compared to the EARSM based on standard $k-\omega$ (WJ_skw), EARSM based on low-Reynolds number $k-\omega$ (WJ_kw), EARSM based on Kok $k-\omega$ (WJ_Kkw marked with small squares) and the Linear EARSM based on standard $k-\omega$ (LWJ_kw). Experimental data from Cook *et al.* (1979).

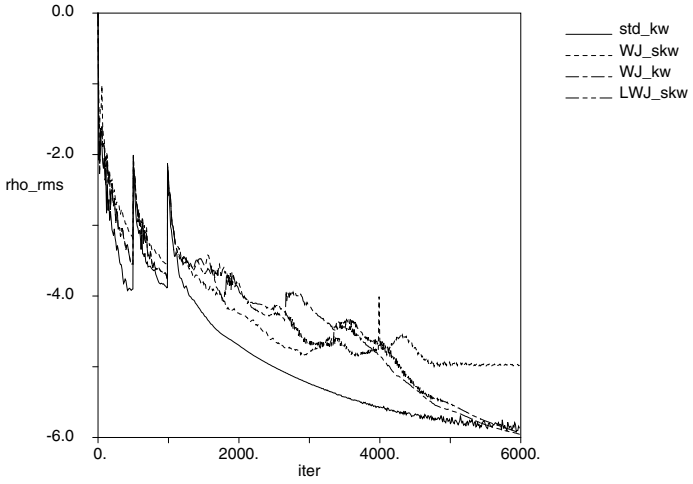

FIGURE 2: ρ -residual convergence history for the RAE2822 wing profile. The standard eddy-viscosity $k-\omega$ model (std_kw) compared to the EARSM based on standard $k-\omega$ (WJ_skw), EARSM based on low-Reynolds number $k-\omega$ (WJ_kw) and the Linear EARSM based on standard $k-\omega$ (LWJ_kw).

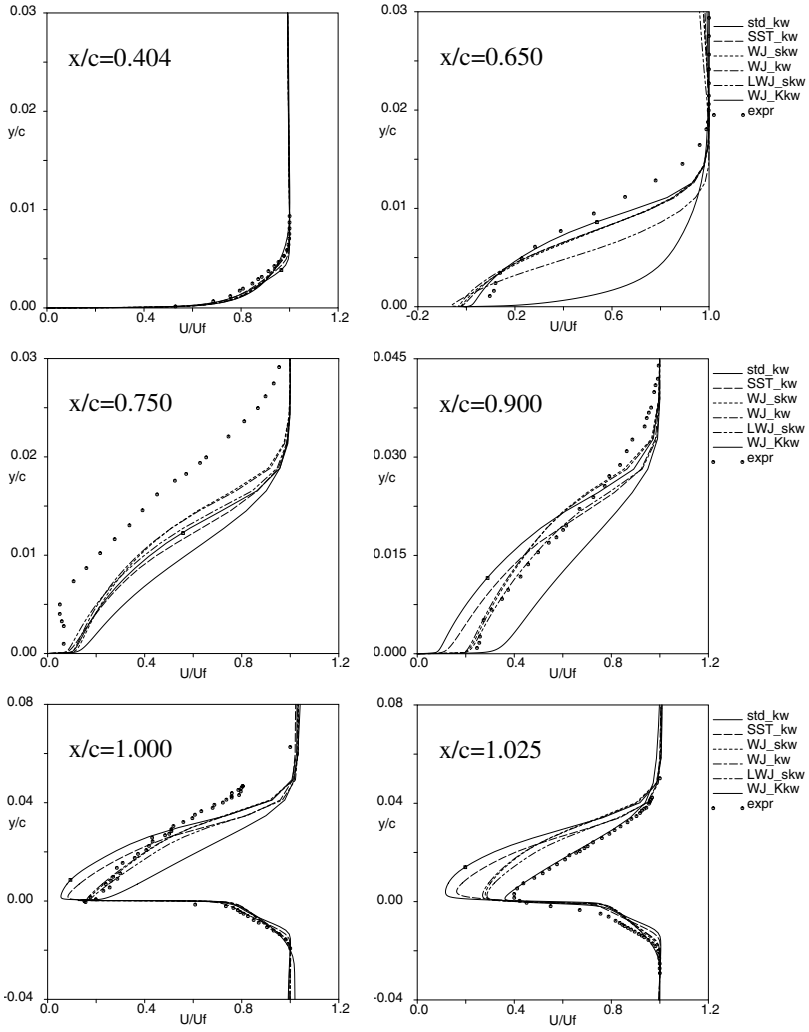

FIGURE 3: Predicted velocity profiles at different x-positions compared to measurements for the RAE2822 wing profile at $Ma = 0.754$, $\alpha = 2.57$ and $Re = 6.2 \cdot 10^6$ (Case 10). The standard eddy-viscosity $k-\omega$ model (std_kw) and Menter SST $k-\omega$ (SST_kw) compared to the EARSM based on standard $k-\omega$ (WJ_skw), EARSM based on low-Reynolds number $k-\omega$ (WJ_kw), EARSM based on Kok $k-\omega$ (WJ_Kkw marked with small squares) and the Linear EARSM based on standard $k-\omega$ (LWJ_kw). Experimental data from Cook *et al.* (1979).

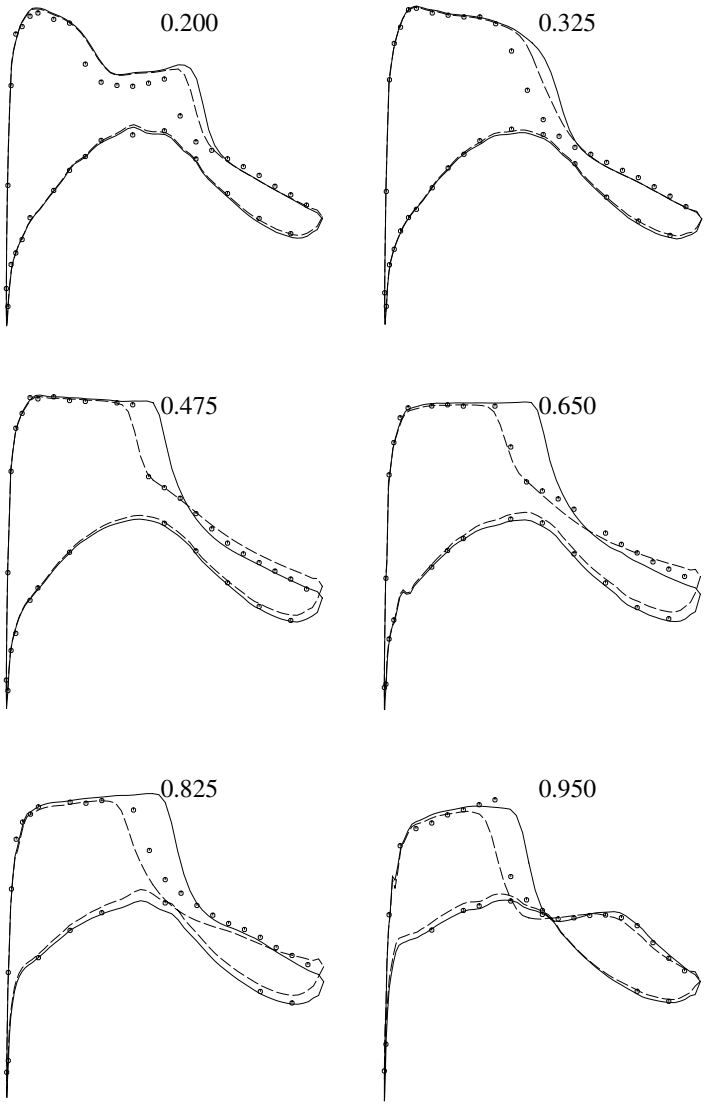

FIGURE 4: Predicted C_p distribution at different spanwise positions compared to measurements for the LANN wing at $Mach = 0.82$, $\alpha = 2.60$ and $Re = 7.16 \cdot 10^6$. The standard eddy-viscosity $k-\omega$ model (——) compared to the EARSM based on standard $k-\omega$ (- – -). Experimental data from Horsten *et al.* (1983).

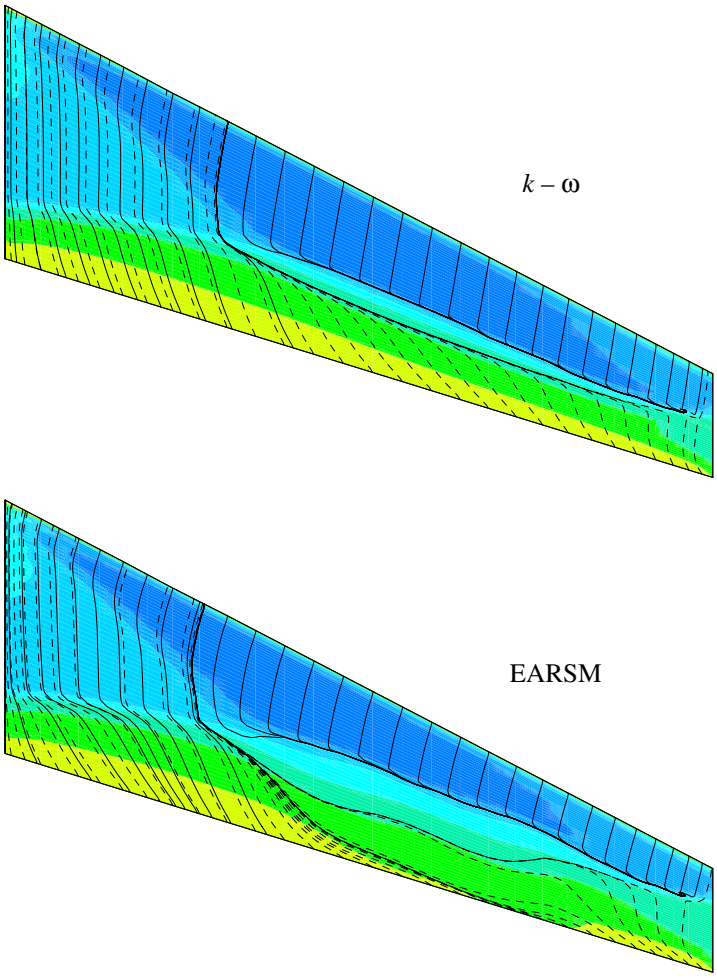

FIGURE 5: Predicted skin friction lines for the LANN wing at $Mach = 0.82$, $\alpha = 2.60$ and $Re = 7.16 \cdot 10^6$. The standard eddy-viscosity $k-\omega$ model (top) compared to the EARSM based on standard $k-\omega$ (bottom).

6. Concluding remarks

The EARSM approach was shown to improve the shock position over standard eddy-viscosity two-equation models, for highly loaded transonic wings, without significal increased computational cost. The EARSM without damping functions with the standard $k-\omega$ model as the platform is recommended for this kind of problems. The additional accuracy in the near-wall region, that the EARSM with damping functions provides, is probably not needed in the cases studied here.

The Kok $k-\omega$ model is an interesting alternative since the erroneously free-stream dependency in standard $k-\omega$ models have been removed. The EARSM based on that

model also shows the best predictions for the RAE2822 case. This combination (EARSM + Kok $k-\omega$) should, thus, be further investigated and tested, especially concerning the free-stream dependency.

The Menter SST model predicts the shock position well for the RAE2822 and could also be recommended for these kind of flow problems. This model is, however, an eddy-viscosity model with an empirical limitation on the turbulent viscosity and thus lacks the generality of the more fundamental EARSM. That is obvious in rotational dominated flows where the EARSM has the correct qualitative behaviour while eddy-viscosity models and in some cases also incomplete quadratic EARSMs fail, reported by Wallin & Johansson (1997).

Acknowledgment

This work has been carried out within the the AVTAC Project (Advanced Viscous Flow Simulation Tools for Complete Civil Transport Aircraft). AVTAC is a collaboration between British Aerospace, DASA, CASA, Dassault Aviation, SAAB, Alenia, DLR, ONERA, CIRA, FFA and NLR. The project is managed by British Aerospace and is funded by the CEC under the IMT initiative (Project Ref: BRPR CT97-0555)

References

[1] Cook, P.H., MacDonald, M.A. & Firmin, M.C.P. 1979 Aerofoil 2822 - Pressure distributions, boundary layer and wake measurements. *AGARD AR 138.*

[2] Durbin, P.A. 1993 Application of a near-wall turbulence model to boundary layers and heat transfer. *Int. J. Heat and Fluid Flow* 14, 316–323.

[3] Eliasson, P. 1999 A robust and positive scheme for viscous, compressible steady state solutions with two-equation turbulence models. *FFA TN 1999-81.*

[4] Gatski, T.B. & Speziale, C.G. 1993 On explicit algebraic stress models for complex turbulent flows. *J. Fluid Mech.* 254, 59–78.

[5] Girimaji, S.S. 1995 Fully-explicit and self-consistent algebraic Reynolds stress model. *ICASE Report No. 95-82*.

[6] Hellsten, A. 1998 On the solid-wall boundary condition of ω in the $k-\omega$-type turbulence models. *Helsinki University of Technology, Report No B-50, Series B.*

[7] Hellström, T., Davidson, L. & Rizzi A. 1994 Reynolds stress transport modelling of transonic flow around the RAE2822 airfoil. *AIAA 94-0309*. 32nd Aerospace Sciences Meeting, Reno, Jan. 1994.

[8] Horsten, J.J., Den Boer, R.G. & Zwaan, R.J. 1983 Unsteady transonic pressure measurements on a semi-span wind tunnel model of a transport-type supercritical wing (LANN model). *AFWAL-TR-83-3039.*

[9] Johansson, A.V. & Wallin, S. 1996 A new explicit algebraic Reynolds stress model. Proc. Sixth European Turbulence Conference, Lausanne, P. Monkewitz (ed). 31–34.

[10] Kok, J.C. 1999 Resolving the dependence on free-stream values for the $k-\omega$ turbulence model. Submitted to AIAA J.

[11] Launder, B.E. Reece, G.J. & Rodi, W. 1975 Progress in the development of a Reynolds-stress turbulence closure. *J. Fluid Mech.* 41, 537–566.
[12] Menter, F.R. 1994 Two-equation eddy-viscosity turbulence models for engineering applications. *AIAA J.* 32, 1598–1604.
[13] Pope, S.B. 1975, A more general effective-viscosity hypothesis. *J. Fluid Mech.* 72 331–340.
[14] Rodi, W. 1972 The prediction of free turbulent boundary layers by use of a two equation model of turbulence. *Ph.D. thesis, University of London.*
[15] Rodi, W. 1976 A new algebraic relation for calculating the Reynolds stresses. *Z. angew. Math. Mech*. 56, T219–221.
[16] Wallin, S & Johansson, A. V. 1996, A new explicit algebraic Reynolds stress turbulence model including an improved near-wall treatment. *Proc. Flow Modeling and Turbulence Measurements VI, Tallahassee, Chen, Shih, Lienau & Kung (eds).*
[17] Wallin, S. & Johansson, A.V. 1997 A complete explicit algebraic Reynolds stress model for incompressible and compressible turbulent flows. *FFA TN 1997-51* (submitted for publication). Also to appear in *J. Fluid Mech*, **403**, 89-132, (2000).
[18] Wilcox, D.C. 1988 Reassessment of the scale-determining equation for advanced turbulence models. *AIAA J.* 26, 1299–1310.
[19] Wilcox, D.C. 1994 Simulation of transition with a two-equation turbulence model. *AIAA J.* 32, 247–255.

Paper 7

7

A ROBUST AND POSITIVE SCHEME FOR VISCOUS, COMPRESSIBLE STEADY STATE SOLUTIONS WITH TWO-EQUATION TURBULENCE MODELS

Peter Eliasson and Stefan Wallin
The Aeronautical Research Institute of Sweden (FFA), Bromma, Sweden

Abstract. An efficient and robust method has been designed for the simulation of the compressible Navier-Stokes equations with two-equations turbulence models. The compressible Navier-Stokes equations are integrated explicitly to steady state and a novel approach is used to maintain the positivity of the turbulent quantities. The novel approach is based on a conservative estimate of the characteristics of the turbulent equations leading to a restriction of the local time step determined by the residual. As steady state is approached the residual and the restriction of the time step is reduced and hence the asymptotic rate of convergence is not affected. Multigrid is used to accelerate the convergence and a similar approach is used when adding the corrections to guarantee a positive scheme. A higher order restriction operator improves the robustness and the performance of the scheme. It is demonstrated that the higher order restriction can improve the rate of convergence, especially for 'bad' grids with large stretchings and locally large variations in grid size. Numerical results are presented for a model problem and on a RAE2822 airfoil.

1. Introduction

The design of efficient and robust numerical algorithms is essential for the simulation of compressible turbulent flows, especially for engineering-type applications. The main objective of this paper is to demonstrate new approaches to gain increased robustness in the iteration of an explicit Navier-Stokes solver coupled with a two-equation turbulence model and accelerated with a multigrid method.

It is well known that positivity of the discrete turbulent variables at any time during iteration is crucial. Unphysical negative values rapidly lead to instability and positivity must therefore be ensured. Various methods exist to achieve this. Ad hoc methods like enforcing the positivity by taking the absolute values of the turbulent quantities often prevents the convergence or cause divergence of the iterative process.

A more classical approach for avoiding the generation of spurious oscillations is to impose TVD-like conditions [10]. Explicit TVD schemes for transport equations have been considered by Harten [8] and implicit schemes by Yee *et al.* [16]. When transport equations for turbulent variables are present additional constraints need to be made to the source term. Jongen & Marx have developed TVD-like criteria for a general advection-diffusion equation with a source term. Both explicit and implicit time integration are considered. They consider separately the convective, viscous and source term of the equation and give a positivity criterion for the advection term that is a weaker require-

ment of a TVD criterion. The central viscous term can not increase the total variation. The negative part of the source term is treated implicitly and the positive part explicitly. A criterion is given on how the linearization of the negative terms must be chosen to maintain positivity. The criterion for the source term often restricts the local time step more than does the stability criterion. In addition, Jongen & Marx consider only the update of the variables in the time integration. They give no criteria of how to maintain positivity of the variables in a multigrid procedure where the variables are updated from prolongated coarse grid corrections.

In this paper an alternative, novel approach is suggested to guarantee positive turbulent variables. The approach is based on an estimate of the spectral radius of the complete turbulent equations and produces an underrelaxation of the local time step based on the residual. The underrelaxation is only active in those regions where the residual is large compared to the positive dependent variable and where the sign of the residual is such that the variable is decreased. The underrelaxation does not affect the asymptotic rate of convergence since the relaxation is only active initially when the solution is far from being converged. This results in a method that is not required to fulfil the TVD criterion for the convection, nor from the positivity requirements setup for the source term to have a positive solution in the iterative time stepping. The only requirement is that a stable time step is chosen.

An explicit Runge-Kutta finite-volume method is used to solve the compressible, Reynolds averaged Navier-Stokes equation. Local time steps are used based on a stability analysis of the convective and viscous terms. A point-implicit treatment of the turbulent source terms is chosen to guarantee stability in the iteration to steady state of the turbulence.

The convergence is further accelerated by using FAS multigrid. To ensure positive variables when the prolongated coarse grid corrections are added, a similar procedure as in the time stepping is introduced. An additional parameter is introduced to scale the underrelaxation, the size of this parameter is investigated numerically.

A higher order restriction operator is used which is basically the transpose of a linear prolongation operator. For some reason, to the authors knowledge this restriction operator has not been used before for CFD calculations. It is demonstrated in this paper that a higher order operator is as important as a higher order (linear) prolongation operator used on a common basis and that a lower order operator may prevent convergence. It is shown that especially when the grid is ‘bad’ with local large variations and when the grid is stretched with high cell aspect ratios the combination of the higher order transfer operators are beneficial.

Numerical results are presented for a model problem and for a 2D RAE2822 airfoil (case 10). The computations are all started from free stream, with or without multigrid. Although the novel approach is not restricted to a specific turbulence model, results are presented fro the k–ε equations only with the near wall treatment by Chien [2]. The focus will not be on the predicted results, only robustness and the rate of convergence are considered.

2. Construction of positive scheme

Finite-volume discretization schemes for a general transport equation are considered integrated to a steady state. The purpose is to investigate the stability and positivity requirements in the time integration. A positive discretization of the advection may be obtained by a TVD like criterion, see e.g. Jongen & Marx [10] where it also shown that the diffusion does not increase the total variation. A positivity requirement of the source term is also given leading to a restriction of the local time step. This requirement is usually more restrictive than the requirement for stability. Below an alternative approach is suggested in which the stability requirement only is required. The positivity is ensured by a an underrelaxation of the time step in the initial stage of the computation.

2.1. 1-D model problem. To investigate the positivity requirements a simple model problem is considered. A scalar, linear semi-discrete model problem with diffusion and a source term is investigated

$$\frac{dq_i}{dt} = R(q) = \frac{\nu}{\Delta x^2}(q_{i+1} - 2q_i + q_{i-1}) + aq_i \tag{1}$$

where q represents a positive, transported quantity (e.g. k or ε), ν represents a positive viscosity, Δx the step length and a is a constant multiplying the source term. The advection term is left out simply to reduce the complexity of the algebra.

$a > 0$ leads to an exponential growth without the presence of the diffusion. The source term may be positive locally in regions where there is a turbulent growth. Positive source terms do not restrict the local time step, they are integrated explicitly and will eventually be balanced by the negative source terms or the diffusion when the turbulence stops to grow. Positive source terms do no possess a threat to turn q negative since q is growing, therefore only negative source terms $a < 0$ are considered which may push q towards zero.

The diffusion term is integrated explicitly, as in the CFD calculation. Without the source term explicit Euler forward integration gives the following stability bound on the time step:

$$\frac{q_i^{n+1} - q_i^n}{\Delta t_v} = \frac{\nu}{\Delta x^2}(q_{i+1}^n - 2q_i^n + q_{i-1}^n) \Rightarrow \Delta t_v \le \frac{\Delta x^2}{2\nu} \tag{2}$$

which is easily verified by a von Neumann analysis. With the negative source term present and explicit integration leads to

$$\frac{q_i^{n+1} - q_i^n}{\Delta t} = \frac{\nu}{\Delta x^2}(q_{i+1}^n - 2q_i^n + q_{i-1}^n) + aq_i^n \Rightarrow \Delta t \le \frac{1}{\frac{2\nu}{\Delta x^2} - \frac{a}{2}} = \frac{\Delta t_v}{1 - \frac{a\Delta t_v}{2}} \tag{3}$$

for a stable time step provided Δt_v is chosen as its maximum. The source term restricts the time step by an additional term in the denominator. To guarantee positivity in the integration (3) the following constraint must be made to the time step:

$$Positivity\colon \Delta t \le \frac{1}{\frac{2\nu}{\Delta x^2} - a} = \frac{\Delta t_v}{1 - a\Delta t_v} \tag{4}$$

When the source term is dominating the positivity requirement restricts the time step by a factor of two.

Jongen & Marx [10] propose to treat negative source terms point implicitly leading to

$$\begin{gathered}\frac{q_i^{n+1} - q_i^n}{\Delta t} = \frac{\nu}{\Delta x^2}(q_{i+1}^n - 2q_i^n + q_{i-1}^n) + aq_i^{n+1} \Rightarrow \\ \left(\frac{1}{\Delta t} - a\right)(q_i^{n+1} - q_i^n) = \frac{q_i^{n+1} - q_i^n}{\Delta t^*} = \frac{\nu}{\Delta x^2}(q_{i+1}^n - 2q_i^n + q_{i-1}^n) + aq_i^n\end{gathered} \tag{5}$$

which increases the stability limit for the time step Δt:

$$\Delta t \le \frac{1}{\frac{2\nu}{\Delta x^2} + \frac{a}{2}} \tag{6}$$

However, the time step used in the time integration is the efficient time step $\Delta t^* = \Delta t/(1 - a\Delta t)$ which is restricted by the same stability and positivity criteria as the explicit scheme, (3) and (4). In either case of explicit or point implicit time integration, the time step has to be restricted due to the source term. In the case of this scalar, one-stage integration problem explicit and point-implicit time integration become identical.

It is not attractive to restrict the time step due to a positivity criterion more restrictive than the stability criterion since it will decrease the rate of convergence. Ideally, the positivity requirement should be used initially only when the residual is large and may cause the solution to turn negative. When the residual becomes smaller the stability limit should determine the size of the time step. Below such an approach is presented.

If the residual is assumed to be negative and large and the residual is dominated by the source term the model problem may be approximated as:

$$\frac{dq_i}{dt} = R(q) \approx aq_i \tag{7}$$

Hence the size of the source term may be estimated as

$$a \approx \frac{R(q)}{q} \tag{8}$$

According to the expression for the time step in the model problem (3) a positive time step Δt_p may be obtained as

$$\Delta t_p \leq \frac{\Delta t}{1 - \Delta t \; min\left(\frac{R(q)}{q}, 0\right)} \tag{9}$$

which ensures that the time step is determined by the stability requirement only as the residual becomes small compared to the solution. Δt is then determined from reasons of stability only, the additional term in the denominator in (9) guarantees positivity. For a point implicit approach, the time step may be determined from the explicit terms (advection and diffusion) which for the example above would lead to

$$\Delta t_p \leq \frac{\Delta t_v}{1 - \Delta t_v \; min\left(\frac{R(q)}{q}, \frac{a}{2}\right)} \tag{10}$$

where Δt_v is given in (2). Note that the time step is only reduced when the residual is negative, i.e. when the solution is decreasing. When it increases the time step is determined from stability reasons only and the expressions (9) and (10) are identical. Note that the expressions (9) and (10) are not identical for negative residuals. (9) is more restrictive for large negative residuals. The expressions (9) and (10) are chosen because of their similar appearance, other choices of time steps are possible that guarantees positivity.

The one-stage integration may be extended to *m*-stage Runge-Kutta schemes. E.g. the 2-stage point-implicit scheme:

$$\begin{aligned} q_i^1 &= q_i^n + \alpha_1 \Delta t \left\{ \frac{\nu}{\Delta x^2}(q_{i+1}^n - 2q_i^n + q_{i-1}^n) + a q_i^1 \right\} \\ q_i^{n+1} &= q_i^1 + \Delta t \left\{ \frac{\nu}{\Delta x^2}(q_{i+1}^1 - 2q_i^1 + q_{i-1}^1) + a q_i^{n+1} \right\} \end{aligned} \tag{11}$$

where α_1 is a Runge-Kutta coefficient. This scheme will, as the one-stage scheme, be integrated with the efficient time step $\Delta t^* = \Delta t/(1 - a\Delta t)$ and Δt^* will be subject to the same stability and positivity requirement as the corresponding explicit time integration with time step Δt. The stability requirement becomes for the explicit scheme:

$$\Delta t \leq \frac{1/\alpha_1}{\frac{4\nu}{\Delta x^2} - a} \tag{12}$$

The positivity requirement may be found for each stage in the scheme to be

$$Positivity\colon \Delta t \leq \frac{2}{\frac{4\nu}{\Delta x^2} - 2a} \tag{13}$$

provided $\alpha \leq 1$. For a dominating source term the positivity requirement is certainly more restrictive. For vanishing source terms ($a \to 0$) Shu [13] gives the necessary CFL-conditions for arbitrary *m*-stage Runge-Kutta to be TVD.

For a general *m*-stage Runge-Kutta scheme a *CFL* criterion the condition (9) may be written

$$\Delta t_p = \frac{\Delta t}{1 - \frac{\Delta t}{CFL_v} min\left(2\frac{R(q)}{q}, 0\right)} \tag{14}$$

for an explicit integration of the viscous and source term where Δt is a stable time step based on the spectral radius of the viscous and source term

$$\Delta t = \frac{CFL_v}{\frac{4\nu}{\Delta x^2} - a} \tag{15}$$

and where CFL_v is the absolute value of the intersection of the stability region with the negative real axis in the complex plane.

For a point implicit approach the equation (10) for a general *m*-stage Runge-Kutta scheme may be written

$$\Delta t_p = \frac{\Delta t_v}{1 - \frac{\Delta t_v}{CFL_v} min\left(2\frac{R(q)}{q}, a\right)} \tag{16}$$

where the time step is based on the spectral radius of the viscous term only:

$$\Delta t_v = \frac{CFL_v}{\frac{4\nu}{\Delta x^2}} \tag{17}$$

The equations (14) and (16) are valid for explicit and point implicit time integration respectively and guarantee a positive and stable time integration for an *m*-stage Runge-Kutta scheme applied to the model problem (1) provided the Runge-Kutta coefficients $0 \leq \alpha_{1 \leq i \leq m} \leq 1$.

2.2. The *k*-ε equations. The positive time steps for the model problem above may easily be extended to two-equation turbulence models As an example the *k*-ε equations are used, but any two-equation turbulence model may be used. The equations for the Chien *k*-ε is:

$$\frac{D}{Dt}\rho k = \nabla\cdot\left(\mu+\frac{\mu_T}{\sigma_k}\right)\nabla k + P - \rho\varepsilon - 2\frac{\mu k}{y^2}$$
$$\frac{D}{Dt}\rho\varepsilon = \nabla\cdot\left(\mu+\frac{\mu_T}{\sigma_\varepsilon}\right)\nabla\varepsilon + (C_{\varepsilon 1}P - C_{\varepsilon 2}f_2\rho\varepsilon)\frac{\varepsilon}{k} - 2\frac{\mu\varepsilon}{y^2}e^{-\frac{1}{2}y^+} \tag{18}$$

where

$$P = S^2\mu_T - \frac{2}{3}\rho k D,\ \mu_T = C_\mu f_\mu \rho\frac{k^2}{\varepsilon} \tag{19}$$

The negative source terms are treated point implicitly and must be accounted for so that a stable time step is obtained. The complete Jacobian of the negative source S^- terms may be used

$$S^- = \begin{pmatrix} -\rho\varepsilon - 2\dfrac{\mu k}{y^2} \\ (-C_{\varepsilon 2}f_2\rho\varepsilon)\dfrac{\varepsilon}{k} - 2\dfrac{\mu\varepsilon}{y^2}e^{-\frac{1}{2}y^+} \end{pmatrix},\ \frac{\partial}{\partial q}(S^-) = \begin{bmatrix} -\dfrac{2\mu}{\rho y^2} & -1 \\ C_{\varepsilon 2}f_2\dfrac{\varepsilon^2}{k^2} - 2C_{\varepsilon 2}f_2\dfrac{\varepsilon}{k} - 2\dfrac{\mu\varepsilon}{y^2}e^{-\frac{1}{2}y^+} & \end{bmatrix} \tag{20}$$

or an estimate of the spectral radius ρ^- of it may be used. In the computations presented in this paper ρ^- is used and approximated as

$$\rho^- = min\left(-2\frac{\varepsilon}{k} - 2\frac{\mu}{y^2\rho}, -1.5C_{\varepsilon 2}f_2\frac{\varepsilon}{k} - 2\frac{\mu}{y^2\rho}e^{-y^+/2}\right) \tag{21}$$

As will be shown using the spectral radius or the complete Jacobian has a small influence on the rate of convergence.

The time step used in the computations is

$$\Delta t^* = \frac{\Delta t}{1 - \dfrac{\Delta t}{CFL}\ min\left(2\dfrac{R(\rho k)}{\rho k}, 2\dfrac{R(\rho\varepsilon)}{\rho\varepsilon}, \rho^-\right)} \tag{22}$$

where Δt is determined from a stability analysis of the convective and diffusive terms of the mean flow [14]. Hence Δt is used to update the mean flow, Δt^* is used for the turbulence. A common time step instead of two separate time steps was chosen for the two turbulent equations since they are closely coupled.

3. Multigrid

To accelerate the convergence of the explicit Runge-Kutta time integration with local time steps, FAS multigrid is used. The multigrid is applied to both the mean flow as well as to the turbulence. Below the positive update in the time integration is extended

to the update of the corrections in multigrid. A higher order restriction operator is also presented.

3.1. Positivity. The dependent variables are updated in the Runge-Kutta time integration but also in the multigrid procedure where a prolongated correction is added to the variables, see e.g. Hackbush [7]. Positivity of the turbulence is then not only of concern in the time integration but also when the multigrid corrections are added.

The corrections are added as:

$$q^{n+1} = q^n + \Delta q \tag{23}$$

where Δq is the correction. There is nothing in the update of the corrections (23) that prevents the turbulent variables to turn negative.

By considering the corrections as residuals the approach from the time integration may be extended. The following modified expression for adding the corrections ensures positivity:

$$q^{n+1} = q^n + \frac{\Delta q}{1 - \beta min\left(\frac{\Delta q}{q^n}, 0\right)} \tag{24}$$

Note that the correction is only reduced when it is negative and that the reduction becomes small as soon as the correction becomes small compared to the solution. An additional parameter $\beta > 1$ has been introduced to keep the turbulence sufficiently far away from zero. In the computations presented below it will be shown that the value of β has very small influence on the rate of convergence provided it is chosen big enough to prevent initial divergence and blow up. β should for most cases be chosen $\beta \geq 10$ for reasons of robustness, in the computations $\beta = 100$ is usually used.

For the k-ε equations the following expression is used:

$$q^{n+1} = q^n + \frac{\Delta q}{1 - \beta min\left(\frac{\Delta k}{k^n}, \frac{\Delta \varepsilon}{\varepsilon^n}, 0\right)} \tag{25}$$

where q is either k or ε and Δq the correction Δk or $\Delta \varepsilon$ respectively. Note that k and ε are equally restricted not to destroy their close coupling.

3.2. A higher order restriction operator. In multigrid the residuals of a fine grid is restricted to coarser grids to form a forcing function on the right hand side [7]. A semi-discrete equation discretized by a finite-volume method is denoted

$$V_l \frac{dq_l}{dt} = R(q_l) + d_l \tag{26}$$

where V_l is the volume of a cell and where subscript $l \geq 1$ denotes the grid level, $l = 1$ being the finest. d_l is the forcing function restricted from finer levels, $d_1 = 0$. For more details see e.g. Rizzi *et al.* [14].

A restriction operator commonly used is the transpose of the simplest prolongation operator, the injection. These restriction and prolongation operators are illustrated in Figure 1 in two space dimensions. Note that the restriction is for the residuals only, to restrict the unknowns a factor of 1/4 multiply fine grid unknowns. This is a result of the finite-volume discretization.

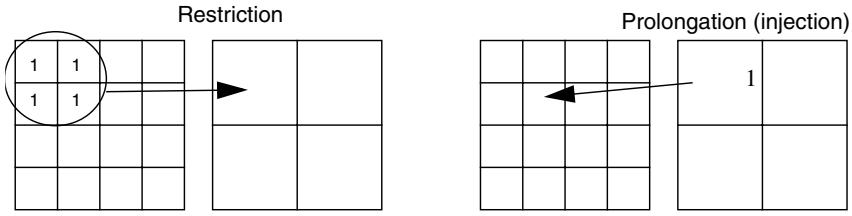

FIGURE 1: Prolongation operator of lowest order (injection) in two dimensions, restriction as its transpose.

The injection prolongation is usually not accurate enough so a linear prolongation operator may be used instead. The linear prolongation may be used to form a higher order restriction by taking the transpose of the prolongation, Figure 2.

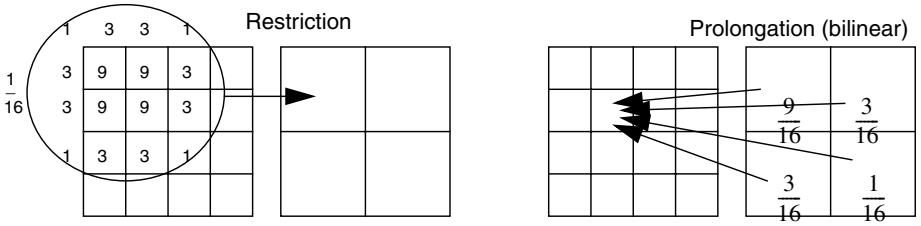

FIGURE 2: Linear prolongation in two dimensions and restriction as its transpose.

The higher order restriction needs values outside the boundaries, it needs boundary conditions on the residual. At solid walls the boundary condition

$$R_0 = -R_1 \tag{27}$$

is used for all residuals. At external boundaries the same boundary condition is used although the boundary condition on these boundaries have negligible impact on the rate of convergence. For more details about the multigrid operators as well as analysis for model problem, see Eliasson [3] and Eliasson *et al.* [4].

Note that the higher order restriction should not be used for the variables. Although it should be possible to apply any consistent operator in theory, in practice the large var-

iations and non-linearities of the turbulent variables often cause problem for this wider operator and hence the lower order, compact operator is used for the variables.

The extension of the operators to three space dimensions is obtained from the transpose of the tri-linear prolongation operator. The coarse grid cell centre forcing function $F_{i,j,k}$ may in three dimensions be obtained as

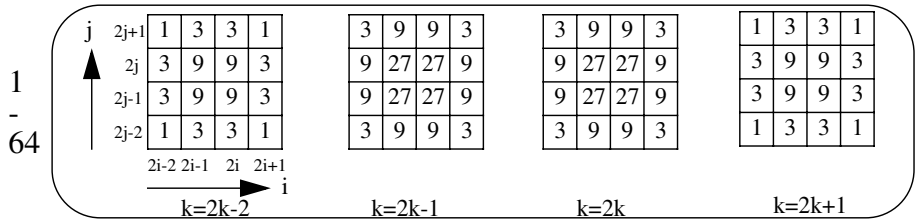

FIGURE 3: Higher order restriction operator in three dimensions. Coarse grid cell centre forcing function $F_{i,j,k}$ as a result.

It will be demonstrated that in some cases the lower order operators prevent convergence.

4. Solution technique

4.1. Time integration. The equations are integrated to steady state using an explicit 5-stage Runge-Kutta scheme with point-implicit treatment of the turbulent negative source terms described above. The Runge-Kutta coefficients are:

$$\alpha_1 = 0.0814,\ \alpha_2 = 0.1906,\ \alpha_3 = 0.342,\ \alpha_4 = 0.574,\ \alpha_5 = 1 \tag{28}$$

The viscous terms and the source terms are calculated in the first stage only. This scheme provides optimum damping for both central and upwind schemes [3], the CFL number in the computations is CFL=1.5.

4.2. Spatial discretization. The mean flow convective terms as well as the turbulent convective terms are discretized using a second order accurate symmetric TVD scheme [11]. Second order accuracy is obtained by using a van Leer limiter for the mean flow applied to the characteristics and a minmod limiter for the turbulence.

An entropy fix is used to prevent unphysical solution, the eigenvalues of the mean flow and turbulence are not allowed to be less than 5% of the spectral radius $|\bar{u}| + c$.

4.3. Coarse grid simplification. On coarser grids the mean flow and the turbulent convective terms are reduced to first order accuracy. The entropy fix is increased to 20% and the turbulent production is set to zero, i.e. it is assumed to be constant from the fine grid.

5. Numerical Results

5.1. Model equation. To investigate the time discretization and the different time step restrictions a model equation is used [15]. The model problem varies in time only and is basically the k-ε equations without convection and near-wall damping:

$$\frac{dq}{dt} = R(q) = V(q) + S(q) = -\alpha \begin{bmatrix} k-1 \\ \varepsilon - 1 \end{bmatrix} + \begin{bmatrix} P_k - \varepsilon \\ (C_{\varepsilon 1} P_k - C_{\varepsilon 2}\varepsilon)\dfrac{\varepsilon}{k} \end{bmatrix} \tag{29}$$

where $q = [k, \varepsilon]^T$ and $V(q)$ represents schematically the viscous terms where α is positive and related to $\mu/\Delta x^2$. $S(q)$ is the source term, $P_k = C_m k^2/\varepsilon$ is the turbulent production and $C_{\varepsilon 1} = 1.45$, $C_{\varepsilon 2} = 1.9$.

The spectral radius to the negative terms of $S(q)$ may be found from the Jacobian

$$J(q) = \frac{\partial S^-}{\partial q} = \frac{\partial}{\partial q} \begin{bmatrix} -\varepsilon \\ -C_{\varepsilon 2}\dfrac{\varepsilon^2}{k} \end{bmatrix} = \begin{bmatrix} 0 & -1 \\ C_{\varepsilon 2}\dfrac{\varepsilon^2}{k^2} & -2C_{\varepsilon 2}\dfrac{\varepsilon}{k} \end{bmatrix} \tag{30}$$

to be

$$\rho^- = -(C_{\varepsilon 2} + \sqrt{C_{\varepsilon 2}(C_{\varepsilon 2} - 1)})\frac{\varepsilon}{k} \tag{31}$$

One stage explicit Euler time integration is made with three different limitations to the time step. In the first approach a strictly positive time step is chosen according to Equation (13):

$$\Delta t = \frac{CFL_v}{\alpha - 2\rho^-} \tag{32}$$

The second time step used is a time step based on stability requirements only

$$\Delta t = \frac{CFL_v}{\alpha - \rho^-} \tag{33}$$

and may therefore initially turn k or ε negative. An 'ad hoc' approach is then used by setting the negative value to 1% of the initial value.

In the third approach the new way of restricting the time step is used in accordance with Equation (14)

$$\Delta t = \frac{CFL_v}{\alpha - \rho^- - min(R(k)/k, R(\varepsilon)/\varepsilon, 0)} \tag{34}$$

or, equivalently, with the notation in Equation (14)

$$\Delta t_p = \frac{\Delta t}{1 - \frac{\Delta t}{CFL_v} min(R(k)/k, R(\varepsilon)/\varepsilon, 0)} \tag{35}$$

where Δt is defined in equation (33).

In Figure 4 and Figure 5 two computations with different values of the parameters are visualized. The results are compared against an exact solution in time. Since a steady state problem is used the focus is the number of iterations required to reach the asymptotic steady state values. The computed results are therefore plotted using the same time step although different time steps (32)-(34) were used in the computations. As can be seen, for both cases the new proposed time integration reaches the asymptotic value fastest.

Other ‘ad hoc’ resetting of negative values can result in both worse and better behaviour than demonstrated below. The example demonstrates the danger with that procedure and the increased robustness with the new proposed time step.

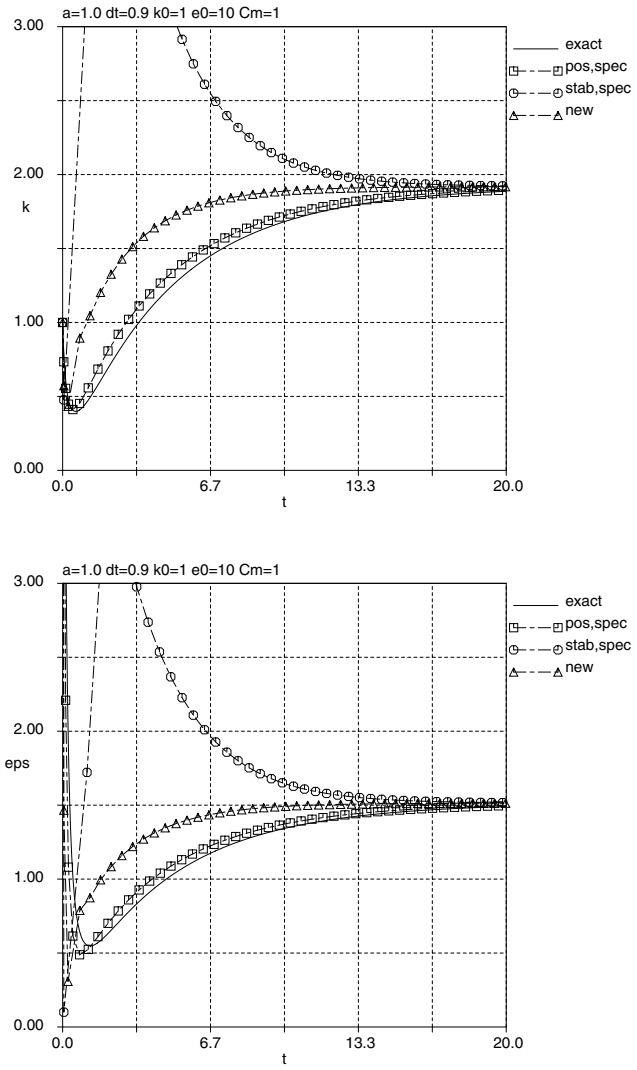

FIGURE 4: Model example with $k_0 = 1$, $\varepsilon_0 = 10$, $\alpha = 1$. Time evolution of k (top) and ε (bottom). ___ exact solution, □ positive time step, O stable time step with ‘ad hoc’ resetting, Δ new proposed time step.

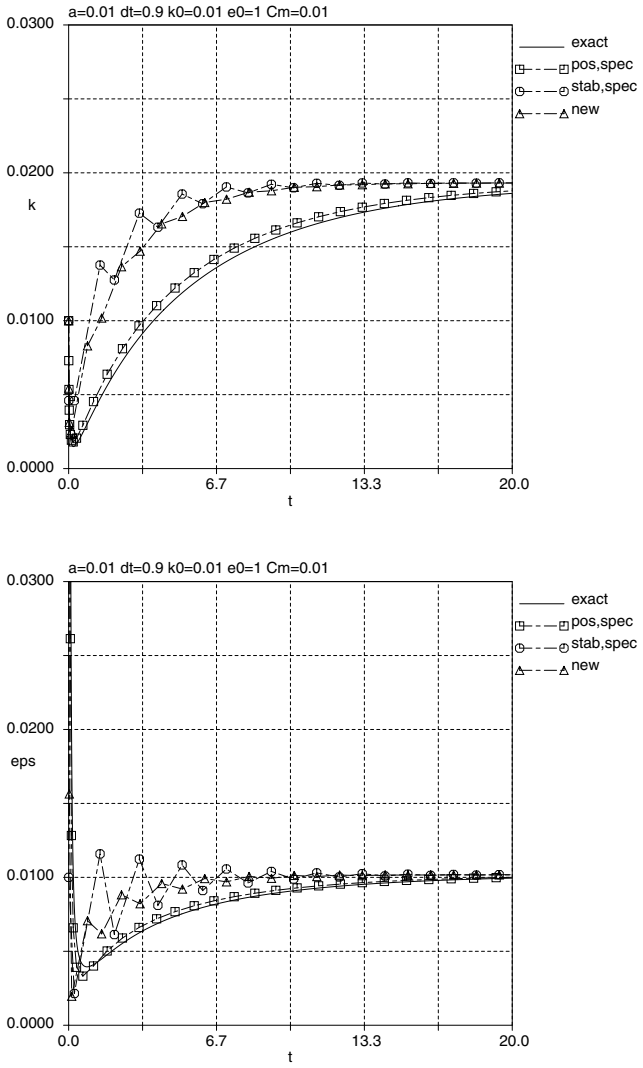

FIGURE 5: Model example with $k_0 = 0.01$, $\varepsilon_0 = 10$, $\alpha = 0.01$. Time evolution of k (top) and ε (bottom). ___ exact solution, □ positive time step, O stable time step with 'ad hoc' resetting, Δ new proposed time step.

5.2. RAE2822 airfoil, Case10. A demanding test case is the transonic flow over a RAE2822 airfoil. This case has been subject for several earlier investigations in Euroval [5] and ECARP [6], the particular case investigated here is denoted *Case 10* and involves shock boundary layer separation. In this paper only aspects concerning robustness and rate of convergence are considered although the case is very interesting concerning the prediction of shock location, leading edge suction peak, skin friction etc.

The flow conditions are

$$M = 0.754, \alpha = 2.57°, Re = 6.2\times10^{6}. \quad (36)$$

The trailing edge of the airfoil is sharp and hence a C-type of grid was used with a size of 257×65 nodes, 65 nodes from the wall to the outer boundary located about 10 chords away. A close up of the grid can be seen Figure 6. The distance to the second layer of nodes from the wall varies from 0.3×10^{-5} at the leading edge to 1×10^{-5} at the trailing edge. Transition is specified at 3% of the chord on both upper and lower side.

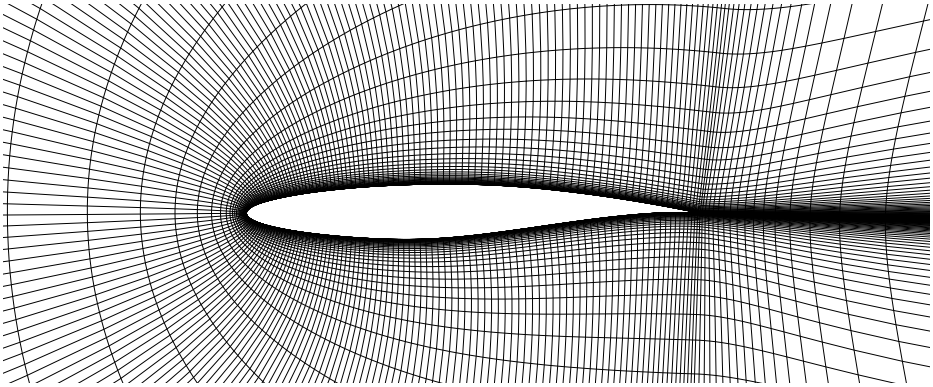

FIGURE 6: C-type of grid around the RAE2822 airfoil used in the calculation with 257×65 nodes.

Unless otherwise stated 3 levels of multigrid with V-cycles is used in the computations as well as a higher order prolongation operator, higher order restriction operator, the restriction damping factor $\beta = 100$ from Equation (25), everything initialized to free stream values and a CFL number of $CFL = 1.5$. No smoothing of the multigrid corrections is applied. The rate of convergence is presented for the density and turbulent kinetic energy residuals.

Without the new proposed time step (22) and correction relaxation (25) the computations starting from free stream values diverge immediately. The option to the new approach would be to drastically reduce the CFL number initially, finding a better initial solution, leave out multigrid initially etc. All of these option imply additional time and cost to find a converged solution which makes the proposed improvements superior. It is difficult though, to quantify the benefits from it since the options involve different procedures in getting a solution.

The rate of converge using 1-4 multigrid levels can be seen in Figure 7.

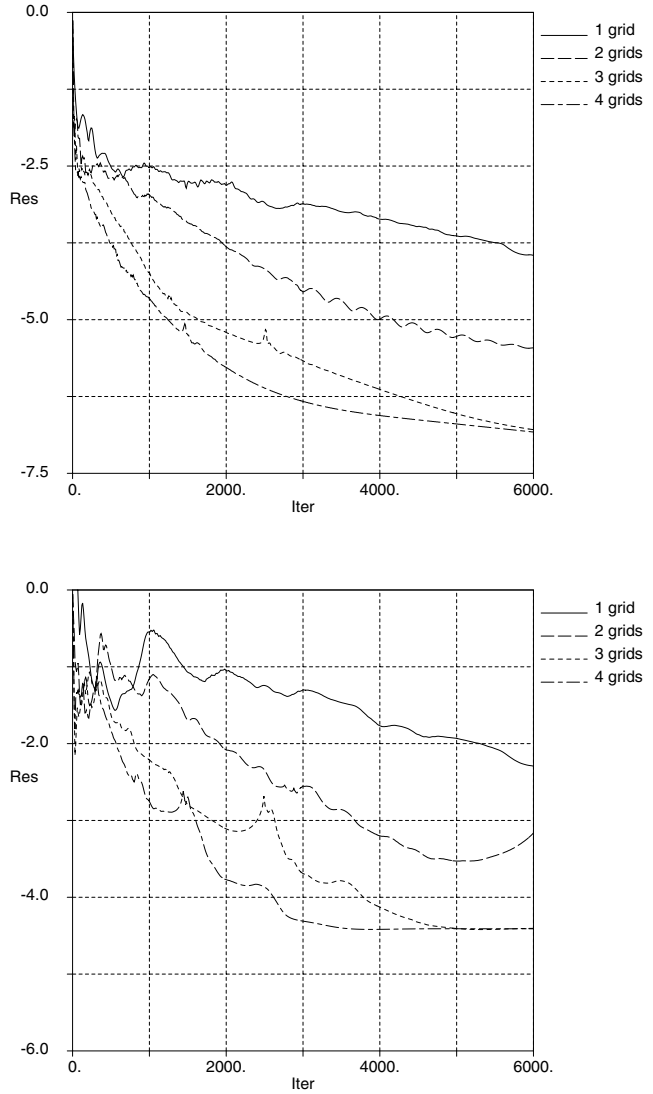

FIGURE 7: Rate of convergence using 1-4 multigrid levels. Top: density residual, bottom: k residual.

As can be seen the speed up is considerable. The residual of the turbulent kinetic energy drops to a constant level from which there is no further decrease.

The ambition has not been to obtain the best possible convergence but to study delta effects on the rate of convergence. The rate of convergence can be further improved by optimizing CFL numbers, using residual smoothing, increasing numerical diffusion etc.

Although the density residual is reduced more than 7 orders of magnitude it is not required for engineering accuracy, e.g. the integrated forces converge to its steady state values within 0.1% in about 1500 iterations using 4 grid levels, see Figure 8

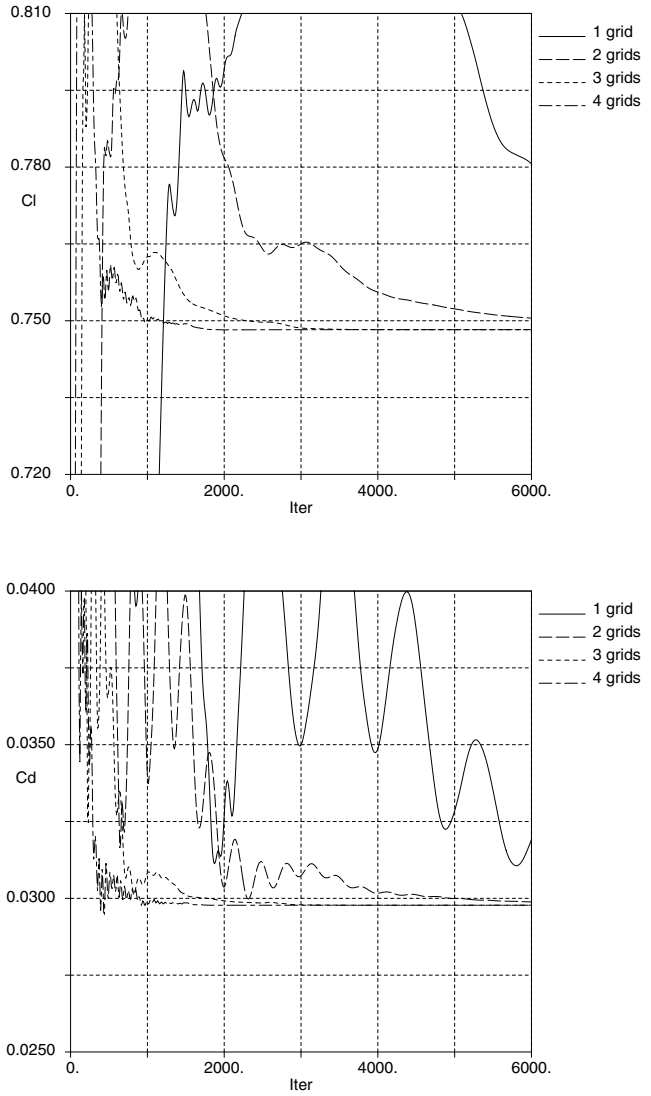

FIGURE 8: Rate of convergence using 1-4 multigrid levels. Top: lift coefficient Cl, bottom: drag coefficient, Cd

The choice of the parameter β in the update of the multigrid corrections in Equation (25) is investigated in Figure 9 using 4 grid levels. The rate of convergence is practi-

cally unchanged for different β provided β is chosen large enough. Divergence is obtained for $\beta = 2$ which is obviously a too low value for this case.

In Figure 10 different restriction operators are used. With a lower order restriction operator the residuals show a somewhat oscillatory behaviour using 3 grid levels although convergence is obtained. With 4 grid levels there is no longer convergence using 4 grid levels.

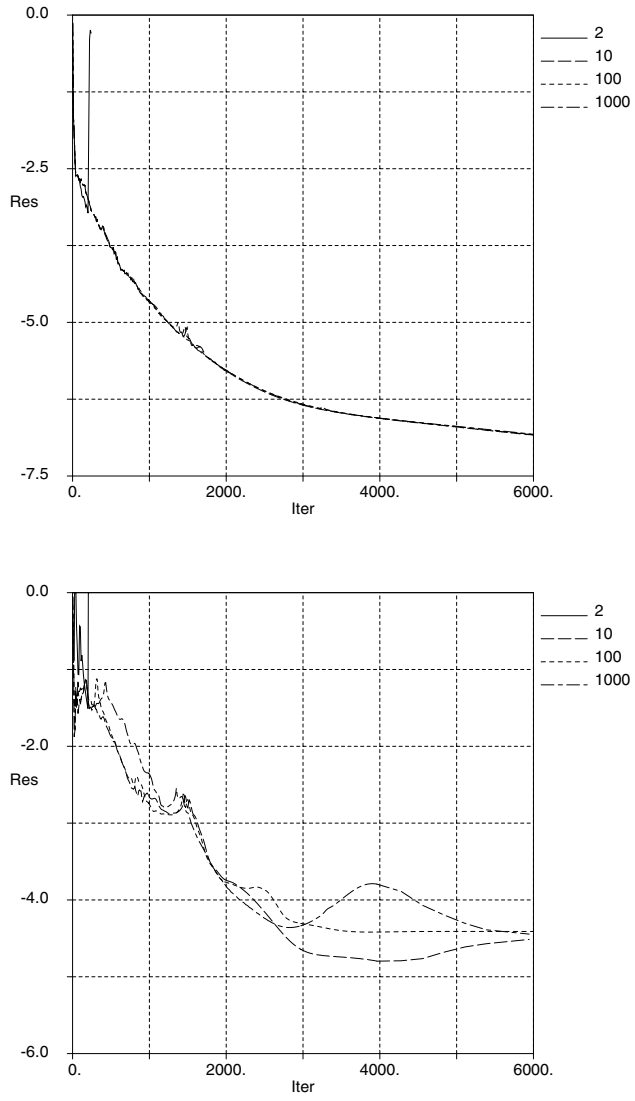

FIGURE 9: Rate of convergence using 4 grids and variation of $\beta = 2, 10, 100, 1000$. Top: density residual, bottom: k residual.

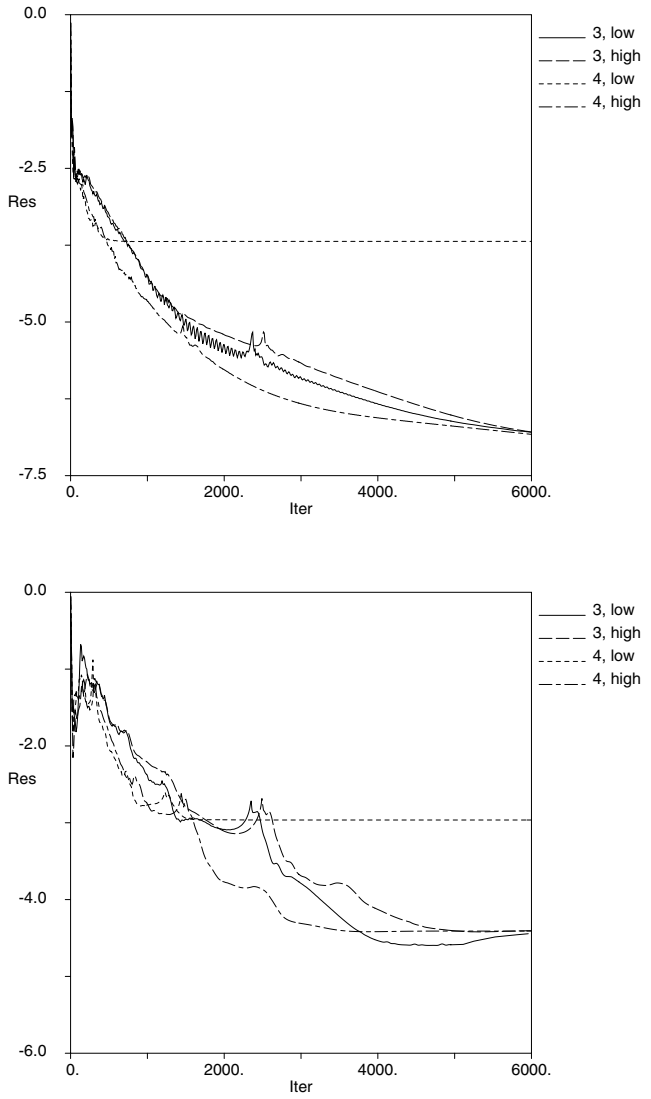

FIGURE 10: Rate of convergence using 3 and 4 multigrid levels with lower and higher order restriction. Top: density residual, bottom: k residual.

The influence of using the full Jacobian in the determination for the local time step instead of the spectral radius can be seen in Figure 11. The difference is very small which justifies the use of the scalar spectral radius.

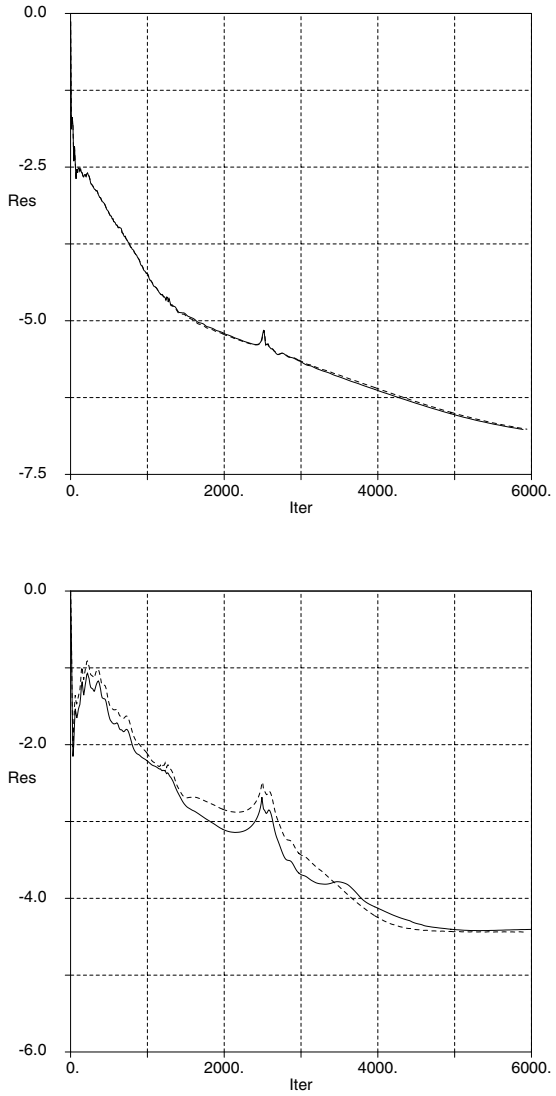

FIGURE 11: Rate of convergence with 3 multigrid levels using spectral radius (straight line) and full Jacobian (dashed line). Top: density residual, bottom: k residual.

In general multigrid is often less robust applied to the turbulent equations due to their stiffness. In many industrial codes multigrid is therefore only applied to the mean

flow equations. In Figure 12 the difference between using multigrid and single grid for the turbulence is plotted. As can be seen the rate of convergence for the density is not affected much whereas the kinetic turbulent kinetic energy converges much slower. This also indicates that the evolution of the mean flow and the turbulence is fairly decoupled.

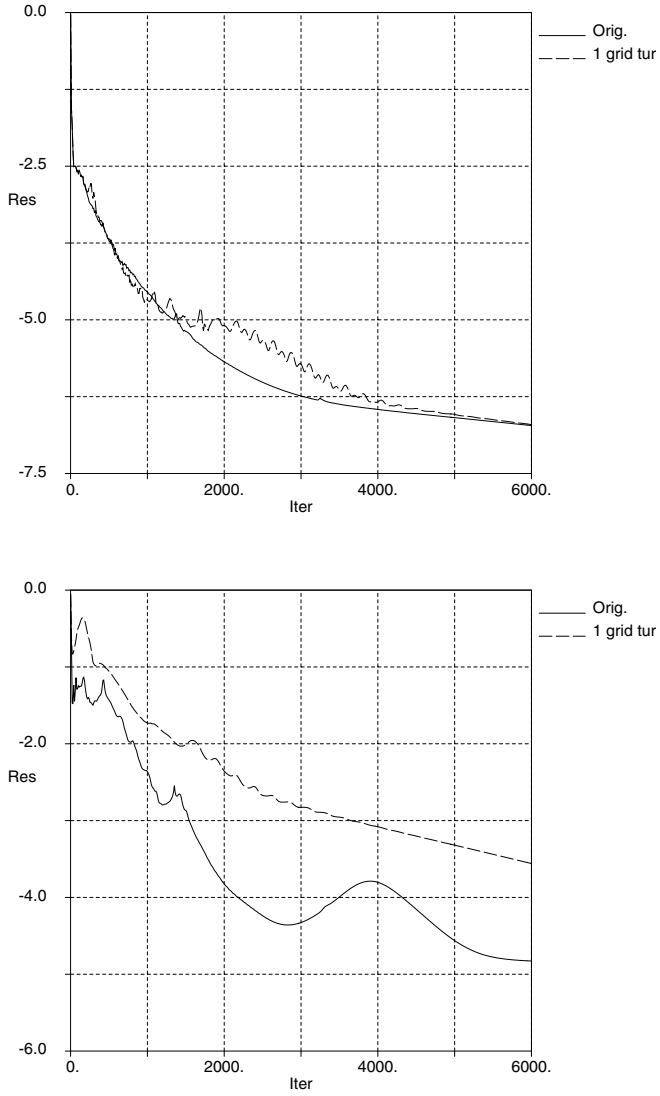

FIGURE 12: Rate of convergence with 4 multigrid levels. Comparison with multigrid applied to all equations (solid line) and multigrid applied only to the mean flow equations (dashed line). $\beta = 1000$. Top: density residual, bottom: k residual.

5.3. Multigrid applied to 'bad grids'. In practical application for complex geometry in three dimensions it not possible to avoid 'bad grids' with large stretchings, grid singularity, high cell skewness etc. These distortions often lead to a degradation in the quality of the solution and in the rate of convergence. In this section the influence of different multigrid transfer operators on grids with large and sudden stretchings to the rate of convergence is carried out.

To simulate a complex 3D grid with large and sudden stretchings, a less complex problem was chosen. Every third point has been removed in the 2D grid of the RAE2822 original grid of 257×65 points. Points are removed in the I-direction, in the J-direction and in both directions. The grids can be seen in Figure 13. The grid sizes and the sizes of the coarser grids in multigrid can be seen in Table 1. Note that for the grid with points removed in both directions only 3 multigrid levels are possible and hence used. Also note that removing points in one directions implies that the grid is made coarser in only one direction between grid levels 3 and 4.

The flow conditions and the numerical conditions are the same as in the previous Section 5.2 .

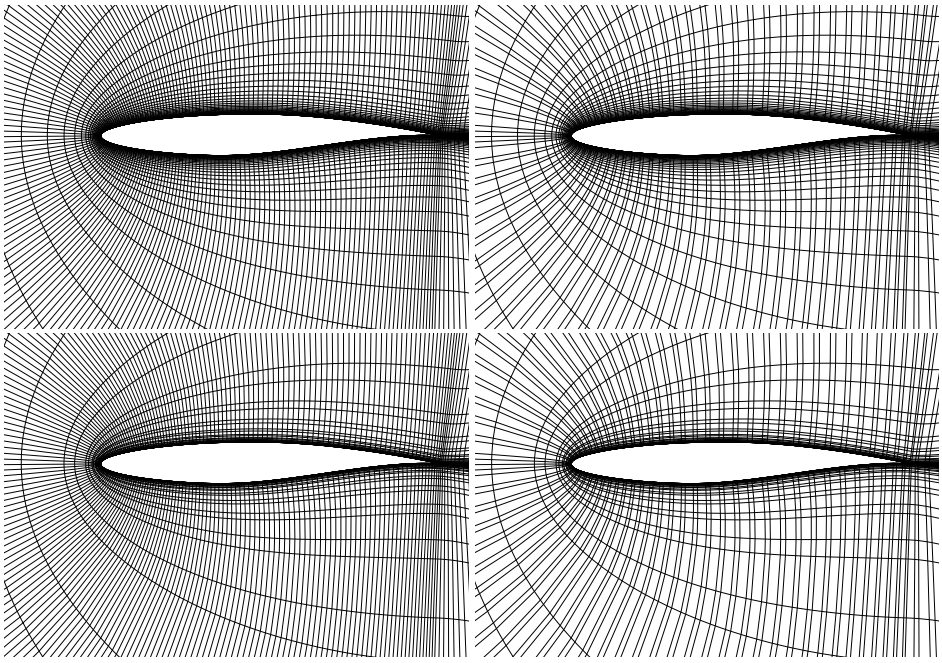

FIGURE 13: .Upper left: original grid. Upper right: grid with every third point removed in I. Lower left: grid with every third point removed in J. Lower right: grid with every third point removed in I and J.

TABLE 1: Size of the original grids and the grids with every third point removed. Sizes of the coarser grids used in multigrid are displayed as well (Grid 2). J is the direction normal to the airfoil to the outer boundary

Original		Removal in I		Removal in J		Removal in I,J	
Grid	Size	Grid	Size	Grid	Size	Grid	Size
1	257×65	1	173×65	1	257×45	1	173×45
2	129×33	2	87×33	2	129×23	2	87×23
3	65×17	3	44×17	3	65×12	3	44×12
4	33×9	4	44×9	4	33×12		

The rate of convergence using the lower and higher order multigrid operators in Figure 1 and Figure 2 for the four grids in Figure 13 can be seen in Figure 14- Figure 17.

It is evident that the combination of higher order prolongation and restriction operators give the best convergence as well as convergence curves with least oscillations. Lower order restriction or prolongation may prevent convergence in some cases. The benefit from the higher order operators is most evident when removing points in the I-direction and hence increasing the local cell aspect ratio. The combination of lower order restriction and prolongation operators give divergence and can usually not be used for problems with more than two multigrid levels.

Finally the rate of converge is plotted in Figure 18 using three multigrid levels for the four different grids with the higher order restriction and prolongation operators. The rate of convergence is improved when removing points normal to the wall (J) which reduces the cell aspect ratio. By removing in the I-direction the convergence becomes slower with higher cell aspect ratios. This is typical for explicit methods.

6. Summary and conclusions

A new way of keeping the turbulent dependent variables positive in the time integration is proposed and evaluated. The local time step in the steady state time integration is restricted by the local residual in such a way that the solution cannot turn negative. The restriction is only initial and the asymptotic rate of convergence is not effected. A similar procedure is used in the update of the variables from the multigrid corrections. The benefits of the proposed method is demonstrated on a model example and on the RAE2822 airfoil at transonic speed.

A higher order restriction operator is demonstrated to give improved rate of convergence in some cases. Especially when the grid has large local variations and the cell

aspect ratio is high it is shown that only with the combination of linear prolongation and higher order restriction convergence is obtained.

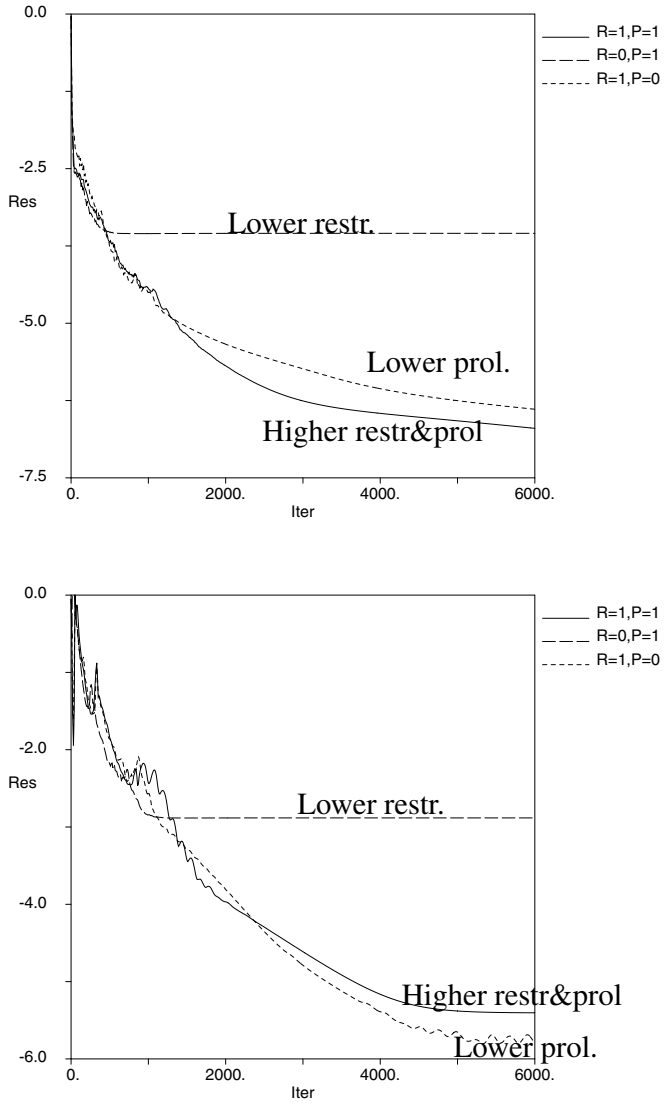

FIGURE 14: Rate of convergence, original grid with 4 multigrid levels. Top: density residual, bottom: k residual.

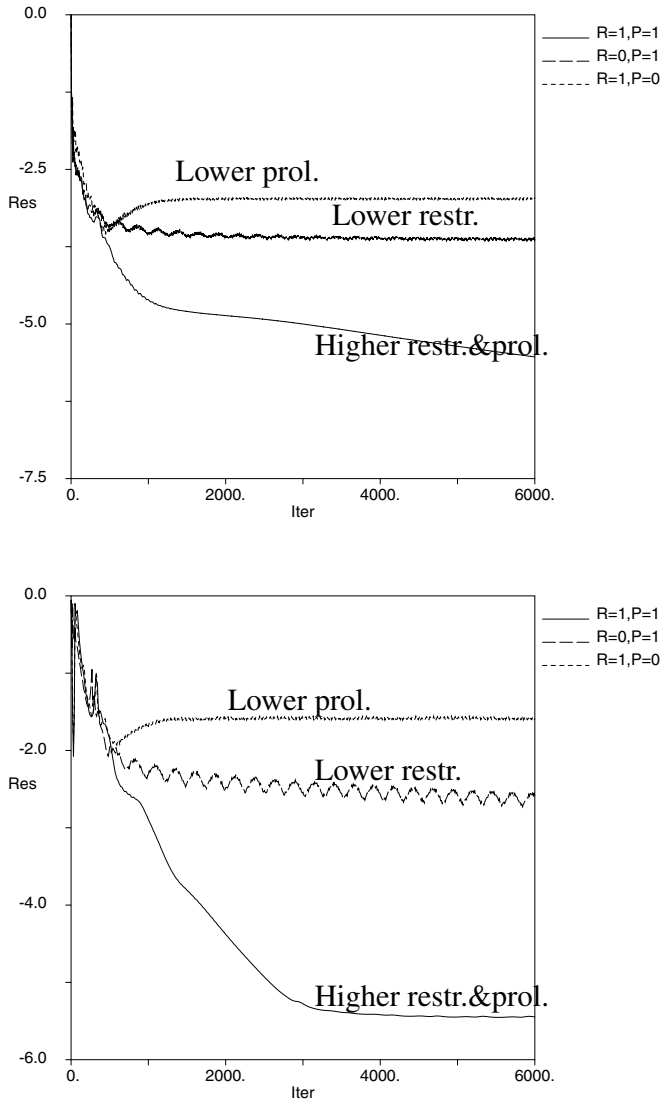

FIGURE 15: Rate of convergence with points removed in I and 4 multigrid levels. Top: density residual, bottom: k residual.

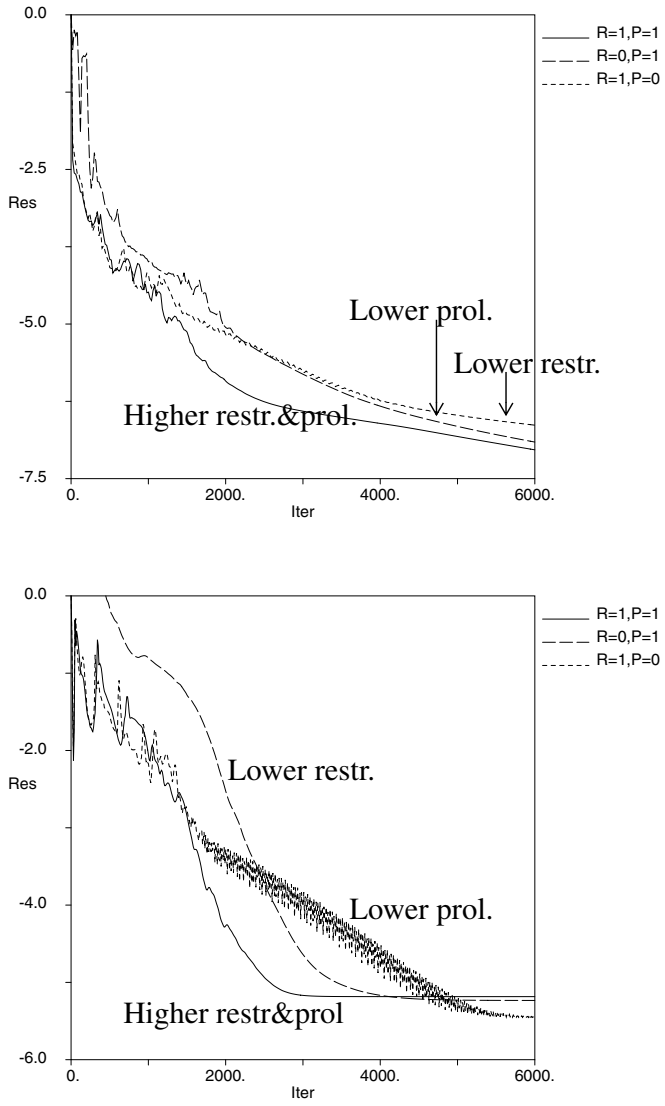

FIGURE 16: Rate of convergence with points removed in J, 4 multigrid levels.
Top: density residual, bottom: k residual.

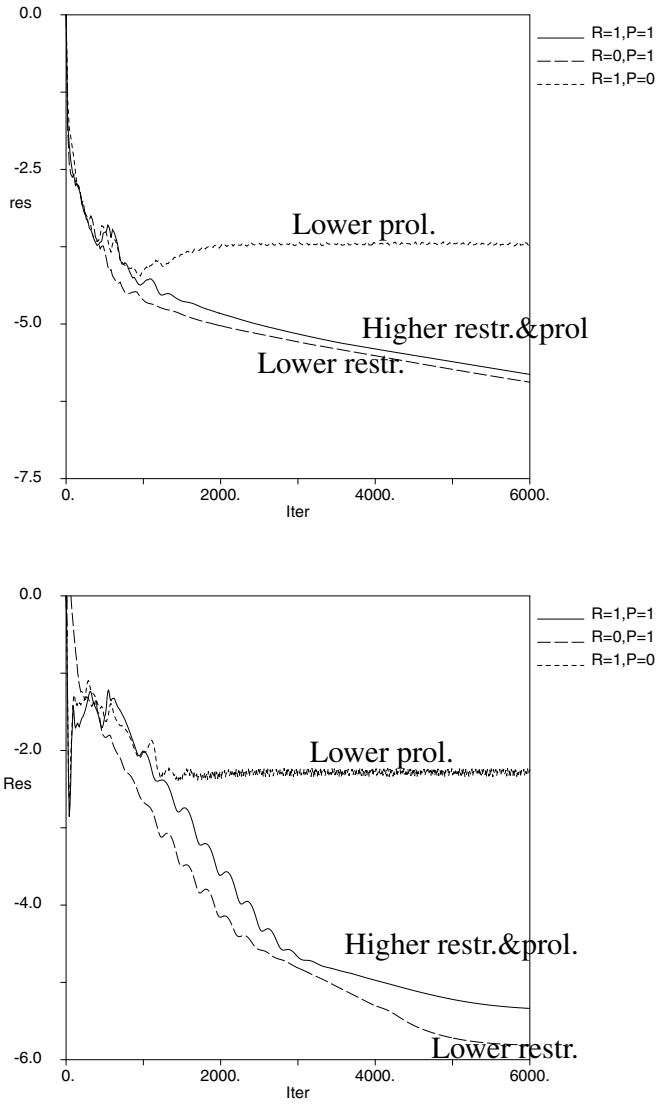

FIGURE 17: Rate of convergence with points removed in I and J, 3 multigrid levels. Top: density residual, bottom: k residual.

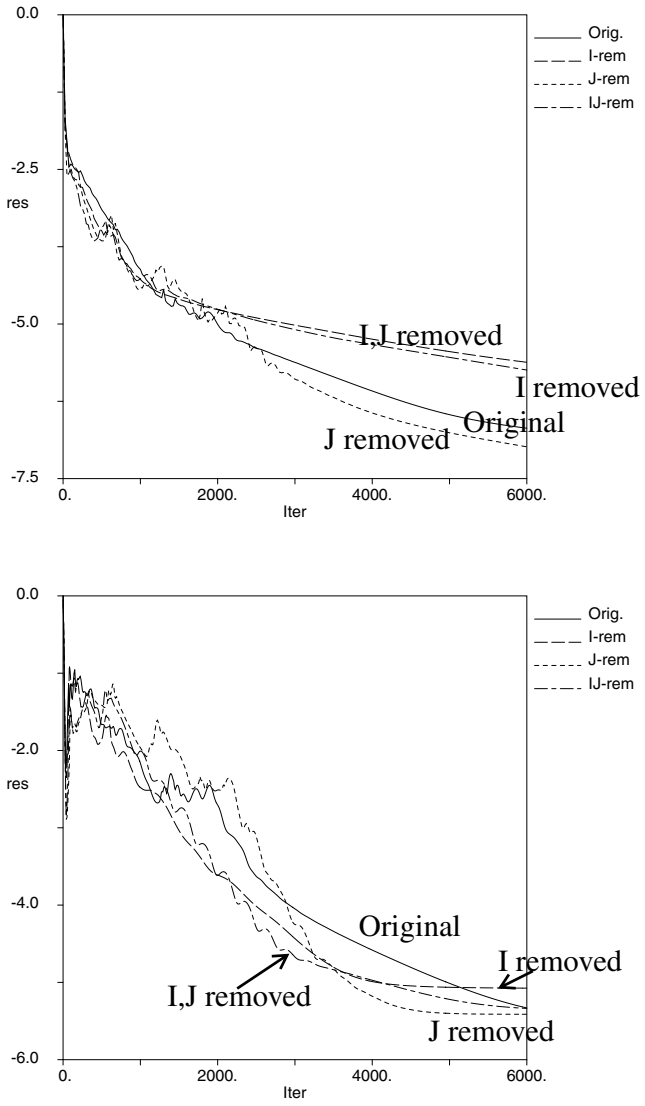

FIGURE 18: .Rate of convergence for the four grids with higher order transfer operators using 3 multigrid levels. Top: density residual, bottom: k residual.

Acknowledgment

This work has been carried out within the the AVTAC Project (Advanced Viscous Flow Simulation Tools for Complete Civil Transport Aircraft). AVTAC is a collaboration between British Aerospace, DASA, CASA, Dassault Aviation, SAAB, Alenia,

DLR, ONERA, CIRA, FFA and NLR. The project is managed by British Aerospace and is funded by the CEC under the IMT initiative (Project Ref: BRPR CT97-0555)

References

[1] Almeida, G.P., Durao, D.F. and Heitor, M. V. (1993) "Wake Flows behind Two-dimensional Model Hills", Experimental and Thermal Fluid Science, vol. 7, pp. 87-101.

[2] Chien, K.Y. (1982) "Prediction of Channel and Boundary Layer Flows with a Low Reynolds Number turbulence Model", AIAA Journal, Vol. 20, No. 1.

[3] Eliasson, P. (1993) "Dissipation Mechanisms and Multigrid Solutions in a Multi-block Solver for Compressible Flow", PhD thesis, TRITA-NA-R9314, ISSN-0348-2952, Stockholm.

[4] Eliasson, P. and Engquist, B. (1995) "The Effects of Dissipation and Coarse Grid Resolution for Multigrid in Flow Problems", 7th Copper Mountain Conf. on Multigrid Methods, NASA Conf. Publication 3339, Colorado.

[5] Haase, W., Bradsma, F., Elsholz, E., Leschziner, M. and Schwamborn, D. (1993) "*EUROVAL - An European Initiative on Validation of CFD Codes*", Notes on Numerical Fluid Mechanics, Vol. 42, Vieweg Verlag.

[6] Haase, W., Chaput, E., Elsholz, E., Leschziner, M.A. and Mueller U.R. (1997) "*ECARP - European Computational Aerodynamics Research Project: Validation of CFD Codes and Assessment of Turbulence Models*", Notes on Numerical Fluid Mechanics, Vol. 58, Vieweg Verlag.

[7] Hackbush, W. (1985) "Multi-Grid Methods and Applications", Springer-Verlag.

[8] Harten, A. (1983) "High Resolution Schemes for Hyperbolic Conservation Laws", Journal of Computational Physics, vol. 49, pp. 357-393.

[9] Hundsdorfer, W., Koren, B. van Loon, M. and Verwer, J. (1995) "A Positive Finite-Difference Advection Scheme", Journal of Computational Physics, vol. 117, pp. 35-46.

[10] Jongen, T. and Marx, Y.P. (1997) "Design of an Unconditionally Stable, Positive Scheme for the K–ε and Two-Layer Turbulence Models", Computers & Fluids, Vol. 26, No. 5, pp. 469-487.

[11] Lacor, C., Zhu, Z.W. and Hirsch, C. (1993) "A New Family of Limiters Within the Multigrid/Multiblock Navier-Stokes code Euranus", AIAA/DGLR 5th Int. Aerospace Planes and Hypersonics Conf., Munich.

[12] Lien, F.S. and Leschziner, M.A. (1993) "Approximation of Turbulence Convection in Complex Flows with a TVD-MUSCL Scheme", Proc. 5th Int. Symp. on Refined Flow Modelling and Turbulence Measurements, Paris, Sep. 7-10, 1993.

[13] Shu, C. (1988) "Total-Variation-Diminishing Time Discretizations", SIAM J. Sci. Stat. Comput., Vol. 9, No. 6.

[14] Rizzi, A., Eliasson, P., Lindblad, I., Hirsch, C., Lacor, C. and Haeuser, J. (1993) "*The Engineering of Multiblock \ Multigrid Software for Navier-Stokes Flows on Structured Meshes"*, Computers and Fluids, Vol. 22, pp. 341-367

[15] Wallin, S. (1996) "Numerical Discretization of Two-Equation turbulence Models in Euranus", FFAP-B-010, Internal report.

[16] Yee, H.C., Warming, R.F. and Harten, A. (1985) “Implicit Total Variation Diminishing (TVD) schemes for Steady-State Calculations”, Journal of Computational Physics, vol. 57, pp. 327-360.